STUDY ON BIOREMEDIATION OF AZO DYES USING NUTRACEUTICAL INDUSTRIAL SPENT AND RESULTANT WASTE AS FILLER MATERIALS TO FABRICATE GREEN COMPOSITES

SYED NOEMAN TAQUI

FACULTY OF SCIENCE
UNIVERSITY OF MALAYA
KUALA LUMPUR

2019

STUDY ON BIOREMEDIATION OF AZO DYES USING NUTRACEUTICAL INDUSTRIAL SPENT AND RESULTANT WASTE AS FILLER MATERIALS TO FABRICATE GREEN COMPOSITES

SYED NOEMAN TAQUI

THESIS SUBMITTED IN FULFILLMENT OF THE REQUIREMENTS FOR THE DEGREE OF DOCTOR OF PHILOSOPHY

DEPARTMENT OF CHEMISTRY
FACULTY OF SCIENCE
UNIVERSITY OF MALAYA
KUALA LUMPUR

2019

UNIVERSITY OF MALAYA

ORIGINAL LITERARY WORK DECLARATION

Name of Candidate: **SYED NOEMAN TAQUI**

Registration/Matric No: SHC130091

Name of Degree: **DOCTOR OF PHILOSOPHY**

Title of Project Paper/Research Report/Dissertation/Thesis ("this Work"):

STUDY ON BIOREMEDIATION OF AZO DYES USING NUTRACEUTICAL INDUSTRIAL SPENT AND RESULTANT WASTE AS FILLER MATERIALS TO FABRICATE GREEN COMPOSITES

Field of Study: **POLYMER CHEMISTRY**

I do solemnly and sincerely declare that:

(1) I am the sole author/writer of this Work;
(2) This Work is original;
(3) Any use of any work in which copyright exists was done by way of fair dealing and for permitted purposes and any excerpt or extract from, or reference to or reproduction of any copyright work has been disclosed expressly and sufficiently and the title of the Work and its authorship have been acknowledged in this Work;
(4) I do not have any actual knowledge nor do I ought reasonably to know that the making of this work constitutes an infringement of any copyright work;
(5) I hereby assign all and every rights in the copyright to this Work to the University of Malaya ("UM"), who henceforth shall be owner of the copyright in this Work and that any reproduction or use in any form or by any means whatsoever is prohibited without the written consent of UM having been first had and obtained;
(6) I am fully aware that if in the course of making this Work I have infringed any copyright whether intentionally or otherwise, I may be subject to legal action or any other action as may be determined by UM.

Candidate"s Signature Date:

Subscribed and solemnly declared before,

Witness"s Signature Date:

Name:

Designation:

STUDY ON BIOREMEDIATION OF AZO DYES USING NUTRACEUTICAL INDUSTRIAL SPENT AND RESULTANT WASTE AS FILLER MATERIALS TO FABRICATE GREEN COMPOSITES

ABSTRACT

The ever-increasing volume of spent/waste from Nutraceutical Industries accumulating into millions of tons is a serious threat to environment. Its disposal by incineration/burning as fuel adds to the carbon foot print. Nutraceutical Industrial Spent (NIS) has no feed or fertilizer value, since it has undergone process using toxic organic solvents. The present study explores the novel concept of using NIS as biosorbent for the remediation of toxic dyes and utilizing the resultant "sludge" as filler/reinforcing material with non-biodegradable plastics to fabricate polypropylene green thermoplastic and unsaturated polyester resin composites. Fennel seed spent, coriander seed spent, and cumin seed spent have been explored for bioremediation of Congo red, Acid Blue 113, Acid Red 119 and metal-complex dye, Acid Black 52 in aqueous solutions and textile industrial effluent. By batch experiments, the operating variables like initial dye concentration, adsorbent dosage, particle size, temperature, contact time and pH were optimized. pH 2 is ideal to remove azo dyes from aqueous solutions using NIS as adsorbent with enhanced adsorption capacity. For comparison, bioremediation of Congo red dye was carried out at almost neutral pH which displayed equally interesting results. The results indicate that broad range of pH 2 to 7 can be used for remediation of bisazo dyes from aqueous solutions. The adsorption methodology was studied using nine models. Of all the adsorption studies thermodynamic analysis showed the adsorption is favorable and endothermic. The low ΔH value indicates that the adsorption is a physical process involving weak chemical interactions like hydrogen bonds and van der Waals interactions. The kinetics revealed that the adsorption process showed pseudo second-order tendencies with the equal influence of intra-particle as well as film diffusion. The process of interaction between the adsorbent and adsorbate is physical and maximum

adsorption takes place between pH of 2 and 4 and at 30^{o}C. The SEM images showed that NIS is highly fibrous matrix with a hierarchical porous structure. By FTIR presence of cellulosic and ligno-cellulosic matter in spent was confirmed and they impart hydrophilic and hydrophobic properties. The thermoplastic composites of polypropylene using dye-adsorbed NIS as filler/reinforcing material were evaluated for physico-mechanical and tribological properties and compared with polypropylene/NIS composites. Flexural strength and flexural modulus of composites were improved by adding dye-adsorbed NIS and NIS into polypropylene matrix. The wear volume of polyprolyene/dye-adsorbed NIS composites and polypropylene/NIS composites increased with increase in sliding distance, applied load and filler loading. Increased filler composition showed adverse impact on abrasive wear. The water absorption characteristics of thermoplastic composites exhibited gradual increase in weight due to hydrophilic nature of lignocellulosic filler. The SEM of surface morphology of fractured composite revealed damage to the matrix at higher dye adsorbed-NIS content. Unsaturated polyester composites of dye adsorbed-NIS and NIS showed improved chemical resistance and dimensional stability but reduced in tensile strength by increasing the filler content. The study infers that utilization of dye adsorbed-NIS as useful industrial materials may lead to creation of more jobs, ecologically alleviating waste disposal problems and helping in ameliorating the environmental pollution.

Keywords: bioremediation, azo dyes, nutraceutical industrial spent, composites

KAJIAN TERHADAP BIOPEMULIHARAAN PEWARNA AZO MENGGUNAKAN BAHAN TELAH-GUNA INDUSTRI NUTRASEUTIKAL DAN BAHAN BUANGAN YANG DIHASILKAN SEBAGAI PENGISI UNTUK MEMFABRIKASIKAN KOMPOSIT HIJAU

Abstrak

Jumlah sisa/bahan terguna semakin meningkat dari Industri Nutraseutikal yang terkumpul berjuta-juta tan merupakan ancaman serius terhadap alam sekitar. Pelupusannya melalui pembakaran sebagai bahan api telah menambah kepada kesan tapak karbon. Bahan terguna Industri Nutraceutical (NIS) tidak mempunyai nilai suapan atau baja, kerana ia telah menjalani proses yang menggunakan pelarut organik toksik. Kajian ini meneroka-kaji konsep baharu menggunakan NIS sebagai penjerap-bio untuk pemulihan pewarna toksik dan menggunakan "enapcemar" yang terhasil sebagai bahan pengisi/pengukuh dengan plastik bukan terbiodegradasi untuk fabrikasi komposit termoplastik hijau polipropilena dan resin poliester tak tepu. Biji adas terpakai, biji ketumbar terpakai dan biji jintan terpakai telah diterokai untuk bioremediasi Congo merah, Acid Blue 113, Acid Red 119 dan pewarna kompleks logam, Acid Black 52 dalam larutan akueus dan bahan buangan perindustrian tekstil. Uji kaji “kelompok”, pembolehubah operasi seperti kepekatan awal pewarna, dos penjerap, saiz zarah, suhu, masa sentuhan dan pH dioptimumkan. pH 2 adalah ideal untuk mengeluarkan pewarna azo daripada larutan akueus menggunakan NIS sebagai penjerap dengan keupayaan penjerapan yang dipertingkatkan. Sebagai perbandingan, pemulihan-bio bagi pewarna Congo merah telah dilakukan pada pH hampir neutral dan menunjukkan hasil yang sama menarik. Keputusan menunjukkan bahawa julat yang luas dari pH 2 hingga 7 boleh digunakan untuk pemulihan pewarna-pewarna bisazo daripada larutan akueus. Metodologi penjerapan telah dikaji menggunakan sembilan model. Daripada semua kajian penjerapan, analisis termodinamik menunjukkan penjerapan adalah baik dan endotermik. Nilai ΔH yang rendah menunjukkan bahawa penjerapan adalah proses fizikal yang melibatkan tidak balas kimia yang lemah seperti tidak balas ikatan hidrogen

dan tindakan van der Waals. Tindak balas kinetiknya mendedahkan bahawa proses penjerapan menunjukkan kecenderungan pseudo-tertib kedua dengan pengaruh yang sama antara intra-zarah dan juga penyebaran filem. Proses interaksi antara penjerap dan bahan terjerap adalah fizikal dan penjerapan maksimum berlaku antara pH 2 dan 4 dan pada 30^{o}C. Imej SEM menunjukkan bahawa NIS adalah matriks yang sangat berserabut dengan struktur berliang berperingkat-peringkat. Melalui FTIR kehadiran bahan selulosa dan ligno-selulosa dalam bahan terguna telah disahkan dan ianya menunjukkan sifat hidrofilik dan hidrofobik. Komposit termoplastik polipropilena menggunakan bahan penjerap NIS sebagai pengisi/bahan pengukuh telah dinilai untuk sifat fizikal-mekanikal dan tribologi dan dibandingkan dengan komposit polipropilena/NIS. Kekuatan fleksural dan modulus lenturan komposit telah diperbaiki dengan menambahkan NIS dan NIS pewarna-dijerap ke dalam matriks polipropilena. Isipadu haus komposit polipropilena/NIS pewarna-terjerap dan komposit polipropilena/NIS meningkat dengan peningkatan jarak gelangsar, beban gunaan dan muatan pengisi. Komposisi pengisi yang meningkat menunjukkan kesan buruk terhadap hausan kasar. Ciri-ciri penyerapan air bagi komposit termoplastik menunjukkan kenaikan beransur-ansur dalam berat disebabkan oleh sifat hidrofilik pengisi lignoselulosik. SEM bagi morfologi permukaan komposit retak mendedahkan kerosakan pada matriks dengan kandungan NIS pewarna-terjerap yang lebih tinggi. Komposit poliester tak tepu yang mempunyai NIS pewarna-terjerap dan NIS menunjukkan rintangan kimia dan kestabilan dimensi yang lebih baik tetapi kurang dalam kekuatan tegangan dengan meningkatkan kandungan pengisi. Kajian ini menyimpulkan bahawa penggunaan NIS pewarna-terjerap sebagai bahan industri yang berguna boleh menjurus kepada terbentuknya lebih banyak pekerjaan, mengurangkan masalah pelupusan sisa secara ekologi dan membantu memulihkan pencemaran alam sekitar.

Kata kunci: bioremediasi, azo pewarna, bahan terguna industri farmaseutikal, komposit

ACKNOWLEDGEMENTS

From the innermost depths of my heart, I thank Almighty for His grace whose everlasting mercy has permitted me to complete the task. My sincere thanks to all those who helped me to accomplish my goal.

I express my profound gratitude and acknowledge the affection, cooperation, inspiration and guidance offered by my guide Prof. Dr. Rosiyah Yahya and Prof. Dr. Aziz Hassan right from the initiation of the work to the preparation of the manuscript. I recall with gusto the experiences I shared with them during my endeavor. It is indeed a rare privilege for me to work under their enduring inspiration and impregnable spirit.

I express my heartfelt thanks to the Dean, Faculty of Science, Prof. Dr. Zanariah Abdullah for her continuous support and encouragement throughout my stay as a Researcher in the campus.

My humble and heartfelt gratitude to Assoc. Prof. Dr. Shamsuddin Ahmed Mohammed Sahadat formerly associated with the Department of Mechanical Engineering who provided me the first platform in the University of Malaya to perceive my Doctoral Studies.

It gives me immense pleasure to express my deep sense of reverence and gratefulness to all the members of the faculty in the Department of Chemistry, University of Malaya, Kuala Lumpur, Malaysia for their commendable help to me for the successful completion of my task. I extend my humble appreciation to all the staff of Faculty of Science for their help.

My sincere thanks are due to the present and past Heads of the Department in Chemistry, University of Malaya, Kuala Lumpur, Malaysia for their cooperation and help during my research programme.

My appreciations to all my colleagues from the Polymer Research Laboratory for their valuable help during my endeavor.

I am very much thankful for the assistance I have received from Prof Syed Akheel Ahmed, Department of Studies in Chemistry, University of Mysore, Manasagangotri, Mysore, India.

My sincere thanks to the authorities of Department of Studies in Chemistry, University of Mysore, Manasagangotri, Mysore, India for providing the facilities to carry out part of my research work. My sincere thanks to all the research scholars of the department for their support, guidance and encouragement during my tenure.

It is a pleasure to express my deep sense of reverence and gratefulness to my friend Mr Nayan Nayak, LAQV-REQUIMTE, Department of Chemistry, Faculty of Science and Technology, Universidade NOVA de Lisboa, Caparica, Portugal for his help during my research work.

It is right time to express my heartfelt thanks to my mother Mrs Ayesha Nasreen and my brothers Mr Syed Raihan Taqui and Mr Syed Usman Taqui, my sister-in-law Mrs Amina Farheen and Master Aahil Syed for their affection and encouragement.

TABLE OF CONTENTS

LIST OF FIGURES

LIST OF TABLES

LIST OF SYMBOLS AND ABBREVIATIONS

α	Brouers-Sotolongo isotherm constant
A_{RP}	Redlich-Peterson constant (mg^{-1})
B_{RP}	Redlich-Peterson constant ($L\ g^{-1}$)
b_{T0}	Toth isotherm constant ($mg\ g^{-1}$)
β_{VS}	Vieth-Sladek isotherm constant
χ^2	Chi-squared
C_o	Initial concentration
C_e	Equilibrium concentration
ΔG^0	Standard free energy
ΔH^0	Enthalpy change
ΔS^0	Entropy change
g	Redlich-Peterson isotherm constant
K_a	Langmuir constant ($L\ mg^{-1}$)
K_{ad}	Dubinin-Radushkevich constant ($mol^2k^{-1}J^{-2}$)
K_{BS}	Brouers-Sotolongo isotherm constant
K_F	Freundlich constant related to adsorption capacity ($mg\ g^{-1}$)
K_J	Jovanovic isotherm constant
K_{rp}	Radke-Prausnitz isotherm model exponent
K_s	Specific wear rate
K_{VS}	Vieth-Sladek isotherm constant

m_{rp}	Radke-Prausnitz isotherm model exponent
n_F	Heterogeneity factor (mg L^{-1})$^{-1/n}$
n_{T0}	Toth isotherm constant (L mg^{-1});
R_L	Separation factor
R^2	Correlation coefficient
q_e	Adsorption capacity (mg L^{-1})
Q_m	Maximum adsorption capacity (mg L^{-1})
q_t	Adsorption capacity at time „t“ (mg L^{-1})
q_s	Dubinin-Radushkevich constant (mg g^{-1})
AB52	Acid black 52
AB113	Acid blue 113
AR119	Acid red 119
CR	Congo red
CR-NICSS	Congo red dye adsorbed nutraceutical industrial coriander seed spent
COD	Chemical Oxygen Demand
DTA	Differential thermal analysis
FFED	Fractional factorial experimental design
FTIR	Fourier transform infrared spectroscopy
MA-g-PP	Maleic anhydride grafted polypropylene
NIS	Nutraceutical industrial spent
NICSS	Nutraceutical industrial coriander seed spent

NICUS	Nutraceutical industrial cumin seed spent
NIFSS	Nutraceutical industrial fennel seed spent
PP	Polypropylene
PP/NICSS	Polypropylene nutraceutical industrial coriander seed spent
PP/CR-NICSS	Polypropylene Congo red dye adsorbed nutraceutical industrial coriander seed spent
PVC	Polyvinyl chloride
SEM	Scanning electron microscopy
SSE	Sum of square errors
TIE	Textile industrial effluent
TGA	Thermogravimetric analysis
USP	Unsaturated polyester resin
USP/NICSS	Unsaturated polyester resin/Nutraceutical industrial coriander seed spent
USP/CR-NICSS	Unsaturated polyester resin/Congo red dye adsorbed nutraceutical industrial coriander seed spent
UTM	Universal testing machine

CHAPTER 1: INTRODUCTION

1.1 Background study

The fundamental ingredients in the evolution of a happy, peaceful and prosperous nation lie in laying strong foundation for sustainable development (Finkbeiner et al., 2010; Glavič & Lukman, 2007; Ness et al., 2007). The pertinent challenges for sustainable development in the twenty-first century are the impact of developmental initiatives towards the environment – air, soil and water. Water is the most vital among the natural resources, and is highly critical for the survival of all living organisms. In the course of human activities water gets affected and the quality gets declined due to the increased of urbanization, population growth, and industrial production and such other factors. Untreated or improperly treated industrial effluents/wastes are the major sources for environmental air, soil and water pollution and these are posing serious threat to the well-being of the ecosystem across the world.

1.2 Resolving environmental concern

1.2.1 Nutraceutical industries

The ascendancy of nutraceuticals over synthetic chemical products during the last quarter of 20th century has made pharmaceutical industry to look at the plant kingdom as potential 'factories' for the production of a wide range of high-value therapeutic agents. This has created a revolution in nutraceuticals and as a result there is going to be great change in the nature of pharmaceutical and food industries by 2025 due to great monetary success. A complete transition from complex mixtures and extracts of 19th century to single-entity prescription up to the last quarter of 20th century has created many therapeutic problems relating to side effects.

Consequently, there was a surge for alternative medicines which led to the resurgence of Traditional Indian Medicine and Traditional Chinese Medicines

(Patwardhan et al. 2005) thereby paving the way for increased dependence on nutraceuticals. Besides, a large quantum of scientific studies concluded and/or in progress on a wide variety of botanicals or phytochemical entities with evidence-based therapeutics acceptable for the global community has led to unparalleled business on herbal drugs and traditional medicines (Birt et al., 2001; Belem, 1999; DeFelice, 1995; Fowler, 2006; Gupta & Sharma, 2006; Kalra, 2003; Ohr, 2005; Patwardhan et al., 2005; Raaman, 2006).

Nutraceutical industries come under agro-industrial sector and of late it is expanding fast. According to the Associated Chambers of Commerce and Industry of India, the Indian Nutraceuticals market is expected to grow from $ 4 Bn in 2015 to $ 10 Bn in 2022. This represents a huge growth of 21% annually (www.mrssindia.com). Nutraceuticals are isolated from food matrix either by steam distillation or through solvent extracted oleoresins from medicine related foods, such as garlic, soybean and coriander to mention a few. The process followed for this generates 50-95% of waste from the total amount of herbs, shrubs, seeds and/or roots used in the process of recovery of the active ingredient(s). Large quantities of cellulosic biomass generated in nutraceutical industries commonly known as Nutraceutical Industrial Spent (NIS) are often disposed by burning; because NIS has no fertilizer or feed value since during processing it undergoes chemical treatment. Though no official figures are available on the Nutraceutical Industrial Spent/waste generated, but, considering the total turn-over it may amount for millions of tons of renewable and biodegradable spent/waste. Thus, there is a greater challenge faced by the nutraceutical industry in handling the generated waste.

Nutraceutical industries of India are processing over 50 varieties of botanicals to isolate and/or recover the principle nutraceutical component generating myriad tons of

spent. Three spent were chosen in this study, they were fennel seed spent, coriander seed spent and cumin seed spent.

(i) Fennel seeds Fennel seed spent Fennel seed spent powder

(ii) Coriander seeds Coriander seed spent Coriander seed spent powder

(iii) Cumin seeds Cumin seed spent Cumin seed spent powder

Figure 1.1: The seeds, spent and spent powders of (i) fennel (ii) coriander (iii) cumin

India is the leading producer of fennel with production of 1.10 x 10^5 tons/year (Bhattacharyya & Sharma, 2004). Fennel is a perennial, pleasant-smelling herb with yellow flowers. This herbaceous plant reaches up to 2 meters in height. Fennel seed *(Foeniculum vulgare)* belongs to the family (*Umbelliferae*) is native to Southern Europe and grown extensively all over Europe, Middle-East, China, India, and Turkey. The seeds are extensively used for culinary, flavoring and medicinal purposes. The seeds are

commonly known in vernacular as *"saunf"* and are rich source of dietary fiber. It contain numerous flavonoids and powerful anti-oxidants which offer protection from cancers, infection, aging and degenerative neurological diseases. It prevents oxidative stress damage and strengthens the immune system. It is one of the nine Anglo-Saxon sacred herbs. Fennel seeds contain 1-3% volatile oil which is composed of about 50 - 60% anethole and about 20% d-fenchone (www.spices.res.in/spices/fennel.php). Other compounds present in fennel are d-α-pinene, d-α-phellandrene, dipentene, methyl chavicol, feniculun, anisaldehyde, and anisic acid (www.spices.res.in). The extraction of oleoresin and/or principle component(s) from fennel seeds involves mechanical, chemical and thermal processes. After the extraction, a large quantity of fennel seed spent is obtained which has no commercial/fertilizer value. The resultant spent obtained is considered as an agro-waste or nutraceutical industrial spent (NIS), is a good biosorbent with least E-factor as it needs no chemical treatment before its use, as needed in case of many agriculture biomasses reported in the literature (Bhattacharyya & Sharma, 2004; Sheldon, 1992).

India is the largest producer, consumer and exporter of coriander having greater share in world export market with annual production of 3.15 x 10^5 tons (Peter, 2006). Coriander belongs to the family *Apiceae* and genus *Coriandrum* also known as Chinese parsley. The herb is a soft hairless plant growing up to 50-cm height and is widely cultivated in southern Europe, southern Africa and Asia. Coriander is known all over the world for its edible, medicinal and antibacterial properties. It is a great source of potassium, iron, vitamins, folic acid, magnesium, and calcium and contains pinene, terpenes, linalool and antiseptic citronelol. Due to its antiseptic property, coriander is widely used in traditional medicine to heal mouth ulcers. The resultant spent generated after extracting active component(s) and/or oleoresin by mechanical, chemical and thermal processes is commonly known as Nutraceutical

Industrial Coriander Seed Spent (NICSS). NICSS has proved to be a good biosorbent with least E-factor (Sheldon, 1992) for the bioremediation of toxic azo dyes from aqueous water.

India is the main producer and consumer of cumin seed. It produces 80% of the world supply and consumes 73% of the total world's cumin seed. Other producers are Syria (7%), Iran (4%), and Turkey (3%). The remaining 6% comes from other countries. In total, around 400,000 metric tons of cumin seed per year are produced worldwide (www.royalspices.com). Cumin is the dried seed of the herb *Cuminum Cyminum L*, a member of the parsley family. Cumin is a thin herbaceous annual plant growing to a height of 30-45 cm. The plant is slender, with a main stem that branches up to five secondary branches from the base; each branch may have 2-3 sub-branches. All the branches attain the same height, giving the plant a uniform canopy. The plant has a branched glabrous stem, 3-5cm in diameter, with a grey or dark green color, having alternate, dissected leaves with fusiform segments, angular, sparsely hairy, bluish green and petioles sheathing the stem at the base. The inflorescence is compound umbel with white or pinkish flowers. The leaves are pinnate or bi-pinnate with thread-like leaflets. The flowers are small and either pink or white colored. The flowers are born in umbels, and each umbel has 5 to 7 umbellate. The fruit is a schizocarp, 4-5 mm long; containing two pericarps with a single seed. The fruit is a lateral fusiform or ovoid achene, containing a single seed. Cumin seeds are similar to fennel and anise seeds in appearance, but are smaller and darker in color. The fruits have eight ridges with oil canals. Seeds are hairy, in some varieties these hairs are prominent, and otherwise it is difficult to see them.

1.2.2 Textile industries – present-day scenario

Ever-increasing population and living standard have continuously put higher demand for textiles and clothing - one of the primary needs of human beings. Today,

textile industries have become one amongst the top ten most polluting industries (www.worstpolluted.org) which produce an astonishing 60 billion kg fabric annually, using up to 9 trillion gallons of water (Zaffalon, 2010). This massive scale of water consumption by the industry is ultimately the key component for creating pollution. Bringing down water footprint and carbon footprint is the ultimate concern for sustainable development of world's textile industry (Zaffalon, 2010). Textile industries use umpteen varieties of chemicals and are one of the major consumers of dyes.

The Indian textile industry, currently valued at around US$ 120 billion, is expected to reach US$ 230 billion by 2020. The industry is next only to agriculture in providing employment with over 45 million people being directly and 20 million people indirectly employed. The industry contributes approximately 2 per cent to India's Gross Domestic Product and 14 per cent to overall Index of Industrial Production (www.ibef.org/industry). The industry has two broad segments. First, the unorganized sector consisting of handloom, handicrafts and sericulture, which are operating on a small scale using traditional tools and methods. The second is the organized sector consisting of spinning, apparel and garments segments applying modern machinery and techniques (www.ibef.org/archives). The former adopts old technologies and uses large quantities of varied synthetic dyes with most of them causing environmental, specifically water pollution. This has created ecological imbalance which is gaining prominence at textile forums and development of alternative and clean technology is gaining momentum. Clean technology can be broadly defined as ''a diverse range of products, services, and processes that harness renewable materials and energy sources, dramatically reduce the use of natural resources, and cut or eliminate emissions and wastes'' (Clift, 1997). E-factor as a metric is relatively simple and easy to understand and draws attention to the quantum of waste produced from a given mass of product"

(Sheldon, 1992). It also pinpoints to the relative wastes generated by different products of the chemical processing.

Textile industry is currently facing major challenges, such as severe competition, over-capacity, falling profit margins and increased environmental considerations. These factors have contributed to shortage of funds for overhead expenditures especially towards R&D and wastewater treatment. Hence, economical removal of color and toxicity from effluents becomes an important issue. The limitations and disadvantages of techniques, methods and procedures led to the resurgence of adsorption as a technique and as a tool of paramount importance. Adsorption techniques, of late, are gaining prominence due to their efficiency in the removal of pollutants that are otherwise too difficult by conventional methods (Yagub et al., 2014).

Leather industries, like textile dyeing and related processes have played yeomen role during the last few decades by augmenting the economy of India (Sarkar, 1981). During this period, many chemicals have been invented, synthesized, developed, and chosen to provide the consumer long life and continued fashion appeal to the garments, furnishings and leather materials. To assure these qualities, the chemicals used had to resist the effects of the environment. Materials used were required to be durable, fast and chemically not degradable. However, these properties that protect the consumer materials also create problems to the textile dyeing and leather industry when the effluents containing these harmful chemicals are released into the environment. The Central Pollution Control Board, India has identified textile and leather industries as most polluting industries affecting human health and ecology in a significant way (www.indiaenvironmentportal.org.in).

India is rich in natural resources and ranks first among major livestock holding countries. According to US based Global Agriculture Information Network report 2016,

India produced approximately 51 million pieces of bovine hides, and 128 million pieces of sheep, lamb, and goat skins during the year 2014 (agriexchange.apeda.gov.in). About 80 percent of these local raw materials are used to produce on average approximately 2 billion square feet of leather per year and contributes to about 10 percent of global supplies. It is endowed with 21% of the world cattle and buffalo and 11% of the world goat and sheep. The annual average rate of the growth of cattle is around 1.5% in India, helping it to maintain its leading position. The total sales of hides and skins industry were approximately $12.5 billion in 2015 and expected to grow by 24 percent in the next five years due to higher demand for finished leather goods from the rising middle class. The total turnover plays a vital role in the national economy in terms of export earnings and employments generation. This sector provides direct employment to more than 2 million people, among them majority represent economically weaker sections. Women employment accounts for 30% share of the total work force (Naidu 2000).

Indian leather industry is spread over organized as well as unorganized sectors. The products manufactured by the organized sector are free from pentachlorophenol, azo dyes and other banned dyes and chromium-free products. There are around 2,000 tanneries in India. The small scale, cottage and artisan sectors account for over 75% of the total production which still use banned dyes and chemicals. From chemical point of view, majority of the dyes used in tanneries are mostly metal-complex dyes. Metal-complex dyes represent an important class of dyes due to their excellent light fastness on substrates. The more important metal-complex dyes are chromium, cobalt and copper complexes with azo ligands and the share of this class of dye is estimated to be approximately 30% in wool dyeing and 40% in polyamide dyeing (Ramasami et al., 1995).

The tanning industry is one of the largest contributors of chromium pollution in India (www.dnaindia.com). Sustenance of tanneries, particularly of small units, is

becoming increasingly difficult due to alarming levels of environmental pollution caused by various tanning operations and practices (Sarkar, 1981) because scientific waste disposal practices are almost absent in unorganized sector (Ramasami et al., 1994). Though official figures regarding waste disposal are not available due to the excessive use of banned dyes, but considering the total turnover of the products, it is envisaged that myriad tons of effluents containing metal-azo dyes are dumped in to the environment. Thus, in such situations remediation of the hazardous metal-dyes using simple, cost-effective and ecofriendly technology assumes paramount importance.

1.2.3 Polymers in use – the displaced paradigm

Depletion of fossil fuels and non-degradability of synthetic polymers have posed a big challenge and made to use waste material(s) and translate them into new products to address the environmental foot print (Hoekstra & Wiedmann, 2014). Petrochemical and textile industries are the major polluters amongst the top fifteen classes of industries (www.worstpolluted.org). Nutraceutical industries are also major polluters producing lots of spent and waste materials. There is an urgent need to harness renewable nutraceutical industrial spent and use non-biodegradable plastic waste and remediate toxic and hazardous waste of textile industries and reuse for the development of green materials.

World plastics production increased from 1.5 million tons (MT) in 1950 to 322 MT in 2015 (committee.iso.org) and the global plastic market is expected to reach USD 654.38 billion by 2020 (prnewswire.com). The rapid rate of plastic production increased the waste and created waste disposal problems. The pollution caused by emissions during their incineration is affecting very badly the air, the water and the food.

Polypropylene (PP) is a low cost, most extensively used engineering plastic (Hashmi et al. 2002). It has multiple properties like flexibility, strength, lightness,

stability, chemical resistance and least absorption of moisture. Although, the changing petrochemical feedstock adversely affects polypropylene market, it's easy processability and simple recycling will partly off-set the economic imbalance. The U.S. based GBI Research group has estimated that world PP consumption will reach 62.4 million tons by 2020 of which the packaging industry is expected to consume around 20.1 million tons. The short half-life of packaging material triggers the generation of waste material.

1.2.4 Problem statement

Dyes are the most prominent group of synthetic organic compounds. They are used extensively in cosmetics, foods, ink, medicine and other materials especially in dying of natural and synthetic materials (Mohammadi et al., 2014). Due to the diverse chemical nature and various types of dyes, no systematic nomenclature has been attempted. Hence, dyes in the present situation, can be classified according to the method of their application to the fiber or on the basis of their chemical structure (Garfield, 2002). The former is of immense significance to the textile industry while, the latter is of fundamental importance to the chemists. Amongst diverse classes of dyes; reactive dyes are extensively used to color fabrics as they possess simple chemical structures that react with the fiber and provide excellent light and wash-fastness by establishing covalent bond with the substrate. Reactive dyes are put under the category of azo dyes. Azo dyes have a high degree of chemical and photolytic stability and this property is of great concern for pollution abatement (Bafana et al., 2011).

Azo dyes constitute the single largest group of synthetic organic compounds. These dyes are diazotized amines coupled to an amine or phenol, with one or more –N=N– linkage commonly known as azo bond. These synthetic compounds containing azo bonds account for about 70% of total world dye production (Carliell et al., 1998) and they are the most common group of synthetic colorants released to the environment. These colorants when mixed with natural water create visible aesthetic color problem

even at low concentration, besides creating serious health risks by their toxicity to aquatic organisms and humans (Anliker et al., 1981; Bafana & Chakrabarti, 2008; Brown & Schoenberg, 2008; Clarke & Anliker, 1980; Kellener et al., 1973; Li et al., 2007; Li et al., 2010; Ramos et al., 2002; Weisburger, 2002).

Azo dyes are unique due to their structural diversity, high molar extinction coefficient, and medium-to-high fastness properties with respect to both light and wetness (Chung, 1983). Due to their simple synthesis, usually in aqueous medium, and unlimited choice in starting products, it is possible to have extremely wide variety of azo dyes. The number of combinations is further extended because one dye molecule can accommodate several azo groups. These diversified and inexpensively produced azo dyes provide a wide spectrum of shades and fastness properties suitable for use on a variety of substrates. Therefore, they are extensively preferred and used with success. This success story is posing a great threat to eco-system (Apostol et al., 2012; Beerbaum & Heidhues, 1996; Chequer et al., 2011; Chequer et al., 2013; Chung, 1983; de Lima et al., 2007; Khan et al., 2006; Organisation for economic cooperation and development, 2005; Puntener & Page, 2004; Puvaneswari et al., 2006; Report by LGC, 1999; Xiaoyue, 1999).

Azo dyes are highly stable in the environment owing to their resistance to natural oxidation and reduction, light exposure and biodegradation. The recalcitrance of azo dyes has been attributed to the presence of sulphonate groups and azo bonds. The electron-withdrawal character of azo groups create electron deficiency making azo compounds less susceptible to oxidative catabolism (Bafana et al., 2007; Carvalho et al., 2008; Işik & Sponza, 2007; Kulla et al., 1983; Liu et al., 2007; Pagga & Brown, 1986; Pinheiro et al., 2004; Wuhrmann et al., 1980). Azo dyes are characterized by a chromophoric azo group −N=N−, whose nitrogen atoms are linked respectively to sp^2-hybridized carbon atoms. At least one among these carbon atoms belongs to an aromatic

carbocycle or heterocycle, whereas, the second carbon atom adjoining the azo group may also be part of an enolizable aliphatic derivative (Hunger et al., 2000). Azo dyes are classified as monoazo-, bisazo- and trisazo-dyes, etc depending on the number of azo groups present. Amongst, these classes, bisazo dyes are extensively used. Three bisazo dyes and one metal-azo dye have been selected in this research. The metal-azo dye is extensively used in tannery industry in India. The structures of azo dyes are presented below:

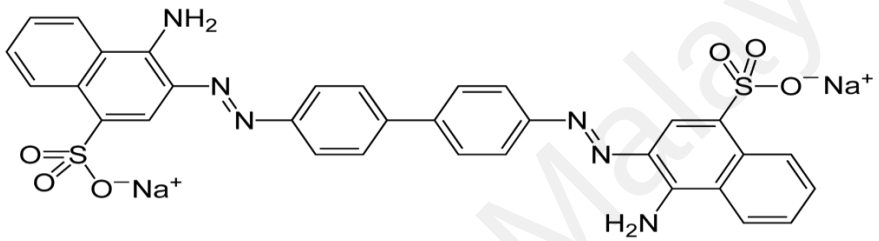

Figure 1.2: Structure of Congo red dye

Congo Red (CR) [1-naphthalenesulfonic acid, 3,3-(4,4-iphenylenebis(azo)bis(4-amino-) disodium salt] is a benzidine-based anionic bisazo dye, which gets metabolized to benzidine, a known human carcinogen (Mall et al. 2005). Although, CR has been banned in many countries still it is widely consumed (Afkhami and Moosavi, 2010) in textile industry. Owing to structural stability, CR is highly resistant to microbial biodegradation.

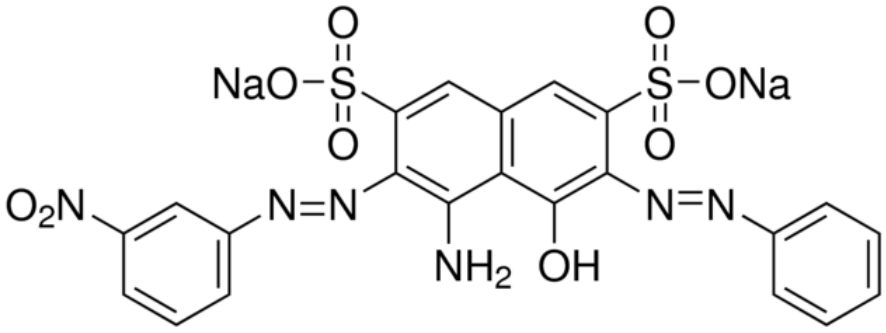

Figure 1.3: Structure of Acid blue 113 dye

Acid Blue 113 (AB113) is categorized as bisazo dye extensively used for dyeing wool, silk and polyamide fibres from a neutral or acid bath to obtain deep shade of navy blue color (Green, 1990). It may ultimately get metabolized to benzidine, a known human carcinogen (de lima et al., 2007). The health problems caused by AB113 will increase, with increased use by textile industry.

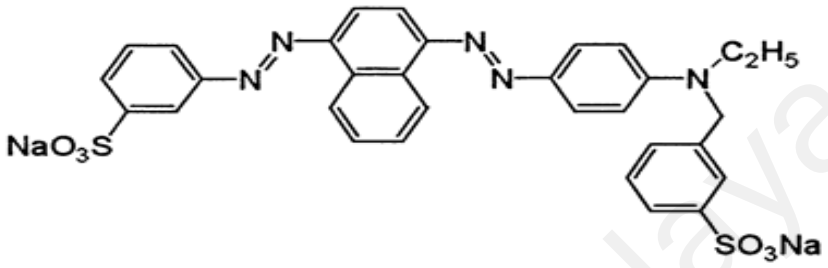

Figure 1.4: Structure of Acid red 119 dye

Acid Red 119 (AR119) is a bisazo dye and is extensively used for leather finishing, wood stains and applicable on polyamides and other coloration.

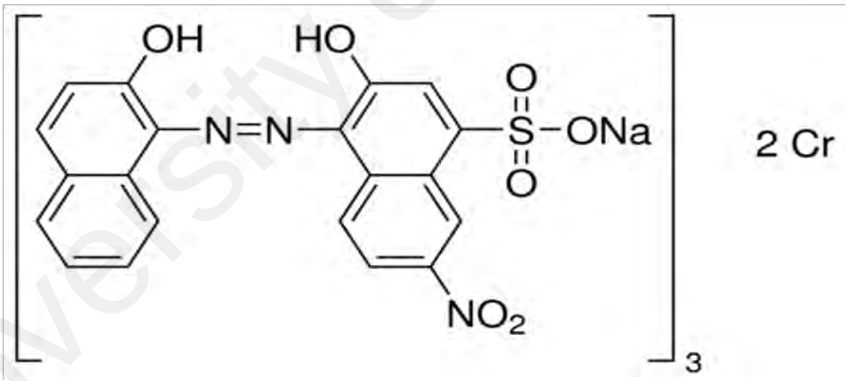

Figure 1.5: Structure of Acid black 52 dye

Acid Black 52 is a monoazo acid chromium-complex dye with high fastness properties and finds wide application in leather industries. Azo dyes and their degradation intermediates vary in their recalcitrance to biodegradation due to their complex structures and xenobiotic nature and in some cases they are both mutagenic and carcinogenic (Chung & Cerniglia, 1992).

1.2.5 Adsorption, biosorption and biosorbent

Adsorption is a mass transfer between the solid and the liquid at the interphase on a two-dimensional surface. The mass accumulated at the interface is the adsorbate and the solid surface is the adsorbent. Biosorption differs from adsorption as the mass transfer phenomenon involving the removal or separation of substances from the solution by biological material. In fact, it is a physico-chemical process involving such mechanisms as absorption, adsorption, ion exchange, surface complexation and precipitation. Biosorbents could be both living (beyond the scope of the thesis) and dead biomass. Majority of the linkage established between the adsorbent and the adsorbate is a surface complex phenomenon involving functional groups as –OH, –COOH, and –SH, to mention a few. Biosorption is used as a successful analytical technique to isolate and recover toxic and/or hazardous substances, precious metals, and other materials. It is very selective under the operating conditions. Comparatively, it has such advantages over other separation techniques, as apparent efficiency without discharging any harmful by-products, cost-effective, eco-friendly, low energy consumption, flexibility at field operations analogous to conventional ionexchange technology and easy to scale up from laboratory to field level (Ahmad et al., 2015; Ali, 2010; Anastopoulos & Kyzas, 2014; Anjaneyulu et al., 2005; Banat et al., 1996; Bello et al., 2013; Crini, 2006; Dawood & Sen, 2014; Demirbas, 2009; Forgacs et al., 2004; Fu & Viraraghavan, 2001; Gupta & Suhas, 2009; Mondal, 2008; Pearce et al., 2003; Robinson & Nigam, 2008; Salleh et al., 2011; Sharma et al., 2011; Sivashankar et al., 2014; Solis et al., 2012; Srinivasan & Viraraghavan, 2010; Tanthapanichakoon et al., 2005; Ngah et al., 2011; Yagub et al., 2014). To achieve and sustain efficient recovery of toxic and/or hazardous materials, appropriate selection of adsorbent is of paramount importance. An ideal biosorbent suitable for the conditions needed should possess the following characteristics:

- it should be available in abundance and at low-cost
- it should have either no or minimal other use(s) so that price rise and increase in demand can be controlled
- it should be in ready-to-use form without requiring any pre-chemical or other kinds of treatments
- it should have such pore structure as to allow maximum adsorption
- it should be amenable to simple and cost-effective technology to reuse the sludge/toxic biomass produced after the remediation process.

1.2.6 Bioremediation of bisazo dyes using low-cost biosorbents

Biosorption of dyes from aqueous solutions is a relatively new process that has proven very promising in the removal of contaminants from aqueous effluents. Biosorbent materials derived from low-cost agricultural wastes can be used for the effective removal and recovery of dyes from wastewater streams. However, no efforts have been made to use the nutraceutical industrial spent for the removal of contaminants from the waste water. The porous structure of Nutraceutical Industrial Spent (NIS) contains cellular spaces which have the tendency to retain water and it can be potential biosorbents. The mechanism of dye adsorption on the adsorbent in color removal process involves following steps: first, diffusion of dye molecules through the solution on to the surface of the materials through molecular interactions and second, diffusion of dye molecules from the surface into interiors of the biosorbent materials.

The factors which may affect the diffusion process are:

- The dye concentration and agitation may affect the first-step of adsorption.
- Biosorption depends on the nature of the dye molecules and pH of the solution.
- The rate determining step in the process, affects the biosorption of dyes on the substrates.

- Several treatment technologies exist for dye removal but the process of biosorption has been found to be effective technology for decolourization of wastewater.
- Adsorption by activated carbon has been found to be an effective technology for removal of dyes from wastewater. However, its use is restricted due to higher cost of activated carbon and difficulties associated with regeneration.

Thus, attempts have been made to explore low-cost and eco-friendly NIS materials as alternative adsorbents for the bioremediation of azo dyes.

1.2.7 Objectives of the study

- To study nutraceutical industrial spent (NIS) as a new class of biosorbent for remediation of toxic dyes from water and textile industrial effluents.
- Development of sustainable adsorption system of dyes using NIS through kinetic, thermodynamics and modelling studies.
- To develop sustainable design for utilization of NIS and dye adsorbed-NIS as filler materials to fabricate Green composites – thermoset and thermoplastics from virgin/recycled polymers.
- To investigate physico-mechanical and wear properties of the fabricated composites.

1.2.8 Scope of the study

By the unprecedented rise in nutraceutical industries and by taking a predominant place in world's economy, it is generating myriad tons of renewable spent/waste. This spent and/or waste is seriously affecting the environment. In such situation, nutraceutical industrial sector, a part of agro-industries cannot sustain for an everlasting period. Thus, to achieve sustainability in nutraceutical sector, there is an urgent need for developing effective management system to utilize the nutraceutical

spent/waste. Reuse, regeneration and recovery are the three components of recycling – and they also constitute the important curative approaches in environmental management.

Biosorption studies were carried out under varying conditions of initial pH, initial dye concentration, adsorbent dosage, particle size of the adsorbent and temperature to assess the adsorption, kinetic and equilibrium thermodynamics. A two-level fractional factorial experimental design (FFED) and analysis of variance (ANOVA) were used to study the influence of each parameter and combination of parameters on the final adsorption capacity of the system. SEM and FTIR techniques and the procedure for the determination of Point of Zero Charge (pZc) were used to characterize the surface properties of virgin spent and dye adsorbed spent. Efforts have also been made to prove NIS as efficient biosrobent for the remediation of bisazo dyes from aqueous system and textile industrial effluent. Also, I have endeavored to use Nutraceutical Industrial Fennel Seed Spent (NIFSS) and Nutraceutical Industrial Coriander Seed Spent (NICSS) as filler materials for the fabrication of polypropylene (PP) and unsaturated polyester resin (USP) thermoplastic and thermoset composites.

A novel concept of using a model bisazo dye Congo Red (CR) adsorbed onto NIFSS (CR-NIFSS) and NICSS (CR-NICSS) as filler materials to fabricate PP green thermoplastic composites, namely, PP/CR-NIFSS and PP/CR-NICSS and unsaturated polyester resin unsaturated polyester resin USP/CR-NICSS and USP/NICSS composites has been studied. The composites were evaluated for physico-mechanical and tribological properties and compared with the thermoplastic composites fabricated using NICSS. Flexural strength and flexural modulus of composites were improved by adding CR-NICSS and NICSS into PP matrix. The abrasive wear behavior, wear volume loss and specific wear rate as a function of abrading distance at 150, 300, 450 and 600 m and different loads of 23.54 and 33.54 N at 200 rpm were determined. The water absorption

characteristics of thermoplastic composites were studied. The surface morphology of tensile fractured PP/CR-NICSS was examined under scanning electron microscope. The influence of water and thermal ageing on tensile strength and physical properties, such as density, surface hardness and effect of chemicals on USP/CR-NICSS and USP/NICSS have been studied. This is in conformity with the present day increasing demand on bio-resources to accomplish the combined utilization of plant products and synthetic polymers, which may give way for producing cheap substitutes for traditional products, and this may have high promise in the future. This thesis is an approach towards that sustainability of nutraceutical industrial waste as shown in Schemes 1-4.

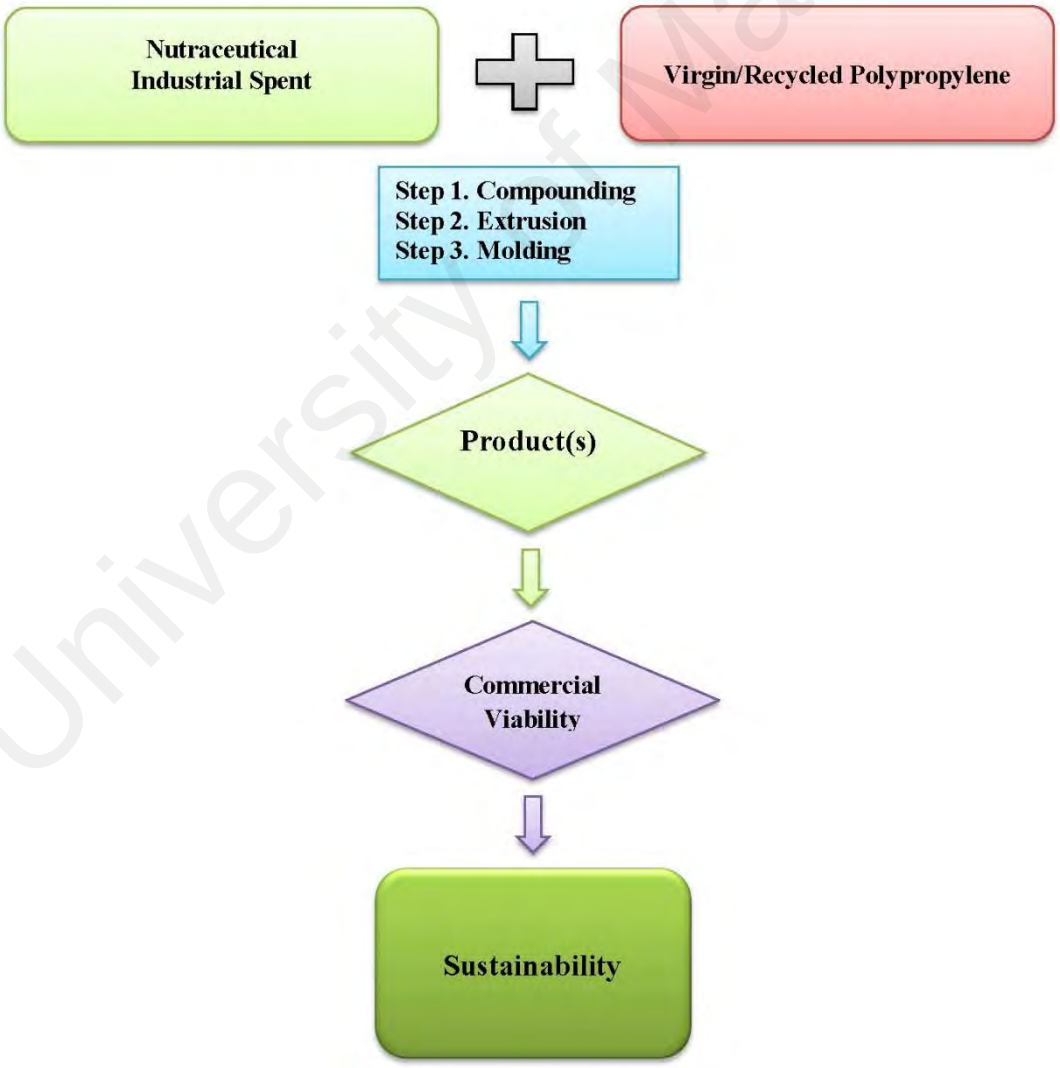

Scheme 1.1: Process of sustainability through use of NIS as filler material for the fabrication of thermoplastics using virgin/recycled polypropylene

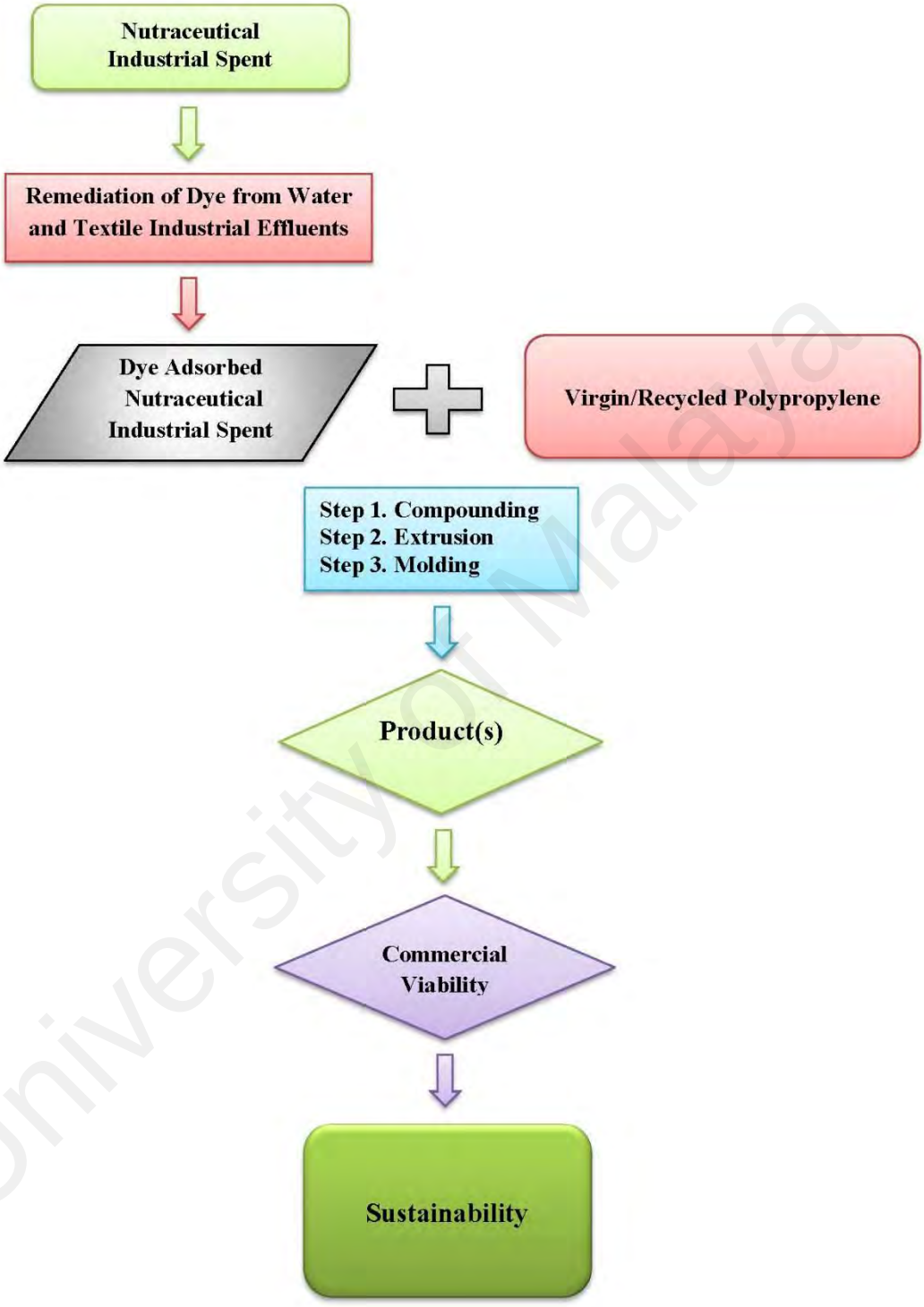

Scheme 1.2: Process of sustainability through the use of NIS as a biosorbent for the remediation of toxic dyes and the resultant dye-adsorbed NIS as filler material for the fabrication of thermoplastics

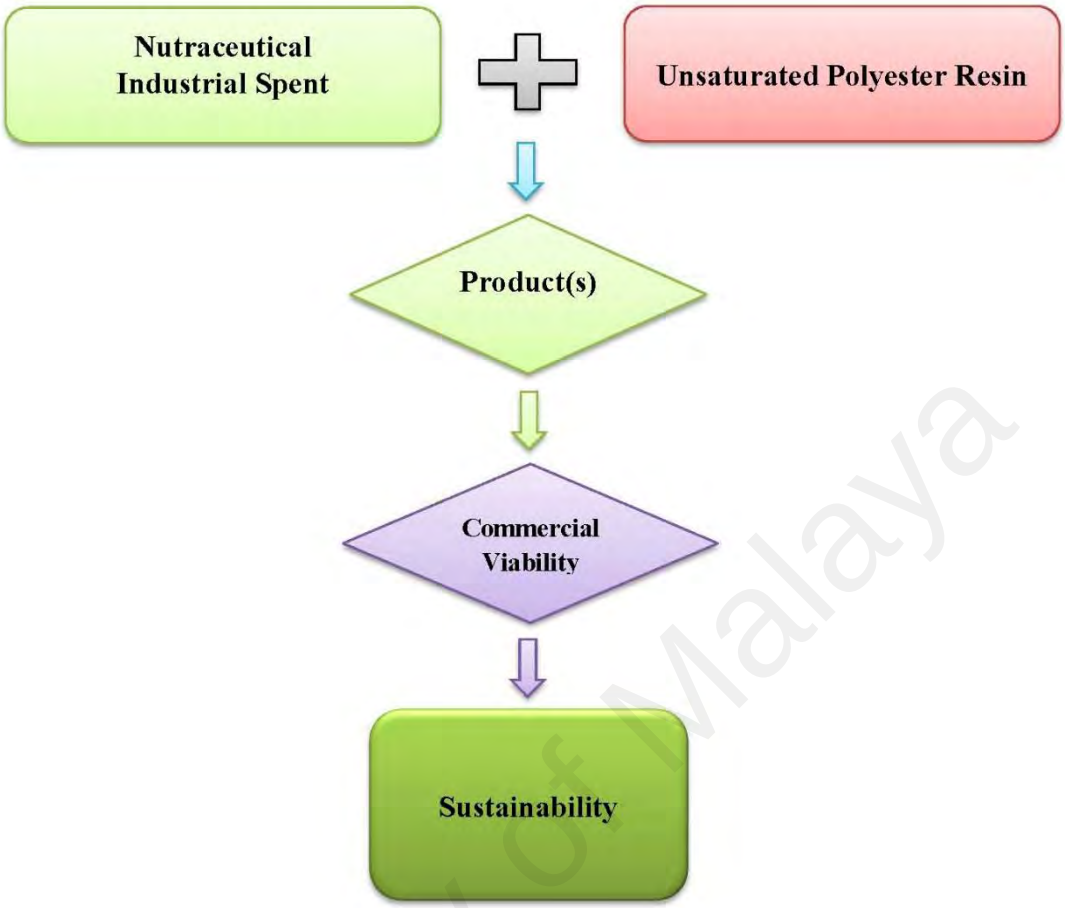

Scheme 1.3: Process of sustainability through use of NIS as filler material for the fabrication of thermosets using virgin/recycled unsaturated polyester

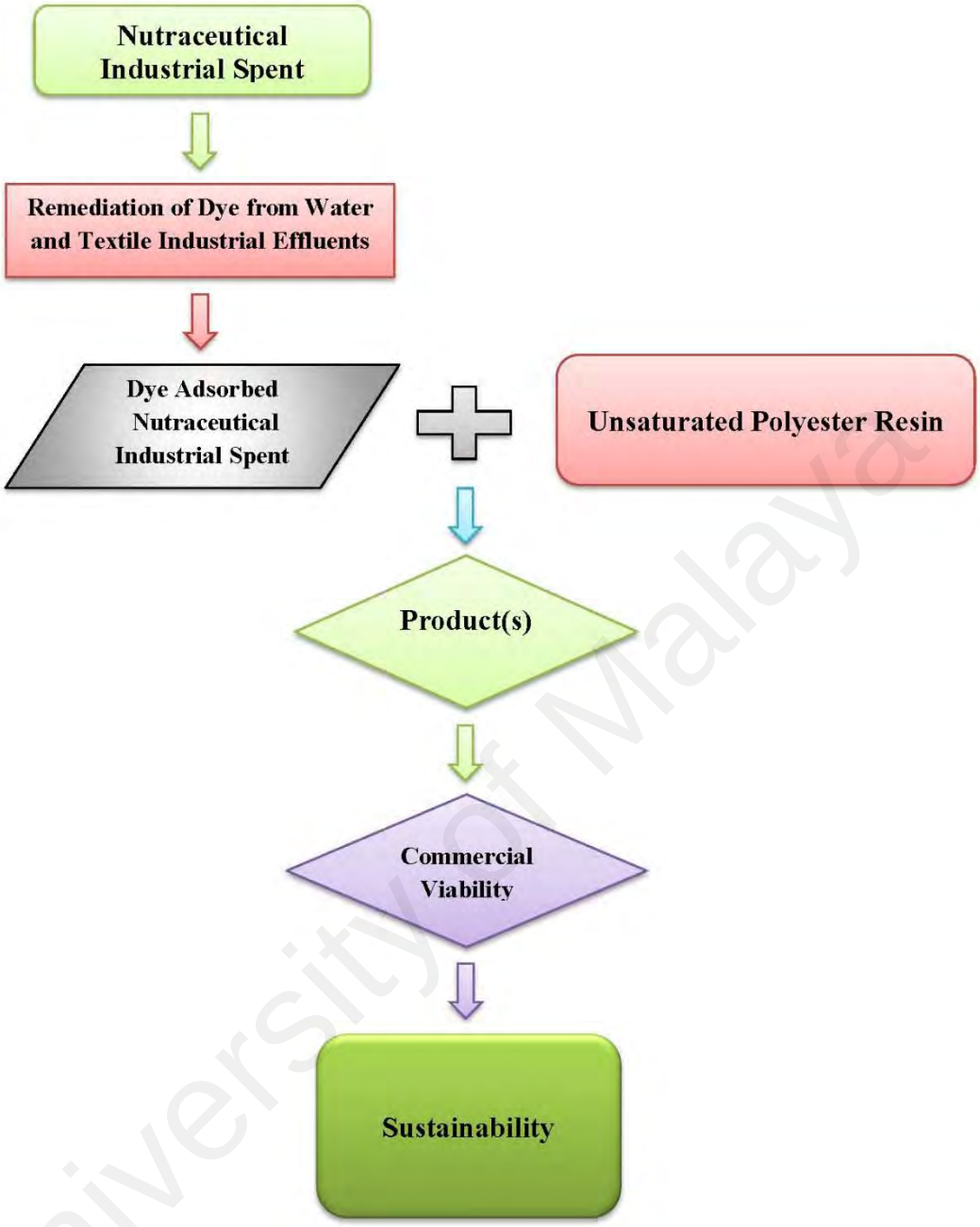

Scheme 1.4: Process of sustainability through the use of NIS as a biosorbent for the remediation of toxic dyes and the resultant dye-adsorbed NIS as a filler material for the fabrication of thermosets

CHAPTER 2: LITERATURE REVIEW

Pollution interest in the potential of dyes has been primarily prompted by the concern over their purported toxicity, carcinogenicity and mutagenicity. Most of the dyes are made up of benzidine and naphthalene derivatives which are known to be transformed into carcinogens due to microbial metabolism. Brightly colored water-soluble dyes are the most problematic to remove from industrial waste, due to their stability and resistance to degradation. Conversely, the ever-increasing stringencies on enforcement of law will continue to ensure that textile and other dye utilizing industries bring down their dye-containing effluent to the required standard level before they are released into the environment.

Azo dyes constitute nearly 70% of commercial synthetic dyes produced and used by textile industry (Carliell et al., 1998). The predominance of azo dyes is due to their ease and cost effectiveness for synthesis, great structural diversity, high molar extinction coefficient, and medium-to-high fastness properties (Chung, 1983). The color fastness, stability and the resistance of dyes to degradation have made color removal from industrial waste waters difficult. The techniques, methods and procedures reported could be categorized into; physical, chemical and biological. High cost of plant establishment, increased operation cost, problem of regeneration, secondary pollutants, sensitivity to changes in wastewater input, interference by wastewater ingredients, and disposal of residual sludge are some associated technological and economical drawbacks of above methods (Azarang et al., 2014; Azarang et al., 2015; Azarang et al., 2015a).

2.1 Physico-chemical methods

Conventional irradiation techniques used in water and wastewater treatments produce high quality water. However, the application of these technologies for reclamation at a large scale is limited due to cost economics and maintenance (El-Gohary et al., 1995). On the contrary, radiation treatment using gamma rays or electron beams is a simple and efficient technique that can eliminate a wide variety of organic contaminants and harmful microorganism (Borely et al., 1998). However, one of the major disadvantages is requirement of sufficient quantities of dissolved oxygen for organic substances to be broken down effectively by radiation. The requirement of constant and adequate supply of oxygen and rapid consumption of oxygen has bearing on the cost of the process.

Direct photolysis of organic dye has proven difficult in the natural environment because the decay rates strongly depend on the dye's reactivity and photosensitivity. Majority of commercial dyes are usually designed to be light resistant. Therefore, recent efforts have been directed towards investigating the photo-degradation of organic dyes by sensitizers or catalysts in aqueous/dispersion systems by UV irradiation.

Photocatalysis is a process of using UV light in combination with H_2O_2 or solid catalyst such as TiO_2 for the decolorization of industrial effluents. While the UV/H_2O_2 process appears to be too slow, costly and little effective for potential full-scale application, the combination of UV/TiO_2 seems more promising (Davies et al., 1994; Dominguez et al., 2005). TiO_2 during photocatalysis generates electron hole pairs when irradiated by the light of wavelength shorter than 380 nm. The organic pollutants are thus oxidized via direct hole transfer or in most cases attacked by the *OH radical formed in the irradiated TiO_2 (Xu, 2001).

Sonochemical degradation methods are relatively new and involve exposing aqueous solutions containing the organic pollutants to ultrasound (Petrier, 1992; Serpone & Colarusso, 1994). Free radical formation in water by ultrasonic irradiation is a less popular technique despite the 'extreme'' conditions by sonic vibrations in liquids for ''high energy chemistry'' (Suslick, 1990). The advantage of using ultrasound rests with the simplicity of its use. Propagation of an ultrasound wave in aqueous solution leads to the formation of cavitation bubbles. A prerequisite for these bubbles is the presence of a dissolved gas (Suslick 1990). The collapse of these bubbles spew extreme conditions such as high temperatures and pressure, which in turn lead to the dissociation of H_2O and the production of radical species such as *OH, HOO*, etc. Higher ultrasound frequencies are especially more favorable for the generation of hydroxide radicals; possibly due to faster production rates (Entezari & Kruus, 1996; Hua & Hoffmann, 1997).

Membrane techniques offer the appeal of recovering and reusing chemicals and dyes for producing reusable water. This method has the ability to clarify, concentrate and most importantly, separate dye continuously from effluent (Xu et al., 1991). Pressure driven membrane processes such as Ultrafiltration (UF) and Nanofiltration (NF) have found many applications in the field of wastewater treatment in recent years (Chakraborthy et al., 2003).

Ion exchange has not been widely used for the treatment of dye-containing effluents or color removal, mainly due to the option that ionexchangers cannot accommodate a wide range of dyes (Slokar & Le Marechal, 1998). Wastewaters containing color is passed over the ion exchange resin until the available exchange sites are saturated. Employing this method, both cationic and anionic dyes can be removed from effluents with partial success. Advantages of this method include no loss of adsorbent on regeneration, reclamation of solvent after use and the removal of soluble dyes. One major disadvantage is the high

operation cost. However, standard ionexchange systems are not widely used for treatment of dye-containing effluents because of their poor performance in the presence of other additives in wastewaters.

2.2 Chemical Methods

Oxidation is the most commonly used chemical decolorisation process due to its simple handling. However, pH and catalysts play an important role in oxidation process. Bright color removal is accomplished by more powerful oxidizing agents such as chlorines, ozone, Fenton's reagents, UV/peroxide, UV/ozone, or other oxidizing techniques or combinations. Chlorine has been proved to be a good dye-oxidizing agent and applied at low capital and operating costs. Nonetheless, the potential of chorine to form undesirable compounds with nitrogen containing components of the wastewater has limited the acceptability of this method (EPRI, 1996).

Hydrogen peroxide (H_2O_2) is one of the widely used agents that need to be activated by ultraviolet light resulting in aromatic ring cleavage of the dye molecules (Raghavacharya, 1997). Fenton's reagent (hydrogen peroxide, activated with Fe (II) salts) is very suitable for the oxidation of toxicants present in wastewaters, which inhibit biological treatment. One of the advantages of this process is substantial reduction of COD, color and toxicity. Nevertheless, due to flocculation, impurities get transferred from the wastewater to the sludge, which is ecologically not desirable.

The use of ozone as an oxidizing agent is prompted due to its high instability compared to chorine and H_2O_2. It can selectively oxidize unsaturated bonds and aromatic structures (Adams & Gorg, 2002). Oxidation by ozone will lead to the degradation of chlorinated hydrocarbons, phenols, pesticides and aromatic hydrocarbons (Xu et al., 1999)

which are highly pH dependent. At low pH ozone may often efficiently target unsaturated chromophoric bonds in a dye molecule via direct reactions. At higher pH, indirect reactions of ozone may lead to a less efficient process by the indiscriminant oxidation of all parts of dye molecule in addition to other scavengers in solution (Adams & Gorg, 2002). Thus, a careful monitoring of the effluent pH is required (Slokar & Le Marechal, 1997). With no residual or sludge formation (Ince & Gönenç, 1997) and no toxic metabolites (Gahr et al., 1994), ozonation leaves the effluent with no colour and low COD suitable for discharge into aqueous systems (Xu et al., 1999). Besides, one of the major advantages is that ozone can be applied in its gaseous state and therefore does not increase the volume of wastewater and sludge. The disadvantage of ozonation is its short half-life (typically being 20 min) demanding continuous application making it a cost-intensive process (Xu et al., 1999). The ozonation process leads to complete decolorisation with a very short retention time; however effective mineralization of the dye was not observed (Peralta-Zamora et al., 1999).

Coagulation and precipitation techniques using hydrolyzing metal salts of iron and aluminium are widely used to promote the formation of aggregates in wastewater and reduce the concentration of colorants and other dissolved organic compounds. Short detention time and low capital cost makes chemical coagulation a widely used technique. The limitations of this method include; high cost of chemicals for precipitation, pH adjustments, problems associated with dewatering and disposing of generated sludge and high concentration of residual cation levels which remains in the supernatant.

Advanced oxidation processes (AOPs) as part of emerging technologies have led their way in the treatment of aqueous waste and are rapidly becoming the technology of choice for many applications (Muthukumar et al., 2005). AOP's have been described as oxidation processes that are based on the generation of hydroxyl (*OH) radical

intermediates (Glaze et al., 1987). The direct photolysis of H_2O_2 by the photon of wavelength shorter than 370 nm produces two (*OH) radicals that can oxidize most organic pollutants. AOPs based upon hydrogen peroxide, ozone and ultraviolet radiation are the most commonly investigated (Apak & Hugül, 1996; De et al., 1999; Aleboyeh et al., 2005). AOPs are capable of achieving desired on-site colour destruction. There are a growing number of successful commercial applications of these AOPs and their combinations (Bigda, 1995; US patent, 1996).

Electrochemical treatment of dye based colored wastewater is considered as one of the advanced processes, and is a potentially powerful method of pollution control, offering high removal efficiencies. Electrochemical processes generally have lower temperature requirement when compared to other non-electrochemical treatments and hence do not require any additional chemicals (Kim et al., 2002). The required equipment and operation is generally simple. The controls are easy and the electrochemical reactors are compact, and prevent the production of unwanted by-products. Electrochemical method shows efficient and economical removal of dyes and high efficiency for degradation of recalcitrant pollutants (Pelegrini et al., 1999). The electrochemical method of oxidation for color removal is more efficient for the treatment of textile dye wastewater for the dyeing stage than for total dyeing and finishing stages. Nevertheless, the main drawbacks are high electricity cost, sludge production and pollution from chlorinated organics.

2.3 Biological methods

Biological methods offer considerable advantages like being relatively inexpensive, having low running costs and the end products of complete mineralization not being toxic. The process can be aerobic (in presence of oxygen), anaerobic (without oxygen) or combined aerobic-anaerobic. Nevertheless, the ability of biological treatment process for

decolorisation of industrial effluents is ambiguous, different and divergent. Observations indicate that dyes themselves are not biologically degradable since microorganisms do not utilize the color constituents as a source of food. Most currently used laboratory methods for biodegradation involve aerobic microorganisms, which utilize molecular oxygen as reducing equivalent acceptor during the respiration process. Yet, environmental conditions with lack of molecular oxygen are not uncommon. In these anoxic and hypoxic environments, microorganisms survive by using sulphates, nitrates and carbon dioxide, etc. as electron acceptors (Birch et al., 1989). With respect to future improvements, research data are increasingly being gathered which indicates that certain dyes are susceptible to anoxic/anaerobic decolorisation. An anaerobic step followed by an aerobic step may represent a significant advancement in biological treatment and decolorisation in the future (Bahorsky, 1998; Ong et al., 2005). An advantage of biological treatment over certain physico-chemical treatment methods is that over 70% of the organic material present that is measured by the COD test may get converted into biosolids. Though this methodology is cost-competitive, and biological treatments are suitable for variety of dyes, the main drawbacks of the biological treatment are low biodegradability of the dyes, less flexibility in design and operation, larger land area requirement and longer times required for decolourisation‑fermentation processes thereby making it incapable of removing dyes from effluent on a continuous basis in liquid state fermentations (Bhattacharyya & Sarma, 2003; Crini, 2006; Robinson et al., 2001).

2.4 Non-conventional low-cost adsorbents and removal of dyes

Cost is actually an important parameter for comparing the adsorbent materials. According to Bailey et al., 1999, an adsorbent can be considered low-cost if it requires little processing, is abundant in nature or is a by-product or waste material from another industry.

Certain waste products from industrial and agricultural operations, natural materials and biosorbent represent potentially economical alternative adsorbents. Many of them have been tested and proposed for dye removal. The by-products from the agricultural and industrial industries could be assumed to be low-cost adsorbents since they are abundant in nature, inexpensive, require little processing and are effective materials.

2.5 Activated carbons from solid wastes

Commercially available activated carbons (AC) are usually derived from natural materials such as wood, coconut shell, lignite or coal, but almost any carbonaceous material may be used as precursor for the preparation of carbon adsorbents (Rozada et al., 2003; Rodriguez-Reinoso, 1997; Pollard et al., 1992). Because of its availability and cheapness, coal is the most commonly used precursor for AC production (Carrasco- Marin et al., 1996; Illan Gomez et al., 1996). Coal is a mixture of carbonaceous materials and mineral matter, resulting from the degradation of plants. The adsorption properties of each individual coal are determined by the nature of the original vegetation and the extent of the physical–chemical changes occurring after deposition (Karaca et al., 2004). Coal based sorbents have been used by Karaca et al., 2004, Mohan et al., 1999, 2002 and McKay et al., 1999 with success for dye removal. However, since coal is not a pure material, it has a variety of surface properties and thus different adsorption properties.

Plentiful agricultural and wood by-products may also offer an inexpensive and renewable additional source of AC. These waste materials have little or no economic value and often present a disposal problem. Therefore, there is a need to valorize these low-cost by-products. So, their conversion into AC would add economic value, help reduce the cost of waste disposal and most importantly provide a potentially inexpensive alternative to the existing commercial activated carbons. A wide variety of carbons have been prepared from

agricultural and wood wastes, such as bagasse (Valix et al., 2004; Juang et al., 2001, 2002; Tsai et al., 2001; Ahmedna et al., 2000), coir pith (Namasivayam & Kavitha, 2002; Namasivayam et al., 2001), banana pith (Kadirvelu et al., 2003), date pits (Banat et al., 2003), sago waste (Kadirvelu et al., 2003), silk cotton hull (Kadirvelu et al., 2003), corn cob (Juang et al., 2002a), maize cob (Kadirvelu et al., 2003), straw (Kannan & Sundaram, 2001), rice husk (Mohamed, 2004; Malik, 2003; Guo et al., 2003; Kannan & Sundaram, 2001), rice hulls (Ahmedna et al., 2000), fruit stones (Aygu¨n et al., 2003), nutshells (Aygu¨n et al., 2003; Ahmedna et al., 2000), pinewood (Tseng et al., 2003), sawdust (Malik, 2003), coconut tree sawdust (Kadirvelu et al., 2000, 2003), bamboo (Wu et al., 1999) and cassava peel (Sivakumar et al., 2001). There are also several reports on the production of AC from various city wastes and industrial by-products such as waste PET bottles (Nakagawa et al., 2004), waste tires (Nakagawa et al., 2004), refuse derived fuel (Nakagawa et al., 2004), wastes generated during lactic acid fermentation from garbage (Nakagawa et al., 2004), sewage sludge (Rozada et al., 2003; Otero et al., 2003a,b; Graham et al., 2001), waste newspaper (Okada et al., 2003), waste carbon slurries (Jain et al., 2003; Gupta et al., 2003) and blast furnace slag (Jain et al., 2003; Gupta et al., 2003).

The excellent ability and economic promise of the activated carbons prepared from by-products have been recently presented and described. Non-conventional activated carbons exhibited high adsorption properties. Juang et al., 2002a reported that the adsorption capacities of activated carbons made from corncob had very large values of 1060–790 mg of dye per g of carbon. However, the adsorption capacities of a carbon depend on the different sources of raw materials, the history of its preparation and treatment conditions such as pyrolysis temperature and activation time. Many other factors can also affect the adsorption capacity in the same adsorption conditions such as surface

chemistry, surface charge and pore structure. A suitable carbon should possess not only a porous texture, but also high surface area. Recently, Guo et al., 2003 showed that the adsorption does not always increase with surface area. Besides the physical structure, the adsorption capacity of a given carbon is strongly influenced by the chemical nature of the surface. The acid and base character of a carbon influences the nature of the dye isotherms.

The adsorption capacity depends also on the accessibility of the pollutants to the inner surface of the adsorbent, which depends on their size. The specific adsorption mechanisms by which the adsorption of dyes takes place on these adsorbents are still not clear. This is because adsorption is a complicated process depending on several interactions such as electrostatic and non-electrostatic (hydrophobic) interactions. Although much has been accomplished in terms of adsorption properties and kinetics, much work is still necessary to identify the adsorption mechanisms clearly.

2.6 Agricultural solid wastes

Raw agricultural solid wastes and waste materials from forest industries such as sawdust and bark have been used as adsorbents. These materials are available in large quantities and may have potential as sorbents due to their physico-chemical characteristics and low-cost. Sawdust is an abundant by-product of the wood industry that is either used as cooking fuel or as packing material. Sawdust is easily available in the countryside at zero or negligible price (Garg et al., 2004). It contains various organic compounds (lignin, cellulose and hemicellulose) with polyphenolic groups that might be useful for binding dyes through different mechanisms. The role of sawdust materials in the removal of pollutants from aqueous solutions has been reviewed (Shukla et al., 2002). Some valuable guidelines can be drawn from the review. Sawdust has proven to be a promising effective material for the removal of dyes from wastewaters (O¨ zacar & Sengil, 2005; Garg et al., 2004,a; Baouab et

al., 2001; Ho & McKay, 1998). The adsorption mechanisms can be explained by the presence of several interactions, such as complexation, ion-exchange due to a surface ionization, and hydrogen bonds. One problem with sawdust materials is that the adsorption results are strongly pH-dependent (Garg et al., 2003, 2004a; Khattri & Singh, 2000; Ho & McKay, 1998). There is a neutral pH beyond which the sawdust will be either positively or negatively charged. Ho & McKay 1998a showed that the adsorption capacity of basic dye is much higher than that of acid dye because of the ionic charges on the dyes and the ionic character of sawdust. Khattri & Singh, 2000 also noted that the adsorption capacity of Neem sawdust was highly concentration dependent. Chemical pretreatment of sawdust has been shown to improve the adsorption capacity and to enhance the efficiency of sawdust adsorption (Garg et al., 2003, 2004,a; Batzias & Sidiras, 2004).

Bark a polyphenol-rich material is an abundant forest residue which has been found to be effective in removing dyes from water solutions. Because of its low-cost and high availability, bark is very attractive as an adsorbent. Bark is an effective adsorbent because of its high tannin content (Bailey et al., 1999; Morais et al., 1999). The polyhydroxy polyphenol groups of tannin are thought to be the active species in the adsorption process. Morais et al., 1999 studied adsorption of Remazol BB onto eucalyptus bark from Eucalyptus globulus. The adsorption capacity at pH = 2.5 and 18^{o} C was found to be 90 mg of dye g^{-1} of dry bark. Parallel adsorption tests, under similar conditions, carried out with a commercial activated carbon and with bark, showed for the latter an adsorption capacity about half that of the former. The authors concluded that there are promising perspectives for the utilization of eucalyptus bark as adsorbent on an industrial scale. However, there are still several important aspects such as the adsorption mechanism to clarify.

Tree fern, an agricultural by-product, has been investigated to remove pollutants from aqueous solutions (Ho et al., 2005; Ho & Mckay, 2003). Tree fern is a complex material containing lignin and cellulose as major constituents. Maximum adsorption capacity of tree fern for basic red 13 was 408 mg g^{-1} (Ho et al., 2005). The capacity increased as the adsorbent particle size decreased. The adsorption mechanism involves chemical bonding and ion-exchange. Other agricultural solid wastes from cheap and readily available resources such as date pits (Banat et al., 2003), pith (Ho & McKay, 1999, 2003; Chen et al., 2001; Namasivayam et al., 1993, 1998, 2001a; Namasivayam & Kadirvelu, 1994; McKay et al., 1987), corncob (Robinson et al., 2002), barley husk (Robinson et al., 2002a), wheat straw (Robinson et al., 2002,a,b; Nigam et al., 2000), wood chips (Low et al., 2000; Nigam et al., 2000) and orange peel (Sivaraj et al., 2001; Namasivayam et al., 1996) have also been successfully employed for the removal of dyes from aqueous solution.

2.7 Industrial by-products

Industrial solid wastes such as metal hydroxide sludge, fly ash and red mud, because of their low- cost and local availability, are classified as low-cost materials and can be used as adsorbents for dye removal (Namasivayam & Sumithra, 2005; Netpradit et al., 2003, 2004,a; Acemioglu, 2004; Janos et al., 2003; Mohan et al., 2002; Gupta et al., 2000; Ho & McKay, 1999b; Namasivayam & Arasi, 1997; Namasivayam et al., 1994; Namasivayam & Chandrasekaran, 1991). Recently, Netpradit et al., 2003, 2004,a studied the capacity and mechanisms of metal hydroxide sludge in removing azo reactive dyes. The sludge is a dried waste from the electroplating industry, which is produced by precipitation of metal ions in wastewater with calcium hydroxide. It contains insoluble metal hydroxides and other salts. The authors demonstrated that metal hydroxide sludge was an effective positively charged adsorbent with a high maximum adsorption capacity (48–62 mg dye g^{-1}

material) for reactive anionic azo dyes. The charge of the dyes is an important factor for the adsorption due to the ion-exchange mechanism.

Fly ash is a waste material originating in great amounts in combustion processes (Wang et al., 2005; Acemioglu, 2004; Mohan et al., 2002; Gupta et al., 1990, 2000; Ramakrishna & Viraraghavan, 1997; Khare et al., 1987). Although it may contain some hazardous substances, such as heavy metals, it is widely utilized in industry in many countries (Janos et al., 2003). However, bagasse fly ash generated in the sugar industry does not contain large amounts of toxic metals and has been widely used for adsorption of dyes (Mohan et al., 2002; Gupta et al., 2000). Fly ash has a surface area of 15.6 $m^2 g^{-1}$ (Wang et al., 2005). Its properties are extremely variable and depend strongly on its origin (Wang et al., 2005; Janos et al., 2003; Ho & McKay, 1999a). Another abundant industrial by-product is red mud (Wang et al., 2005; Namasivayam & Arasi, 1997; Namasivayam & Chandrasekaran, 1991). Waste red mud is a bauxite processing residue discarded in alumina production. Namasivayam & Arasi 1997 proposed red mud as adsorbent for the removal of congo red. The maximum capacity was 4.05 mg g^{-1}. Wang et al., 2005 showed that physical and chemical treatment can significantly change the adsorption capacity.

2.8 The Challenges ahead

The challenges encountered in transferring the data, process and/or products to industrial applications are summarized below:

- The variability in the material characteristics and the availability of the resource that is controlled by the demand at the commercial level can discourage industrial users (Guibal, 2004).
- The applicability of low-cost adsorbents such as chitosan, peat, zeolites, biomass, fly ashes and red mud for water treatment depends strongly on their origin (Wang et

al., 2005; Kargi & Ozmihci, 2004; Varma et al., 2004; Guibal, 2004; Kumar, 2000; Calzaferri et al., 2000; Altin et al., 1998).

- The characteristics of the particles can also introduce hydrodynamic limitations and column fouling, which limits the use of the materials for large-scale columns.
- The adsorption process will provide an attractive technology if the low-cost sorbent is ready for use. However, physical and chemical processes such as drying, autoclaving, crosslinking reactions or contacting with organic or inorganic chemicals are proposed for improving the adsorption capacity and the selectivity.
- The pre-treatment methods are not cost effective at large scale.
- Performance is dependent on the type of material used. Each low-cost adsorbent has its specific advantage in wastewater treatment.
- The effectiveness of treatment depends not only on the properties of the adsorbent and adsorbate, but also on the following environmental conditions and variables used for the adsorption process: pH, ionic strength, temperature, existence of competing organic or inorganic ligands in solution, contact time and adsorbent concentration. Despite the fact that industrial effluents contain several pollutants simultaneously, little attention has been given to adsorption of pollutants from mixtures (Aksu, 2005). The development of the adsorption process requires further investigation in the direction of testing low-cost adsorbents with real industrial effluents.
- There is little literature containing a full study of comparisons between adsorbents. The comparison of adsorption performance depend not only the parameters related to the experimental conditions and the effluent, but also on the analytical method used for decontamination tests (batch method, column, reactors, etc.). Thus, a direct

comparison of data obtained using different low-cost adsorbents is difficult because of inconsistencies in the data presentation (Babel & Kurniawan, 2003; Bailey et al., 1999).

- There is a lack of data concerning the reproducibility of the adsorption properties and the equilibrium data, commonly known as adsorption isotherms. In view of industrial developments of the various kinds of adsorbents described in the literature, the physical and chemical stability of the materials and the reproducibility of the adsorption properties are of utmost importance. Unfortunately, there is little information on this subject.
- The design and efficient operation of adsorption processes also requires equilibrium adsorption data for use in kinetic and mass transfer models (Allen et al., 2004). These models play an important role in predictive modeling for analysis and design of adsorption systems. Additional work on this subject is needed. The present research work is an attempt to fill the gap.

In summary, different physical, chemical, and biological techniques have been applied to treat effluent containing dyes and heavy metals. Physical methods are often not only expensive, but are greatly affected by other wastewater constituents, and create serious problems with respect to the disposal of the concentrated sludge. Its use is limited to small-scale *in situ* removal. In addition, the main problem of toxicity of dyes still remains largely unsolved (Shu et al., 2015, 2016a, b). The chemical techniques are often expensive and, although the dyes are removed, but the accumulation of concentrated toxic and/or hazardous sludge may create disposal problem. There is also possibility of occurrence of secondary pollution problem because of excessive chemical use. High consumption of electrical energy and chemical reagents are common problems. The advanced oxidation

processes which are essentially photochemical or electrochemical methods involving generation of very powerful oxidizing agents such as hydroxyl radicals, have been applied with success for pollutant degradation. Although, these methods appear very efficient, their prohibitively high cost makes them commercially not feasible (Eskandarian et al., 2014; Husain et al., 2010; Srinivasan & Mishra, 2008). Biological treatment is the most economical alternative when compared with physical and chemical processes. It has such advantages as efficiency, versatility, lower construction and operation costs, robustness and eco-friendliness. Biological treatment unlike physical and chemical methods mineralizes the pollutant, leading to complete detoxification and overcomes the problems of sludge disposal and secondary pollution (Lee et al., 2015; Khehra et al., 2005). However, one of the major drawbacks of bioremediation is the slowness of the process, which limits its application at field level.

High competition, over capacity, falling profit margins and increased environmental considerations are making textile and dye industries to adopt low-cost techniques, methods and/or procedures to address the problem of pollution. In this context, adsorption as a technique and a tool and low-cost adsorbents assumes paramount importance.

Low-cost adsorbents may be classified into two groups; namely, inorganic and organic. The former includes slag, sludge, fly ash, red mud, coal, lignite to name a few.

While the latter embraces agriculture and agro-industrial waste. Nutraceutical industrial spent falls under the latter category, which is renewable, eco-friendly, thermally, mechanically and chemically processed ready-to-use by-product available in myriad tons and qualifies as a suitable candidate as adsorbent for the remediation of dyes in textile and leather industries.

CHAPTER 3: METHODOLOGY

3.1 Materials

3.1.1 Adsorbate

The Congo Red (CR) dye also commonly known as Direct Red 28 [C.I. = 22,120; CAS Number 573-58-0 chemical formula = $C_{32}H_{22}N_6Na_2O_6S_2$; molecular weight = 696.66; absorbance maximum (λ_{max}) = 497 nm] ; Acid Blue 113 (AB113) dye also commonly referred to as Neutral Blue 5R; [C.I. = 26360; CAS Number: 3351-05-1; chemical formula = $C_{32}H_{21}N_5Na_2O_6S_2$; molecular weight = 681.65; absorbance maximum (λ_{max}) = 566 nm] ; Acid Red 119 (AR119) dye; C.I = 262085; CAS Number: 12220-20-1; chemical formula = $C_{31}H_{25}N_5Na_2O_6S_2$; molecular weight = 637.67; absorbance maximum ($\lambda_{max)}$ = 526 nm and Acid Black 52 (AB52) dye (C.I. 15711; CAS Number: 5610-64-0; chemical formula = $C_{20}H_{12}N_3NaO_7S$; molecular weight = 461.38; absorbance maximum (λ_{max} = 571 nm) were supplied by Sigma-Aldrich, USA and were used without further purification.

3.1.2 Adsorbent

NIFSS, NICSS and NICUS were procured from a local factory which processes seeds to extract the oleoresin. The spent were dried in the sunlight, crushed and ground using ball mill and sieved as per ASTM standards to get the following particle sizes: ≤ 90 μm; ≥ 90 μm ≤ 125 μm; ≥ 125 μm ≤ 177 μm; ≥ 177 μm ≤ 355 μm; ≥355 μm ≤ 500 μm and ≥ 500 μm ≤ 710 μm. Major part of the experiments was carried out using NIS ≥ 125 μm and ≤ 177 μm (ASTM 80 mesh particles).

3.1.3 Surface characterization

The surface morphology of Nutraceutical Industrial Spent and dye adsorbed-NIS was visualized by Scanning Electronic Microscope (LEO 435 VP model, Japan). The functional groups present in the adsorbent were identified by FTIR. Infrared spectra of

the control samples, NIS and the dye-adsorbed NIS samples were obtained using a FTIR spectrometer (Inter-spec 2020, Spectro Lab, UK).

3.1.4 Determination of point of zero charge

The surface charge of NIS was determined by preparing stock solution of 0.1 M KCl. Fifty ml each of 0.1 M KCl were transferred to seven 250-ml Erlenmeyer flasks and pH was adjusted initially to 2.0 and 12.0 by using HCl and NaOH. NIS (0.05 g) was added to each flask. After allowing for 24 h the final pH was measured by pH meter (Systronics-802, India). Graph of pH_{final} *vs.* $pH_{initial}$ was plotted.

3.1.5 Batch adsorption experiments

The experiments were conducted in batches with varying parameters. However, the common preliminary preparation involved the setting up of 250-mL flasks with 50 mL working aqueous solution of dye of known concentration. After the initial preparation was complete, 50 mg of NIS was introduced into each flask. A temperature-controlled shaker was used to agitate the contents of the flasks at 165 rpm for 3 h. Evaluations were then conducted based on the effects of varying parameters such as, dosage of NIS (0.025, 0.050, 0.075, 0.100, 0.150, 0.200, 0.300 g/50 ml); dye concentration (25, 50, 75, 100, 125, 150, 175, 200, 300, 400 and 500 mg/L); pH (2, 4, 6, 7, 8, 10 and 12) and temperature (303 K, 313 K and 323 K) with different dye concentration. The samples were centrifuged for five minutes to remove the leftover particulate matter. A UV– Vis Spectrophotometer (Perkin Elmer-Lambda 25, USA) was used to measure the absorbance of the filtrate at λ_{max}. Controls were maintained by using the adsorbent in distilled water and an adsorbent-free dye. The adsorbed amount of dye at equilibrium, q_e (mg g^{-1}) was calculated by using Eq. (3.1).

$$q_e = (C_0 - C_e)\frac{V}{W} \quad \textbf{(3.1)}$$

where C_0 and C_e are concentrations (mg L^{-1}) of the dye at initial and equilibrium respectively, V is solution volume (L) and W is adsorbent weight (g).

The same procedure was conducted in kinetic studies also, except the aqueous samples were pre-set at time specific intervals. The concentrations of the dye were also determined. The amount of the dye adsorbed at any time, qt (mg/g), was calculated using Eq. (3.2).

$$q_t = (C_0 - C_t)\frac{V}{W} \tag{3.2}$$

where C_t (mg L^{-1}) is the concentration of the dye measured at time t. Initial concentrations of the dye and an adsorption time of 60 min (5 min intervals) were studied. For determining the optimum amount of adsorbent per unit mass of adsorbate, 50 mL dye solution was brought in contact with varying amounts (0.500–6.000 g L^{-1}) of NIS till equilibrium was attained. To determine the influence of pH on dye adsorption, 50 mg of NIS along with 50 mL of the dye solution of concentration 100 mg L-1 were agitated on an orbital shaker. The experiment was repeated with varying pH values in range of 2.0–12.0. Equilibrium was reached after 140–150 min with constant agitation speed of 165 rpm. The dye concentration was measured using a double beam UV/Vis spectrophotometer at λ_{max}. The pH was adjusted with dilute HCl and/or NaOH. Solution pH was determined by pH meter (Systronics 802, India). The extent of removal of dye was determined by the following equation:

$$Dye\ removal\ efficiency\ \% = \frac{(C_0 - C_e)}{C_0} \times 100 \tag{3.3}$$

All biosorption experiments were performed in triplicate in the laboratory and results are presented as averages of the replicates.

3.1.6 Adsorption isotherms, adsorption kinetics and thermodynamic parameters

The process of adsorption describes a dynamic separation of solute from a solution onto an adsorbent. Equilibrium is established when the solute being adsorbed onto the adsorbent equal to the amount being desorbed. Thus, the adsorption equilibrium may be defined as the ratio between the adsorbed amount and that which is remaining in the solution. This can be established when the adsorbate phase contacts the adsorbent for sufficient time, under given experimental conditions. This results in establishing a dynamic balance with the interface concentration. Under the equilibrium condition the solution concentration remains almost constant. By plotting solid phase concentration against liquid phase concentration it is possible to depict the equilibrium adsorption isotherm. Thus, to understand the mechanism of adsorption it is essential to study the interaction between the adsorbent and adsorbate. This can be done by fitting the adsorption data to different adsorption isotherms. Langmuir, Freundlich, Temkin, Jovanovic, Redlich-Peterson, Radke-Prausnitz, Vieth-Sladek, Brouers-Sotolongo and Toth are the most accepted adsorption isotherm models used for studying the mechanism of equilibrium adsorption for single solute systems at ambient temperature. Also the results of parameters studied in different models provide information about interaction mechanisms, surface properties and affinities of the adsorbent and helps to describe the interaction between the adsorbate and adsorbent.

Langmuir isotherm (Langmuir, 1916) assumes that adsorption takes place on a homogeneous surface with equal energy and all points on it–which are equally available for interaction with the adsorbate. This assumption holds good only in the case of monolayer adsorption, which suggests that there is no transmigration of the adsorbate molecule on the surface. Since the Langmuir isotherm is derived from thermodynamic principles, an important metric called the separation factor (R_L), can be estimated (Webber & Chakkravorti, 1974). The separation factor provides indication of whether

the adsorption in the system studied is unfavourable ($R_L > 1$), linear ($R_L = 1$), favourable ($0 < R_L < 1$), or irreversible ($R_L = 0$). The Langmuir equations are as shown below:

$$q_e = \frac{Q_m K_a C_e}{1 + K_a C_e}$$

$$R_L = \frac{1}{1 + K_a C_0} \qquad \textbf{(3.4)}$$

where, q_e *is* the amount of dye adsorbed on to adsorbent (mg g^{-1}) at equilibrium; C_e is the equilibrium concentration (mg L^{-1}) of the dye in solution. The values of Q_m and K_a are determined from the intercept and the slope of q_e *vs* C_e, where, Q_m is the monolayer adsorption capacity (mg g^{-1}) and K_a is the Langmuir constant (L mg^{-1}) related to the free energy of adsorption.

Another adsorption mechanism is that proposed by Freundlich. This isotherm assumes that heterogeneous layers of adsorbate can be formed and an empirical model can be used to describe this process (Freundlich, 1906). The metric called the heterogeneity factor (n_F) can be estimated from the Freundlich isotherm, which indicates whether the nature of adsorption is linear ($n_F = 1$), chemisorption ($n_F < 1$), or a physisorption ($n_F > 1$). This parameter can also be used to quickly identify if a process follows normal Langmuir isotherm ($1/n_F < 1$) or cooperative adsorption ($1/n_F > 1$). The capacity of adsorption by adsorbent is related to the dye concentration at equilibrium which follows the equation:

$$q_e = K_F C_e^{1/n_F} \qquad \textbf{(3.5)}$$

One of the expanded forms of Langmuir isotherm is the Jovanovic isotherm (Jovanovic, 1969) which describes a model considering a monolayer and no lateral interactions, but with an added exponential term to account for deviances of the experimental results from the Langmuir isotherm. Jovanovic isotherm (Jovanović 1969)

is one of the expanded forms of Langmuir isotherm model. The equation for Jovanovic model is given below:

$$q_e = Q_m(1 - e^{(K_J C_e)}) \quad \textbf{(3.6)}$$

where, K_J is the Jovanovic constant, q_e is the amount of dye adsorbed on to adsorbent (mg g^{-1}) at equilibrium; C_e is the equilibrium concentration (mg L^{-1}) of the dye in solution. The model describes formation of a monolayer with no lateral interactions. The added exponential term K_J accounts for deviances of the experimental results from the Langmuir isotherm.

Temkin isotherm, considers the interaction between adsorbate molecules assuming that the adsorption heat of all molecules decreases linearly when the layer is covered and the adsorption has maximum energy distribution of uniform bond (Temkin & Pyzhev, 1940).

$$q_e = RT/b_T \ln A_T + (RT/b) \ln C_e \quad \textbf{(3.7)}$$

Dubinin-Radushkevich (Dubinin, 1947) isotherm is another empirical model which initially formulated for the adsorption process following a pore filling mechanism. The equation for Dubinin-Radushkevich isotherm is illustrated below:

$$q_e = q_s[\exp(-K_{ad}\varepsilon^2)] \quad \text{where} \quad \varepsilon = RT \ln\left[1 + \frac{1}{C_e}\right] \quad \textbf{(3.8)}$$

where, q_s (mg g^{-1}) is a constant in the Dubinin-Radushkevich isotherm model which are related to adsorption capacity q_e (mg g^{-1}), K_{ad} (mol^2/kJ^2) is a constant in related to the mean free energy of adsorption, R ($J^{-1}mol^{-1}K$), and T (K) is the absolute temperature.

Redlich–Peterson isotherm is an improvement of the Langmuir-Freundlich equations (Redlich & Peterson, 1959) with a correction exponent '*g*'. The equation can either represent the Langmuir isotherm (*g*=1) or the Freundlich isotherm (*g*=0).

The equation of Redlich-Peterson isotherm is given as:

$$q_e = \frac{A_{RP} C_e}{1 + B_{RP} C_e^g} \quad \textbf{(3.9)}$$

where, $A_{RP,}$ B_{RP} and g are Redlich-Peterson constants, q_e is the amount of dye adsorbed on to adsorbent (mg g^{-1}) at equilibrium; C_e is the equilibrium concentration (mg L^{-1}) of the dye in solution.

Another empirically determined isotherm model is the Toth isotherm (Toth, 1971). The Toth isotherm tries to explain the heterogeneous adsorption systems by building on the Langmuir isotherm. The mathematical equation is shown below:

$$q_e = Q_m C_e (b_{To} + C_e^{n_{To}})^{-1/n_{To}} \quad \textbf{(3.10)}$$

The models used to understand the mechanism of adsorption are of higher order equations. The validity of data fitting cannot be confirmed only by R^2 value because it is used with linear models only. Hence χ^2 values are considered as they provide a better statistic because if model data are similar to the experimental data, then χ^2 would be a small number and vice versa.

Radke-Prausnitz isotherm model is used for wide concentration range and the correlation is usually predicted by high χ^2 value (Radke & Prausnitz, 1972).

$$q_e = \frac{K_{RP} Q_m C_e}{(1 + K_{RP} C_e)^{m_{RP}}} \quad \textbf{(3.11)}$$

A better isotherm for combining the Langmuir and Freundlich isotherms is the Sips isotherm (Sips, 1948). The Sips equation is reduced to the Freundlich equation at low adsorbate concentrations and Langmuir isotherm at high adsorbate concentrations.

$$q_e = \frac{Q_m (K_s C_e)^{m_S}}{(1 + K_S C_e)^{m_S}} \quad \textbf{(3.12)}$$

The Vieth-Sladek isotherm (Vieth & Sladek, 1965) deals with adherence of the dye molecules onto the surface of the adsorbent. The equation of the isotherm is as follows:

$$q_e = K_{VS}C_e + \frac{Qm\beta_{VS}C_e}{1+\beta_{VS}C_e} \quad \textbf{(3.13)}$$

where, K_{VS} and β_{VS} are Vieth-Sladek constants, q_e is the amount of dye adsorbed on to the adsorbent (mg g^{-1}) at equilibrium, Q_m is the maximum adsorption capacity and C_e is the equilibrium concentration (mg L^{-1}) of the dye in solution.

Brouers-Sotolongo isotherm (Brouers et al., 2005) is the mathematical equation consists of K_{BS} and α variable that characterize the adsorption power and the active site distribution of the adsorbent–adsorbate system. Its equation is presented below:

$$q_e = Q_m[(1-\exp(-K_{BS}(C_e)^{\alpha})] \quad \textbf{(3.14)}$$

where, K_{BS} and α are Brouers-Sotolongo constants, q_e is the amount of dye adsorbed on adsorbent (mg g^{-1}) at equilibrium, Q_m is the maximum adsorption capacity and C_e is the equilibrium concentration (mg L^{-1}) of the dye in solution.

The rate limiting step in the adsorption process is determined by fitting experimental data to the pseudo-first-order and pseudo-second-order kinetic equations. The kinetic data for both adsorption and desorption were analyzed by non-linear analyses (MS Excel 2010) using six different kinetic models: pseudo-first order (Lagergren, 1898), pseudo-second order (Ho & McKay, 1998a), Intra-particle diffusion by Weber-Morris model (Alkan et al., 2007), Dumwald-Wagner model (Wang et al., 2004) and Film Diffusion model (Boyd et al., 1947). All the models were fitted using the nonlinear least-square method. The controlling mechanism of the adsorption process was found out by fitting the experimental data to the appropriate kinetic equations.

Pseudo-first-order $q = q_e\ (1-e^{-k1t})$ **(3.15)**

Pseudo-second-order $q = \dfrac{q_e^2\ k_2 t}{1+q_e k_2 t}$ **(3.16)**

Intraparticle diffusion $q_t = k_i t^{0.5}$ **(3.17)**

Webber-Morris $q_t = k_{id}t^{1/2} + C$ **(3.18)**

Dumwald-Wagner $log\ (1-F^2) = -K/2.303\ t$ **(3.19)**

Film Diffusion $ln\ (1\text{-}q_t/q_e) = -R^1t$ **(3.20)**

Initial CR concentration in the water is vital for kinetics and the initial CR concentrations employed during the kinetic studies were 25, 50 and 100 µg ml^{-1} which are similar when compared with other studies reported (Hameed & El-Khaiary, 2008; Ahmad & Kumar, 2010). By studying the kinetics at different temperatures (303 K, 313 K and 323 K) it was possible to understand the changes in rate of adsorption with changes in temperature.

Energy and entropy are the key factors in determining the possibility and stability of any molecular interaction. Standard Gibbs free energy change (ΔG°) is an indicator of the degree of spontaneity of a process i.e., a process is feasible and spontaneous only if this value is negative. To calculate these parameters, the vant Hoff and Gibbs-Helmholtz equations were used:

$K_L = C_o/C_e$ **(3.21)**

$\Delta G° = -RT \ln K_L$ **(3.22)**

$\ln K_L = \Delta S°/R - \Delta H°/RT$ **(3.23)**

Where K_L is the thermodynamic equilibrium constant (L mol^{-1}) and T is the temperature (K). C_0 and C_e are the initial and equilibrium concentration (mg L^{-1}) of dye in solution respectively.

3.1.7 Statistical optimization of process parameters

Five or six (sixth factor being particle size) factors influencing the adsorption process on the final adsorption capacity were studied and these included: adsorption time (A), process temperature (B), initial dye concentration (C), adsorbent dosage (D) and initial pH (E). These are the independent variables which were to be optimized for adsorption capacity which is the dependent response variable at fixed orbital shaking at 165 rpm. A standard experimental design was prepared comprising 5 or 6 factors at 2

levels (Table 1). Analysis of variance was performed on the responses which yielded a general quadratic regression equation. Surface and contour plots were prepared which indicated graphically the effect of individual as well as interaction effects between parameters on the adsorption capacity.

Table 3.1: Experimental range of individual factors for RSM studies

Factor	Name	Units	Minimum	Maximum
A	Time	minutes	0	180
B	Temperature	^{0}C	27	50
C	Concentration	mg/L	25	500
D	Absorbent dosage	g/L	0.500	6.00
E	pH		2	12

3.1.8 Application of remediation method using NIS to textile industrial effluent

Different processes employed in textile industry generate waste water with varied compositions containing, large amounts of suspended solids, highly fluctuating pH, variable temperature, intense color and COD concentration (Kumar et al., 2007). Therefore, it is difficult to identify a specific dye in industrial effluent due to matrix effect (Talarposhti et al., 2001). A simple procedure was developed to compare remediation of AB113 dye in water as also in textile industrial effluent.

3.1.8.1 Textile industrial effluent (TIE)

Effluent samples were collected from a local textile industry which operates in two shifts. Six random TIE samples were collected in 10-L polyethylene containers from the end of the pipe where the effluent enters into the treatment plant. Among the six samples, three were collected from first and second shifts consecutively on three working days. All textile industrial effluent samples collected were transferred to a 100-L barrel and stirred manually to get uniform concentration. The resulting TIE solution was used as control sample for analyses. Sampling, preparation and preservation

methods followed while collecting the effluent samples from the industries were in accordance with standard methods (Standard methods for the examination of water and wastewater, 2002).

3.1.8.2 Preparation of dye in distilled water and textile industrial effluent

Two grams of AB113 were transferred to two 2-L standard flasks. The dye was dissolved in distilled water (Solution 1) and in TIE (Solution 2). The resulting solutions were stirred to uniform concentration and were made up to the mark with water and TIE respectively.

3.1.8.3 Blank experiment

Five hundred mL of distilled water were transferred to one-liter conical flask containing 5-cm Teflon coated magnetic bar. Five grams of NIS were added and the solution stirred at about 700 rpm for 15 min using a magnetic stirrer. The solution was filtered using No 42 Whatman filter paper and the filtrate solution was compared with the solution obtained after remediation of dye loaded-TIE.

3.1.9 Procedures

3.1.9.1 Measurement of the absorbance of stock solutions

An aliquot solution of TIE was filtered through Buchner funnel apparatus using No 42 Whatman filter paper and the absorbance of the filtrate was measured using UV-Vis Spectrophotometer (Perkin Elmer-Lambda 25, USA) with a maximum absorbance scale of 3.0. All absorbances were measured within this range. However, in case of concentrated solutions, the absorbance was measured after appropriate dilution and the resultant absorbance was multiplied by the dilution factor to get the absorbance of concentrated solution. This procedure was repeated to measure the absorbance of Solution 1 and Solution 2.

3.1.9.2 Measurement of molar absorption coefficient (ε) of the dye

Six different concentrations of the dye were prepared in distilled water and the absorbance was measured at 566 nm using distilled water as reference. A graph of absorbance vs. concentration was plotted. ε was measured from the slope of the linear portion of the curve or by using mathematical formula ε = A/cl where A is specific absorption coefficient for concentration c (mol L^{-1}) for a path length of 1 cm. Specific absorption coefficient or absorbency index is the absorbance per unit path length and unit concentration. In case of the latter the εAB113 was calculated as the mean of six values as follows:

$$\varepsilon_{dye} = \varepsilon_1 + \varepsilon_2 + \varepsilon_3 + \varepsilon_4 + \varepsilon_5 + \varepsilon_6/6$$

Step 1: Five hundred mL of Solution 1 were transferred to one-liter conical flask. Five gram of NIS was added to the conical flask and the solution was agitated using magnetic stirrer at about 700 rpm. At the end of 15 min the agitation was stopped and solution was filtered through No 42 Whatman filter paper using Buchner funnel apparatus. If the filtrate is not clear the filtration was repeated and absorbance recorded.

Step 2: The dye-adsorbed NIS on the filter paper of the Step 1 was carefully transferred from a Buchner funnel to a watch glass and kept in an oven at 60°C for 24 h for drying. The dried powder was scrapped using spatula and transferred to a watch-glass.

Step 3: Second portion of 5 g NIS was added to the conical flask containing filtrate solution from Step 1 and agitation was continued on a magnetic stirrer at about 700 rpm for 15 min. At the end of 15 min the agitation was stopped and solution was filtered through No 42 Whatman filter paper using Buchner funnel apparatus. If the filtrate is not clear the filtration was repeated and absorbance recorded.

Step 4: The dye-adsorbed NIS on the filter paper of the Step 3 was carefully transferred from a Buchner funnel to a watch glass and kept in an oven at 60°C for 24 h for drying.

The dried powder was scrapped using spatula and transferred to a watch-glass.

Step 5: Third portion of 5 g NIS was added to the conical flask containing filtrate solution from Step 3 and agitation was continued on a magnetic stirrer at about 700 rpm for 15 min. At the end of 15 min the agitation was stopped and solution was filtered through No 42 Whatman filter paper using Buchner funnel apparatus. If the filtrate is not clear the filtration was repeated and absorbance recorded.

Step 6: The dye-adsorbed NIS on the filter paper of the Step 5 was carefully transferred from a Buchner funnel to a watch glass and kept in an oven at 60°C for 24 h for drying. The dried powder was scrapped using spatula and transferred to a watch-glass.

Step 7: Fourth portion of 5 g NIS was added to the conical flask containing filtrate solution from Step 5 and agitation was continued on a magnetic stirrer at about 700 rpm for 15 min. At the end of 15 min the agitation was stopped and solution was filtered through No 42 Whatman filter paper using Buchner funnel apparatus. If the filtrate is not clear the filtration was repeated and absorbance recorded.

Step 8: The dye-adsorbed NIS on the filter paper of the Step 7 was carefully transferred from a Buchner funnel to a watch glass and kept in an oven at 60°C for 24 h for drying. The dried powder was scrapped using spatula and transferred to a watch-glass.

Step 9: Steps 1 to 8 were repeated with Solution 2.

The powder and filtrate solutions after the adsorption of constituents of Solution 2 on NIS are shown in Figure 13b and 13c.

Preliminary trial study revealed that better results could be obtained by scaling up to two-orders of the adsorbent and the adsorbate and to one order of the volume of the solution. In an interesting observation Solution 2 showed about 20% decrease in absorbance compared to Solution 1. This may be due to the absorbance of the dye by

varied undefined constituents present in TIE. Also, it was observed that additional fresh samples of the adsorbent after every 15 min enhanced the efficiency of removal of the dye from TIE. The recovery of the dye and allied substances from Solution 2 after 15, 30, 45 and 60 min was observed. This observation is in accordance with the kinetic results according to which the solute adsorbs quickly onto the surface of the particles forming a film which then gets retarded further diffusion thereby bringing change in absorption rates.

The experiment was scaled up to 10 g, 20 g, and 50 g of NICSS using 1, 2, and 5 L of Solution 2 taken in polyethylene beakers. The solutions were vigorously stirred using a magnetic stirrer and the procedure repeated as indicated earlier and the results obtained were almost uniform. All experiments were carried out in triplicate and the mean of three results are reported. The coefficients of variance of all results did not vary from ± 2% error.

3.1.10 Preparation of dye adsorbed coriander seed spent

The NICSS with particle sizes of ≤90 μ; ≥90 μ ≤ 125 μ; ≥125 μ ≤ 177 μ; ≥177 μ ≤ 355 μ; ≥355 μ ≤ 500 μ and ≥500 μ ≤710 μ, were dried in an oven at 60^{o}C for about 24 h. Three litre of distilled water containing 300 g of Congo red dye were transferred to a 5L beaker containing 1 kg NICSS. The pH was adjusted to 2 using HCl and the solution was stirred for 166 min at 165 rpm. The solution was filtered using a Büchner funnel and the dye adsorbed NICSS was washed with water. The resulting dye adsorbed spent was air dried and kept in an oven at 60^{0}C for about 12 h. The lumps formed during the adsorption process were crushed into powder and used for further study to fabricate thermoplastic and thermoset biocomposites. Preliminary investigation on different particle sizes revealed only two sizes (90 μ ≤ 125 μ; ≥125 μ ≤ 177 μ) gave encouraging and similar results. The ≥125 μ ≤ 177 μ sizes was selected for further

studies as it requires less labour compared to 90 μ ≤ 125 μ and extensively used for the fabrication of composites.

3.1.11 Compounding and specimen preparation of thermoplastic biocomposites

Polypropylene (PP) (H110MA) (melt flow index 11 g/10 m at 231°C under 2.16 kg load) supplied by Reliance Industries, India was used as matrix polymer for the fabrication of thermoplastic biocomposites. NIFSS/NICSS and CR-NIFSS/CR-NICSS were oven dried at 105^0C for 24 h. Maleic anhydride-graftF-PP (MAg-PP) was used as coupling agent for NIFSS/NICSS and CR-NIFSS/CR-NICSS (wt/wt,%) 10, 20, 30, 40, and 50% were initially mixed thoroughly with PP. The mixture was melt blended by adding to a 28 mm fully inter-meshing, co-rotating twin screw extruder with segmented screw and barrels. The extrudes were collected, cooled and granulated into pellets. The pellets of PP/NIFSS or PP/NICSS and PP/CR-NIFSS or PP/CR-NICSS composites are shown in Figure 3.1.

(a) (b)

Figure 3.1: Compounded pellets of (a) PP/NICSS and (b) PP/CR-NICSS

The blends were injection moulded into standard ASTM D 638-94b, ASTM D 790-92 and ASTM D 256-93a and subjected to tensile, flexural and impact tests using 60 ton L&T made multipoint twin toggle, close loop, injection moulding machine. The temperature at different zones in injection moulding ranged from 170 to 175^0C (from feed zone to nozzle). The injection moulded dumb-bell specimens were conditioned in a

desiccator for 3 days at ambient temperature before testing and the specimens are shown in Figure 3.2. Three-body wear test samples (25 * 75 * 3.2 mm) were cut from injection moulded 100-mm diameter circular disks. Mechanical tests (tensile and flexural) were performed using Shimadzu make universal testing machine (UTM) (model AGIS10, 10 KN).

Figure 3.2: Injected moulded dumb-bell specimen of PP/NICSS and PP/CR-NICSS

Tensile tests were conducted in accordance with ASTM D 638-94b, using specimen Type I (dimensions—165 * 13.2 * 3.2 mm) and at crosshead speed of 50 mm/min. Flexural strength was determined as per ASTM D 790-92 with a support span of 100 mm and crosshead speed of 2.8 mm/min. Five samples from each set were tested, and mean values are reported which had standard deviation within the analytical limits and coefficient of variance 62%. Thermogravimetric analysis (TGA) and differential thermal analysis (DTA) were used to study the thermal stability of biocomposites. Specimen Preparation of Thermoset Composites USP was procured from a local industry. Thermoset composites with 2, 5, 10, 15, and 20% (on weight percent basis) of NICSS and 10% dye adsorbed NICSS (on weight percent basis) were prepared. Methyl ethyl ketone peroxide (2%) was used as catalyst. The mixture was homogenized using

liquid mixing stirrer. The slurry was poured on a glass plate containing a frame of required dimensions. The thermoset formed was placed under a pressure plate for about 3 h. The sample obtained was studied for physico-mechanical and thermal properties.

3.1.12 Measurements

3.1.12.1 Physico-mechanical properties

The surface hardness was measured as per ASTM D 2240 and the density of the composite was measured using ASTM D 792-00. Specimens were tested for water absorption according to ASTM D 570-98 method. A 50 mm disc with 3-mm thickness specimen sample of each composition was immersed in distilled water at room temperature and change in weight was recorded at the end of 48 h. The water absorption was calculated as in Eq. 3.24:

$$\text{Water absorption (\%)} = M_2\text{-}M_1 \times 100/M_1 \quad \textbf{(3.24)}$$

where M_1 and M_2 are the mass of sample before and after immersion respectively.

Tensile properties were measured using UTM, Shimadzu make UTM (model AGIS10, 10 KN) with crosshead speed of 50 mm/min as per ASTM D 638-94b method. Flexural tests were performed using the same UTM machine as per ASTM D 790-92 method with 5 mm/min rate. Three samples of each set were tested and mean values are reported.

3.1.12.2 Theoretical calculation of tensile properties

A series of values for the parameters B in Turcsanyi model and Sato and Furukawa models have been obtained through a program written in MATLAB software (Version 7.2). All these values were substituted in the respective equations sequentially and the resulting values nearest to the experimental result were chosen.

3.1.12.3 Three-body abrasive wear

The three-body abrasive wear was measured using rubber wheel abrasion test rig as per ASTM G65. The abrasive particles of AFS 60 grade angular shaped silica sand with sharp edges were used. The abrasive particles were fed at the contacting face between the rotating rubber wheel and the test sample. The initial weight of the samples was taken in a high precision electronic balance (0.1 mg accuracy, Mettler, Toledo) before subjecting to wear analysis. The abrasive particles were introduced between the test specimens and rotating abrasive wheel composed of chlorobutyl rubber tyre. The test specimen was pressed against the rotating rubber wheel at a specified load, applied by means of lever arm while a controlled flow of abrasives abraded the test surface. The rotation of the abrasive wheel was such that its contact face moved in the direction of sand flow. The pivot axis of the lever arm lied within a plane, which was approximately tangent to the rubber wheel surface and normal to the horizontal diameter along which the load was applied. At the end of a set test duration, the specimen was removed, thoroughly cleaned and again weighed (final weight). At least two tests were performed and the average values are reported. The abrasive wear studies were carried with two different loads (23.54 and 33.54 N) and at a constant sliding velocity of 2.15 m/s. Composite specimens were abraded at varying abrading distances (150–600 m) varied in steps of 150 m at appropriate time intervals. Weight loss was measured at regular test intervals using an electronic balance. The wear loss was determined by the loss in weight, which was then converted into wear volume using measured density data. The specific wear rate (Ks) was calculated from the below mentioned Eq. 3.25:

$$K_s = \frac{\Delta V}{L \times d} m^3 / Nm \qquad \textbf{(3.25)}$$

where, ΔV is the volume loss in m^3, L is the load in Newton and d is the abrading distance in meters. Scanning electron microscopy (SEM) of model JSMIT 300 (JEOL,

Japan) was used to study the morphological features of tensile fractures samples and surface composite specimen features.

3.1.12.4 Testing of thermosets

The polyester composites formed were tested for tensile strength as per ASTM D 638-95 method using 4302 model Houns Field UTM, UK. The tensile tests were carried out on dumb-bell shaped specimens in UTM with cross-head speed of 50 mm/min. Five samples were tested at room temperature for each formulation and the mean values are reported. Physical properties such as density and surface hardness were determined according to ASTM D 792-00 and ASTM D 2240 methods, respectively. The surface hardness was measured using Shore D Durometer (M/s. P.S.I Sales, India).

The resistance of composites was tested as per ASTM D 543-06 for chemicals including, 10% (V/V) nitric acid, 10% (V/V) hydrochloric acid, 10% (V/V) acetic acid, 10% (V/V) sodium hydroxide, 10% (V/V) ammonium hydroxide and distilled water. For this the dried and pre-weighed samples of unfilled and CR-NICSS and NICSS filled USP thermoset composites were immersed in different chemicals at room temperature. After one week the samples were taken out and washed with distilled water and the solvent adhering to the surface was removed by using soft tissue paper. The final weights of the samples were measured and percent weight loss/gain was determined.

CHAPTER 4: SUSTAINABLE DESIGN TO DEVELOP COMPOSITES USING CONGO RED DYE-ADSORBED NUTRACEUTICAL INDUSTRIAL SPENT AS FILLER MATERIALS

4.1 Adsorption studies of Congo Red (CR) onto Nutraceutical Industrial Fennel Seed Spent (NIFSS)

4.1.1 Surface characterization

IR spectra of CR-NIFSS reveal shifting, disappearance and appearance of new peaks. This is attributed to the involvement of functional groups during adsorption process (Figure 4.1). Absorption at 3442 cm^{-1} is due to the stretching of hydroxyl groups of cellulose, hemicellulose and lignin present in NIFSS. The bands at 2925 cm^{-1} and 2856 cm^{-1} is due to the C-H stretching of saturated carbon. The bands at 1651 cm^{-1} are due to C=C stretching. The bands at 1380 cm^{-1} and 1245 cm^{-1} are assigned to C-O vibrations and O-H bending respectively. Bands at 1318 cm^{-1} and 1244 cm^{-1} are assigned to OH bending and C-O vibration respectively. The finger print region of the biological material NIFSS indicates complex bands and it is difficult to get an accurate assignment of the peaks without the help of standard sample. However, the presence of cellulose and lignin indicates that the spent possibly displays both hydrophilic and hydrophobic properties.

The surface characterization of NIFSS done through SEM showed a highly porous structure (Figures 4.2a, 4.2b). After the adsorption of CR some pores got completely filled with the adsorbate forming a thin film over the particle. Determination of point of zero charge at intersection of two plots (Figure 4.3) confirms that at pH 7.0 NIFSS have zero charge.

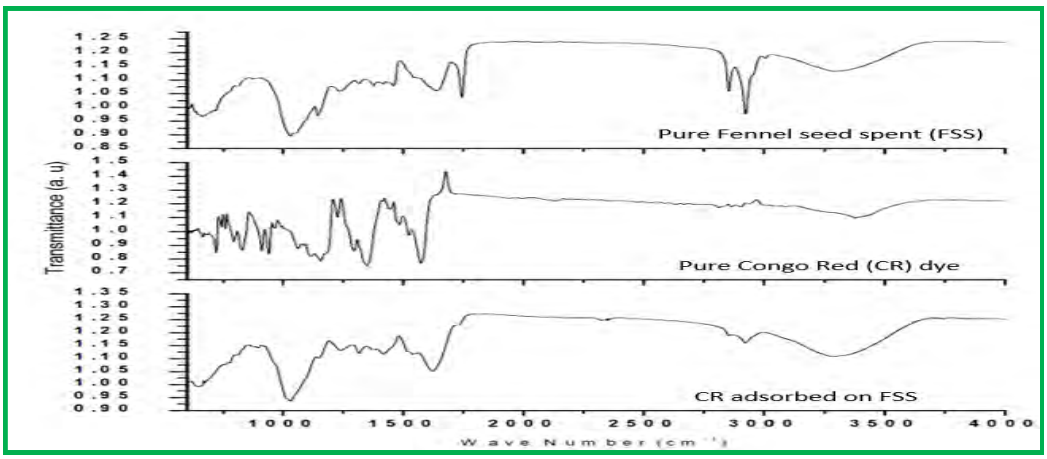

Figure 4.1: FTIR spectra of NIFSS, CR dye and CR dye-adsorbed on NIFSS

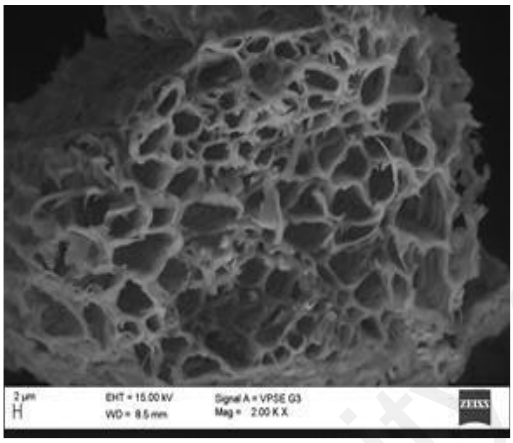

Figure 4.2a: SEM image of NIFSS

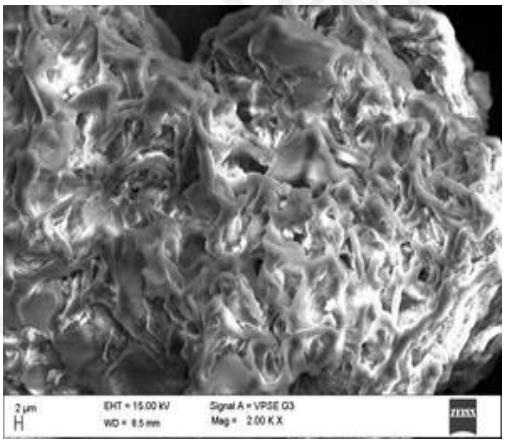

Figure 4.2b: SEM image of CR dye adsorbed NIFSS

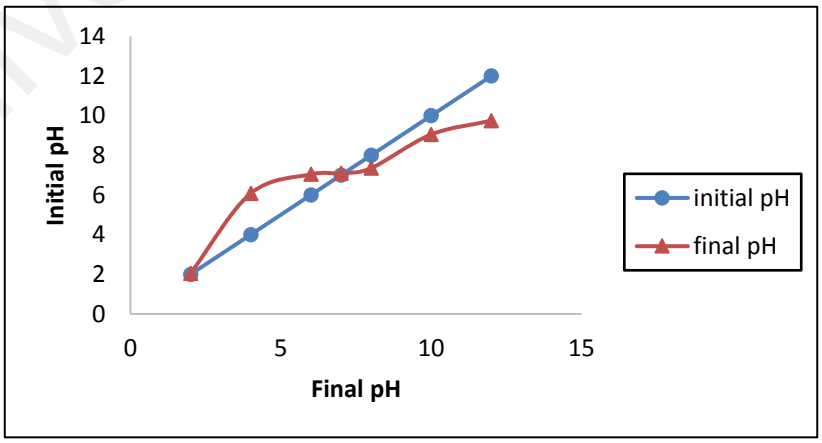

Figure 4.3: Point of zero charge of NIFSS

4.1.2 Batch adsorption studies of CR-NIFSS system

In order to achieve maximum adsorption, it is necessary to optimize the various parameters.

4.1.2.1 Effect of pH

The pH of the process is one of the most important parameters for the adsorption process as it controls the adsorption capacity by its influence on the adsorbent surface properties and ionic forms of dye in the solution. When the pH was at 2, NIFSS showed the highest adsorption capacity (Figure 4.4). However, when the pH was increased from 2 to 8, adsorption decreased gradually and again at pH 10 it increased slightly and then decreased even further at pH 12. It was found that the maximum CR adsorbed on NIFSS was at pH 2.0 - 4.0 (q_e = 35.5 mg g^{-1}) with initial concentration of CR is 100 mg L^{-1}. Conversely, the adsorption capacity of NICSS increased marginally from pH 2 to pH 4 and gradually decreased till pH 12. This observation can be explained as follows: In acidic pH, an excess of H^+ ions compete with cations of the dye for adsorption sites. When the surface charge density gets lowered with the increase of pH solution, the repulsion between the positively charged dye and the surface of the adsorbent gets lowered. This result is shown in Figure 4.4.

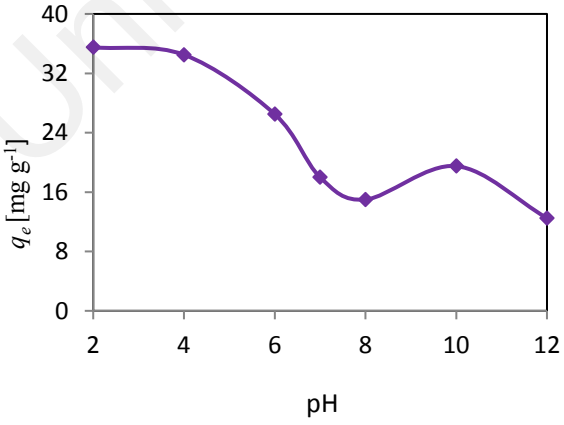

Figure 4.4: Effect of pH on adsorption of CR dye on NIFSS

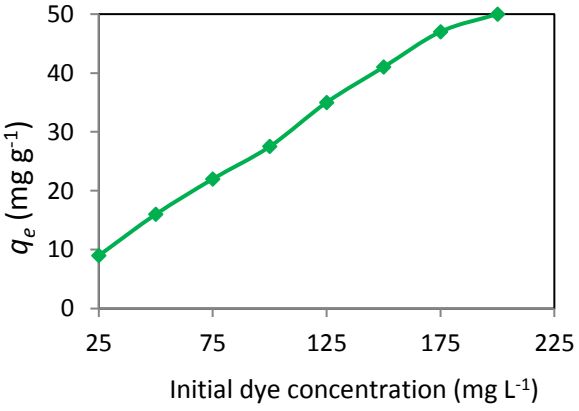

Figure 4.5: Effect of initial dye concentration on adsorption of CR dye on NIFSS

4.1.2.2 Effect of initial dye concentration

The dye uptake of NIFSS increased with the increase in dye concentration from 25 to 175 mg L^{-1} respectively. Thereafter, it attains almost saturation limit as is seen from the Figure 4.5. This indicates that there is an increase in the driving force of the concentration gradient due to the increase in the initial dye concentration. Adsorption was rapid initially due to the dye getting adsorbed onto exterior surface. Later, the dye molecules, probably entered into pores (interior surface), which is relatively a slow process. The adsorption of CR was more with higher concentration and remained almost constant after equilibrium time and higher concentration beyond 175 mg L^{-1}.

4.1.2.3 Effect of particle size of the adsorbent

The maximum adsorption capacity was studied for initial CR concentration of 200 mg L^{-1} at pH 2 by different particle sizes of NIFSS. The results of both the adsorbents were almost similar. The data are detailed below: ≤ 90 μm (65 mg L^{-1}); ≥ 90 μm ≤ 125 μm (60 mg L^{-1}); ≥ 125 μm ≤ 177 μm (50 mg L^{-1}); ≥177 μm ≤ 355 μm (42 mg L^{-1}); ≥355 μm ≤ 500 μm (31 mg L^{-1}) and ≥ 500 μm ≤ 710 μm (20 mg L^{-1}). The results infer that adsorption of dye decreases with the increase in the size of the adsorbent particle. The observation is in conformation with the expected results as surface area decreases with increase in particle size. An optimum size of ≥ 125 μm ≤ 177 μm (80 mesh ASTM) was selected in this studies for two reasons: first, 80 mesh particle is widely employed in the fabrication of composites and second, sieving smaller size particles will take longer period and adding to the cost of the process.

4. 2 Adsorption isotherms, kinetic and thermodynamic modeling of CR-NIFSS system

The predicted maximum adsorption capacity (Q_m) value of 119.037 mg g^{-1} using Langmuir isotherm is significantly higher compared to the experimental value (35.5 mg g^{-1}) (Figure 4.6a). The separation factor R_L for the concentration range of

25–100 mg L^{-1}, the values obtained between 0.80 and 0.38 indicate favorable adsorption of Congo red dye on the NIFSS. The decrease in R_L with increase in the initial concentration of the dye indicates that the adsorption is more favorable at high concentrations as expected. The heterogeneity factor obtained using Freundlich isotherm values of n_F = 1.38 and $1/n_F$ = 0.72 indicates that the adsorption is physisorption and fits to the normal Langmuir isotherm. The fitting of the Langmuir and Freundlich isotherms with respect to the experimentally obtained data (R^2 = 0.995) is shown in Figure 4.7a. Looking at Q_m, χ^2 and R^2 values Langmuir appears to better fit than Jovanovic model (Table 4.1). The 'g' value of 0.765 obtained using Redlich–Peterson isotherm indicates that the adsorption behavior tends towards Langmuir isotherm (Figure 4.6b). The value of Q_m = 145.77 mg g^{-1} found for the Sips isotherm is very close to that estimated from the Langmuir isotherm. On the other hand, from the Radke-Praustnitz isotherm (Radke & Prausnitz, 1972) predicted Q_m of 60.92 mg g^{-1}, was obtained which was closest to the experimentally obtained Q_m value. The fits of Sips isotherm (R^2 = 0.994), the Radke-Praustnitz isotherm (R^2 = 0.994), and the Toth isotherm (R^2 = 0.997) to the experimental data are shown in Figure 4.6c. The Jovanovic isotherm shows Q_m value of 74.27 mg g^{-1} which is almost similar to Radke-Prausnitz isotherm value. But, the Q_m value of 129.3 mg g^{-1} found for Vieth-Sladek isotherm (Vieth & Sladek, 1965) is the third highest calculated value. The fits of Vieth-Sladek (R^2 = 0.994), Redlich-Peterson (R^2 = 0.994) and Jovanovic (R^2 = 0.994) isotherms to the experimental data are shown in Figure 4.6b.

From the isotherms analysis and the knowledge about most important parameters (Q_m, χ^2 and R^2), the isotherms can be arranged according to their capacity to predict or their efficiency in predicting the experimental behavior of the CR-NIFSS system. With respect to Q_m value (closest to actual value to farthest from actual value): Radke-Prausnitz > Jovanovic > Langmuir > Vieth-Sladek > Sips > Toth. While, with

respect to χ^2 (in descending order): Sips > Toth > Redlich-Peterson > Radke-Praustnitz > Langmuir > Vieth-Sladek > Freundlich > Jovanovic.

The estimated parameters are shown in Tables (4.2 and 4.3). Based on the coefficients of determination (R^2) and chi-square values (χ^2) the pseudo-second-order model was best fit with the experimental data for all initial CR concentrations (25, 50 and 100 μg ml^{-1}). It is interesting to observe that the rate of adsorption at the very beginning of the process is very high and then slows down over time to become stagnant as it achieves the maximum adsorption potential. As expected the adsorption capacity (q_e) seems to increase with increase in temperature. Consequently, based on these results, the adsorption processes were found not to be the rate-limiting step.

The data also indicates that the adsorption process occurs in multiple steps involving transport of solute molecules from the bulk solution to the solid-surface of the adsorbent and then the diffusion of the solute molecules into the interior of the pores of the fennel spent. In order to understand solute movement, the data was analyzed to study the effects of diffusion. The Weber-Morris model (Figure 4.8) is routinely used to describe the molecular diffusion and defines that solute up take varies with t½ rather than with time of contact (t). Therefore, a plot of q_t versus t½ should yield a straight line passing through origin whose slope (k_{int}) is the diffusion rate constant. However, adsorption kinetics is not always controlled by a single mechanism. As seen in our experimental data, all solute concentrations multiple levels of linearity can be observed. For lower initial concentration (25 μg ml^{-1}) at lower temperature, the rate of adsorption is high and then it appears to be a shift in the rate following a different linear trajectory until finally the rate stabilizes with respect to time. However, at higher temperatures the rate seems to be more linear. It can also be seen that at higher concentrations of solute (100 μg ml^{-1}) it seems to be less apparent changes in the rate of adsorption.

(a)

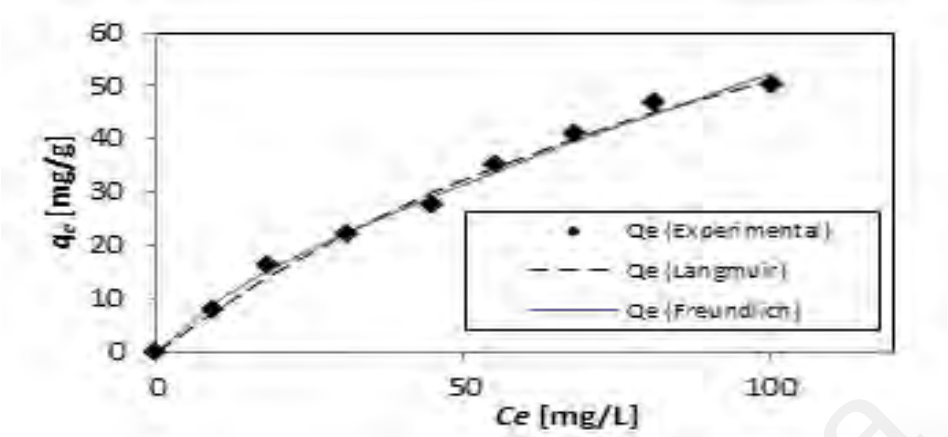

(b)

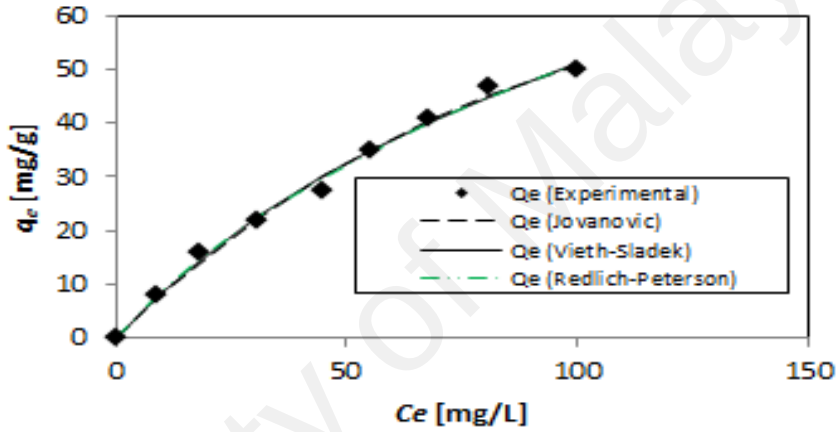

(c)

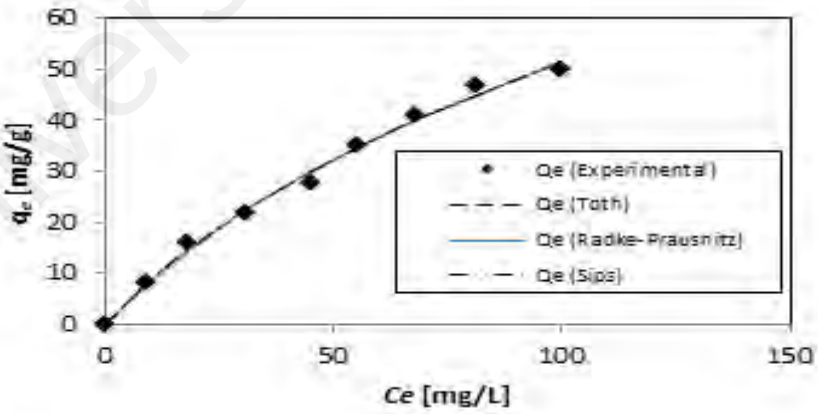

Figure 4.6: Fitting of data to a) Langmuir and Freundlich, b) Jovanovic, Vieth-Sladek and Redlich-Peterson, c) Toth, Radke-Prausnitz and Sips adsorption isotherms on AB113-NIFSS system

Table 4.1: Calculated and statistical parameters for adsorption isotherm models of CR-NIFSS system

Error Functions	Two-parameter isotherms						Three-parameter isotherms									
	Langmuir		Freundlich		Jovanovic		Redlich-Peterson		Toth		Radke-Prausnitz		Sips		Vieth-Sladek	
	Q_m	119.037	K_F	1.89	Q_m	74.27	A_{RP}	1.03	Q_m	222.27	Q_m	60.92	Q_m	145.76	Q_m	129.29
							B_{RP}	0.029	n_{TO}	0.657	K_{rp}	0.015	K_s	0.004	K_{VS}	0.025
	K_S	0.008	n_F	1.386	K_J	0.012	g	0.765	b_{TO}	33.395	m_{rp}	0.648	m_s	0.884	β_{VS}	0.007
SSE	15.9		18.6		16.2		15.6		15.5		15.9		15.1		15.9	
χ^2	0.604		0.640		0.668		0.520		0.513		0.553		0.500		0.611	
R^2	0.99		0.99		0.99		0.99		0.99		0.99		0.99		0.99	

Table 4.2: Experimentally determined and theoretically predicted parameters for absorption kinetics models of CR-NIFSS system

Initial concentration [µg ml^{-1}]	Temp [K]	q_e *expt* *[mg g^{-1}]*	Pseudo-first order				Pseudo-second order			
			Q_m *pred*				Q_m *pred*			
			[mg g^{-1}]	k^1	R^2	$\chi 2$	*[mg g^{-1}]*	k^2	R^2	χ^2
100	303	31	25.28	0.228	0.84	14.65	27.26	0.015	0.86	14.26
	313	32	27.34	0.252	0.77	16.34	29.71	0.014	0.84	15.41
	323	34	30.15	0.261	0.84	17.70	32.21	0.015	0.89	17.11
50	303	16.5	14.32	0.170	0.91	5.77	15.64	0.018	0.94	5.24
	313	17	14.44	0.270	0.90	6.48	15.46	0.031	0.95	6.12
	323	20	18.08	0.155	0.93	7.50	19.84	0.013	0.93	7.11
25	303	8.5	7.73	0.330	0.90	4.16	8.13	0.084	0.93	4.05
	313	9	8.20	0.323	0.85	4.75	8.65	0.075	0.90	4.60
	323	10	8.32	0.184	0.72	5.47	9.10	0.032	0.77	5.13

Table 4.3: Calculated parameters for diffusion models of CR-NIFSS system

Initial concentration [µg ml^{-1}]	Temp [K]	Film diffusion $R^{\|}$ [min^{-1}] R^2		Weber-Morris k_{ist} [mg g^{-1} s$^{0.5}$] R^2		Dumwald-Wagner K [min^{-1}] R^2	
25	303	0.060	0.90	0.67	0.92	0.053	0.91
	313	0.062	0.92	0.68	0.94	0.055	0.93
	323	0.032	0.98	0.58	0.98	0.026	0.98
50	303	0.038	0.93	1.40	0.94	0.032	0.96
	313	0.028	0.83	1.20	0.87	0.024	0.88
	323	0.042	0.91	1.70	0.94	0.036	0.93
100	303	0.023	0.76	1.78	0.89	0.019	0.78
	313	0.031	0.94	1.94	0.96	0.027	0.96
	323	0.032	0.89	1.97	0.93	0.034	0.88

Table 4.4: Thermodynamic parameters of CR-NIFSS system

Initial concentration [µg ml^{-1}]	Temperature [K]	ΔG° [kJ mol^{-1}]	ΔS° [J mol^{-1} K^{-1}]	ΔH° [kJ mol^{-1}]	ln A	Ea [kJ mol^{-1}]
100	303	-1.90	46.23	12.05	4.73	1.29
	313	-2.52				
	323	-2.82				
50	303	-2.31	75.03	20.60	9.20	13.62
	313	-2.52				
	323	-3.83				
25	303	-2.57	42.17	10.21	17.62	38.44
	313	-2.97				
	323	-3.42				

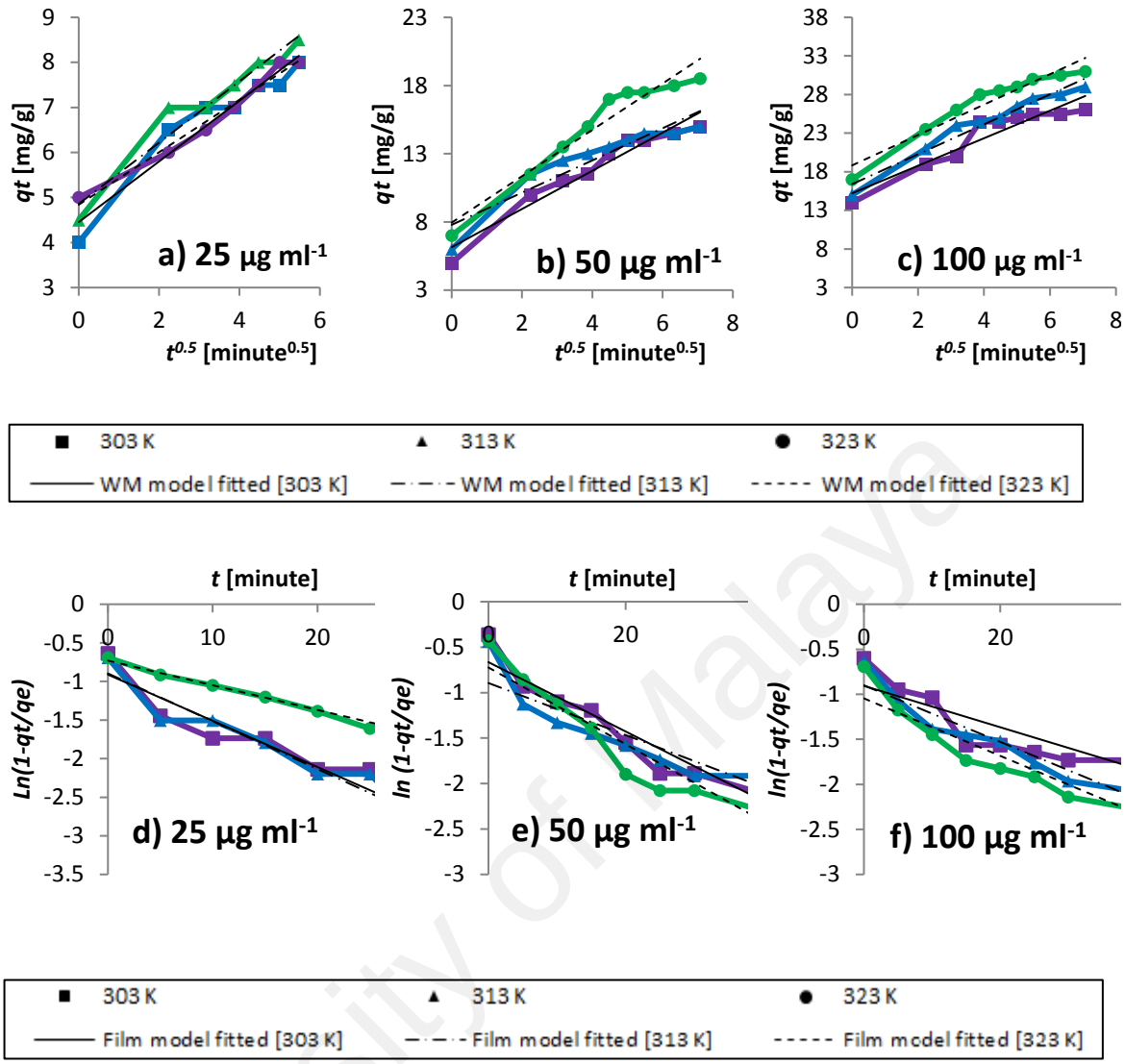

Figure 4.7: Kinetics data fitted to the with initial concentration of CR-NIFSS Weber-Morris model: a) 25 µg ml^{-1}, b) 50 µg ml^{-1}, c) 100 µg ml^{-1} and Film diffusion model: d) 25 µg ml^{-1}, e) 50 µg ml^{-1}, and f) 100 µg ml^{-1}

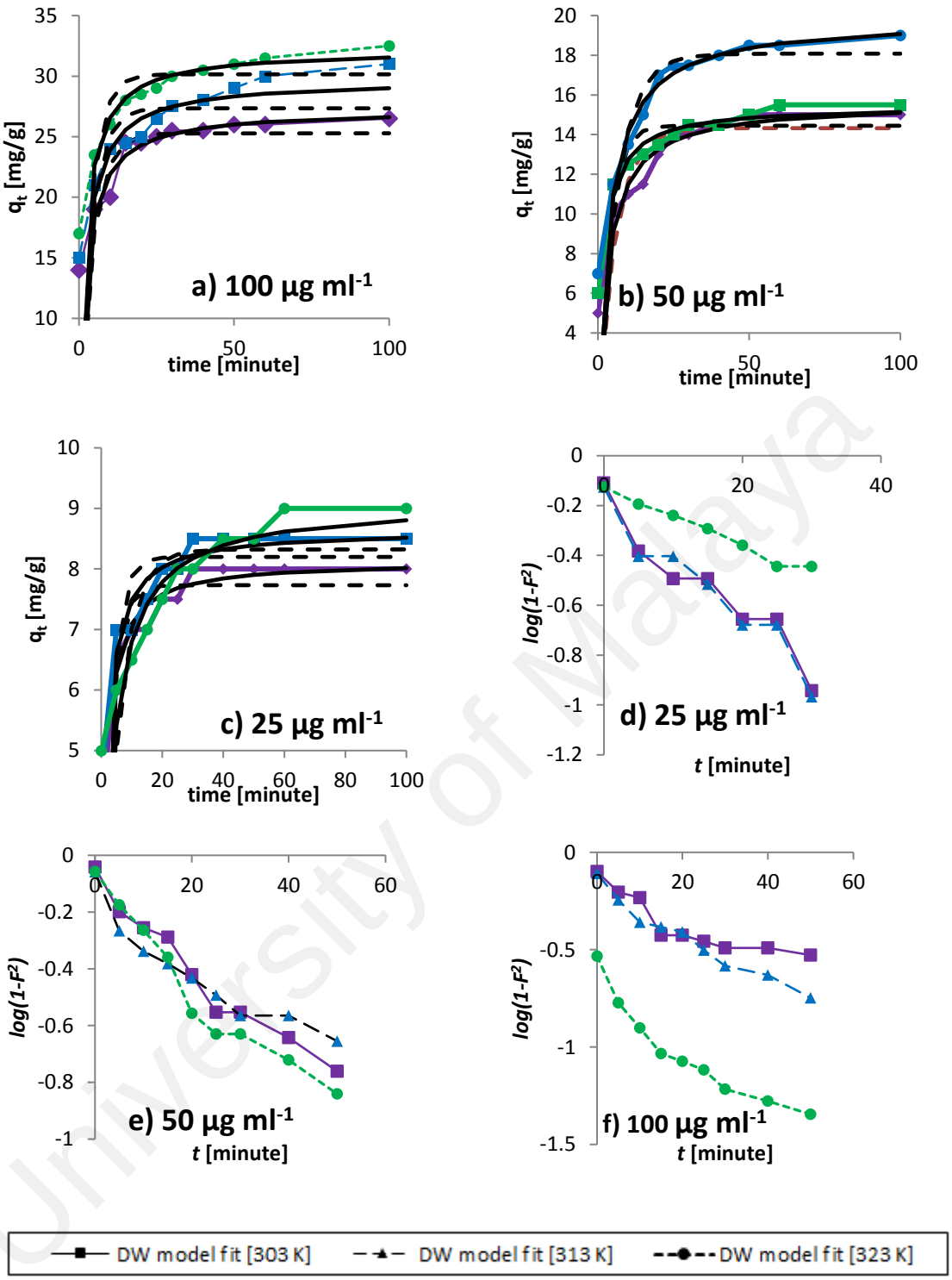

Figure 4.8: Kinetic model fits of initial concentration of CR-NIFSS at different temperatures a) 100 µg ml^{-1}, b) 50 µg ml^{-1}, c) 25 µg ml^{-1} and Dumwald –Wagner model fits: d) 25 µg ml^{-1}, e) 50 µg ml^{-1} and f) 100 µg ml^{-1}

This can be especially be seen when fitting the higher temperature data to the film diffusion model (Figure 4.7) as seen in the figure above it can be affirmed that the data shows good adherence to the model with high R^2 and χ^2 values and gives the liquid

film diffusion constant $R^{|}$ (Table 4.3). This shows that at higher temperatures the rate of adsorption is very negligibly hindered by diffusional limitations.

This implies that diffusion is the rate limiting process. The solute initially absorbs quickly onto the surface of the particles forming a film which then retards further diffusion – which explains the changes in the absorption rates. The Dumwald-Wagner model (Figure 4.8) has been used to calculate the true absorption rate constant (K) with corrections for the observed diffusion effects (Table 4.3).

The thermodynamic parameter estimates are provided in Table 4.4. The positive ΔH° value indicates the endothermic nature of adsorption. The ΔG° is negative for all studied temperatures indicating that the adsorption of CR onto NIFSS would follow a spontaneous and favorable trend. The ΔG° value decreases with increase in temperature indicating an increase in adsorption at higher temperatures. The positive value of ΔS° suggests good affinity of CR towards adsorbent and increased randomness at the solid solution surface. The relatively low value of ΔH° suggests that the adsorption process is physical as the standard enthalpy change for chemical reaction is normally >200 kJ mol^{-1}. It is further confirmed by activation energy values of the adsorption process at different initial concentrations (25, 50 and 100 μg ml^{-1}) which ranged from ~1-38 kJ mol^{-1} using the Arrhenius equation and the kinetic constant from the pseudo-second order model (Table 4.4).

4.3 Adsorption studies of Congo Red (CR) onto Nutraceutical Industrial Coriander Seed Spent (NICSS)

4.3.1 Surface characterization

IR spectra of NICSS provide the information of the functional groups present (Figure 4.9). Absorption at broad band around 3291 cm^{-1} in NICSS is attributed to the surface hydroxyl groups, linked in cellulose and adsorbed water; band at 2920 cm^{-1} is attributed to the stretching vibrations of -CH bonds in alkane and alkyl groups, whereas,

band at 1615 cm^{-1} is due to C=C stretching of olefins. The band at 1417 cm^{-1} indicates methyl groups. The band at 1026 cm^{-1} is due to the cellulose present in the adsorbent. After adsorption, band at 3291 cm^{-1} of hydroxyl group confirms CR adsorption on NICSS. Band at 2916 cm^{-1} is shifted to 2922 cm^{-1}, it is attributed to the stretching vibrations of –CH bonds in alkane and alkyl groups where carbon is bonded with hydrogen bonds. The band at 1615 cm^{-1} is shifted to 1586 cm^{-1} due to imine group of CR and C=C stretching. The band at 1417 cm^{-1} is shifted to 1365 cm^{-1} after adsorption, which may be attributed to CH_3 group of CR and C aryl-N bond.

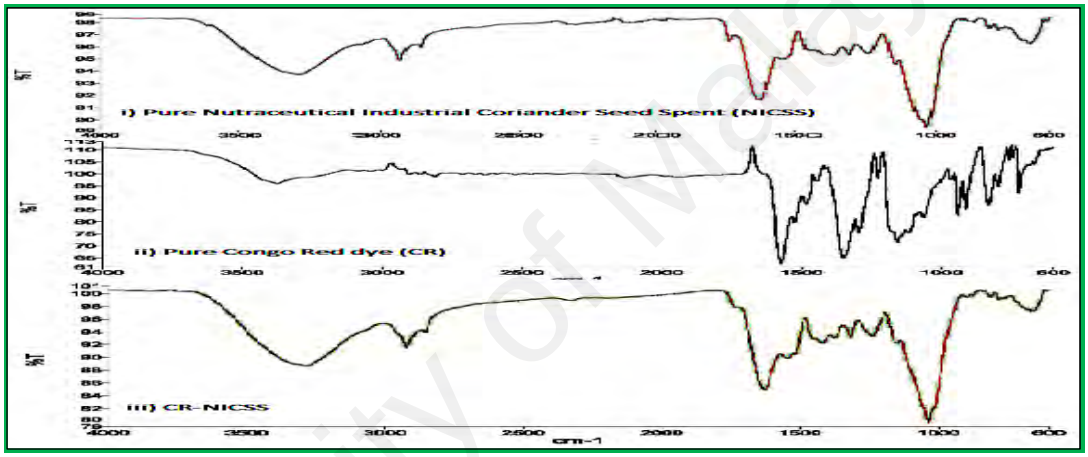

Figure 4.9: FTIR spectra of NICSS, CR dye and CR dye adsorbed on NICSS

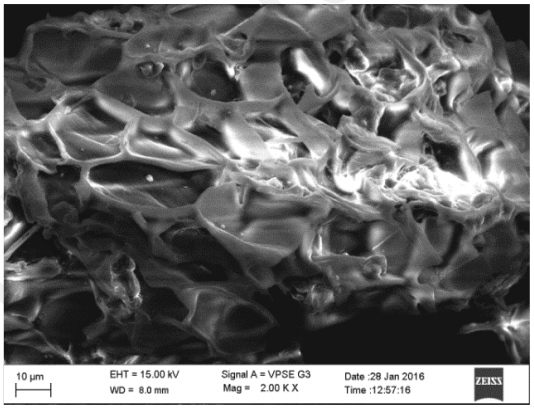

Figure 4.10a: SEM image of NICSS

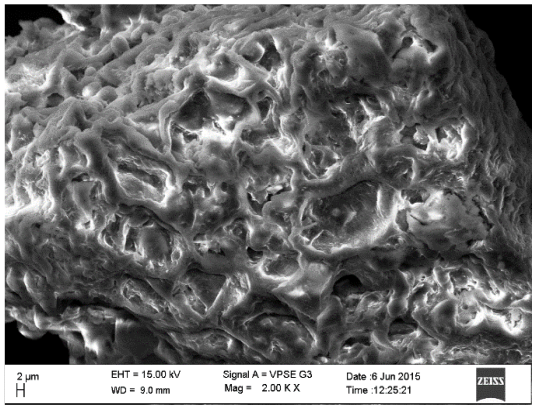

Figure 4.10b: SEM image of CR dye adsorbed NICSS

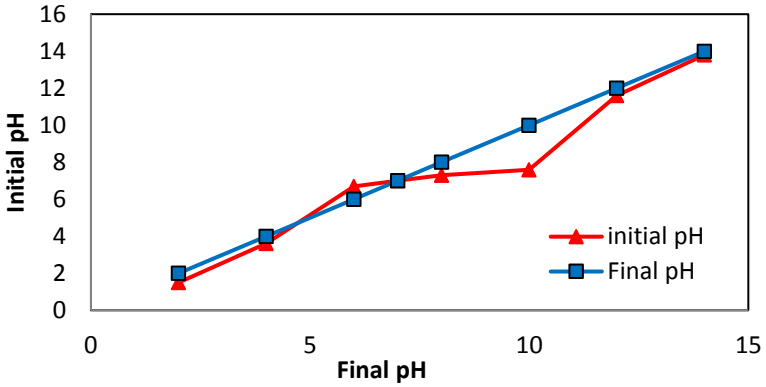

Figure 4.11: Point of zero charge of NICSS

The NICSS morphology obtained by SEM displayed fibrous and porous structure in the Figure 4.10a. This structure enhances the dye adsorption as seen in Figure 4.10b where the pores and void between the spaces are occupied by the dye. Determination of point of zero charge at intersection of two plots (Figures 4.11) confirms that at pH 7.1 NICSS have zero charge.

4.3.2 Batch adsorption studies of CR-NICSS system

Optimization of various parameters is necessary to achieve maximum adsorption of the dye onto the adsorbent.

4.3.2.1 Effect of pH

pH as a parameter controls the adsorption capacity by influencing adsorbent surface properties and ionic forms of dye. The adsorption capacity of NICSS slightly increased with increase in solution pH and maximum adsorption capacity of CR was under acidic condition. In acidic pH an excess of H^+ ions compete with cations of the dye for adsorption sites. When the surface charge density gets lowered with increased solution pH, the repulsion between the positively charged dye and the surface of the adsorbent gets lowered. This results in increased adsorption as depicted in Figure 4.12.

4.3.2.2 Effect of initial dye concentration

The dye uptake increased from 8.5 to 60 mg g^{-1} of NICSS with the increase in dye concentration from 25 to 300 mg L^{-1} respectively (Figure 4.13). This indicates that there is an increase in the driving force of the concentration gradient due to the increase in the initial dye concentration. Adsorption was rapid initially due to the dye getting adsorbed onto exterior surface. Later, the dye molecules, probably entered into pores (interior surface), which is relatively a slow process. The adsorption of CR was more with higher concentration and remained almost constant after equilibrium time.

4.3.2.3 Effect of adsorbent dosage

The influence of adsorption of the dye onto NICSS increased with enhancement in adsorbent dosage in the range 0.025-0.200 g/50 ml. This may be due to the binding of almost all dye molecules on the adsorbent surface and the establishment of equilibrium between dye molecules onto the adsorbent. Hence dye adsorption increased with adsorbent dosage and remained at equilibrium after certain adsorbent dosage as shown in Figure 4.14.

4.3.2.4 Effect of temperature

Temperature, an influencing factor in the adsorption process was studied at 30^{o}C, 40^{o}C and 50^{0}C and the results are shown in Figure 4.15. It can be observed that with the increase in temperature, the adsorption capacity enhanced marginally, which indicates that the process is exothermic in nature. The enhancement in adsorption with temperature may be due to the increase in the mobility of the dye molecule with increase in their kinetic energy and the enhanced rate of intra-particle diffusion of adsorbate with the rise in temperature. The slight increase in removal of dye due to increasing temperature may be due to higher interaction between adsorbate and adsorbent.

4. 4 Adsorption isotherms, kinetic and thermodynamic modeling of CR-NICSS system

The equilibrium experiments were conducted for different initial concentrations of CR in the range of 25-200 mg L^{-1}. The adsorption of the dye onto adsorbent using Langmuir Model (Table 4.5) assumes the monolayer adsorption on to the surface of adsorbent containing finite number of identical adsorption sites of uniform energies. The separation factor R_L in Langmuir isotherm denotes whether the adsorption in the system is unfavorable ($R_L > 1$), linear ($R_L = 1$), favorable ($0 < R_L < 1$) or irreversible ($R_L = 0$).

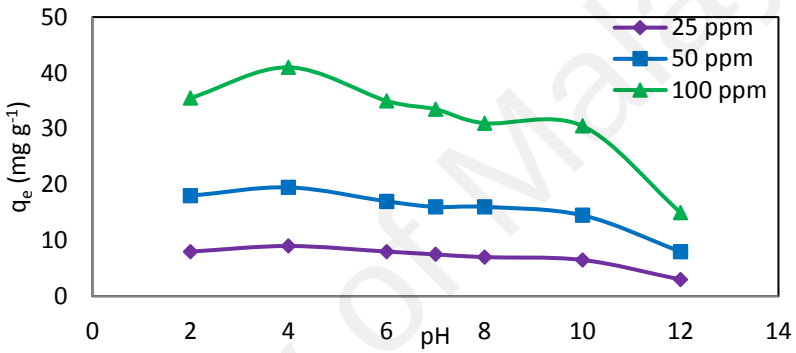

Figure 4.12: Effect of pH on adsorption of CR dye on NICSS

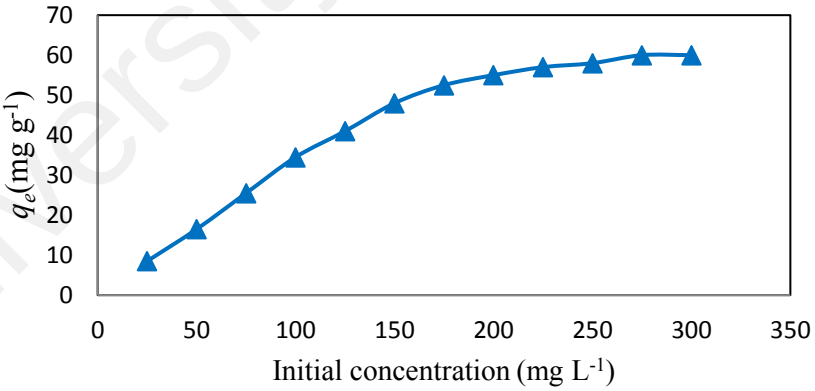

Figure 4.13: Effect of initial dye concentration on adsorption of CR dye on NICSS

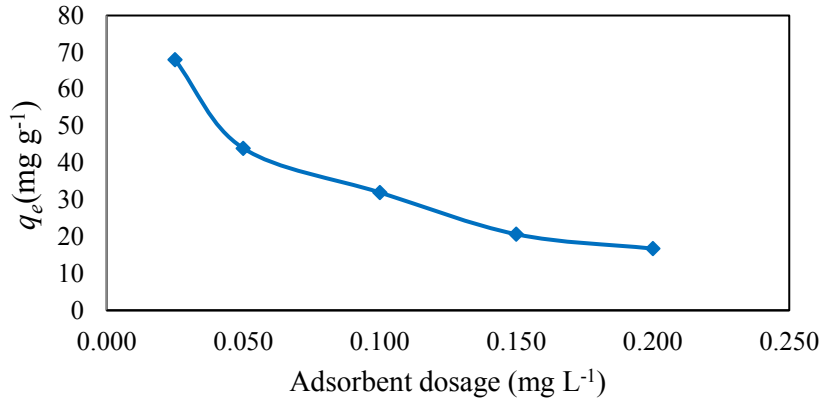

Figure 4.14: Effect of adsorbent dosage on adsorption of CR dye on NICSS

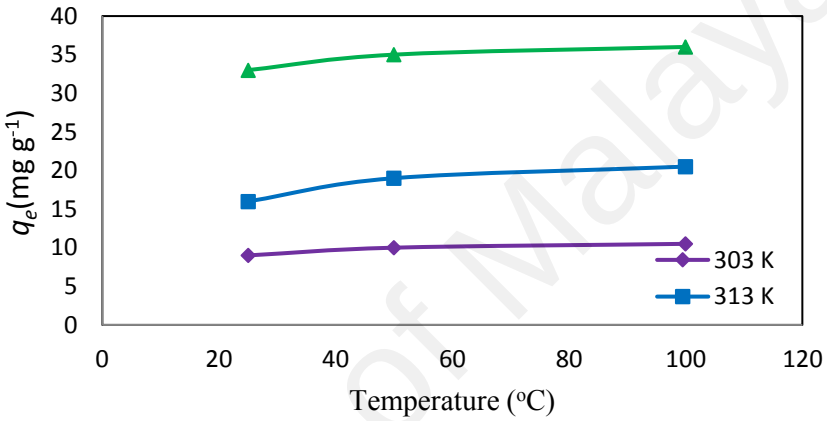

Figure 4.15: Effect of temperature on adsorption of CR dye on NICSS

The R_L value calculated ranges from 0.74 to 0.26 which indicates favorable adsorption of CR on NICSS. The decrease in R_L with increase in the initial concentration indicates that the adsorption is more favorable at higher concentration. A large difference in Q_m (105.40 mg g^{-1}) and q_e (60 mg g^{-1}) values made it necessary to explore other adsorption isotherm models. In the present study, the values of n_F = 1.54 and $1/n_F$ = 0.65 indicate that the adsorption is physisorption and favors normal Langmuir isotherm. The fitting of Langmuir and Freundlich isotherms to the experimental data R^2 = 0.98 where R^2 is the correlation coefficient shows that the data fits well. The results are presented in Figure 4.16 Hence it is inferred that the adsorption of CR on NICSS is favorable and the process is physisorption. Jovanovic considers a model as a monolayer with lateral interactions (Q_m 68.92 mg g^{-1}). The low value of heat of adsorption B = 22 J mol^{-1} indicates the adsorption is mainly a physical phenomenon.

The fit to experimental data (R^2 = 0.98) in Figure 4.16 shows that the Temkin isotherm is adequate to explain the adsorption of CR onto NICSS along with the Langmuir isotherm. In brief, the four two-parameter models studied suggest that the interaction of CR on NICSS is linear, favorable and physical and the results are presented in Table 4.5.

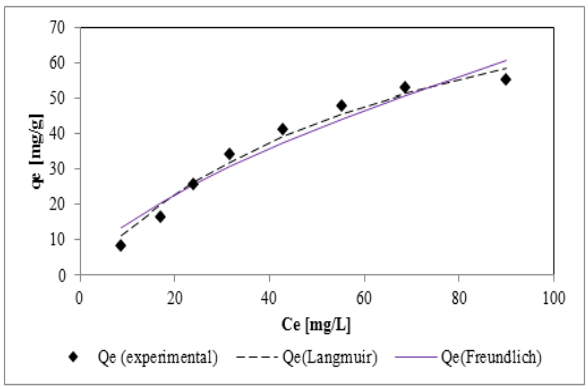

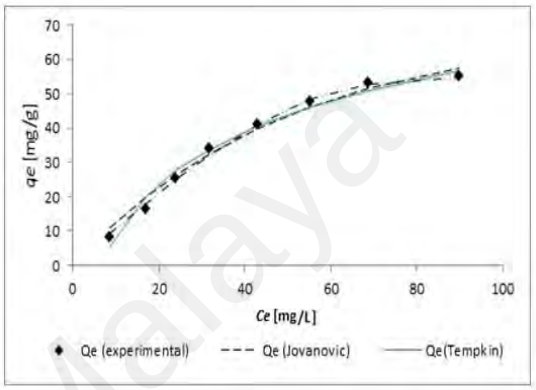

Figure 4.16: Fitting of adsorption data to Langmuir, Freundlich, Jovanovic and Temkin adsorption isotherm of AB113-NICSS system

Table 4.5: Calculated and statistical parameters for adsorption isotherm models of CR-NICSS system

Error Functions	Two-parameter isotherms							
	Langmuir		Freundlich		Jovanovic		Tempkin	
	Q_m	105.40	K_F	3.29	Q_m	68.92	b_T	114.51
	K_S	0.01	n_F	1.54	K_J	0.02	K_T	0.15
SSE	48.6		114.2		35.8		36.9	
χ^2	2.50		5.78		2.01		2.20	
R^2	0.98		0.95		0.99		0.98	

The kinetic studies were carried out at initial CR concentrations of 25, 50 and 100 µg ml^{-1} at temperatures 303, 313, and 323 K respectively. The data were analyzed by non-linear curve fitting (MS Excel 2010) by using different kinetic models i.e., pseudo-first order (Largegren, 1898) and pseudo-second order (Ho and McKay, 2008). While the intra-particle diffusion was analyzed by Weber-Morris model (Alkan et al.,

2007), Dumwald-Wagner model (Wang et al., 2004) and Film Diffusion model (Boyd et al., 1947). The estimated parameters are shown in Tables 4.6 and 4.7.

The pseudo-second order model showed more accurate prediction of adsorption capacities (R^2 closest to 1). Consequently, the adsorption processes were found not to be the rate-limiting step. The data indicates that the adsorption involves transport of solute molecules from the bulk solution to the solid-surface of the adsorbent and diffusion of the solute molecules into the interior of the pores of the NICSS. The solute movement was analyzed from the data with respect to diffusion.

The Weber-Morris model is routinely used to describe molecular diffusion and defines that solute uptake varies with t½ rather than with time of contact (t). Therefore, a plot of q_t vs. t½ should yield a straight line passing through origin whose slope (k_{int}) is the diffusion rate constant. However, adsorption kinetics is not always controlled by a single mechanism. As seen in the experimental data in Figure 4.17, all solute

Table 4.6: Experimentally determined and theoretically predicted parameters for absorption kinetics models of CR-NICSS system

Initial concentration	Temp		Pseudo-first order				Pseudo-second order				Avrami				
[ppm]	[K]	$q_{e\ expt}$ [mg/g]	$Q_{m\ pred}$ [mg/g]	k_1	R^2	χ^2	$Q_{m\ pred}$[mg/g]	k_2	R^2	χ^2	$Q_{m\ pred}$[mg/g]	k_{AV}	n_{AV}	R^2	χ^2
100	303	36	31.20	0.361	0.62	0.39	33.00	0.230	0.85	0.15	31.20	0.36	1	0.62	0.39
	313	37.5	31.63	0.420	0.51	0.36	33.10	0.030	0.77	0.17	31.63	0.42	1	0.51	0.36
	323	38	32.93	0.370	0.45	0.68	34.94	0.021	0.75	0.32	32.93	0.37	1	0.45	0.68
50	303	19.5	17.66	0.150	0.93	0.32	20.50	0.009	0.93	0.44	17.65	0.15	1	0.93	0.31
	313	20.5	18.11	0.400	0.42	0.34	19.15	0.042	0.77	0.14	18.11	0.40	1	0.42	0.34
	323	19	16.51	0.250	0.57	0.72	18.17	0.020	0.83	0.28	16.51	0.25	1	0.57	0.72
25	303	10.5	9.04	0.320	0.67	0.14	9.65	0.060	0.92	0.03	9.04	0.32	1	0.67	0.14
	313	11	9.46	0.330	0.43	0.31	10.18	0.060	0.75	0.14	9.46	0.33	1	0.43	0.31
	323	11	9.21	0.380	0.46	0.18	9.75	0.078	0.77	0.08	9.21	0.38	1	0.46	0.18

Table 4.7: Calculated parameters for diffusion models of CR-NICSS system

Initial concentration	Temp	Film diffusion model		Weber-Morris model		Dumwald-Wagner	
		$R^{\|}$ [min^{-1}]	R^2	k_{ist}[$mg.g^{-1}.s^{-0.5}$]	R^2	K [min^{-1}]	R^2
100	303	0.027	0.96	1.295	0.94	0.024642	0.97
	313	0.02	0.96	1.115	0.95	0.018424	0.95
	323	0.033	0.96	1.49	0.97	0.031091	0.95
50	303	0.046	0.93	1.685	0.76	0.040993	0.95
	313	0.034	0.95	0.758	0.99	0.031781	0.94
	323	0.044	0.99	1.134	0.97	0.040993	0.99
25	303	0.0248	0.91	0.422	0.92	0.022569	0.92
	313	0.0378	0.96	0.52	0.96	0.035006	0.95
	323	0.0228	0.95	0.398	0.97	0.020727	0.95

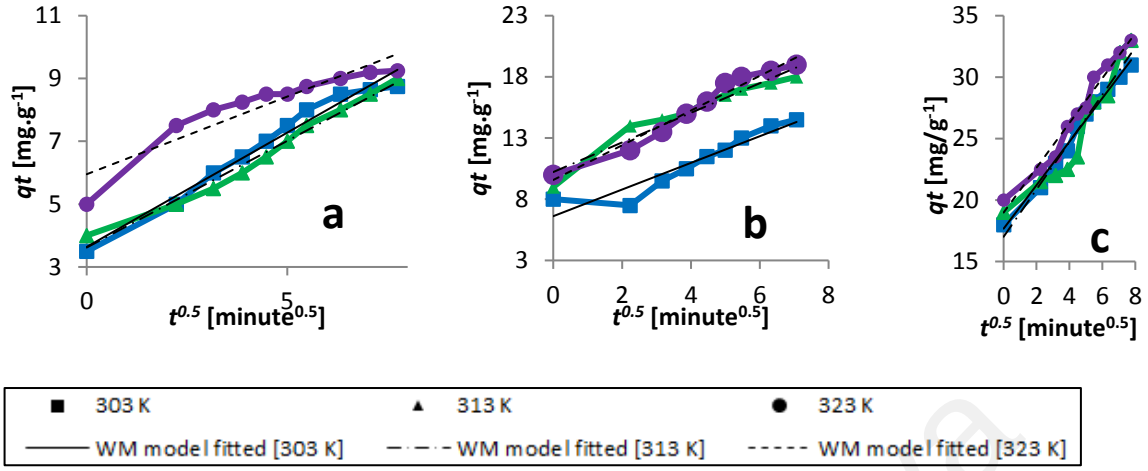

Figure 4.17: Weber-Morris model fits for a) 25 µg ml^{-1}, b) 50 µg ml^{-1} and c) 100 µg ml^{-1} of initial concentration of CR on NICSS system at different temperatures

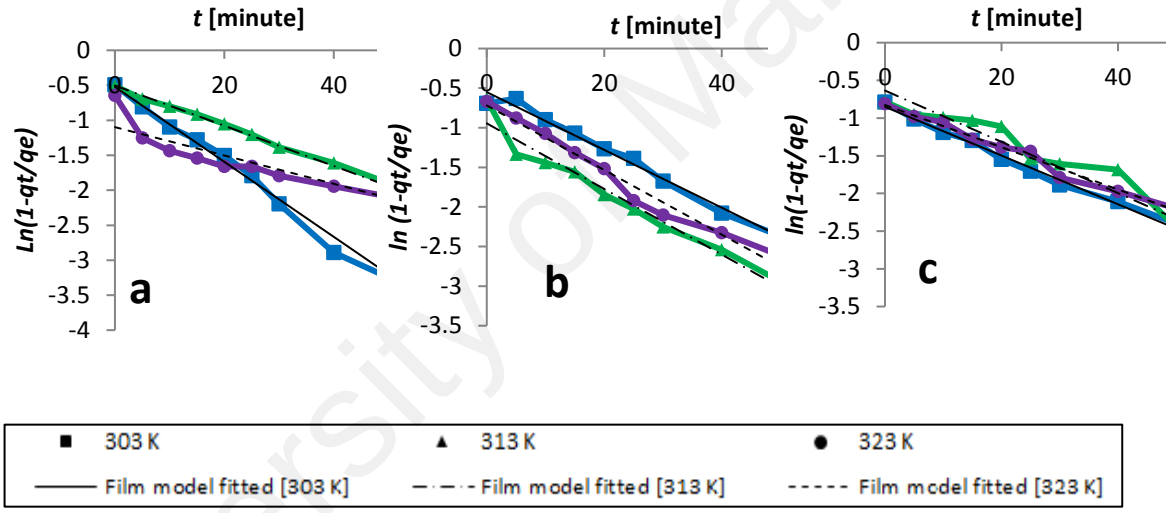

Figure 4.18: Film diffusion model fits for a) 25 µg ml^{-1}, b) 50 µg ml^{-1} and c) 100 µg ml^{-1} of initial concentration of CR on NICSS system at different temperatures

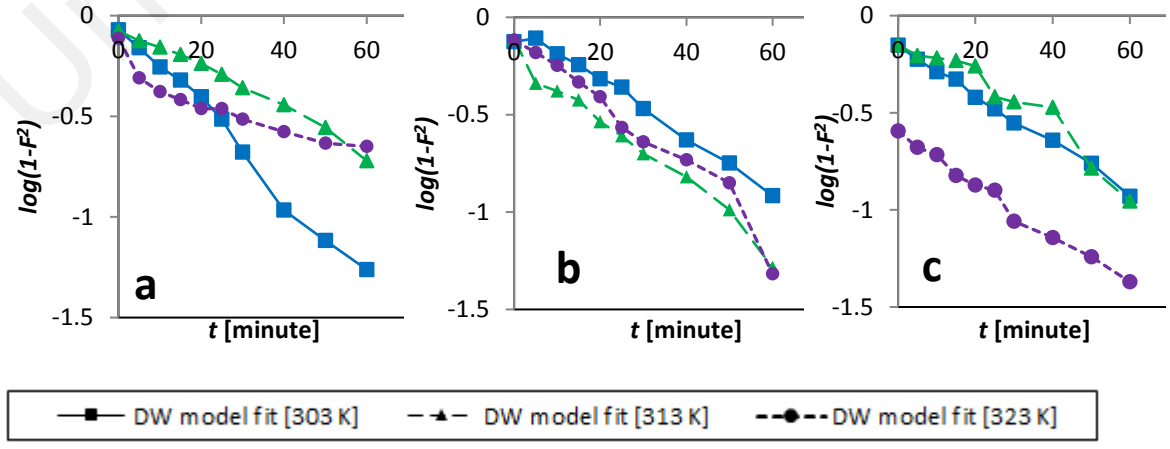

Figure 4.19: Dumwald-Wagner model fits for a) 25 µg ml^{-1}, b) 50 µg ml^{-1} and c) 100 µg ml^{-1} of initial concentration of CR on NICSS system at different temperatures

Table 4.8: Calculated thermodynamic parameters of CR-NICSS system

Initial concentration [μg ml^{-1}]	Temp [K]	ΔG° [kJ mol^{-1}]	ΔS° [J mol^{-1} K^{-1}]	ΔH° [kJ mol^{-1}]
	303	-1.84897		
100	313	-2.38445	52.42892	14.0332
	323	-2.89706		
	303	-2.30827		
50	313	-2.65862	55.0736	14.44308
	323	-3.41845		
	303	-1.64733		
25	313	-2.13642	54.68617	14.94026
	323	-2.74356		

concentrations multiple levels of linearity can be observed. For lower initial concentration (25 μg ml^{-1}) at lower temperature, the rate of adsorption is high and then it appears to be a shift in the rate following a different linear trajectory until finally the rate stabilizes with respect to time. However, at higher temperatures the rate seems to be more linear. It can also be seen that at higher concentrations of solute (100 μg ml^{-1}) there seems to be less apparent changes in the rate of adsorption. This can especially be seen when fitting the higher temperature data to the film diffusion model of Boyd et al., 1947. As seen in the Figure 4.18, it can be affirmed that the data shows good adherence to the model with R^2 values of 0.99 and gives the liquid film diffusion constant R| (Table 4.7). This shows that at higher temperatures the rate of adsorption is very negligibly hindered by diffusional limitations. This implies that diffusion is the rate limiting process. The solute initially absorbs quickly onto the surface of the particles forming a film which then retards further diffusion – which explains the changes in absorption rates. The Dumwald-Wagner model has been used to calculate the true absorption rate constant (K) as seen in Figure 4.19 with corrections for observed diffusion effects (Table 4.7).

The ΔG° is negative for all studied temperatures indicating that the adsorption of CR on NICSS follows a spontaneous and favorable trend. The decrease in ΔG° with

increase in temperature indicates increase in adsorption at higher temperatures. The positive value of ΔS° suggests good affinity of CR towards the adsorbent and increased randomness at the solid solution surface (Table 4.8).

4.5 Statistical optimization by fractional factorial experimental design

The first step of the optimization was to determine and fit an appropriate model regression to the experimental data obtained based on a fractional factorial experimental design (FFED).

$$q_e = 32.82 + 7.08 \times A + 1.5 \times B + 19.98 \times C - 23.38 \times D - 11.07 \times AB + 4.6 \times AC + 0.34 \times BC \pm 8.75 \times CE - 5.18 \times A^2 - 0.02 \times B^2 - 4.69 \times C^2 + 10.61 \times D^2 - 4.08 \times E^2$$

The optimal values of the variables determined by maximization of the second-order polynomial equation with interaction terms obtained by multiple regression analysis based on a FFED model and the input parameters were established as a pH of 2.5, a biosorbent dosage of 0.027 g L^{-1} and an initial dye concentration of 190 mg L^{-1} with an adsorption time of 166 minutes. The predicted adsorption capacity for those optimal values was 100 mg g^{-1}.

The fit of the quadratic polynomial equation to the experimental data was confirmed by both the regression coefficient, which is quite high with a value of 0.978, and the analysis of variance (ANOVA) (Table 4.9). The *p*-value for the *f*-test with a value lower than 0.5 indicates that the equation is a statistically significant regression model. Thus it can be successfully used in optimization of Congo red biosorption. The results confirm the accuracy of approximation by the quadratic equation. The statistical significance of each operating factor was evaluated by *f*-test and *p*-values (Table 4.9). The *f*-test for testing the significance of the individual terms of the model is based on the test statistic that is calculated by dividing a regression coefficient by its variance. The results of f-test and associated *p*-values with confidential level >95% reveal that the

most significant are A, C, D, AC and CE effects, while the others seems to be unimportant. The last step of the statistical optimization was the analysis of the 3D-response surface plots (Figure 4.21 - 4.23) as a function of two-independent variables, which served the purpose of determining the interaction effects between two parameters keeping the others at a fixed value (in this case the optimum value). Statistical process optimization, in a given range of parameter values, allows not only for calculating the optimal condition, but also for determining the effect of the process conditions on the biosorption. In can be observed that lower the biosorbent dosage (D) and pH (E), higher the adsorption capacity (q_e).The values of the regression coefficients, in Equation 1, indicate the effect the parameter has on the adsorption capacity. Positive values indicate incremental effect, for example, an increase in the initial dye concentration (C) causes a significant increase in adsorption capacity. Likewise, a negative value indicates a detrimental effect, as seen in the case of pH (E), i.e., an increase in pH decreases the adsorption capacity of the adsorbent. This is graphically represented in the 3D-surface and 2D-contour plots (Figure 4.20 - 4.22).

As the values of processing time, process temperature and initial dye concentration increase there is an observable increase in absorption capacity, whereas, when considering their combined effect (i.e., for example effect of process time and process temperature on adsorption capacity) there is almost negligible effect (reflected by the coefficient value). Similarly, individually, the adsorbent dosage and pH have negative values for co-efficient, indicating that as their value increases the adsorption capacity decreases.

The dependence of the adsorption capacity on the initial dye concentration indicates the occurrence of a maximum of about 100 mg L^{-1}, which was confirmed by maximization of obtained quadratic polynomial expression. Increasing the dose of

adsorbent should lead to almost complete removal of a pollutant from an aqueous solution and the results reflect this.

Table 4.9: ANOVA for Fractional factorial experimental design

Source	Coefficient	Sum of Squares	Degree of freedom	Mean Square	*f* value	*p* value
Model	--	18927.87	14	1351.99	402.6	< 0.0001**
A	7.08	764.21	1	764.21	227.56	< 0.0001**
B	1.5	34.62	1	34.62	10.31	< 0.0001**
C	19.98	1739.82	1	1739.82	518.08	< 0.0001**
D	-23.38	1469	1	1469	437.43	< 0.0001**
E	-11.07	256.26	1	256.27	76.31	< 0.0001**
AB	-0.07	0.15	1	0.15	0.045	0.833
AC	4.6	181.57	1	181.57	54.07	< 0.0001**
BC	0.34	0.97	1	0.97	0.29	0.592
CE	-8.75	81.67	1	81.67	24.32	< 0.0001**
A^2	-5.18	325.74	1	325.74	96.99	< 0.0001**
B^2	-0.02	0.007	1	0.007	0.002	< 0.0001**
C^2	-4.69	100.66	1	100.66	29.97	0.055
D^2	10.61	202.3	1	202.3	60.24	< 0.0001**
E^2	-4.08	74	1	74	22.04	0.149
Residual	--	426.5	127	3.36		
Lack of fit	--	422.7	123	3.44	3.63	0.107
Total	--	19354.37	141			

Significant figures

Suggestive significance (p value: $0.05<p<0.10$)
Moderately significant (p value: $0.01<p\leq 0.05$)
**Strongly significant (p value: $p\leq 0.01$)

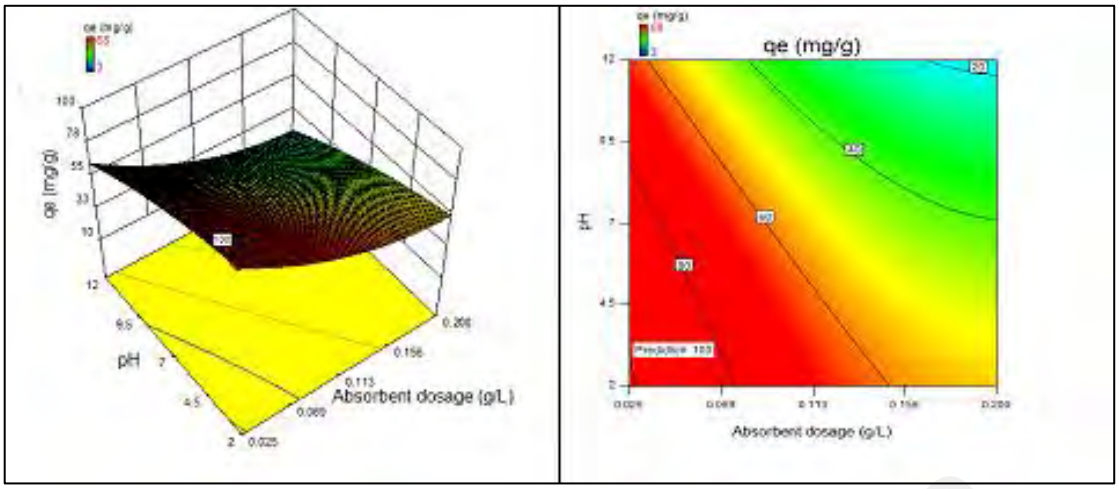

Figure 4.20: 2D-contour plot and 3D-surface plot showing the variation of adsorption capacity with adsorbent dosage and pH

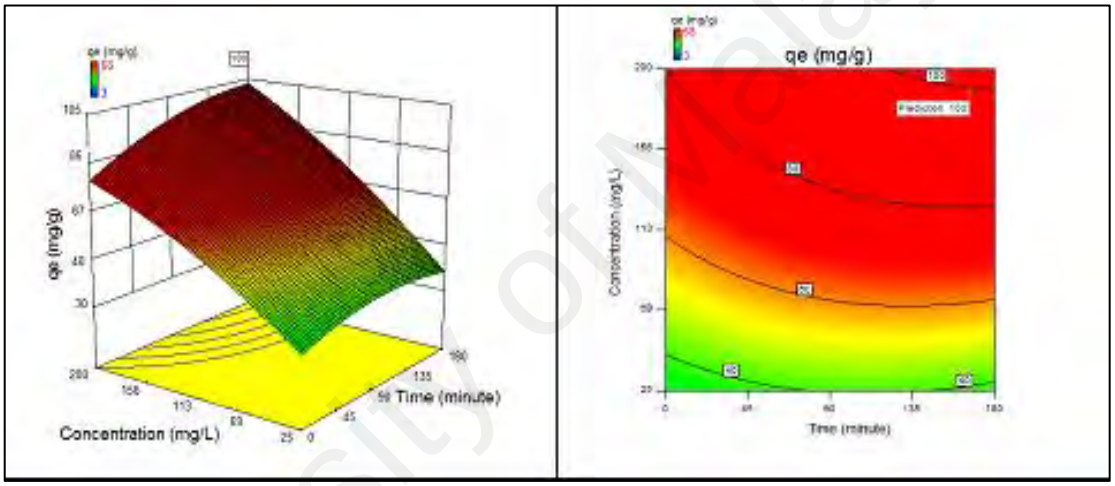

Figure 4.21: 2D-contour plot and 3D-surface plot showing the variation of adsorption capacity with time and concentration

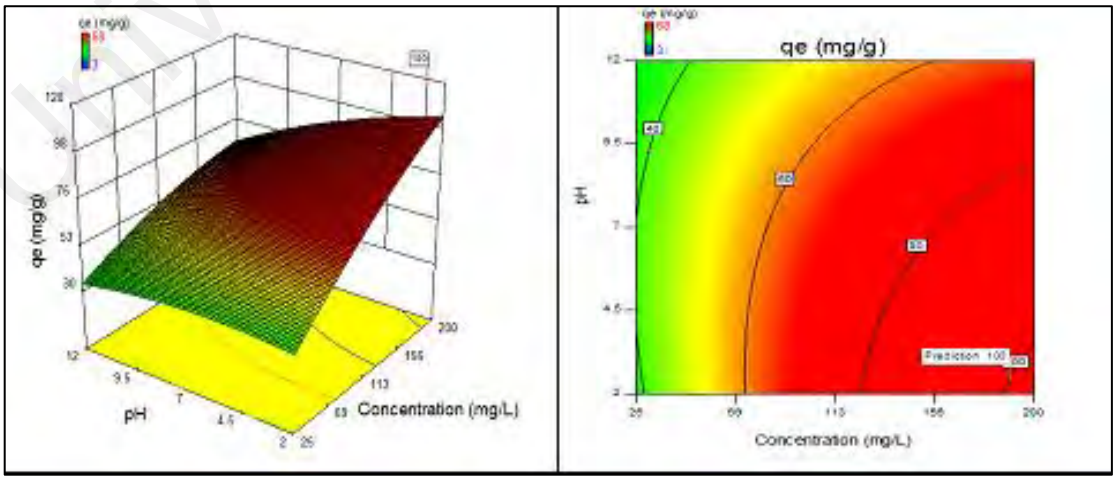

Figure 4.22: 2D-contour plot and 3D-surface plot showing the variation of adsorption capacity with concentration and pH

4.6 Tensile strength

The tensile strengths of Polypropylene/Congo red dye adsorbed on NICSS (PP/CR-NICSS) and PP/NICSS composites are shown in Figure 4.23. The tensile strength of the composites reduced from 28.76 to 21.84 MPa and from 29.6 to 20.89 MPa with increase in PP/CR-NICSS and PP/NICSS content respectively. Lu et al., 2005 reported that from 10 to 40% wt. the mechanical properties of wood plastic composites increased at low weight percentages of filler and gradually decreased with increase in filler content. Dänyädi et al., 2007 reported that, at large wood plastic content considerable particle aggregation takes place, leading to the reduction in strength due to the filler's failure to sustain the stress transferred from the polymer to the filler. In general, addition of lignocellulosic natural fillers/fibers in a non-polar polymer matrix is limited because of the difference in surface nature of the constituents. Consequently, the ultimate tensile strength decreases with increase in the reinforcement content (Mutje et al., 2007, Malkapuram et al., 2009).

Combination of CR-NICSS and NICSS with MA-g-PP enhanced the compatibility with PP matrix. MA-g-PP lowered the surface tension of CR-NICSS and NICSS and increased wettability with the PP matrix. The formation of ester linkage between the anhydride group of MA-g-PP and hydroxyl groups of the natural filler has been reported (Nicolais & Narkis, 1971).

The tensile strength values obtained have been analyzed and the tensile strength of the composites was also calculated theoretically using Nicolais and Narkis model (Nicolais & Narkis, 1971) as given below in equation 4.1;

$$\sigma_{comp} = \sigma_{PP}\left(1 - 1.21\phi_f^{\,2/3}\right) \qquad \textbf{(4.1)}$$

where, σ_{comp} and σ_{PP} represent the tensile strengths of composite and neat PP, respectively. ϕ_f is the volume fraction of filler. The calculated tensile strength value

differs from the experimental result because no adhesion between matrix and filler (Figure 4.24).

4.7 Tensile modulus

The tensile modulus of composites increased from 1363 to 1659 MPa and 1359 to 1636 MPa with increase in CR-NICSS and NICSS content from 10 to 50 % wt respectively (Table 4.10). Filler addition restricts the mobility of PP chains and hence, the tensile modulus is increased. The tensile modulus of PP/CR-NICSS and PP/NICSS composites are shown in Figure 4.24. Two models were used to evaluate tensile modulus theoretically. Kerner's Model is given below;

$$E_{comp} = E_{PP}\left[1.0 + \left(\frac{\phi_f}{1-\phi_f}\right)\left(\frac{15(1-\upsilon)}{(8-10\upsilon)}\right)\right] \quad \textbf{(4.2)}$$

where, E_{comp} and E_{PP} represent the Young's modulus of the composite and neat PP, respectively. υ is the Poisons ratio of PP and it was taken as 0.4 (Biron, 2012). The values obtained by Kerner's model are plotted in Figure 4.25. The experimental values are different from the theoretical values obtained from Eq. (2) as the model assumes no interaction between matrix and filler.

The model formulated by Sato & Furukawa, 1963 which incorporates an adhesion parameter, ξ is as given below;

$$E_{comp} = E_{PP}\left[\left(1 + \frac{{\phi_f}^{2/3}}{2-2{\phi_f}^{1/3}}\right)(1-\psi\xi) - \frac{{\phi_f}^{2/3}\psi\xi}{\left(1-{\phi_f}^{1/3}\right)\phi_f}\right] \quad \textbf{(4.3)}$$

where, $\psi = \left(\frac{\phi_f}{3}\right)\left[\frac{1+{\phi_f}^{1/3}-{\phi_f}^{2/3}}{1-{\phi_f}^{1/3}+{\phi_f}^{2/3}}\right]$

In Eq. (3), the value of ξ was found to be 0.82. Sato & Furukawa, 1963 suggested that the filler gets detached from the matrix due to the poor adhesion. The adhesion scale varies from 0 to 1 for perfect adhesion to no adhesion. In the present

study, the value of 0.4 indicates a slight adhesion between matrix and filler, which might have resulted due to MA-g-PP.

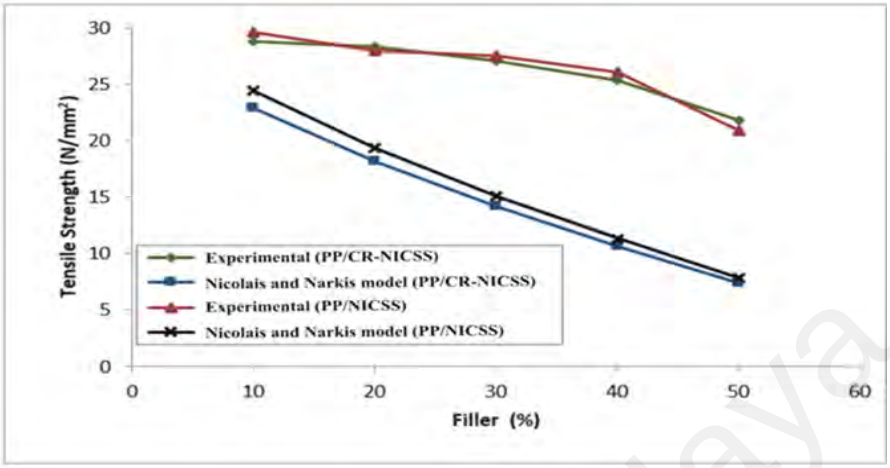

Figure 4.23: Variation in tensile strength with filler content

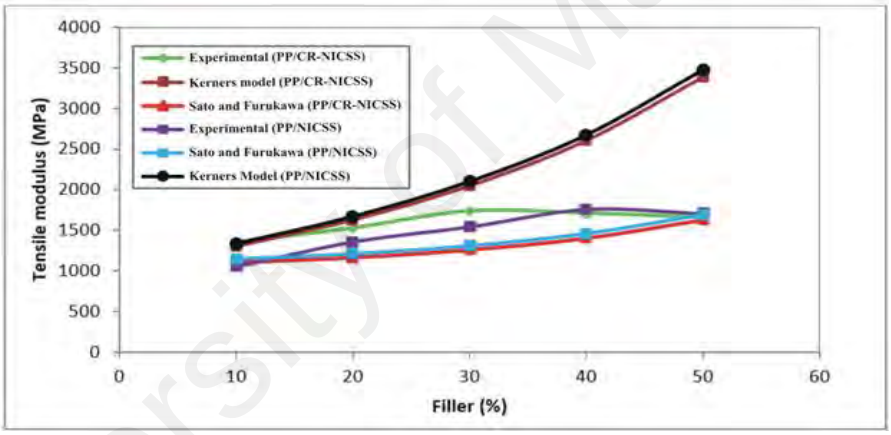

Figure 4.24: Variation in tensile modulus with filler content

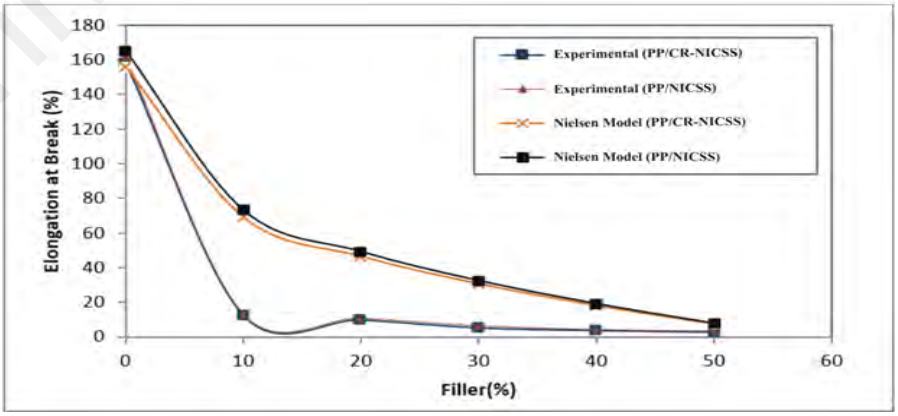

Figure 4.25: Variation in elongation at break with filler content

4.8 Tensile elongation at break

Biofillers cause a remarkable reduction in elongation at break. About 98% reduction in elongation at break was recorded for 50% of filler content compared to neat PP. This is in agreement with previous reports on wood-particle thermoplastic composites (Robin & Breton, 2001; Park & Balatinecz, 1997). More than 77% reduction in elongation at break was recorded with 50% filler content as compared to 10% filler composites (Figure 4.25). This is due to filler material, which severely affects ductility of PP. Figure 4.25 shows the plot of elongation at break versus percent CR-NICSS and NICSS content in composites. As the CR-NICSS and NICSS loading increases, elongation at break gets reduced drastically as the rigid CR-NICSS and NICSS do not elongate.

Nielsen model has been used to determine theoretical values of elongation at break by applying following equation 4.4;

$$\varepsilon_{comp} = \varepsilon_{PP}\left(1 - k\phi_f^{1/3}\right) \quad \textbf{(4.4)}$$

where, ε_{comp} and ε_{PP} are elongation at break values for the composite and neat PP, respectively. In eq. (6), k is an adjustable parameter which depends on filler geometry. k value was determined by trial and found to be 1.3. The calculated elongation at break is plotted in Figure 4.25. The experimental values are lower than those predicted by the model. Bataille et al., 1984 reported that when mica was added as filler, in PVC the predicted value deviated. In most compatibilized composites, tensile strength values increased while elongation reduced.

4.9 Flexural properties

Stiffness of composite materials is an important engineering property in load bearing and structural applications (Neagu et al., 2006). The bio-fillers serve as useful reinforcement materials of plastics to get increased stiffness. Flexural strength of

composites increased after incorporation of CR-NICSS and NICSS into PP matrix (Table 4.11).

Table 4.10: Effect of filler loading on tensile properties with filler content

Composition (%)		Tensile strength (MPa)		Tensile modulus (MPa)		Tensile elongation at break (%)	
PP	Filler						
		PP/CR-NICSS	PP/NICSS	PP/CR-NICSS	PP/NICSS	PP/CR-NICSS	PP/NICSS
100	00	31.0	31.0	1041	1041	158	158
90	10	28.76	29.6	1363	1359	12.4	13.2
80	20	28.37	27.95	1532	1543	9.8	10.7
70	30	27.35	27.53	1739	1759	5.2	6.4
60	40	25.38	26.03	1713	1706	3.7	4.1
50	50	21.84	20.89	1659	1636	2.8	3.2

Table 4.11: Effect of NICSS filler loading on flexural properties of PP/NICSS composites

Composition (%)		Flexural strength (MPa)		Flexural modulus (MPa)	
PP	Filler	PP/CR-NICSS	PP/NICSS	PP/CR-NICSS	PP/NICSS
100	00	30.9	30.9	899	899
90	10	47.3	48.4	1430	1497
80	20	48.2	49.3	1598	1612
70	30	51.4	50.9	1764	1785
60	40	52.1	51.7	2247	2314

Table 4.12: Effect of NICSS filler loading on Physical properties of PP/CR-NICSS PP/NICSS composites

Filler (% wt)	Density (g/cm^3)		Surface hardness (Shore D)		Water absorption (%) in 48 h	
	PP/CR-NICSS	PP/NICSS	PP/CR-NICSS	NICSS-PP	PP/CR-NICSS	PP/NICSS
Neat PP	0.911	0.911	71	71	0.01	0.01
10	0.938	0.938	75	74	0.14	0.15
20	0.996	0.996	76	77	0.29	0.31
30	1.012	1.012	79	80	0.76	0.81
40	1.059	1.059	81	83	2.87	2.67

Increase in flexural strength was observed for 40 % CR-NICSS and NICSS filled composites. The flexural modulus increased from 899 to 2247 MPa and 899 to 2314 MPa with increase in filler content of CR-NICSS and NICSS composites, respectively. This increase in flexural properties can be attributed to better dispersion of CR-NICSS and NICSS particles in PP matrix and also better stress transfer from matrix to filler via compatibilizer.

4.10 Water absorption

Water absorption by PP composites in 48 h immersion is shown in Table 4.12. The PP matrix does not absorb moisture (Bledzki et al., 2005) and the moisture is absorbed only by the lignocellulosic component in the composites. Lignocellulosic fillers contain numerous free -OH groups in the cellulosic cell wall materials, which interact with water molecules by hydrogen bonding. The absorption of water by biobased composites is largely dependent on the availability of free –OH groups on the surface of the reinforcing filler. The interfacial adhesion between matrix and filler through MA-g-PP causes fewer void content in the interfacial region, and also more hydrophilic groups as hydroxyls are blocked by the coupling effect (Espert et al., 2004), which could decrease the extent of moisture absorption by the composite. The reason being that, there are three main regions where the adsorbed water in the composite can reside: the cell wall, the lumen (via porous tubular), and the voids between lignocellulosic material and PP in the case of weak interface adhesion. Since voids and the lumens of fillers/fibers of lignocellulosic materials are filled with melt polymer during extrusion, the penetration of water by capillary action into the deeper parts of composite gets prevented. This suggests that the water absorption might have occurred in the surface layer. It is obvious that CR-NICSS and NICSS cause slightly higher values of moisture uptake, compared to the unfilled composites.

During extrusion, the cellular structure of the filler gets collapsed and/or filled in by the PP, which reduces the void volume of the original cellular structure (Aurrekoetxea et al., 2008). Due to the high melt viscosity of the molten PP, the smaller cells of lignocellulosic filler cannot be filled by the matrix and the high external pressure is not compensated, consequently the cell structure collapses. However, in case of bigger cells, the molten PP was filled in the cavity and compensates the external pressure.

4.11 Wear properties

Wear volume as a function of abrading distances of neat PP and its composites with PP/CR-NICSS and PP/NICSS for loads of 23.54 and 33.54 N are presented in Figures 4.26 to 4.33. Wear volume increased with higher applied load for all composites, which is manifested by the deeper grooving on the sample surface and more material removal from the sample with increasing load. Abrasive particles penetrate deeper into the softer PP, forming deeper furrow tracks. The wear tracks formed by the abrasive particles further deepen by increasing the load from 23.54 to 33.54 N. The interaction between the abrasives and the composite surfaces results in the formation of stresses at the contact points. The extent of material deformation is primarily depends on the magnitude of these stresses. From the Figures 4.26 to 4.33 it is clear that, wear volume increases with higher filler content. At lower filler content, dispersion of CR-NICSS and NICSS in matrix is good and hence its wetting with PP matrix is better. Consequently, particle resists from getting debonded from matrix. Whereas at higher filler content, CR-NICSS and NICSS particles get agglomerated due to hydrogen bonding between CR-NICSS and NICSS particles (strong filler-filler interaction) as a result of the interaction between CR-NICSS and NICSS particles with PP matrix is reduced and CR-NICSS and NICSS particles can be easily deboned from the matrix.

Weight loss increases with higher sliding distance at all applied loads because of progressive material removal with sliding distance. The temperature at the contact region during abrasion increases with higher sliding distance, which further causes loosen of bond and more material removal. CR-NICSS-PP and NICSS-PP composites with lower CR-NICSS and NICSS content exhibited minimum weight loss at all applied loads.

The specific wear rates data display a sudden dip at lower abrading distance followed by a steady state. It can be further explained with a proposed wear mechanism of the CR-NICSS and NICSS composites. There are two possible damage features. First, scratching of filler particles along the sliding direction. This is controlled by the interfacial adhesion characteristics of the filler with the matrix. If the interfacial adhesion is strong to prevent debonding of filler particles, scratching could take place to the filler particles. Second, if the sliding force is higher than the interfacial adhesion, debonding followed by detachment of filler particles could occur. On the other hand if the filler particles are exposed to the counter face, there is no possibility of detachment due to the deep embedding of the filler particles in the bulk of the composite (Figures 4.26-4.33). However, there is a possibility of generating cracks close to the filler particles and perpendicular to the sliding direction due to the side shear force. This can be clarified by examining the worn surface of the composite. In order to determine the wear mechanism responsible for the observed wear loss, the morphology of the worn surfaces of samples of 20, 30 and 50% of PP/CR-NICSS were examined using SEM and the results are shown in Figures 4.34-4.36.

Wear mechanism has following steps: (i) plastic deformation of matrix, (ii) microcutting, (iii) microploughing of the composites and (iv) debonding of CR-NICSS and NICSS from matrix. After CR-NICSS and NICSS debonding, abrasive particles could easily detach the debris of CR-NICSS and NICSS from the sample. Hard abrasive

particles ploughed out of the debris from the sample and subsequently deepen the grooves. In wear processes of reinforced polymer composites, interaction of the matrix with the reinforcement is a significant parameter. It has been observed that at lower filler loading, increases the bonding between filler and matrix did not allow to the debonding of CR-NICSS and NICSS from the matrix and even created hindrance in the path of asperities which resulted in reducing of material loss.

In brief, incorporation of filler into a polymer matrix may either enhance or reduce the tensile strength of the composite. Fiber type reinforcements normally improve the tensile strength as the fibers can support stresses transferred from the polymer. But in irregularly shaped fillers, the strength of the composites decreases as the filler cannot bear the stress transferred from the polymer matrix.

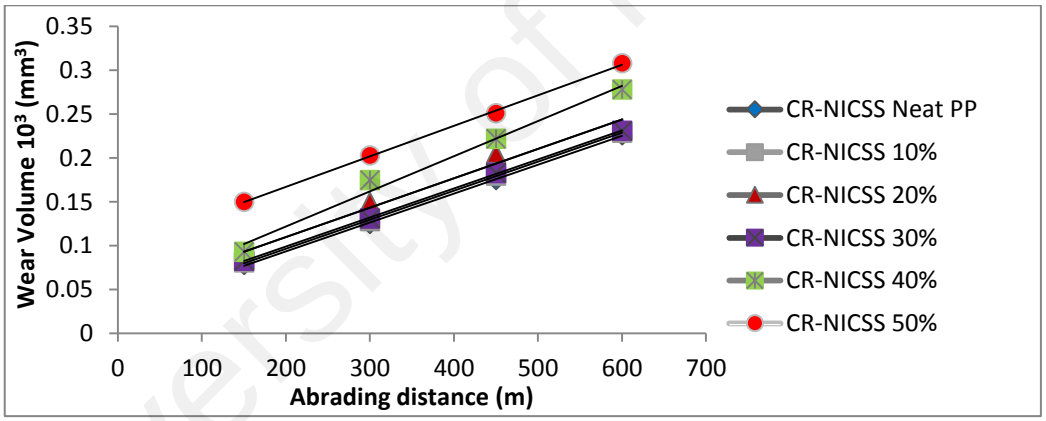

Figure 4.26: Wear volume of neat PP and PP/CR-NICSS composites at 23.54 N

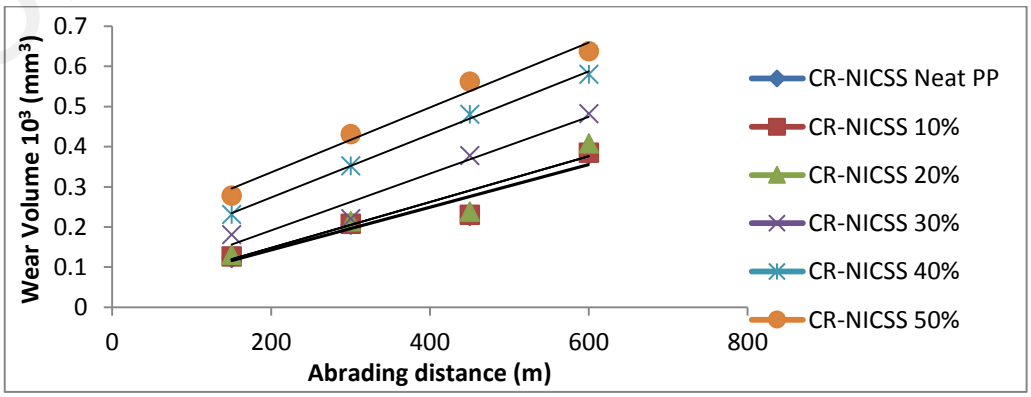

Figure 4.27: Wear volume of neat PP and PP/CR-NICSS composites at 33.54 N

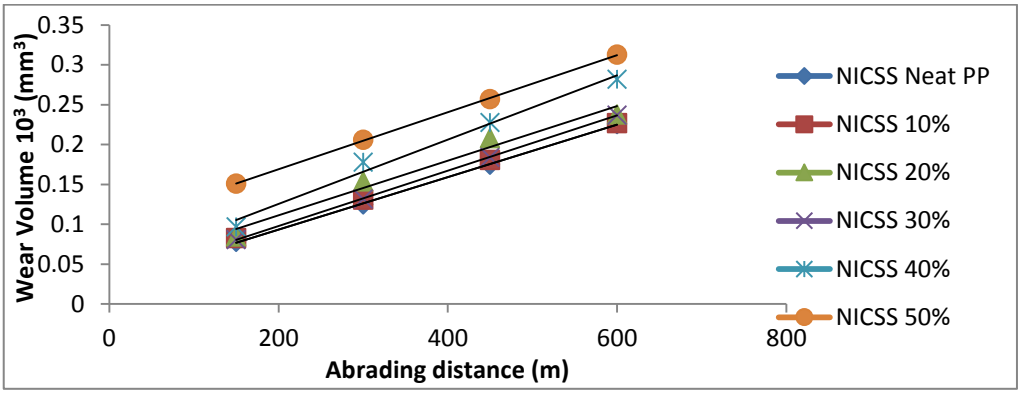

Figure 4.28: Wear volume of neat PP and PP/NICSS composites at 23.54 N

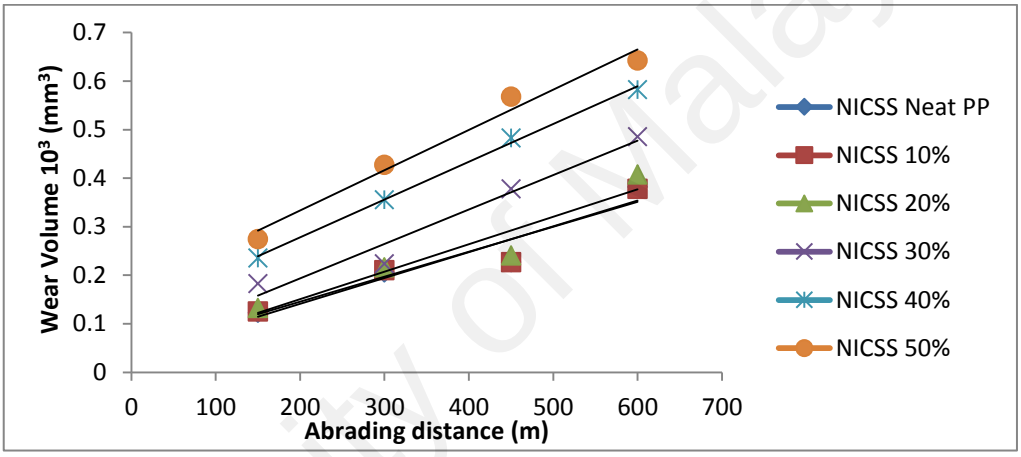

Figure 4.29: Wear volume of neat PP and PP/NICSS composites at 33.54 N

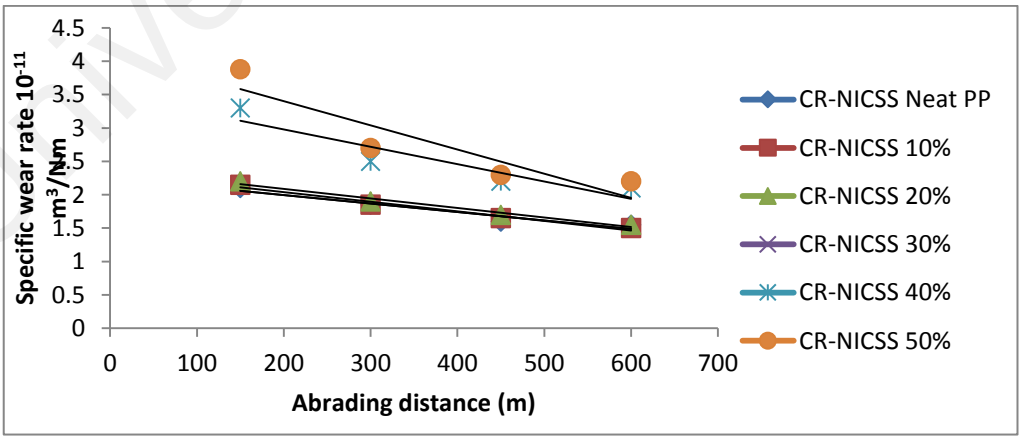

Figure 4.30: Specific wear rate of neat PP and PP/CR-NICSS composites at 23.54 N

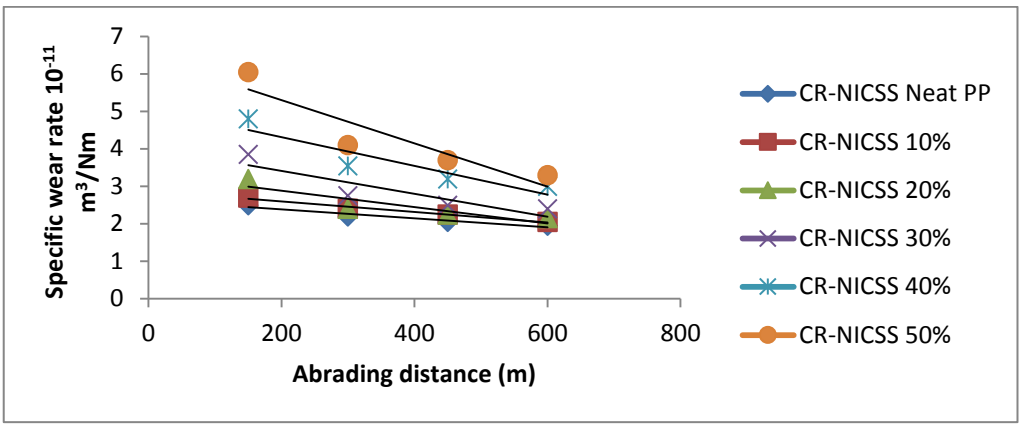

Figure 4.31: Specific wear rate of neat PP and PP/CR-NICSS composites at 33.54 N

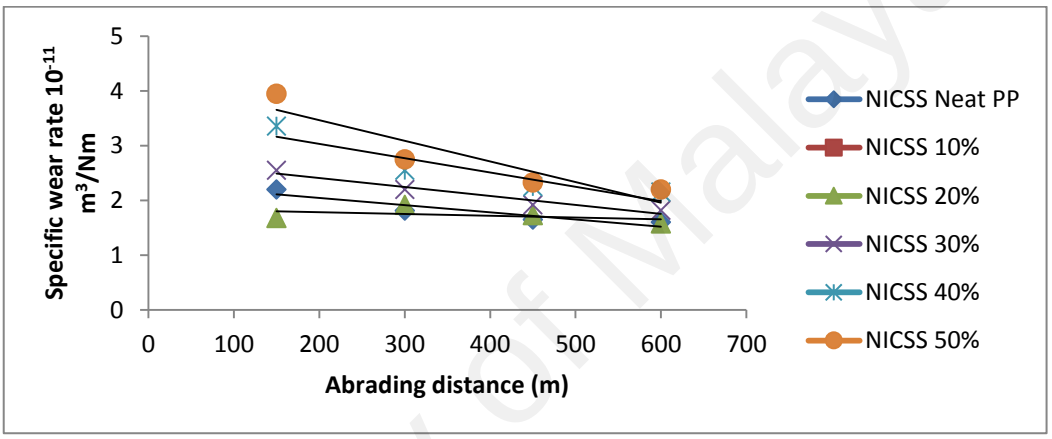

Figure 4.32: Specific wear rate of neat PP and PP/NICSS composites at 23.54 N

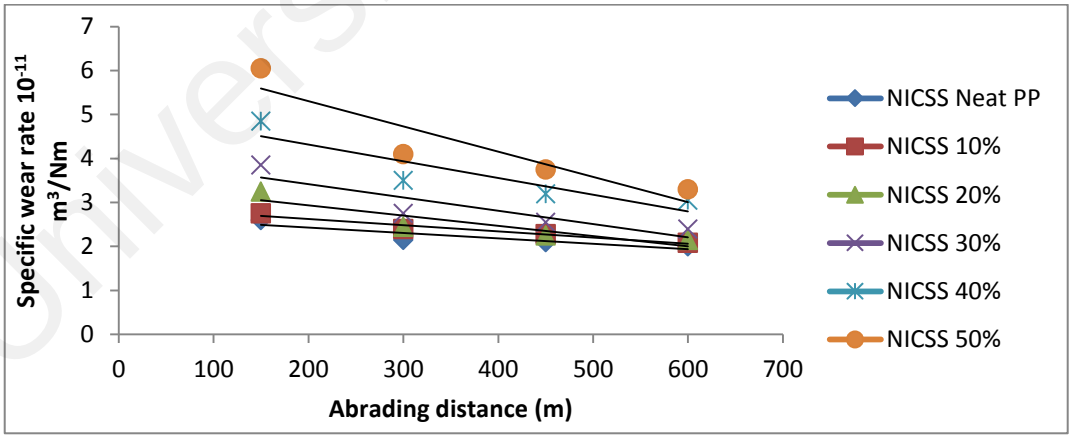

Figure 4.33: Specific wear rate of neat PP and PP/NICSS composites at 33.54 N

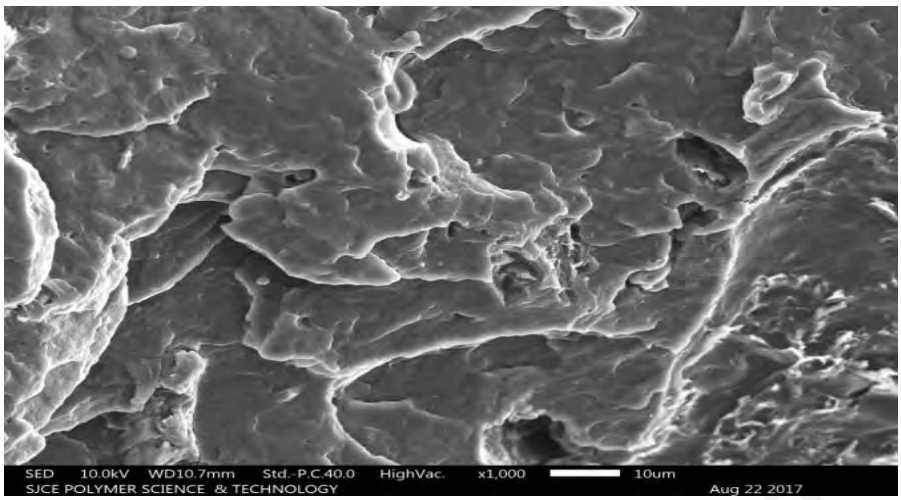

Figure 4.34: SEM image of CR-NICSS-20% PP 1K Tensile at break

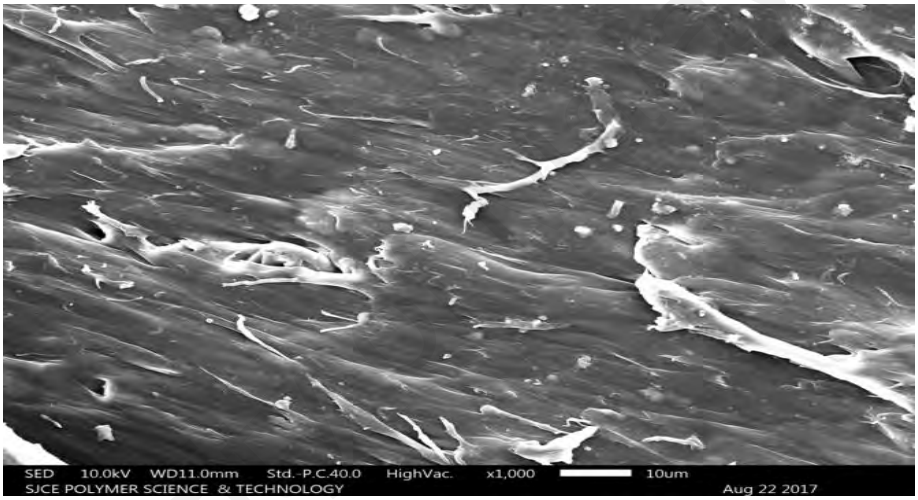

Figure 4.35: SEM image of CR-NICSS-30% PP 1K Tensile at break

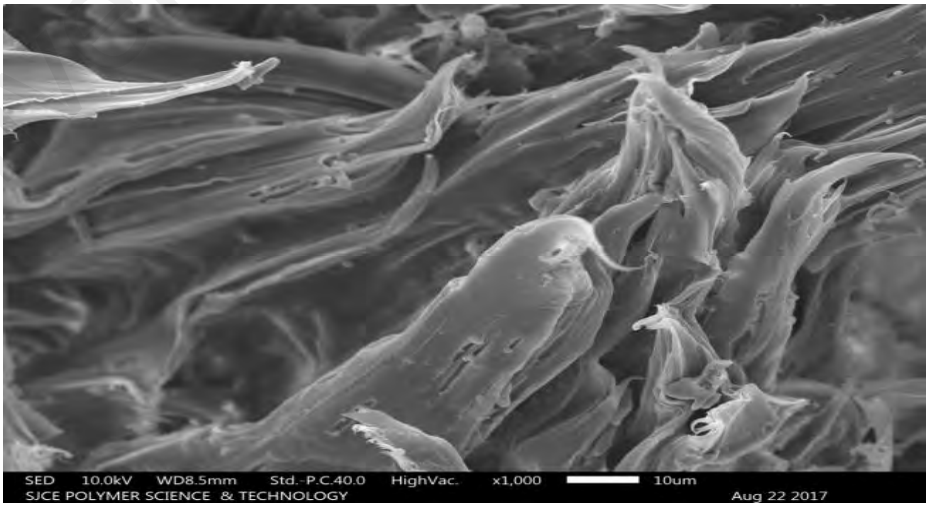

Figure 4.36: SEM image of CR-NICSS-50% PP 1K Tensile at break

4.12 Thermal stability

TGA has proved to be a suitable method to investigate the thermal stability of polymeric systems (Hatakeyama & Quinn, 1999). Thermal degradation and mode of decomposition under the influence of heat is highly recommended for the optimization of process parameters. All the PP/NICSS and PP/CR-NICSS composites were stable up to 400-450^{0}C. The threshold decomposition temperature gives an indication of the highest processing temperature that can be adopted. A small difference is seen between CR-NICSS and NICSS as fillers. It is inferred that almost 10% of the Congo red dye adsorbed onto NICSS will have minimum influence on the thermal stability of the resulting composites as seen in TGA and DTA curves (Figures 4.37-4.40).

4.13 USP/CR-NICSS and USP/NICSS thermosets

The CR-NICSS and NICSS fillers appear to act as particulate filler. The density, surface hardness, void content and specific tensile strength of USP/CR-NICSS and USP/NICSS composites are shown in Table 4.13. Neat resin cast had higher tensile strength of 44.7 MPa than the filled composites. The tensile strength of USP/ CR-NICSS and USP/NICSS composites decreased with increasing CR-NICSS and NICSS content (Table 4.13). In most cases, tensile strength of filled systems is lower than that of unfilled polymers (Yang et al., 2004; Raj et al., 1990). These results manifest that decreasing interfacial adhesion and homogeneity with increase in CR-NICSS and NICSS loading. The CR-NICSS and NICSS particles tend to agglomerate due to lignin and hydroxyl groups on the cellulose. These agglomerates behave like larger size particles, thus reducing the effective adhesion surface (Albano et al., 2001). Weak interfacial bonding causes partially separated microspaces between filler and polymer matrix, which obstructs stress propagation, when tensile stress is loaded and induces brittleness (Ramaraj, 2007).

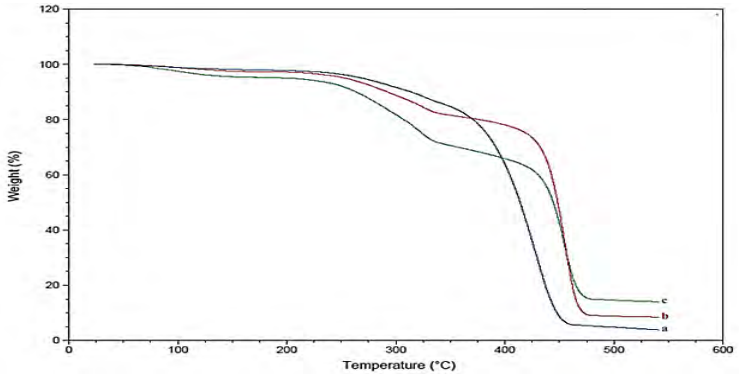

Figure 4.37: Thermogravimetric curves of (a) PP/CR-NICSS; 80:20 (b) PP/CR-NICSS; 70:30 and (c) PP/CR-NICSS; 50:50

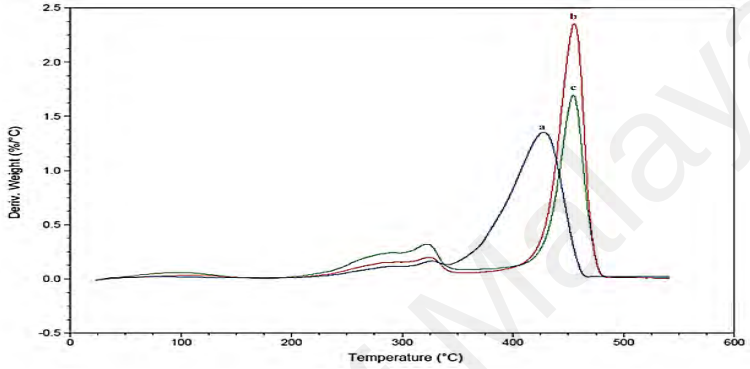

Figure 4.38: Differential thermal analysis curves of (a) PP/CR-NICSS; 80:20 (b) PP/CR-NICSS; 70:30 and (c) PP/CR-NICSS; 50:50

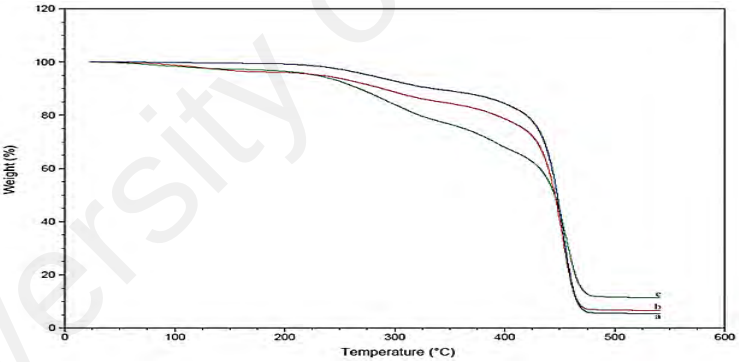

Figure 4.39: Thermogravimetric curves of (a) PP/NICSS; 80:20 (b) PP/NICSS; 70:30 and (c) PP/NICSS; 50:50

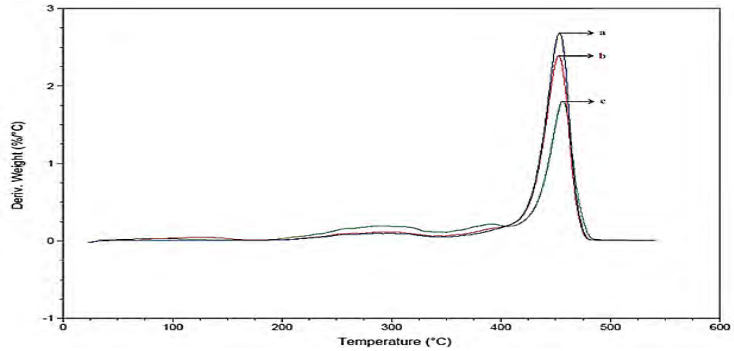

Figure 4.40: Differential thermal analysis curves of (a) PP/NICSS; 80:20 (b) PP/NICSS; 70:30 and (c) PP/NICSS; 50:50

CR-NICSS and NICSS particles may hinder the crosslinking and reduce the interaction between polymer networks, thereby reducing the strength of composite. Mechanical properties of composites depend on filler content, particle size and shape, extent of adhesion between filler and polymer matrix and degree of dispersion of the filler within the matrix. As the surface area of CR-NICSS and NICSS increases, good particle dispersion in the matrix polymer enhances interfacial adhesion between the filler and polymer (Maiti & Lopez, 1992; Lin et al., 2002). By the increase in CR-NICSS and NICSS loading, the tensile strength of composites decreased compared to neat USP. This can be attributed to the poor compatibility between the polar hydrophilic CR-NICSS and NICSS and the USP matrix. This indicates that the poor adhesion between USP and CR-NICSS and NICSS, as also between matrix and CR-NICSS and NICSS is supported by the theoretically obtained tensile strength as presented in Table 4.13.

Table 4.13 shows that unfilled USP neat resin cast had density of 1.224 g/cc. After incorporating CR-NICSS and NICSS, density of composites slightly increased as compared to unfilled USP system. The increase of density is attributed to the incorporation of high density filler (1.32 g/cc) in low dense USP matrix. The density of the composites was 1.227 – 1.241 g/cc. The theoretical density calculated as shown in equation 5 for composites by weight additive principle, which states that:

$$d = w_1 d_1 + w_2 d_2 \quad \textbf{(4.5)}$$

where, d is the density of the composite, w_1 and w_2 are the weight fractions of the constituents and d_1 and d_2 are the corresponding densities. The theoretically obtained density values are slightly lower compared to corresponding experimentally obtained values (Table 4.13). This may be due to void formation and poor interfacial adhesion between matrix with CR-NICSS and NICSS in the composites.

Surface hardness of the unfilled USP is 89.0 shore D and for CR-NICSS and NICSS filled USP composites, it is 90.3 – 92.0 shore D. These results indicate slight

increase in the dimensional stability after incorporation of CR-NICSS and NICSS filler. This is one of the important properties required for engineering applications. Influence of water ageing on the tensile strength of the fabricated 80-120 mesh TS incorporated USP composite was measured by immersing the composites in distilled water for 24 h at room temperature (Table 4.14) and also in boiling water for 2 and 4 hours (Table 4.15). Only a marginal reduction in tensile strength of the composite was observed due to contact with water at room temperature as the hydrophilic filler is encapsulated by hydrophobic polymer matrix. This can be attributed to the plasticization effect by the adsorbed water. The percent reduction in tensile strength was more for samples exposed to boiling water compared to water ageing at room temperature. This is due to the increase in water uptake at higher temperature as the matrix volume expands at higher temperature and water molecules penetrate into the polymer matrix and weaken the intermolecular interaction between the chains. Also slight leaching of CR-NICSS and NICSS was observed due to Congo red.

CR-NICSS and NICSS filled USP composites were subjected to thermal ageing at 300^{o}C for 2 and 4 h and the influence of thermal ageing on tensile strength was studied (Table 4.16). Neat resin cast a slight improvement in tensile strength in 2 and 4 h thermal ageing. This may be due to the increase in crosslink density of USP after post curing. But in filled system there was marginal reduction in tensile strength after thermal ageing as compared to the corresponding samples before thermal ageing. This may be attributed to the presence of CR-NICSS and NICSS, which might have hindered further crosslink of USP and CR-NICSS and NICSS might have degraded at elevated temperature.

Table 4.13: Physico-mechanical properties of neat resin and USP/CR-NICSS and USP/NICSS composites

Filler Content (% by weight)		Densities of neat resin g/cc and USP composites				Surface hardness (shores)±2		Void content (%)		Specific tensile strength (KNm/kg)	
CR-NICSS	NICSS	USP/CR-NICSS		USP/NICSS		USP/CR-NICSS	USP/NICSS	USP/CR-NICSS	USP/NICSS	USP/CR-NICSS	USP/NICSS
		Experimental	Theoretical	Experimental	Theoretical						
0	0	1.221	-	1.221	-	89.0	89.0	-	-	37.0	37.0
5	5	1.225	1.228	1.229	1.228	90.6	90.2	0.45	0.47	25.8	25.6
10	10	1.226	1.230	1.218	1.230	91.6	91.8	0.89	0.91	25.1	25.0
15	15	1.236	1.240	1.238	1.240	92.0	0.98	0.98	0.97	21.6	21.4
20	20	1.245	1.241	1.249	1.241	92.2	1.07	1.08	1.04	19.0	19.2

Table 4.14: Effect of distilled water ageing on tensile strength of USP/CR-NICSS and USP /NICSS composites

Filler content %	Tensile strength (MPa) Without ageing		Tensile strength (MPa) after 24 h ageing	
	USP/CR-NICSS	USP/NICSS	USP/CR-NICSS	USP/NICSS
0	44	44	40	40
5	32	34	25	26
10	31	33	25	26
15	27	28	26	27
20	25	26	28	28

Table 4.15: Effect of boiling water ageing on tensile strength of USP/CR-NICSS and USP /NICSS composites

% Weight Filler content	Tensile strength (MPa) USP/ CR-NICSS			Tensile strength (MPa) USP/NICSS		
	Without ageing	2h ageing	4h ageing	Without ageing	2h ageing	4h ageing
0	46	35	35	46	35	35
5	34	18	18	35	19	19
10	32	22	16	32	21	17
15	30	20	16	30	20	16
20	26	18	16	26	18	16

Table 4.16: Influence of thermal ageing at 300^0C on tensile strength of USP/CR-NICSS and USP /CR-NICSS composites

Filler material Weight %	USP/CR-NICSS Tensile strength (MPa)			USP/CR-NICSS composites Tensile strength (MPa)		
	Without ageing	2h ageing	4h ageing	Without ageing	2h ageing	4h ageing
0	45	47	47	45	47	47
5	32	27	20	32	28	22
10	32	22	18	32	21	18
15	28	18	17	27	18	17
20	25	16	16	25	16	16

Table 4.17: Resistance of neat USP; USP/CR-NICSS (I) and USP/NICSS (II) composites to chemicals

Chemical reagents	Percentage change in weight after 7 days								
	Neat USP	5%		10 %		15%		20%	
		I	II	I	II	I	II	I	II
Water	1.18	2.19	2.21	3.18	3.20	3.46	3.46	5.12	5.13
10% Acetic acid	0.31	0.11	0.13	0.33	0.35	0.27	0.28	0.73	0.74
10 % Hydrochloric acid	0.35	0.40	0.41	0.48	0.50	0.51	0.52	0.53	0.56
10% Nitric acid	0.37	0.42	0.43	0.62	0.64	0.68	0.70	0.70	0.72
10% Ammonium hypochlorite	0.68	0.65	0.67	0.71	0.73	0.74	0.75	0.78	0.80
10 % Sodium hydroxide	2.93	3.23	3.35	4.30	4.40	5.86	5.91	7.43	7.44

The effects of chemicals on the USP composite specimens are given in (Table 4.17). It is clear from the (Table 4.17) that the unfilled USP CR-NICSS and NICSS filled USP composites showed good resistance to all chemical reagents tested except 10% (w/v) NaOH. Unfilled USP system showed least resistance to 10% (w/v) NaOH. With increase in the percentage weight of filler material the weight loss also increased. Standard deviation of the 5 replicates was well within 2%.

CHAPTER 5: DEVELOPMENT OF SUSTAINABLE AZO DYES ADSORPTION SYSTEM USING NUTRACEUTICAL INDUSTRIAL SPENT

5.1 Acid blue 113 – NIFSS system

5.1.1 Surface Characterization

The NIFSS surface was characterized by SEM which displayed a tortuous porous structure (Figure 5.1a). Upon adsorption it is observed that some of the pores are completely filled with the adsorbate (AB113 dye) forming a thin film over the particle (Figure 5.1b). The IR spectra of NIFSS (Figure 5.2) provide the information of the functional groups present which are detailed in 4.1.1. After adsorption of AB113 dye on NIFSS, it has been observed in the IR spectrum that the broad bands between 3200-3550 cm^{-1} due to N-H stretching of $-NH_2$ group in AB113 dye and between 3100-3500 cm^{-1} due to the hydroxyl groups of NIFSS has disappeared which confirms the formation of hydrogen bonds between $-NH_2$ and hydroxyl groups. In addition, the disappearance of a strong peak at 1500 cm^{-1} for N-N stretching in AB113 dye confirms the strong adsorption of the dye on NIFSS. Finally, based on the disappearance of IR absorption frequencies, it attributes that to a large extent AB113 dye has adsorbed on NIFSS.

5.1.2 Effect of parameters on adsorption process

5.1.2.1 Effect of pH

The adsorption capacity was highest at pH 2 (Figure 5.3). When the pH was increased from 2 to 6, adsorption capacity decreased considerably, while, between pH 6 to 10 q_e values decreased marginally. Thereafter, rapid decrease in q_e value was observed till pH 12. The higher values of the adsorption capacity of the NICSS at pH 2 is attributed to the formation of OH_2^+ ions on the NIFSS surface in the presence of large amounts of H^+ ions. NIFSS is a cellulosic material and it is a well-established fact that it contains hydroxyl groups in each separate elementary unit. Decrease in pH results in the increase in the number of OH_2^+ ions on the surface of NICSS. AB113 is a bisazo dye and

exhibits anionic charge in solvent of high polarity, such as water. The q_e= 94.00 mg g^{-1} and q_e = 50.00 mg g^{-1} at pH 2 and 7 respectively was observed with an initial AB113 dye concentration of 100 mg L^{-1}.

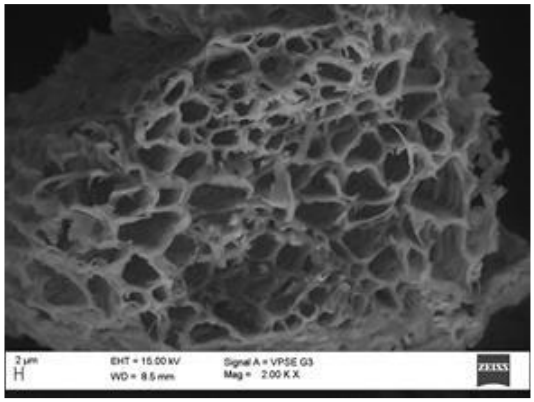

Figure 5.1a: SEM image of NIFSS

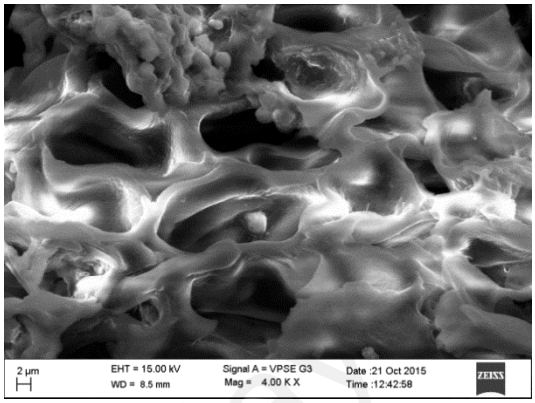

Figure 5.1b: SEM image of AB113-NIFSS

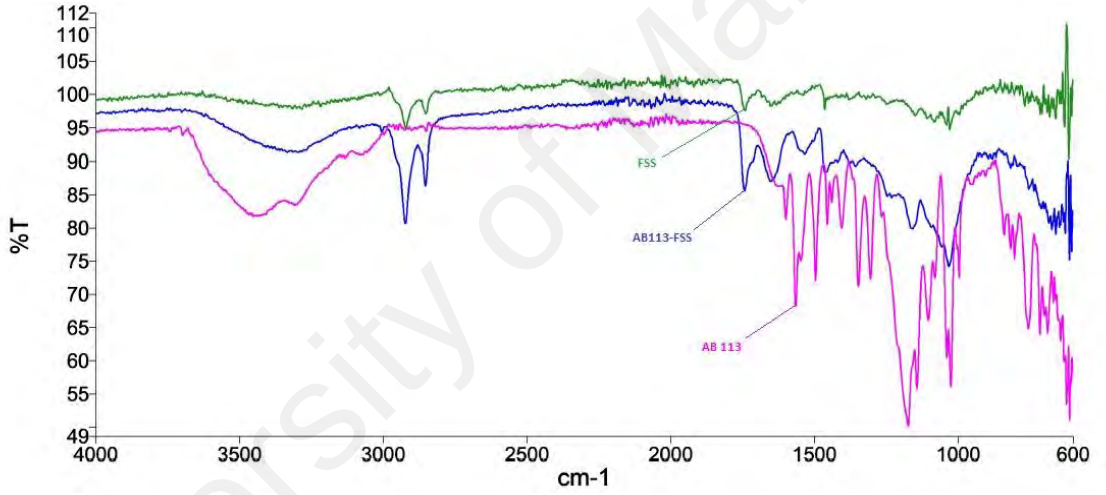

Figure 5.2: FTIR spectra of NIFSS, AB113 dye and AB113 dye adsorbed onto NIFSS

5.1.2.2 Effect of initial dye concentration

The maximum AB113 dye removal by NIFSS was at pH 2.0 with initial concentration of 100 mg L^{-1}. The q_e value increases with increase in initial dye concentration as shown in Figure 5.3 and reached maximum in the range 100-200 mg L^{-1} solution concentration. Thereafter, % q_e value remained almost constant uptill 300 mg L^{-1} and decreased drastically till 500 mg L^{-1}. The mass transfer phenomena of the dye on to the adsorbent are akin to the increasing driving force generated by the increasing concentration gradient of AB113 dye in the solution phase. This leads to equilibrium adsorption until saturation is attained.

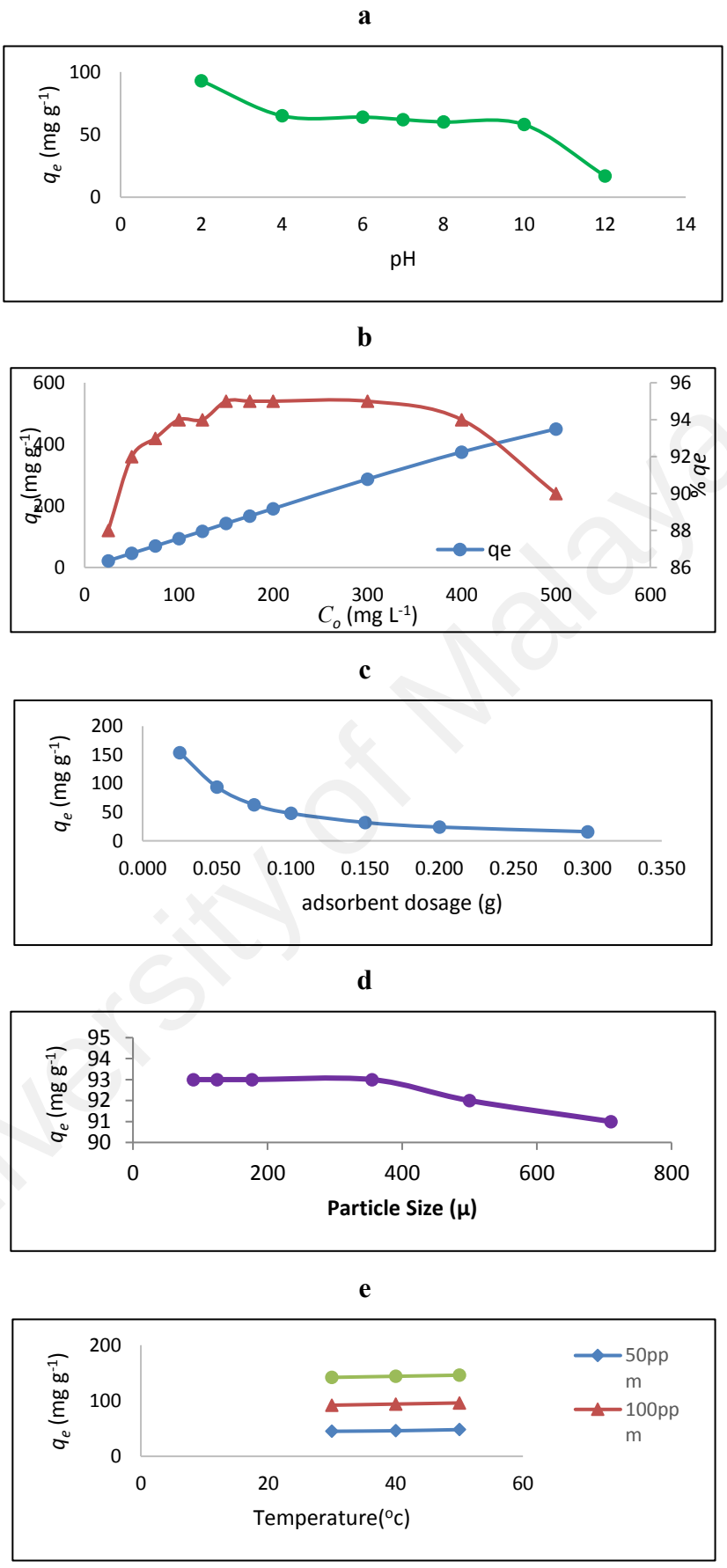

Figure 5.3: Effect of a) pH, b) initial dye concentration and percent q_e, c) adsorbent dosage, d) particle size and e) temperature onto AB113-NIFSS system

5.1.2.3 Effect of adsorbent dosage

This parameter has high influence on the q_e value. The adsorbent dosage of AB113 dye adsorption in the range of 0.025-0.300 g in 50 ml of solution was investigated. It was observed that the extent of AB113 dye removal increased with increase in adsorbent dose. But, beyond the limit as shown in Figure 5.3, any increase in the adsorbent dose did not result in any significant change in the amount of the dye adsorbed. This is a result of the binding of dye molecules on to the adsorbent surface when equilibrium was reached between dye molecule on the adsorbent and in the solution.

5.1.2.4 Effect of particle size

Maximum adsorption capacity was studied for initial AB113 dye concentration of 100 mg L^{-1} at almost neutral pH. The experiments were performed at different particle size of ≤ 90 μm; ≥ 90 μm ≤ 125 μm; ≥ 125 μm ≤ 177 μm; ≥177 μm ≤ 355 μm; ≥355 μm ≤ 500 μm and ≥ 500 μm ≤ 710 μm. The adsorption of dye decreased with the increase in the size of the adsorbent particle (Figure 5.3). The observation is in conformity with the expected results as surface area always decreases when there is increase in adsorbent particle size. The size of ≥ 125 μm ≤ 177 μm (80 mesh ASTM) was selected for further studies because 80 mesh particle is widely employed in fabrication of composites and sieving to lower size particles takes longer period and adds to the cost of the process.

5.1.2.5 Effect of temperature

To understand the influence of temperature on adsorption, studies were done at 30–50 °C with three dye concentrations and the results are shown in Figure 5.3. It can be observed that with increase in temperature, the adsorption capacity decreases gradually, which indicates that the process is endothermic in nature. Increase in adsorption at higher temperature may be a result of higher mobility of dye molecule with decrease in kinetic energy and enhanced rate of intra-particle diffusion.

5.1.2 Adsorption isotherms, kinetic and thermodynamic modeling of AB113-NIFSS system

The equilibrium experiments were conducted for different initial concentrations of AB113 dye in the range of 25-500 mg L^{-1}. The Q_m value of 709.42 mg g^{-1} obtained for the Langmuir isotherm is too high from the experimental value of q_e (93.00 mg g^{-1}). However, R^2 value of 0.95 proves that this isotherm has good fit with experimental data. The R_L values calculated were between 0.049 to 0.204 indicate favourable adsorption of AB113 dye on to NIFSS. The decrease in R_L with an increase in the initial concentration indicates that the adsorption is more favourable at high concentration. However, the large difference between Q_m (709.42 mg g^{-1}) and q_e (93.00 mg g^{-1}) has made me to explore other adsorption isotherm models. In the present study, the values of n_F = 1.757 and $1/n_F$ = 0.569 obtained from Freundlich isotherm equation indicate that the adsorption is physisorption and favours normal Langmuir Isotherm. The values of K_F and n_F are calculated from the intercept and slope of the plot ln q_e *versus* ln *Ce*. The fitting of Freundlich isotherm to the experimental data has R^2 value of 0.89, where R is the correlation coefficient shows that the process is linear. It could be inferred that the adsorption of AB113 dye on to NIFSS is favourable at experimental conditions and the process is physisorption. Since, no concrete inference was derived from Langmuir and Freundlich models regarding the system being homogenous or heterogeneous, an attempt has been made to explore higher models to fit in the data. The Q_m value of 499.48 mg g^{-1} derived from Jovanovic isotherm is high to the experimental value of q_e = 94.00 mg mg g^{-1}. Thus, Jovanovic model fits closer to the experimental q_e value as compared to Langmuir isotherm (Figure 5.4). In brief, the three complimentary two-parameter models studied, suggest that the interaction of AB113 dye on NIFSS is linear, favourable and physical in nature (Table 5.1). For academic curiosity five three-parameter isotherm models, namely Redlich-Peterson, Brouers-Sotolongo, Vieth-Sladek, Toth and Radke-Prausnitz were also studied.

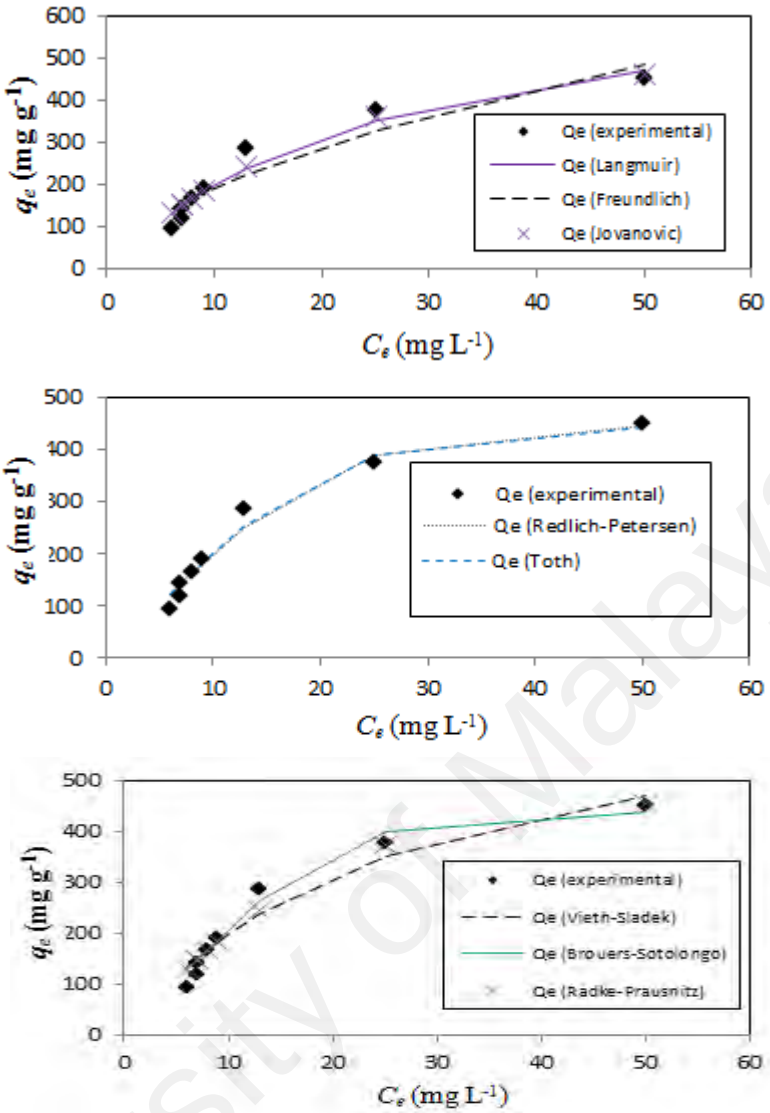

Figure 5.4: Fitting of adsorption data to Langmuir, Freundlich, Jovanovic, Redlich-Petersen, Toth, Vieth-Sladek, Brouers-Sotolongo and Radke-Prausnitz adsorption isotherm of AB113-NIFSS system

The *'g'* value = 1.910 obtained from Redlich–Peterson isotherm indicates that the adsorption tends towards Langmuir isotherm. The Q_m value of 438.50 mg g^{-1} obtained for this Brouers-Sotolongo isotherm is also high from the experimental value of Q_m (94.00 mg g^{-1}). However, the R^2 value of 0.98 shows a good prediction of this isotherm model to the experimental data in Figure 5.4. Vieth-Sladek model predicts Q_m value of 709.40 mg g^{-1} which is a prediction compared to other models studied. Lower value of χ^2 signifies closer similarity with the experimental data shown in Figure 5.4 and Table 5.1. Toth isotherm (R^2 = 0.98) to the experimental data are shown in Figure 5.4. Radke-Praustnitz isotherm predicted Q_m of 6319680 mg

g^{-1}, was obtained which was too far to the experimentally obtained Q_m value. The estimated parameters are shown in Table 5.2.

The experimental data at initial AB113 dye concentrations (50, 100 and 150 μg ml^{-1}) at different temperatures are presented in Figure 5.5. The Dumwald-Wagner model (Figure 5.6) calculates the true absorption rate constant (K) with corrections for observed diffusion effects (Table 5.3). The Weber-Morris model (Figure 5.6) defines that solute uptake varies with $t^{½}$ rather than time of contact (t). At lower initial concentration (50 μg ml^{-1}) and at lower temperature, the adsorption rate is high and then there is a shift in the rate following a different linear trajectory and finally the rate stabilizes with respect to time. But at higher temperatures the rate is more linear. Higher concentration of solute (150 μg ml^{-1}) there are less apparent changes in the adsorption rate. This is more so when higher temperature data is fitted to the film diffusion model of Boyd et al., 1947. It is inferred from the Figure 5.6 that the data shows good adherence to the model with high R^2 and χ^2 values and gives the liquid film diffusion constant $R^{|}$ (Table 5.3). ΔH° and ΔS° can be determined from the slope and the intercept of the van't Hoff plots of ln (K_L) vs. 1/T and E_a can be determined from the slope and the intercept of the van't Hoff plots of ln K_2 versus 1/T as shown in Figures 5.7a and 5.7b.

The thermodynamic parameter estimates are provided in Table 5.4. The positive ΔH° value suggests the endothermic nature of adsorption and the negative ΔG° values indicate the feasibility and spontaneity of the adsorption process. The ΔG° is negative for all studied temperatures indicating that the adsorption of AB113 dye onto NIFSS would follow a spontaneous and favorable trend. The ΔG° value decreases with increase in temperature indicating an increase in adsorption at higher temperatures. The positive value of ΔS° suggests good affinity of AB113 dye towards the adsorbent and increased randomness at the solid solution surface.

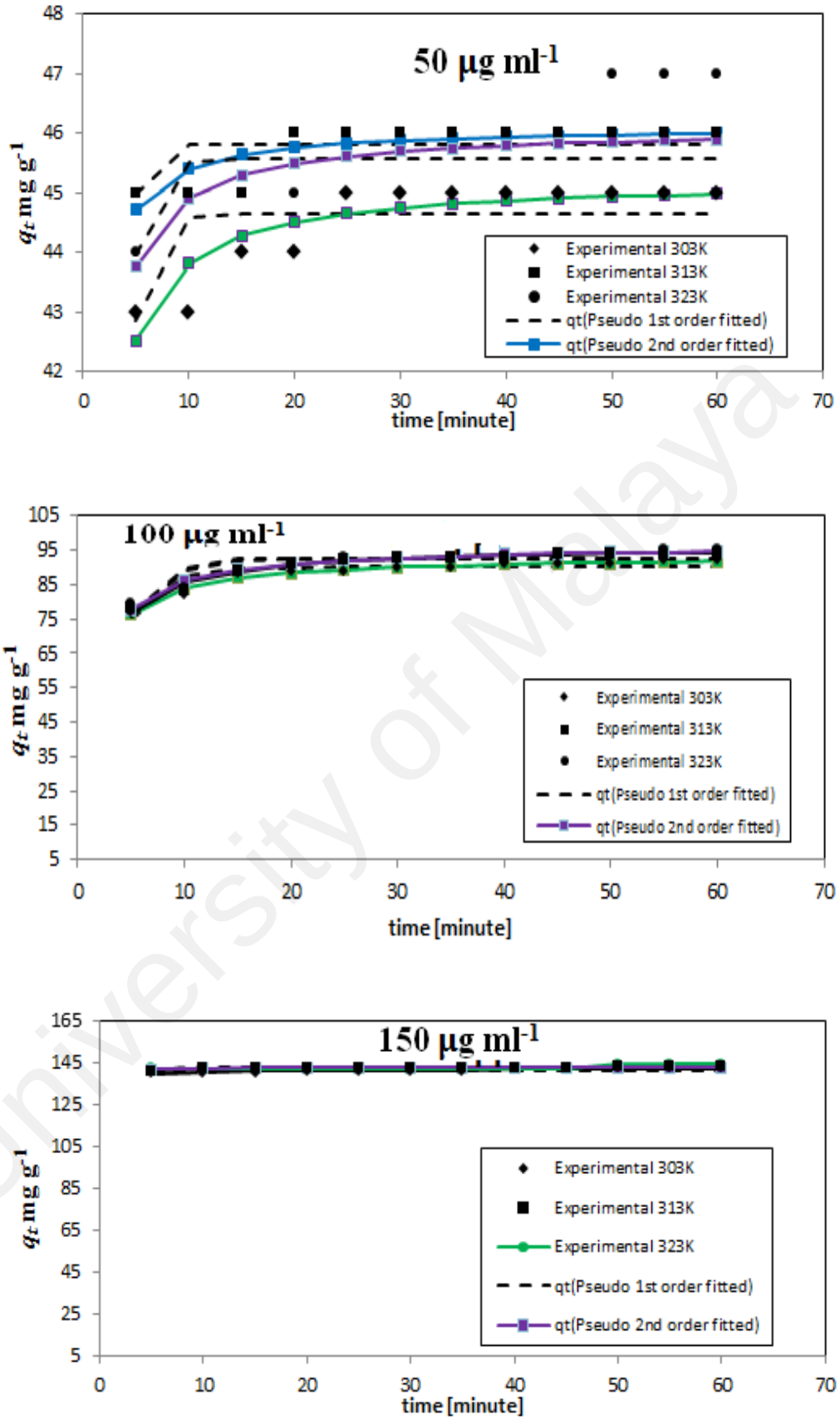

Figure 5.5: Kinetic model fits for 50, 100 and 150 µg ml^{-1} initial concentration of AB113 dye onto NIFSS system at different temperatures

Table 5.1: Calculated and statistical parameters for adsorption isotherm models of AB113-NIFSS system

Error Functions	Two-parameter isotherms						Three-parameter isotherms									
	Langmuir		Freundlich		Jovanovic		Redlich-Peterson		Toth		Radke-Prausnitz		Vieth-Sladek		Brouers-Sotolongo	
	Q_m	709.42	K_F	52.04	Q_m	499.48	A_{RP}	21.20	Q_m	453.40	Q_m	6319680	Q_m	709.4	Q_m	438.50
							B_{RP}	0.001	n_{T0}	3.316	K_{rp}	3.87E-06	K_{VS}	1E-07	K_{BS}	0.021
	K_S	0.039	n_F	1.757	K_J	0.051	g	1.91	b_{T0}	28432.810	m_{rp}	5118.073	β_{VS}	0.039	α	1.469
SSE	6247.2		11894.9		4884.6		3281.4		2822.1		4087.7		6247.2		2092.8	
χ^2	38.852		64.909		33.026		21.349		18.944		28.689		38.852		11.292	
R^2	0.95		0.89		0.96		0.97		0.98		0.97		0.95		0.98	

Table 5.2: Experimentally determined and theoretically predicted parameters for adsorption kinetics models of AB113-NIFSS system

Initial concentration	Temp		Pseudo-first order				Pseudo-second order			
[µg ml^{-1}]	[K]	$q_{e\ expt}$ [mg g^{-1}]	$Q_{m\ pred}$ [mg g^{-1}]	k_1	R^2	χ^2	$Q_{m\ pred}$ [mg g^{-1}]	k_2	R^2	χ^2
50	46	86	44.65	6.44E-01	0.38	0.10	45.22	6.95E-02	0.78	0.10
	47	89	45.82	7.97E-01	0.28	0.04	46.12	1.39E-01	0.66	0.02
	48	92	45.57	6.69E-01	0.29	0.18	46.10	8.13E-02	0.57	0.11
100	93	128	89.98	3.59E-01	0.78	0.59	93.37	9.59E-03	0.97	0.08
	95	130	92.38	9.24E+01	0.77	0.79	65.88	1.71E-03	0.76	1.65
	96	133	92.68	3.51E-01	0.75	0.78	96.43	8.69E-03	0.97	0.10
150	144	169	141.28	9.38E-01	0.20	0.04	141.80	8.09E-02	0.58	0.02
	145	172	142.27	9.42E-01	0.41	0.02	142.59	1.21E-01	0.55	0.01
	146	175	142.55	1.11E+00	0.03	0.06	142.84	1.50E-01	0.15	0.05

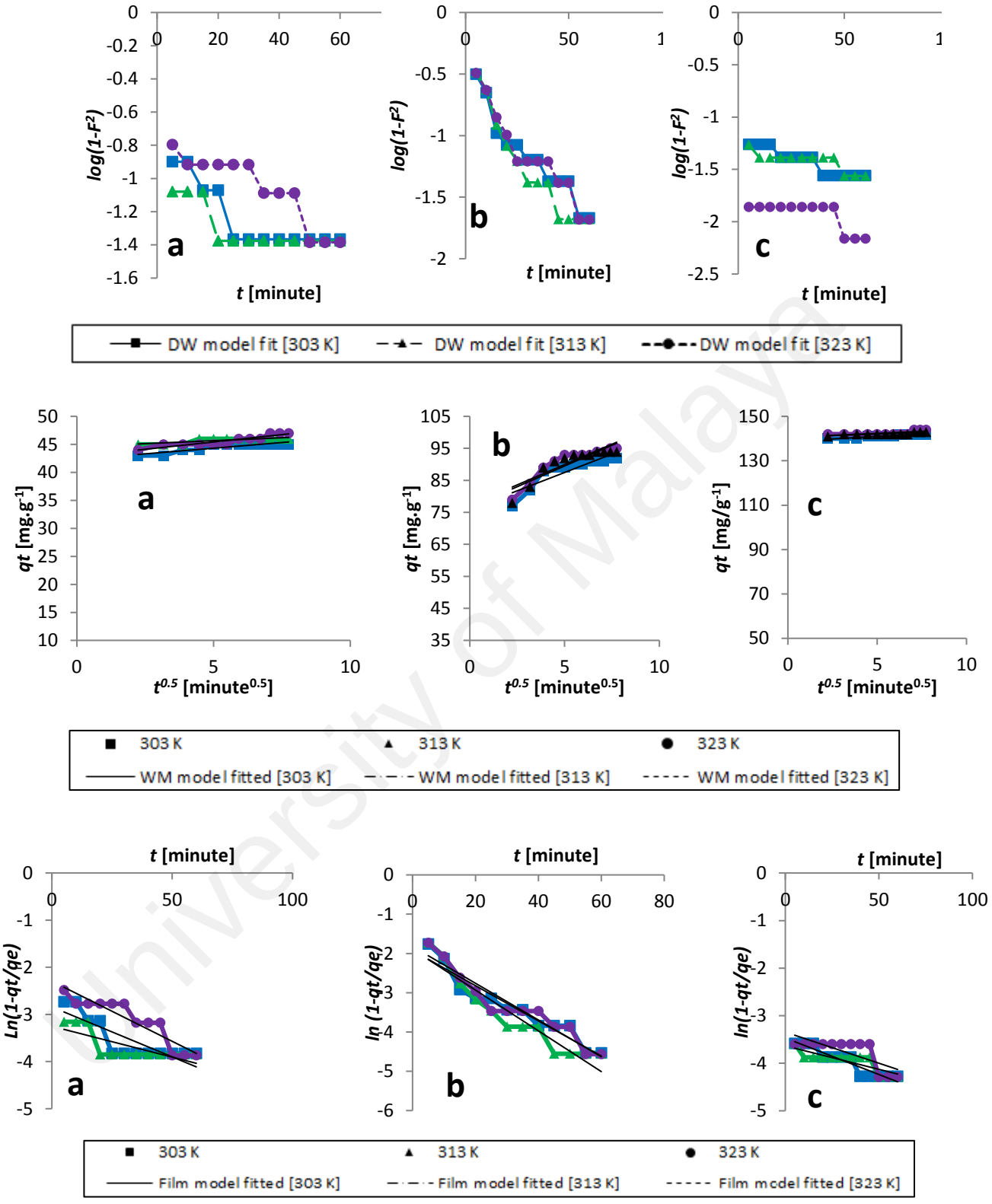

Figure 5.6: Kinetics data fitted to the Dumwald-Wagner model, Webber-Morris model and Film diffusion model with initial concentration of AB113-NIFSS system a) 50 µg ml^{-1}, b) 100 µg ml^{-1} and c) 150 µg ml^{-1}

Table 5.3: Calculated parameters for diffusion models of AB113-NIFSS system

Initial concentration	Temp	Film diffusion		Weber-Morris		Dumwald-Wagner	
[µg ml^{-1}]	[K]	$R^{|}$ [min^{-1}]	R^2	k_{ist} [mg g^{-1} s$^{-0.5}$]	R^2	K [min^{-1}]	R^2
50	303	0.0212	0.69	0.40	0.78	0.002	0.69
	313	0.0131	0.57	0.21	0.66	0.035	0.77
	323	0.0255	0.86	0.52	0.86	0.008	0.43
100	303	0.0448	0.92	2.29	0.79	0.044	0.92
	313	0.0519	0.91	2.59	0.79	0.051	0.91
	323	0.0468	0.92	2.54	0.82	0.046	0.92
150	303	0.0154	0.88	0.45	0.89	0.015	0.88
	313	0.0099	0.69	0.27	0.67	0.808	0.69
	323	0.0131	0.57	0.35	0.46	0.013	0.57

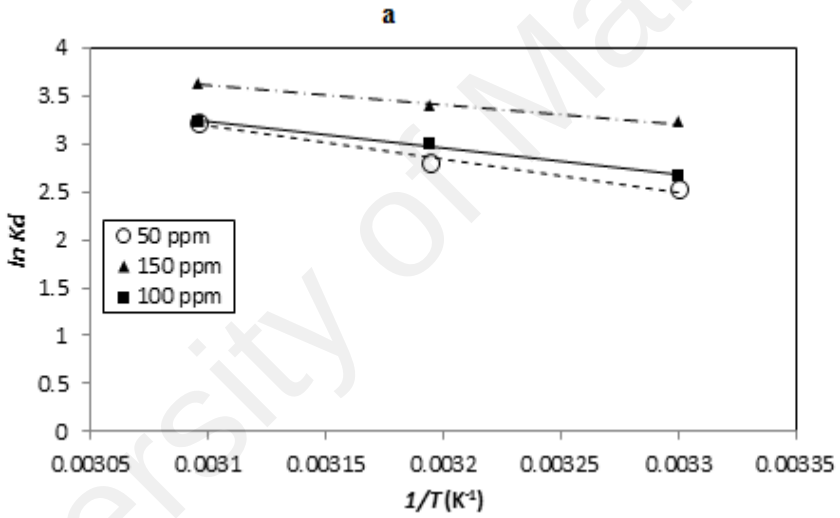

Figure 5.7a: Plot of thermodynamic equilibrium constant versus 1/T to determine the enthalpy and Gibbs free energy of the process of AB113-NIFSS system

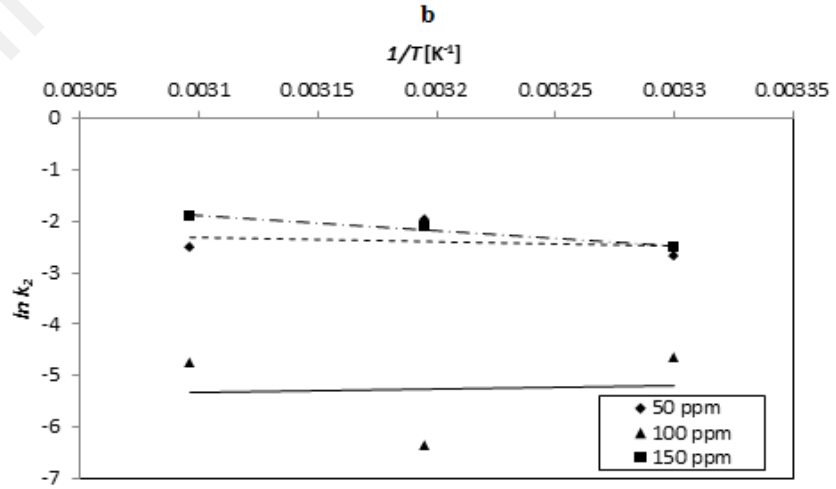

Figure 5.7b: Plot of pseudo – second order kinetic constant versus 1/T to determine the activation energy of the process of AB113-NIFSS system

Table 5.4: Thermodynamic parameters of AB113-NIFSS system

Initial concentration [μg ml^{-1}]	Temperature [K]	ΔG° [kJ mol^{-1}]	ΔS° [J mol^{-1}K^{-1}]	ΔH° [kJ mol^{-1}]	ln A	E_a [kJ mol^{-1}]
50	303	-6.36	113.68	28.14	0.27	6.91
	313	-7.32				
	323	-8.64				
100	303	-6.69	97.51	22.81	-7.35	-5.46
	313	-7.79				
	323	-8.64				
150	303	-8.11	81.05	16.47	7.51	25.19
	313	-8.86				
	323	-9.73				

The extremely low values of ΔH° suggests that the adsorption process is physical as the standard enthalpy change for chemical reaction is normally >200 kJ mol^{-1}. This has been further confirmed by activation energy values of the adsorption process at different initial concentrations (50, 100 and 150 μg ml^{-1}) which ranged from ~-5.46 to 25.19 kJ mol^{-1} using the Arrhenius equation and the kinetic constant from the pseudo-second order model (Table 5.4).

5.1.4 Statistical optimization by fractional factorial experimental design (FFED)

The comparison graph for actual versus predicted values using FFED (Figure 5.8) indicates a strong relationship between the experimental and predicted responses. The regression equation obtained from the study is shown below:

$$\text{Adsorption} = 89.4+61.56.6*A+28*B+113.3*C-59.5-21.2*E-8.4*AB-63.11*A^2+0.004*B^2-20.55*C^2+52.87*D^2-48.37*E^2 \quad \textbf{(5.1)}$$

Maximum adsorption obtained by the statistical optimization experiment using regression analysis with optimized conditions established at pH of 2, adsorbent dosage of 0.500 g L^{-1}, and an initial dye concentration of 209.47 mg L^{-1} for an adsorption time of 126.62 min with orbital shaking of 165 rpm at temperature 49.95°C was 236.18 mg g^{-1}.

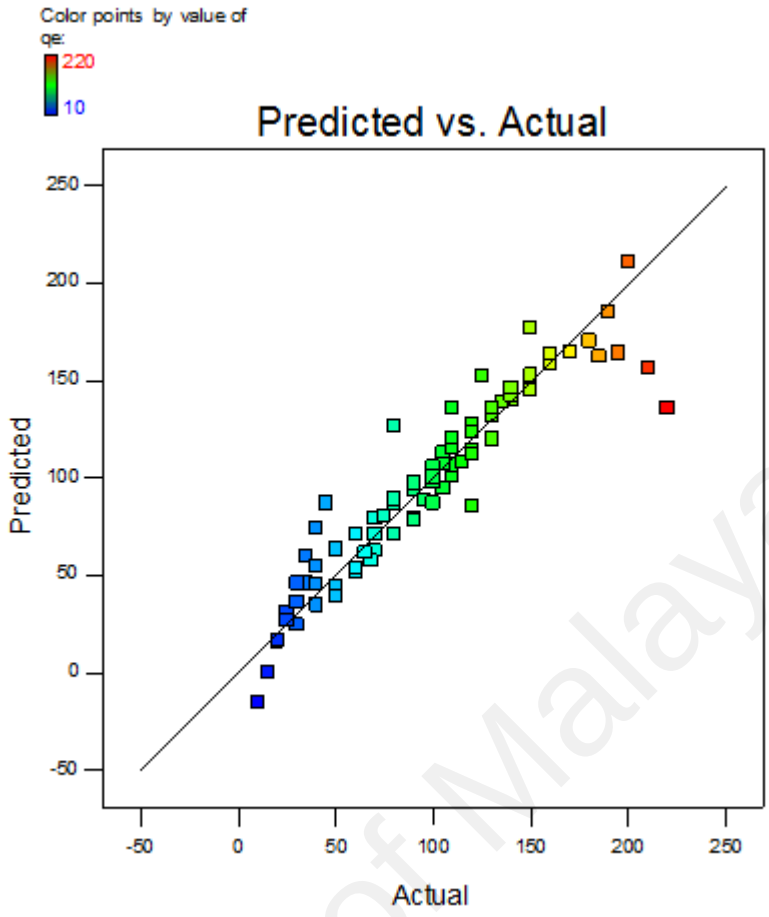

Figure 5.8: Comparison graph for actual versus predicted values of AB113-NIFSS system

Analysis of Variance (Table 5.5) shows the significance of individual and combined effect of the factors. Significance of factors were considered at confidence interval of 95% with p-value < 0.05%. In this study A, B, C, D, AB, A^2 and C^2 are significant model terms, E is moderately significant and rest of the variables are insignificant. The derived statistical model seems to be relevant as per the adjusted R^2 value of 85.8%. This high R^2 value and coefficient of variance of 19.50% signify that the model suitably fits the experimentally determined data. As the values of process time and initial dye concentration increase there is an observable increase in adsorption capacity (Figure 5.9). Whereas, when considering their combined effect there is almost negligible effect.

Table 5.5: ANOVA for fractional factorial experimental design of AB113-NIFSS system

Source	Sum of Squares	Degree of freedom	Mean Square	*F* Value	*P*- Value
Model	179497.3	11	16317.93	44.4735	< 0.0001**
A	47015.75	1	47015.75	128.1385	< 0.0001**
B	16988.58	1	16988.58	46.30131	< 0.0001**
C	56236.35	1	56236.35	153.2687	< 0.0001**
D	13717.61	1	13717.61	37.38649	< 0.0001**
E	2829.371	1	2829.371	7.711274	0.007**
AB	113.685	1.000	113.685	0.310	0.580
A^2	21545.17	1	21545.17	58.72001	< 0.0001**
B^2	0.000159	1	0.000159	4.33E-07	0.999477
C^2	760.4977	1	760.4977	2.072689	0.154545
D^2	3042.676	1	3042.676	8.292622	0.005**
E^2	4037.602	1	4037.602	11.00423	0.001**
Residual	24950.13	68	366.9136		
Lack of fit	17675.13	65	271.925	0.112134	0.99995
Total	7275	3	2425		

Significant figures
Suggestive significance (P value : $0.05<P<0.10$)
Moderately significant (P value : $0.01<P \leq 0.05$)
** Strongly significant (P value : $P \leq 0.01$)

The values of the regression coefficients, as seen in equation, indicate the effect the parameter has on the adsorption capacity. Positive values indicate incremental effect, for example, an increase in the adsorption time causes a significant increase in adsorption capacity.

2D-contour plots and 3D-response surface plots as function of two independent variables provided the interaction effects between two parameters keeping others at a fixed value. Process optimization statistically in a given range of parameter values, allows for calculating the optimal condition and determines the effect of process conditions on adsorption. The 3D-graphs plotted for adsorption time against all other factors indicates that it has a positive effect on the adsorption capacity. By increasing

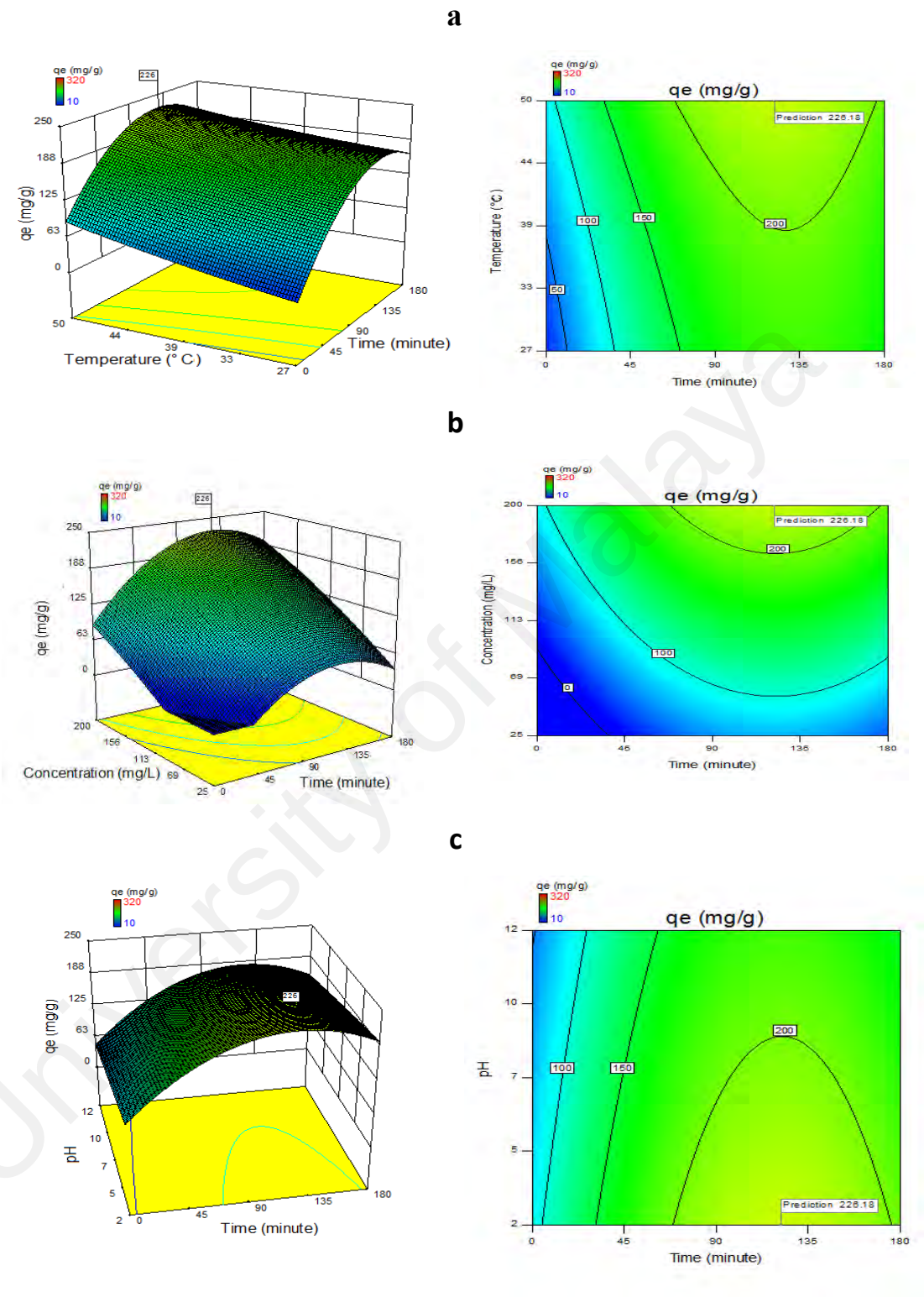

Figure 5.9: 3D-surface plot and 2D-contour plot of AB113-NIFSS system showing the variation of adsorption capacity with (a) time versus temperature, (b) time versus concentration and (c) time versus pH

time along with particle size and dye concentration, it is possible to improve the absorption capacity. The absorption maximum is achieved at an absorption time of 125.62 min. The quadratic model developed for process optimization is found to be beneficial for predicting the maximum adsorption capacity and understanding the interaction between independent variables as well as their effect on adsorption process.

5.1.5 Measurement of molar absorption coefficient (ε) of the dye

Six different concentrations (1.00×10^{-4}; 1.25×10^{-4}; 2.50×10^{-4}; 5.00×10^{-4}; 7.50×10^{-4} and 10.00×10^{-4}) of AB113 dye were prepared in distilled water and the absorbance was measured at 566 nm using distilled water as reference (Figure 5.10a). The ε_{AB113} value was calculated as per the procedure detailed 3.1.9.2.

5.1.6 Application of proposed method to textile industrial effluent (TIE)

The powder and filtrate solutions after the adsorption of constituents of Solution 2 on NIFSS are shown in Figures 5.10b and 5.10c. Preliminary trial study revealed that better results could be obtained by scaling up to two-orders of the adsorbent and the adsorbate and to one-order of the volume of the solution. In an interesting observation the Solution 2 showed about 32% decrease in absorbance compared to Solution 1. This may be due to the absorbance of the dye by varied undefined constituents present in TIE. Also, it was observed that additional fresh samples of the adsorbent after every 15 min enhanced the efficiency of removal of the dye from TIE. The recovery of the dye and allied substances from Solution 2 to an extent of 63%, 77%, 89% and 95% after 15, 30, 45 and 60 min respectively was observed. This observation is in accordance with the kinetic results according to which the solute adsorbs quickly onto the surface of the particles forming a film which then gets retarded further diffusion thereby bringing change in absorption rates.

a

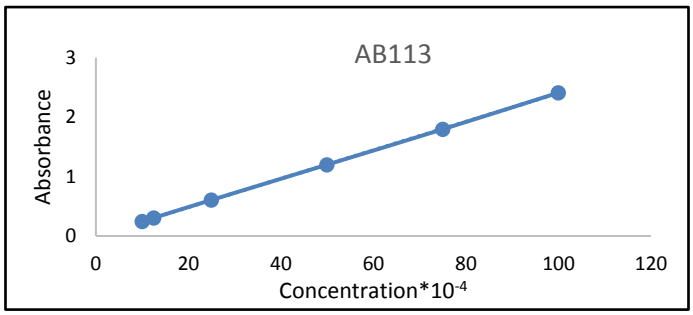

Figure 5.10a: Determination of molecular extinction coefficient of AB113 dye

b

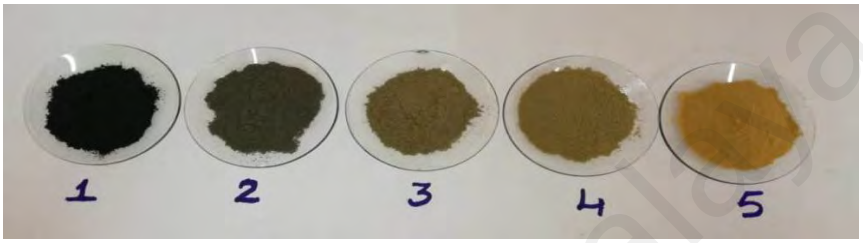

Figure 5.10b: Powders 1 to 4: Fresh samples of NIFSS added to AB113-TIE solution after every 15 min, filtered and the residue dried in oven. Sample 5: NIFSS

c

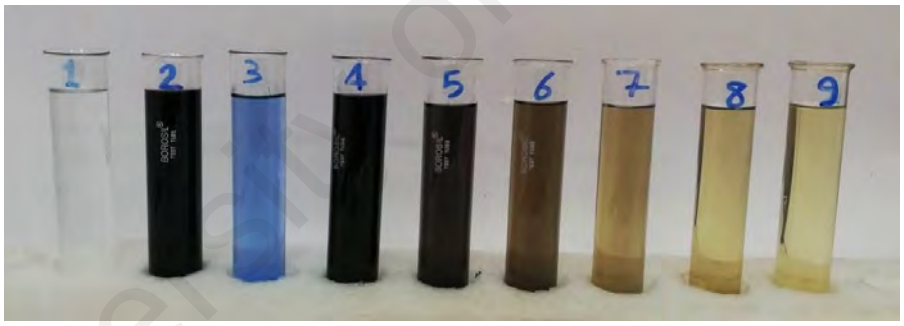

Figure 5.10c: Color of the solutions before and after adsorption: 1. Distilled water; 2. AB113 dye in distilled water; 3. TIE; 4. AB113 dye in TIE; 5. Filtrate after adsorption of dye on NIFSS after 15 min; 6. 30 min; 7. 45 min; 8. 60 min; 9. Filtrate of NIFSS in distilled water

5.1.6.1 Scale up experiments up to three orders

Scaling up of the experiment was done by using 10 g, 20 g, and 50 g of NIFSS and using 1, 2 and 5 L of Solution 2 using polyethylene beakers. Solutions were stirred using magnetic stirrer and the procedure as described earlier was repeated. Uniform results were obtained. Experiments were done in triplicate and the averages are reported. The coefficients of variation of results did not exceed in all cases ± 2% error.

The scale up experiments done to the extent of about three orders (restricted to adsorbent) compared to its initial set up has yielded promising results. The quantity and content of effluents from industry may vary so the results cannot be exactly predicted always from the initial data. Such limitation is a serious problem in such studies. In order to pin pointedly focus the results larger pilot scale studies are necessary. However, the enhanced scale experimental data will certainly yield promising reliability about the process, and it will definitely prove the principles of the method when subjected for development on a bigger scale in industrial environment.

5.1.6.2 Regeneration of the adsorbent and cost analysis

Regeneration of dye-loaded NIFFS enables its re-use and recovery of the adsorbed material. Regeneration of NIFFS is not advisable since the process cost along with the cost of solvents will be very higher as compared to the sorbents cost alone used in the process. In addition we should also consider the enhancement of E-factor (Sheldon 1992) which is not affordable as the planet is not in a position to bear increased load of environmental toxicants. The better approach for the disposal of the waste process materials could be to use the current method which is under development which is to fabricate thermosets and thermoplastics. Work on which has been reported in Chapter 4.

Section 5.2 AB113-NICSS system and Section 5.3 AB113-NICUS behave almost similar to AB113-NIFSS. The figures and the tables are incorporated in Appendix A1 and Appendix A2 respectively.

5.2 Acid red 119 – NIFSS system

5.2.1 Surface Characterization

The NIFSS surface was characterized by SEM which displayed a tortuous porous structure (Figure 5.11a). Upon adsorption it is observed that some of the pores are completely filled with the adsorbate (AR119 dye) forming a thin film over the particle (Figure 5.11b). The IR spectra of NIFSS and AR119-NIFSS are similar as detailed in 5.1.1.

5.2.2 Effect of parameters on adsorption process

5.2.2.1 Effect of pH

The adsorption capacity of NIFSS was the highest when pH was at 2 **(**Figure 5.12**)**. As pH increased the q_e value decreased marginally and the similar behavior was observed uptill pH 12. The chemistry of NIFSS is already described in earlier section 5.1.2.1. It was found that the maximum AR119 dye removal by NIFSS was at pH 2.0 (q_e= 95.00 mg g^{-1}) with initial concentration of 100 mg L^{-1}.

5.2.2.2 Effect of initial dye concentration

Maximum adsorption capacity of 50 mg g^{-1} was reached for initial AR119 dye concentration of 200 mg L^{-1} (Figure 5.13). Higher dye concentration decreased the adsorption capacity.

5.2.2.3 Effect of adsorbent dosage

The amount of AR119 dye adsorbed on to NIFSS decreased as the amount of adsorbent dose increased. The results are presented in Figure 5.13.

5.2.2.3 Effect of particle size

Maximum adsorption capacity was studied for initial AR119 dye concentration of 100 mg L^{-1} at neutral pH. The experiments were performed at different particle size of ≤ 90 μm; ≥ 90 μm ≤ 125 μm; ≥ 125 μm ≤ 177 μm; ≥177 μm ≤ 355 μm; ≥355 μm ≤

500 µm and ≥ 500 µm ≤ 710 µm. The adsorption of dye decreased with the increase in the size of the adsorbent particle (Figure 5.13).

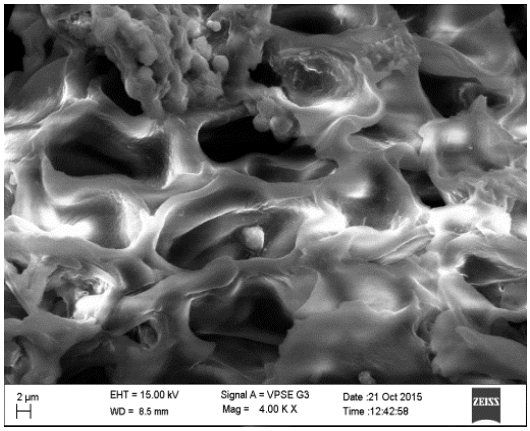

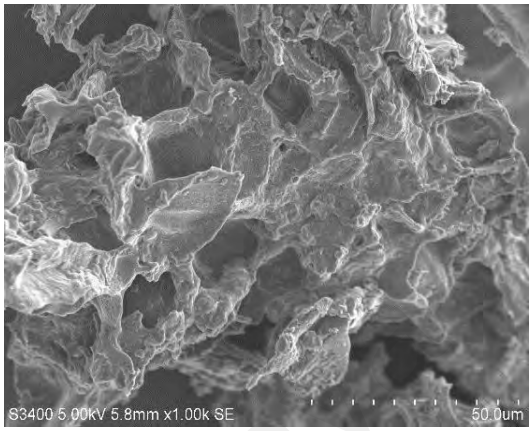

Figure 5.11a: SEM image of NIFSS **Figure 5.11b:** SEM image of AR119-NIFSS

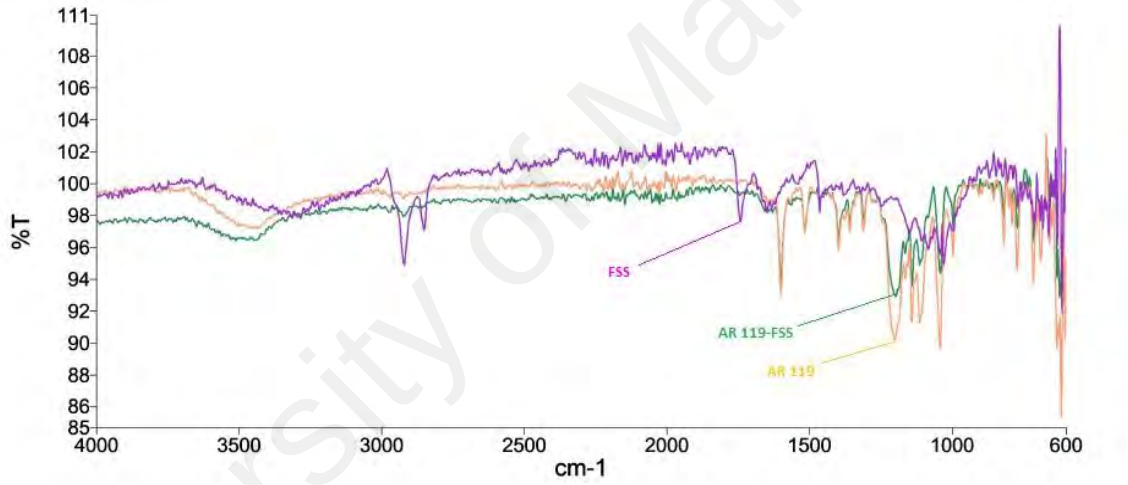

Figure 5.12: FTIR spectra of NIFSS, AR119 dye and AR119- NIFSS system

5.2.2.5 Effect of contact time on dye adsorption

The effect of contact time and the adsorption of AR119 dye onto NIFSS were allowed to take place for 15, 30, 45, 60, 90, 120, 150 and 180 minutes. In the initial 60 min it showed rapid adsorption to an extent of about 80%. But as the contact time increased, there was slow increase in adsorption until 90 min then gradually it reached equilibrium in about 180 min. The results are shown in Figure 5.13. Aggregation of dye molecule with increase in contact time makes dye molecule to defuse deeper into adsorbent structure with higher energy.

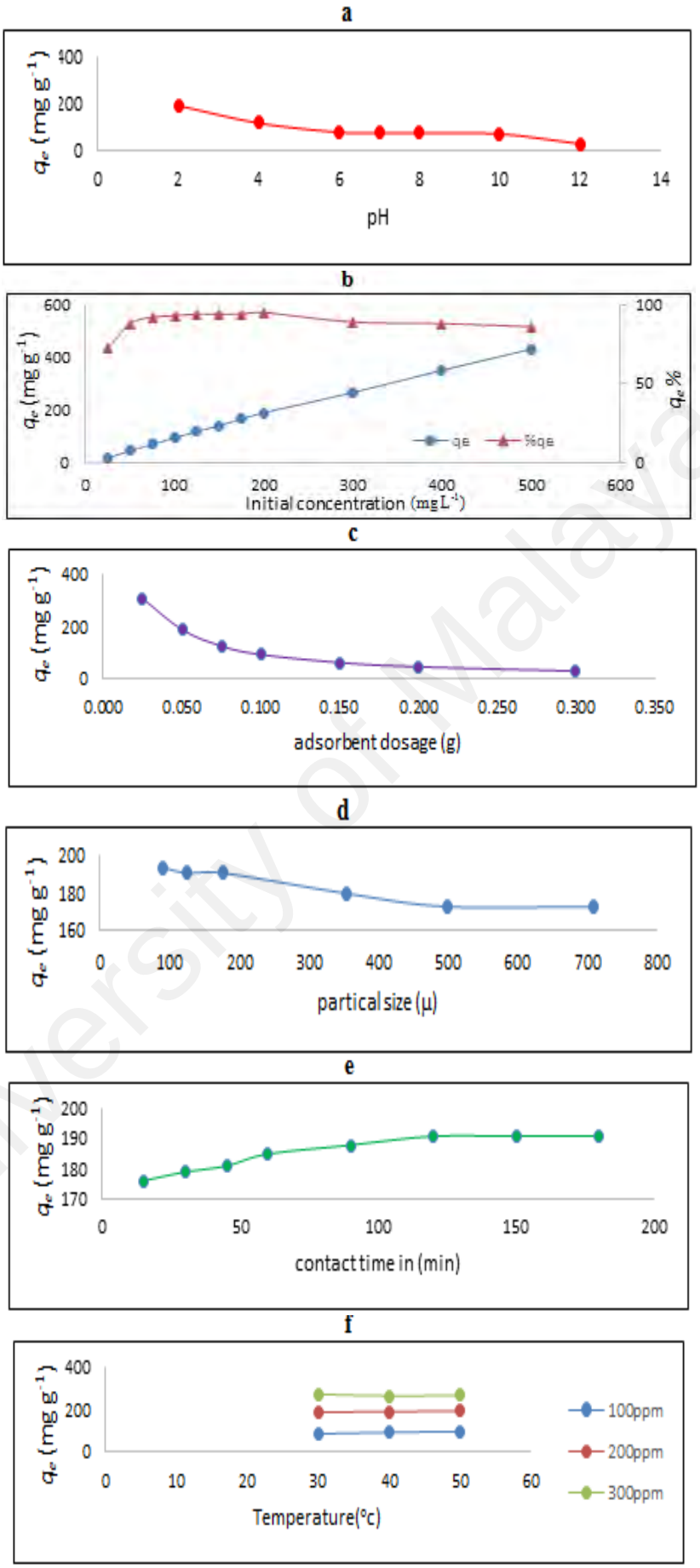

Figure 5.13: Effect of a) pH, b) initial dye concentration with percent q_e, c) adsorbent dosage, d) particle size, e) contact time and f) temperature onto AR119-NIFSS system

This aggregation negates the influence of contact time as the mesopores get filled up and start offer resistance to diffusion of aggregated dye molecules in adsorbents.

5.2.2.6 Effect of temperature

The adsorption studies were carried out at 30˚C-50˚C with three different dye concentrations and the results are shown in Figure 5.13. It can be observed that with increase in temperature, the adsorption capacity decreases gradually, which indicates that the process is endothermic in nature. Increase in adsorption at higher temperature may be as a result of higher mobility of dye molecule with decrease in kinetic energy and enhanced rate of intra-particle diffusion.

5.2.3 Adsorption isotherms, kinetic and thermodynamic modeling of AR119-NIFSS system

The Q_m value of 577.55 mg g^{-1} obtained for Langmuir isotherm is too high compared to the experimental value of q_e (95.00 mg g^{-1}). However, R^2 value of 0.95 proves that this isotherm has good fit with experimental data. The R_L values calculated were between 0.055 to 0.227 indicate favourable adsorption of AR119 dye on to NIFSS. The decrease in R_L with an increase in the initial concentration indicates that the adsorption is more favourable at high concentration. However, the large difference between Q_m (577.55 mg g^{-1}) and q_e (95.00 mg g^{-1}) has made me to explore other adsorption isotherm models. The values of n_F = 1.819 and $1/n_F$ = 0.549, obtained from Freundlich isotherm equation indicate that the adsorption is physisorption and favours normal Langmuir Isotherm. It could be inferred that the adsorption of AR119 dye on to NIFSS is favourable at experimental conditions and the process is physisorption. The Q_m value of 421.34 mg g^{-1} derived from Jovanovic isotherm is high to the experimental value of q_e = 95.00 mg g^{-1}. Thus, Jovanovic model fits closer to the experimental q_e value as compared to Langmuir isotherm (Figure 5.14). In brief, the three complimentary two-parameter models studied, suggest that the interaction of AR119

dye on NIFSS is linear, favourable and physical in nature (Table 5.6). For academic curiosity six three-parameter isotherm models, namely Redlich-Peterson, Vieth-Sladek, Brouers-Sotolongo, Toth, Sips and Radke-Prausnitz were also studied.

The *'g'* value = 0.452 obtained indicates that the adsorption tends towards Langmuir isotherm. Vieth-Sladek isotherm model predicts Q_m value of 180.80 mg g^{-1} which is a prediction compared to other models studied. Lower value of χ^2 signifies closer similarity with the experimental data shown in Figure 5.14 and Table 5.6. The Q_m value of 1401224.00 mg g^{-1} obtained from Brouers-Sotolongo isotherm is also high from the experimental value of q_e (95.00 mg g^{-1}). However, the R^2 value of 0.97 shows a good prediction of this isotherm model to the experimental data in Figure 5.14. Toth isotherm (R^2 = 0.97) to the experimental data are shown in Figure 5.14. The value of Q_m = 29532.90 mg g^{-1} obtained from Sips isotherm has more deviation from experimental value when compared to the value obtained for Langmuir isotherm. Radke-Praustnitz isotherm predicted Q_m of 5.60 mg g^{-1}, was obtained which was not close to the experimentally obtained Q_m value.

In summary, the models used to understand the mechanism of adsorption are of higher order equations. The validity of data fitting cannot be confirmed only by R^2 value because it is used with linear models only. Hence χ^2 values are considered as they provide a better statistic because if model data are similar to the experimental data, then χ^2 would be a small number and vice versa. All the eight isotherm models, gave values for the important parameters (Q_m, χ^2 *and* R^2) which are shown in Table 5.6. The estimated parameters are shown in Table 5.7.

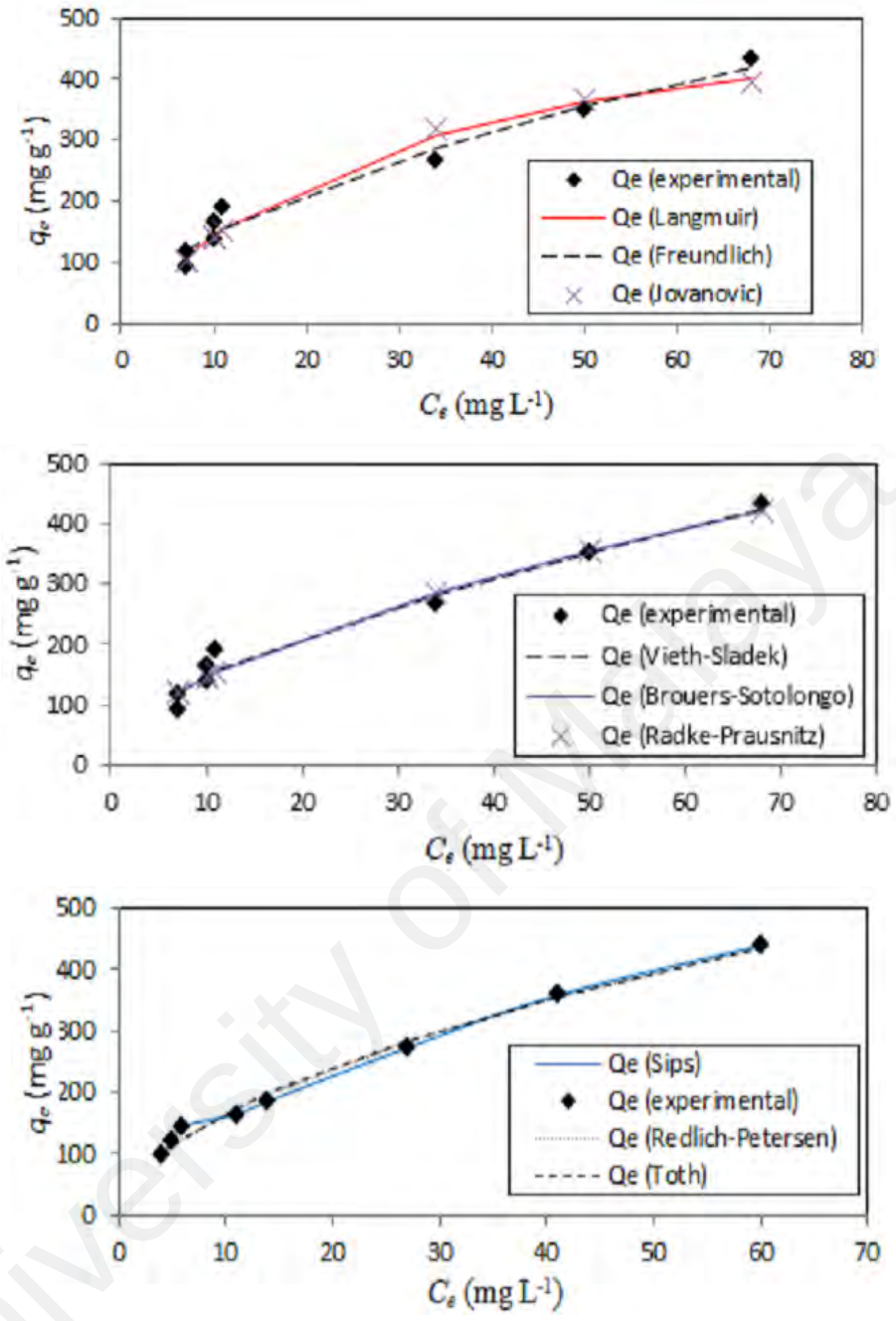

Figure 5.14: Fitting of adsorption data to Langmuir, Freundlich, Jovanovic, Vieth-Sladek, Brouers-Sotolongo, Radke-Prausnitz, Sips, Redlich-Petersen and Toth adsorption isotherm of AR119-NIFSS system

Table 5.6: Calculated and statistical parameters for adsorption isotherm models of AR119-NIFSS system

Error Functions	Two-parameter isotherms						Three-parameter isotherms									
	Langmuir		Freundlich		Jovanovic		Redlich-Peterson		Toth		Radke-Prausnitz		Sips		Vieth-Sladek		Brouers-Sotolongo	
	Q_m	575.55	K_F	41.37	Q_m	421.34	A_{RP}	3200.20	Q_m	72747.30	Q_m	5.60	Q_m	29532.90	Q_m	180.80	Q_m	1401224
							B_{RP}	76.742	n_{TO}	0.099	K_{rp}	38.832	K_s	6.41E-06	K_{vs}	3.824	K_{BS}	2.95E-05
	K_S	0.034	n_F	1.819	K_J	0.041	g	0.452	b_{TO}	1.664	m_{rp}	0.451	m_s	0.549	β_{vs}	0.156	α	0.549
SSE	4629.3		2924.5		6298.2		2925.2		2991.2		2924.3		2924.9		2512.8		2924.6	
χ^2	21.018		18.886		26.618		18.873		18.644		18.870		18.890		17.417		18.886	
R^2	0.95		0.97		0.94		0.97		0.97		0.97		0.97		0.97		0.97	

Table 5.7: Experimentally determined and theoretically predicted parameters for adsorption kinetics models of AR119-NIFSS system

Initial concentration	Temp		Pseudo-first order				Pseudo-second order			
[μg ml^{-1}]	[K]	$q_{e\ expt}$ [mg g^{-1}]	$Q_{m\ pred}$ [mg g^{-1}]	k_1	R^2	χ^2	$Q_{m\ pred}$ [mg g^{-1}]	k_2	R^2	χ^2
100	303	97	95.02	3.83E-01	0.64	0.02	95.96	3.10E-02	0.88	0.03
	313	95	93.01	4.50E-01	0.30	0.02	93.62	5.15E-02	0.62	0.01
	323	99	97.60	5.08E-01	0.20	0.01	98.01	7.91E-02	0.50	0.01
200	303	191	186.39	2.94E-01	0.74	0.15	190.72	6.43E-03	0.97	0.02
	313	193	180.86	1.81E+02	0.56	0.96	65.88	1.71E-03	0.76	1.65
	323	196	189.41	4.35E-01	0.31	0.06	190.81	2.23E-02	0.58	0.04
300	303	276	263.14	3.32E-01	0.44	0.34	268.12	5.94E-03	0.74	0.16
	313	268	258.04	3.92E-01	0.69	0.04	260.36	1.26E-02	0.94	0.01
	323	271	264.64	3.15E-01	0.45	0.47	270.74	4.84E-03	0.79	0.18

Based on coefficients of determination (R^2) and chi-square values (χ^2) the pseudo-second order model fitted better than pseudo-first order with the experimental data at all initial AR119 dye concentrations (100, 200 and 300 μg ml^{-1}) at different temperature in Figure 5.15. The rate of adsorption was very high initially and slowed down gradually to become stagnant when it reached the maximum adsorption. The adsorption capacity (q_e) increased with increase in temperature. These results show that the adsorption processes were not rate-limiting. The data also show that adsorption process occurred in multiple steps where the solute molecules move from the bulk solution to solid surface followed by diffusion of the solute molecules to the pores of the NIFSS.

The Dumwald-Wagner model (Figure 5.16) calculates the true absorption rate constant (K) with corrections for observed diffusion effects (Table 5.8). The Weber-Morris model (Figure 5.16) defines that solute uptake varies with $t^{½}$ rather than time of contact (t). Therefore a plot of q_t vs. $t^{½}$ should yield a straight line passing through origin whose slope (k_{int}) is the diffusion rate constant. Adsorption kinetics is not always controlled by single mechanism. It is evident from our experimental data that at all solute concentrations there is multiple levels of linearity. At lower initial concentration (100 μg ml^{-1}) and at lower temperature, the adsorption rate is high and then there is a shift in the rate following a different linear trajectory and finally the rate stabilizes with respect to time. But at higher temperatures the rate is more linear.

At higher concentration of solute (300 μg ml^{-1}) there are less apparent changes in the adsorption rate. This is more so when higher temperature data is fitted to the film diffusion model of Boyd et al. 1947. It is inferred from the Figure 5.16 that the data shows good adherence to the model with high R^2 and χ^2 values and gives the liquid film diffusion constant $R^{|}$ (Table 5.8).

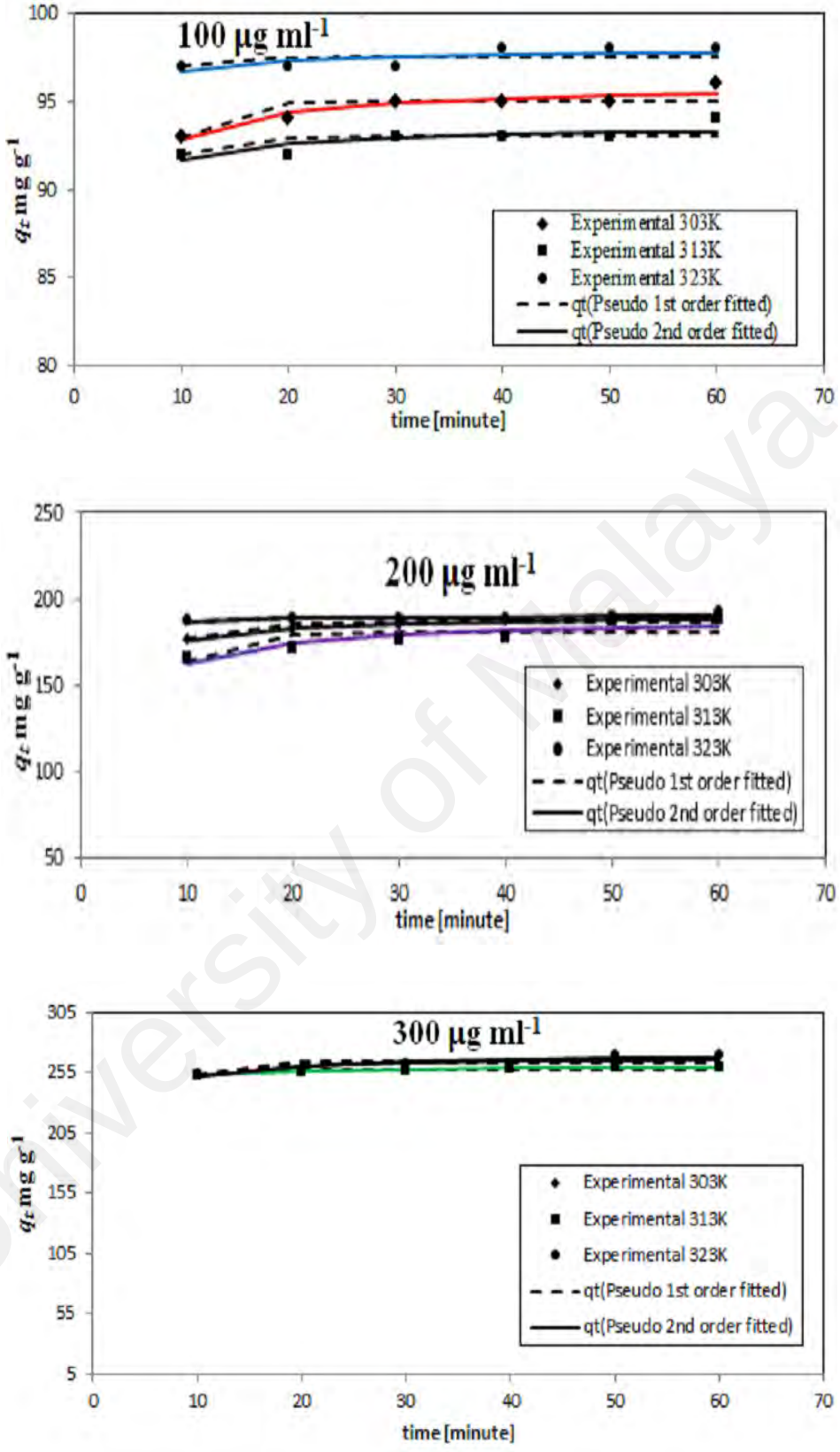

Figure 5.15: Kinetic model fits for 100, 200 and 300 µg ml^{-1} initial concentration of AR119 dye onto NIFSS system at different temperatures

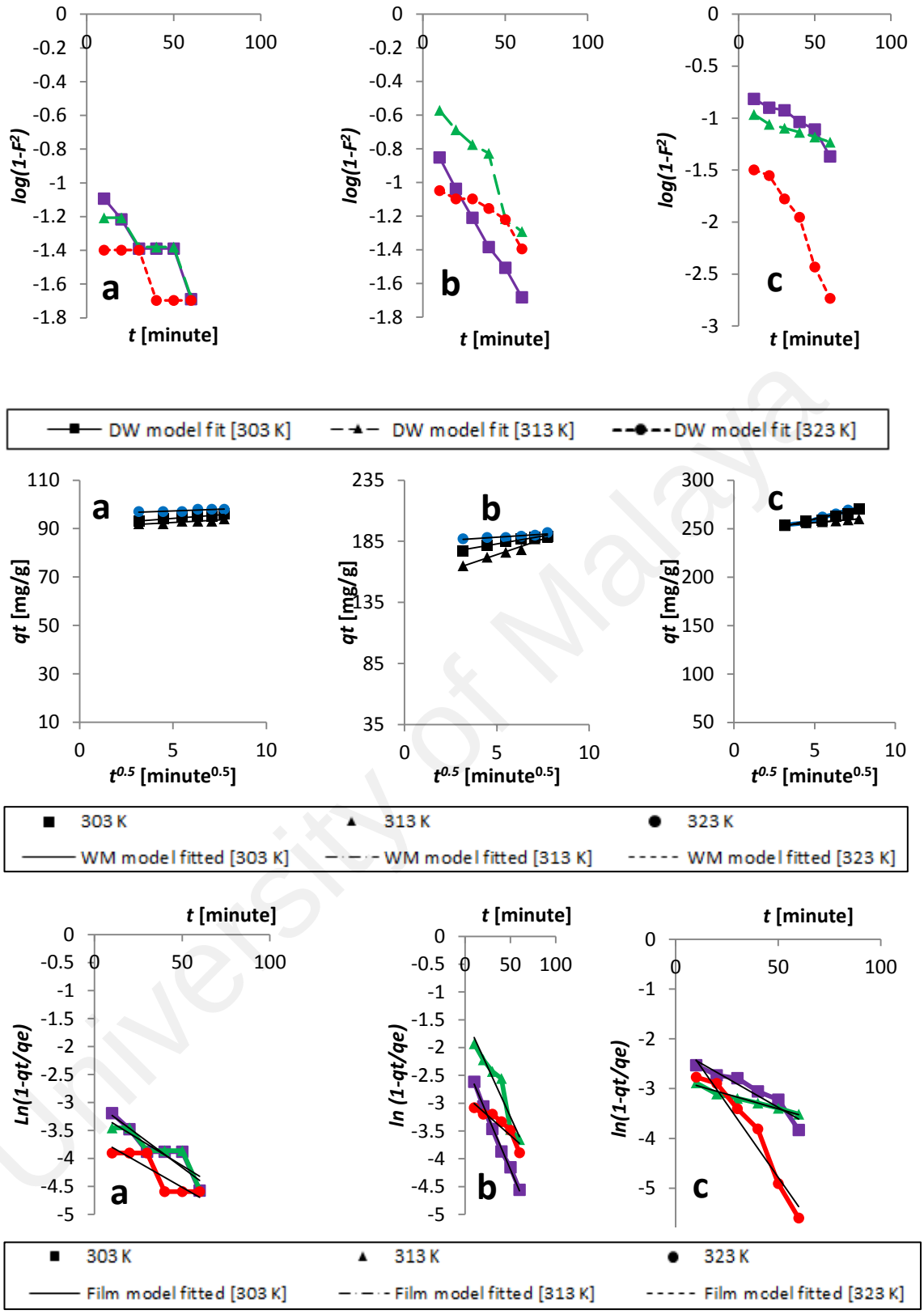

Figure 5.16: Kinetics data fitted to the Dumwald-Wagner model, Webber-Morris model and Film diffusion model with initial concentration of AR119-NIFSS system a) 100 µg ml^{-1}, b) 200 µg ml^{-1} and c) 300 µg ml^{-1}

Table 5.8: Calculated parameters for diffusion models of AR119-NIFSS system

Initial concentration	Temp	Film diffusion model		Weber-Morris model		Dumwald-Wagner	
[µg ml^{-1}]	[K]	$R^{|}$ [min^{-1}]	R^2	k_{ist} [mg g^{-1} s$^{-0.5}$]	R^2	K [min^{-1}]	R^2
100	303	0.0233	0.86	0.57	0.91	0.023	0.86
	313	0.0192	0.79	0.40	0.83	0.019	0.79
	323	0.0178	0.77	0.28	0.74	0.018	0.77
200	303	0.0384	0.99	2.59	0.96	0.004	0.99
	313	0.0357	0.92	5.09	0.96	0.035	0.92
	323	0.0144	0.85	0.97	0.85	0.014	0.85
300	303	0.0235	0.90	3.84	0.97	0.023	0.90
	313	0.0117	0.97	1.44	0.98	0.115	0.97
	323	0.0589	0.84	3.84	0.97	0.059	0.94

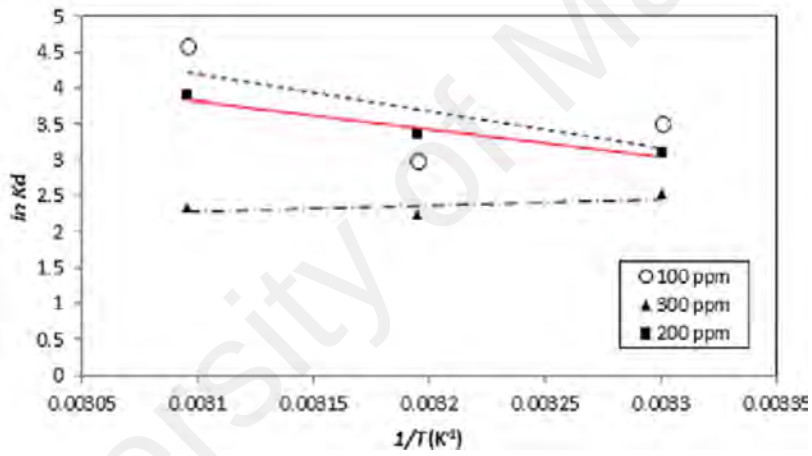

Figure 5.17a: Plot of thermodynamic equilibrium constant versus 1/T to determine the enthalpy and Gibbs free energy of the process of AR119-NIFSS system and

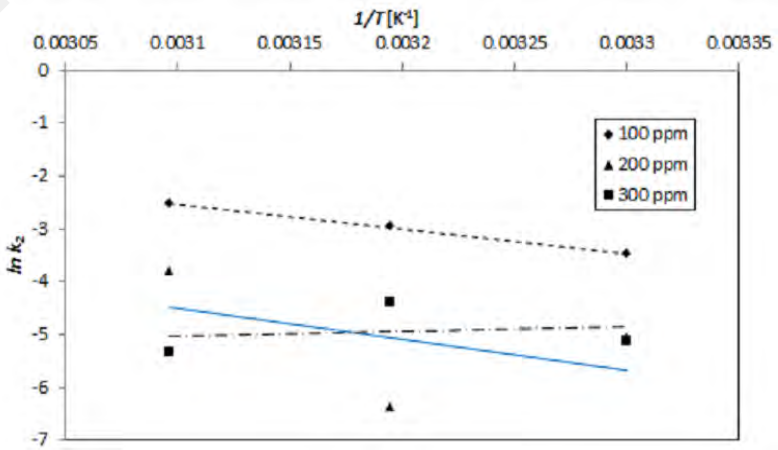

Figure 5.17b: Plot of pseudo – second order kinetic constant versus 1/T to determine the activation energy of the process of AR119-NIFSS system

ΔH° and ΔS° can be determined from the slope and the intercept of the van't Hoff plots of ln (K_L) vs. 1/T and E_a can be determined from the slope and the intercept of the van't Hoff plots of ln K_2 versus 1/T as shown in Figure 5.17a and 5.17b.

The thermodynamic parameter estimates are provided in Table 5.9. The activation energy values of the adsorption process at different initial concentrations (100, 200 and 300 μg ml^{-1}) ranged from ~-7.86 to 406.49 KJ mol^{-1} using the Arrhenius equation and the kinetic constant from the pseudo second order model (Table 5.19).

Table 5.9: Thermodynamic parameters of AR119-NIFSS system

Initial concentration [μg ml^{-1}]	Temperature [K]	ΔG° [KJ mol^{-1}]	ΔS° [J $mol^{-1}K^{-1}$]	ΔH° [KJ mol^{-1}]	ln A	E_a [KJ mol^{-1}]
100	303	-8.83	1419.16	363.84	11.67	317.02
	313	-7.79				
	323	-12.37				
200	303	-7.81	1111.91	273.09	13.73	406.49
	313	-8.72				
	323	-10.50				
300	303	-6.36	45.43	-65.38	-7.86	-7.86
	313	-5.82				
	323	-6.27				

5.2.4 Statistical optimization by fractional factorial experimental design

The comparison graph for actual versus predicted values (Figure 5.18) indicates a strong relationship between the experimental and predicted responses. The regression equation obtained from the study is shown below:

$$\text{Adsorption}=-50.0+9.5*A-1.2*B+191.7*C-15.7*D-102.2*E-75.9*F-2.6*AB+12.6*AC-1.3*BC-17.3*A^2+5.9*B^2-20.4*C^2+3.2*D^2+107.8*E^2+45.2*F^2 \quad (\mathbf{5.2})$$

The optimized values of variables could be determined by maximizing the second-order polynomial equation using interaction products obtained by multiple regression analysis is as per FFED. Maximum adsorption obtained by the statistical optimization experiment was 750.00 mg g^{-1} with optimized conditions established as a pH of 2.03, adsorbent dosage of 6.000 g L^{-1}, adsorbent particle size of 99 μ and an

initial dye concentration of 994.00 mg L^{-1} for an adsorption time of 166.00 min with orbital shaking of 165 rpm at temperature 20°C.

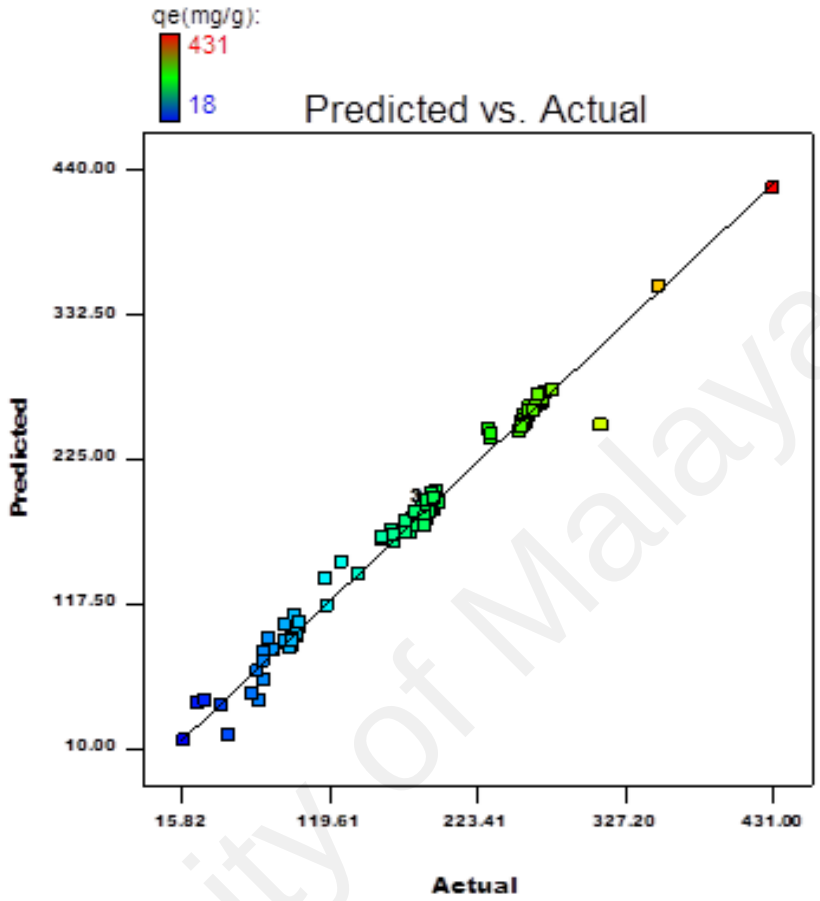

Figure 5.18: Comparison graph for actual versus predicted values of AR119-NIFSS system

Experiments were carried out with different combinations of five independent variables to study the individual as well as combined effects. Analysis of Variance (Table 5.10) obtained from the quadratic regression analysis clearly shows the significance of individual and combined effect of these factors. Significance of factors were considered at confidence interval of 95% with p-value < 0.05%. In this study A, C, D, E, F, AC, A^2, B^2, C^2, E^2 and F^2 are significant model terms and rests of the variables are insignificant. The RSM model is highly significant with model *F-Value* of 422. The predicted R^2 value of 86% is in reasonable agreement with the adjusted R^2 value of 98%. High R^2 value of 98.5% and coefficient of variance (CV) of 6 % assure that model can be used to navigate the design space. As the values of process time and initial dye

concentration increase there is an observable increase in adsorption capacity (Figure 5.19), whereas, when considering their combined effect there is almost negligible effect. Hence, none of the 2D-contour plots and 3D-diagrams is included in the text. The values of the regression coefficients, as seen in equation, indicate the effect the parameter has on the adsorption capacity. Positive values indicate incremental effect, for example, an increase in the adsorption time causes a significant increase in adsorption capacity.

Statistical process optimization, in a given range of parameter values, allows not only for calculating the optimal condition, but also for determining the effect of the process conditions on the adsorption. 3D graphs plotted for time against all other factors indicates that time have a positive effect on adsorption capacity. By increasing time along with temperature, particle size and dye concentration, we can increase the process of adsorption. Maximum time of 166 min has shown maximum adsorption. Increase in temperature has positive effect on adsorption capacity. As temperature increases adsorption capacity decreases. Particle size does not make much difference for the adsorption capacity. Graphs plotted for initial dye concentration against other variables indicates that increase in the initial concentration have positive effect for adsorption capacity. It is observed that initial dye concentration is directly proportional to the adsorption capacity. Positive values indicate incremental effect, for example, an increase in the Temperature (B) causes a significant increase in adsorption capacity.

Table 5.10: ANOVA for fractional factorial experimental design of AR119-NIFSS system

Source	Sum of Squares	Degree of freedom	Mean Square	F Value	P- Value
Model	635122.2	15	42341.5	422.2	< 0.001**
A	872.0	1	872.0	8.7	0.0040**
B	27.5	1	27.5	0.3	0.6019
C	232468.5	1	232468.5	2318.2	< 0.001**
D	1004.8	1	1004.8	10.0	0.0021**
E	44310.7	1	44310.7	441.9	< 0.001**
F	27362.2	1	27362.2	272.9	< 0.001**
AB	63.9	1	63.9	0.6	0.4267
AC	691.1	1	691.1	6.9	0.0101*
BC	7.7	1	7.7	0.1	0.7828
A^2	2106.3	1	2106.3	21.0	< 0.001**
B^2	423.0	1	423.0	4.2	0.0427*
C^2	919.0	1	919.0	9.2	< 0.001**
D^2	9.8	1	9.8	0.1	0.7554
E^2	13306.9	1	13306.9	132.7	< 0.001**
F^2	3658.8	1	3658.8	36.5	< 0.001**
Residual	9526.6	95	100.3		
Total	644648.8	110			

Significant figures
Suggestive significance (p value: $0.05 < p < 0.10$)
* Moderately significant (p value: $0.01 < p \leq 0.05$)
** Strongly significant (p value: $p \leq 0.01$)

The quadratic model developed for process optimization is found to be benifical for predicting the maximum adsorption capacity and understanding the interaction between independent variables as well as their effect on adsorption process. From statistical optimization there is almost 74% increase in adsorption from 431 mg g^{-1} to 750 mg g^{-1}.

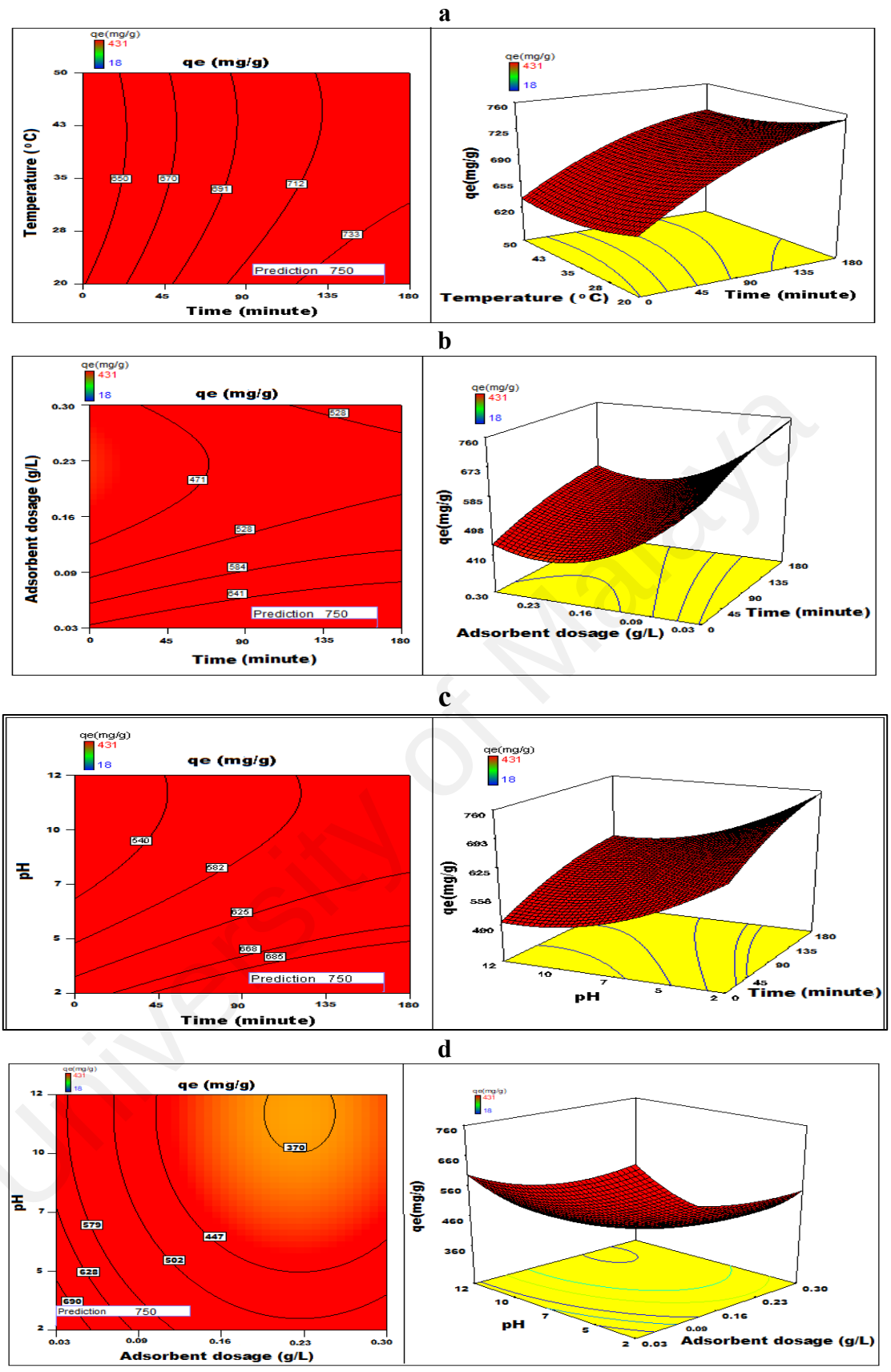

Figure 5.19: 2D-contour plot and 3D-surface plot of AR119-NIFSS systrem showing the variation of adsorption capacity with a) time versus temperature, b) time versus adsorbent dosage, c) time versus pH and d) adsorbent dosage versus pH

5.2.5 Measurement of molar absorption coefficient (ε) of the dye

Six different concentrations (1.00 x 10^{-4}; 1.25 x 10^{-4}; 2.50 x 10^{-4}; 5.00 x 10^{-4}; 7.50 x 10^{-4} and 10.00 x 10^{-4}) of AR119 dye were prepared in distilled water and the absorbance was measured at 526 nm using distilled water as reference (Figure 5.20a).

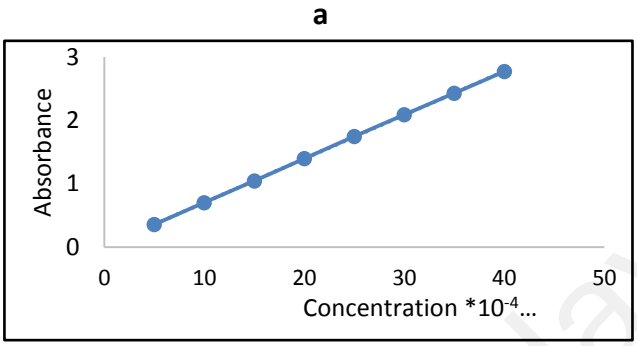

Figure 5.20a: Determination of molecular extinction coefficient of AR119 dye

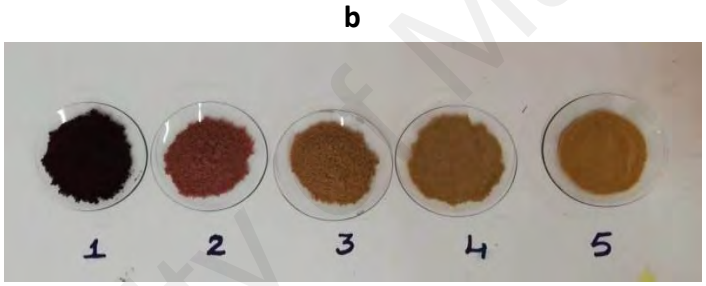

Figure 5.20b: Powders 1 to 4: Fresh samples of NIFSS added to AR119-TIE solution after every 15 min, filtered and the residue dried in oven. Sample 5: NIFSS

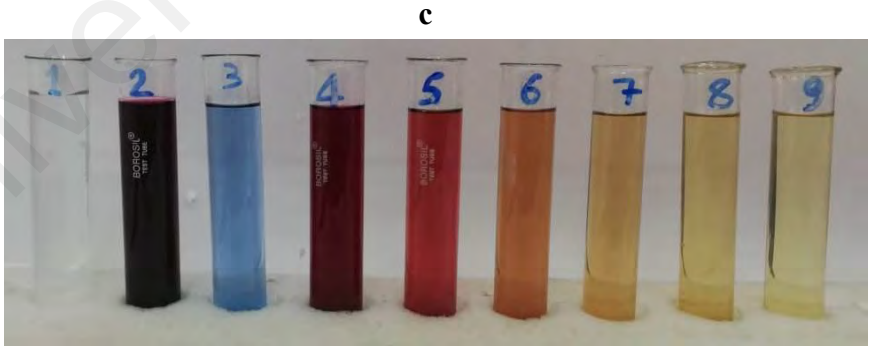

Figure 5.20c: Color of the solutions before and after adsorption: 1. Distilled water; 2. AR119 dye in distilled water; 3. TIE; 4. AR119 dye in TIE; 5. Filtrate after adsorption of dye on NIFSS after 15 min; 6. 30 min; 7. 45 min; 8. 60 min; 9. Filtrate of NIFSS in distilled water

5.2.6 Application of proposed method to textile industrial effluent (TIE)

The powder and filtrate solutions after the adsorption of constituents of Solution 2 on NIFSS are shown in Figures 5.20b and 5. 5.20c. Preliminary trial study revealed that better results could be obtained by scaling up to two-orders of the adsorbent and the adsorbate and to one order of the volume of the solution. In an interesting observation the Solution 2 showed about 21% decrease in absorbance compared to Solution 1. This may be due to the absorbance of the dye by varied undefined constituents present in TIE. Also, it was observed that additional fresh samples of the adsorbent after every 15 min enhanced the efficiency of removal of the dye from TIE. The recovery of the dye and allied substances from Solution 2 to an extent of 75%, 85%, 94% and 96% after 15, 30, 45 and 60 min respectively was observed. This observation is in accordance with the kinetic results according to which the solute adsorbs quickly onto the surface of the particles forming a film which then gets retarded further diffusion thereby bringing change in absorption rates. Scale up experiments up to three orders and regeneration of the adsorbent and cost analysis is detailed in 5.1.6.1 and 5.1.6.2.

Section 5.5 AR119-NICSS system and Section 5.6 AR119-NICUS behave almost similar to AR119-NIFSS. The figures and the tables are incorporated in Appendix A3 and Appendix A4 respectively.

5.3 Acid black 52 – NIFSS system

5.3.1 Surface Characterization

Surface characterization of NIFSS done through SEM showed slightly porous structure (Figure 5.21a). Upon adsorption (Figure 5.21b) of AB52 dye some pores got completely filled with the adsorbate forming a thin film over the particle. The disappearance of peaks between 3284-3471 cm^{-1} and 1529 cm^{-1} after adsorption of AB52 on NIFSS confirms the following: formation of hydrogen bonds between -NH_2 and hydroxyl group and strong adsorption of AB52 dye onto NIFSS (Figure 5.22). Finally, based on the disappearance of IR absorption frequencies, it attributes that to a large extent AB52 dye has adsorbed on NIFSS.

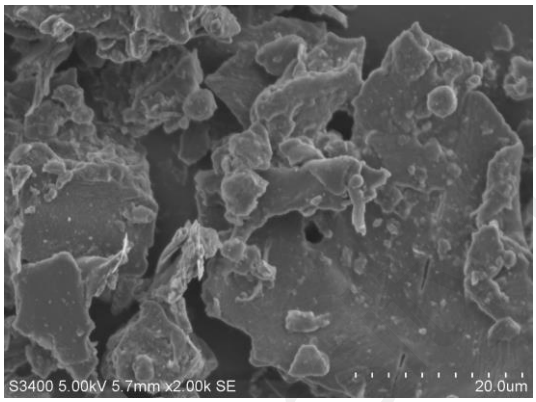

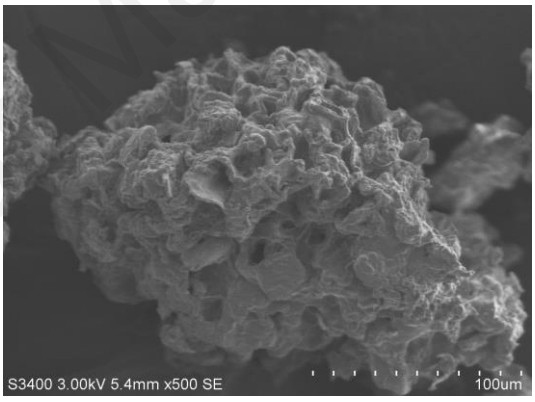

Figure 5.21a: SEM image of NIFSS **Figure 5.21b:** SEM image of AB52-NIFSS

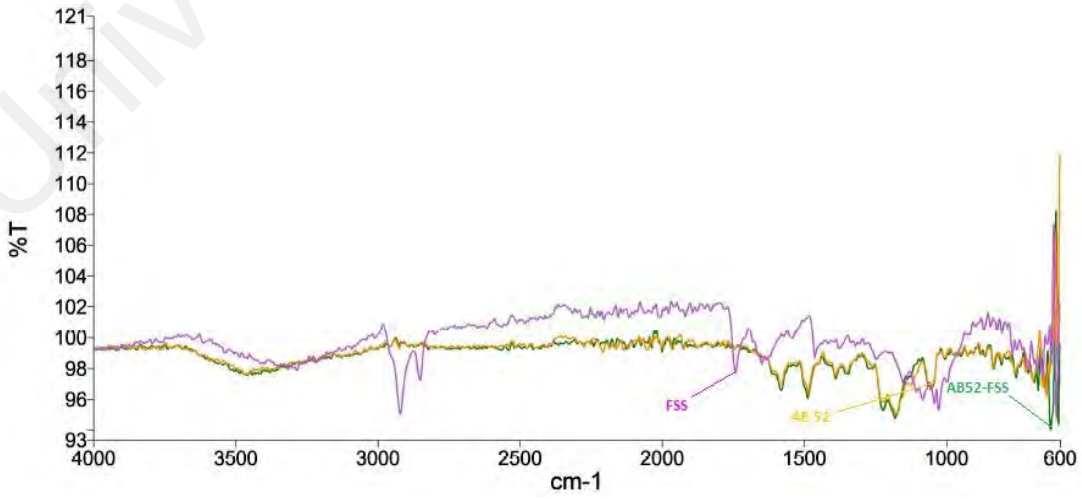

Figure 5.22: FTIR spectra of AB52 dye, NIFSS and AB52 dye adsorbed onto NIFSS

5.3.2 Effect of parameters on adsorption process

5.3.2.1 Effect of pH

At pH 2, the results displayed highest adsorption capacity **(**Figure 5.23**)** and when pH increased from 2 to 4 adsorption decreased drastically. From pH 4 to 10 there is a marginal decrease in the adsorption capacity. Thereafter it remained almost constant till pH 12. The decrease in the dye removal capacity at higher pH is similar to the adsorption made earlier. The maximum AB52 dye removal by NIFSS was at pH 2.0 q_e= 94.00 mg g^{-1} with initial concentration of 500 mg L^{-1}.

5.3.2.2 Effect of initial dye concentration

The q_e value increases with increase in initial dye concentration as shown in Figure 5.23. The %q_e value increased with increase in concentration and reaches maximum in the range of 100-500 mg L^{-1} concentration solution. Thereafter, % q_e value remains almost constant (Figure 5.23).

5.3.2.3 Effect of adsorbent dosage

The effect of adsorbent dosage on AB52 dye adsorption was investigated in the range of 0.025-0.300 g in 50 ml of the solution (0.500-6.000 g L^{-1}). It was observed that the percent AB52 dye removal increased with increase in adsorbent dose. The transfer of AB52 dye onto NIFSS enhanced with higher adsorbent dose. Beyond the limit as shown in Figure 5.23 any further increase in the adsorbent dose did not significantly alter the yield of adsorbate. This is due to the binding of almost all dye molecules on to the adsorbent surface and reaching equilibrium between dye molecule onto the adsorbent and in the solution. The results are depicted in Figure 5.23.

5.3.2.4 Effect of adsorbent particle size

Maximum adsorption capacity was determined for initial AB113 concentration of 100 mg L^{-1} at neutral pH. Different particle sizes of ≤ 90 µm; ≥ 90 µm ≤ 125 µm; ≥

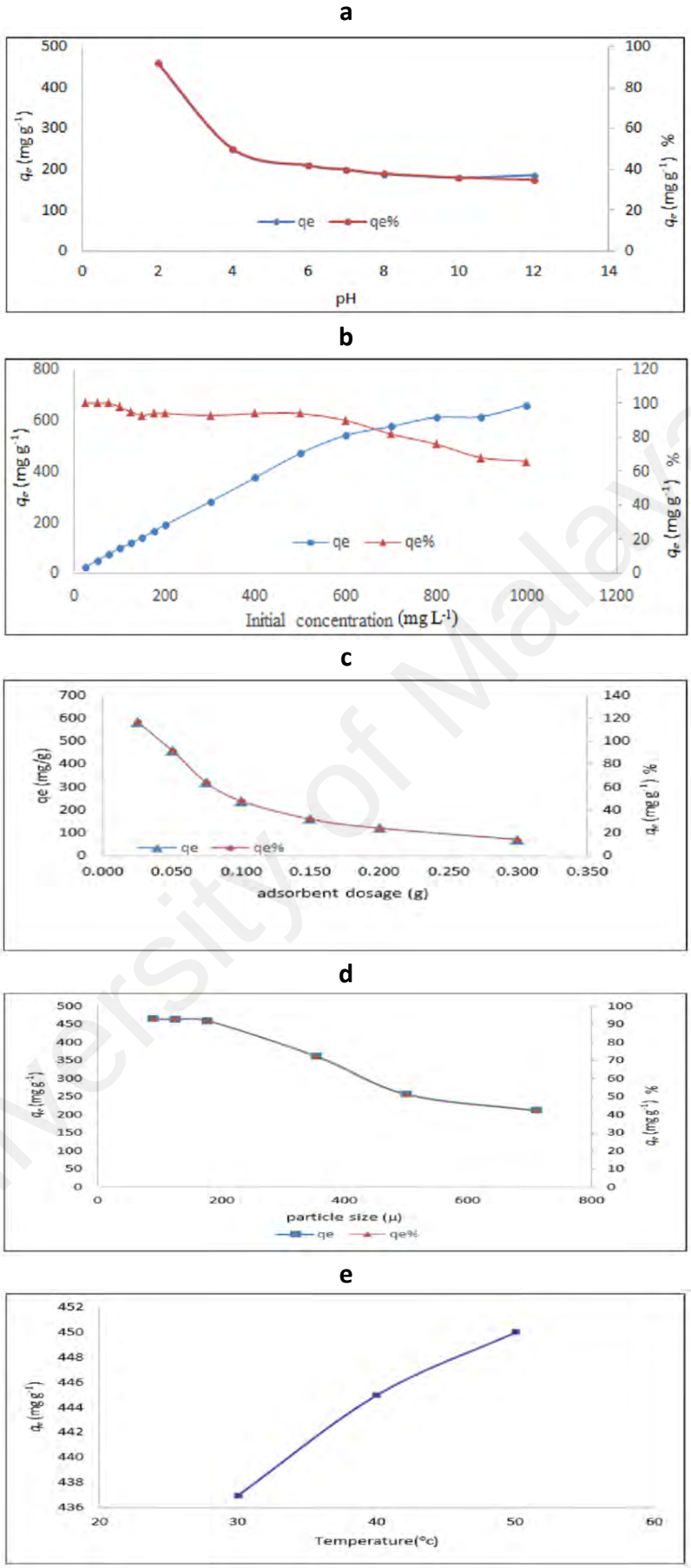

Figure 5.23: Effect of a) pH, b) initial dye concentration with percent q_e, c) adsorbent dosage, d) particle size and e) temperature onto AB52-NIFSS system

125 μm ≤ 177 μm; ≥177 μm ≤ 355 μm; ≥355 μm ≤ 500 μm and ≥ 500 μm ≤ 710 μm were used in the experiment. The adsorption of dye decreased with the increase in the size of the adsorbent particle (Figure 5.23).

5.3.2.5 Effect of temperature

Adsorption studies were carried out at 500 μg ml^{-1} dye concentrations and the results are shown in Figure 5.23. It was observed that with increase in temperature, the adsorption capacity increased indicating endothermic nature of the process. The enhancement in adsorption with temperature may be due to the increase in the mobility of the dye molecule with decrease in their kinetic energy and the enhanced rate of intra-particle diffusion phenomenon.

5.3.3 Adsorption isotherms, kinetic and thermodynamic modeling of AB52-NIFSS system

The Q_m value of 2419975 mg g^{-1} obtained for Langmuir isotherm is too high compared to the experimental q_e value of 94.00 mg g^{-1}. However, the R^2 value of 0.95 indicates good fitting of this isotherm to the experimental data. The R_L values calculated were between 0.997 and 0.999 indicating favourable adsorption of AB52 dye on to NIFSS. The decrease in R_L value with increase in initial concentration indicates that the adsorption is more favourable at high concentration. The large difference between Q_m (2419975 mg g^{-1}) and q_e (94.00 mg g^{-1}) made me to explore other adsorption isotherm models. The values of n_F and $1/n_F$ are 1.087 and 0.543 respectively which indicate that the adsorption is physisorption and favours normal Langmuir Isotherm. The fitting of Freundlich isotherm to the experimental data has provided a correlation coefficient R^2 value of 0.83 which shows that the process is linear. It could be inferred that the adsorption of AB52 dye on to NIFSS is favourable under the experimental conditions and the process is chemisorption. Since, no definite inference could be derived from Langmuir and Freundlich models regarding whether

the system is homogenous or heterogeneous, authors have explored higher models to fit in the data. The Q_m value of 43996.2 mg g^{-1} obtained in Jovanovic isotherm is too high compared to the experimental value of q_e is 94.00 mg g^{-1}. Thus, Jovanovic model value is nearer to the experimental q_e value as compared to Langmuir isotherm (Figure 5.24). The results of Langmuir and Freundlich are presented in Table 5.11 suggesting that the interaction of AB52 dye on NIFSS is linear, favourable and chemical in nature. For academic interest five other three-parameter isotherm models, namely, Toth, Sips, Radke-Prausnitz, Vieth-Sladek and Brouers-Sotolongo were also studied.

The Q_m value of 708884.1 mg g^{-1} obtaining in Toth isotherm is more as compared to the experimental q_e value of 94.00 mg g^{-1} and also that of Langmuir isotherm value of 2419975 mg g^{-1}.The value of Q_m = 530089.7 mg g^{-1} found for the Sips isotherm is very far to that estimated from the Langmuir isotherm (Figure 5.24). Radke-Prausnitz isotherm predicted Q_m of 0.04 mg g^{-1} was very low to the experimentally obtained q_e value. Vieth-Sladek isotherm model predicts Q_m value of 1569817 mg g^{-1} which is a predicted value compared to other models studied. The Q_m value of 2720657 mg g^{-1} obtained from Brouers-Sotolongo isotherm is too high than the experimental value of 94.00 mg g^{-1}. Even, the R^2 value of 0.83 is not a good prediction of this isotherm model to the experimental data (Figure 5.24).

These models illustrated are used to understand the mechanism of adsorption and they are of higher order equations. The validity of data fitting cannot be confirmed by R^2 value alone as it is used only with linear models. Thus, χ^2 values provide a better indication because if model data are similar to the experimental data, then χ^2 would be a small number and *vice versa*. All the nine isotherm models, gave values for important parameters (Q_m, χ^2 and R^2) as shown in Table 5.11. Disparity in the values obtained for the parameters of all models studied along with experimental

values (q_e) will be of some interest to the scientific community; especially to the mathematical modeling researchers who can think of developing new model that can help for better understanding of the adsorption phenomenon occurring in AB52-NIFSS system. The estimated parameters are shown in Table 5.12.

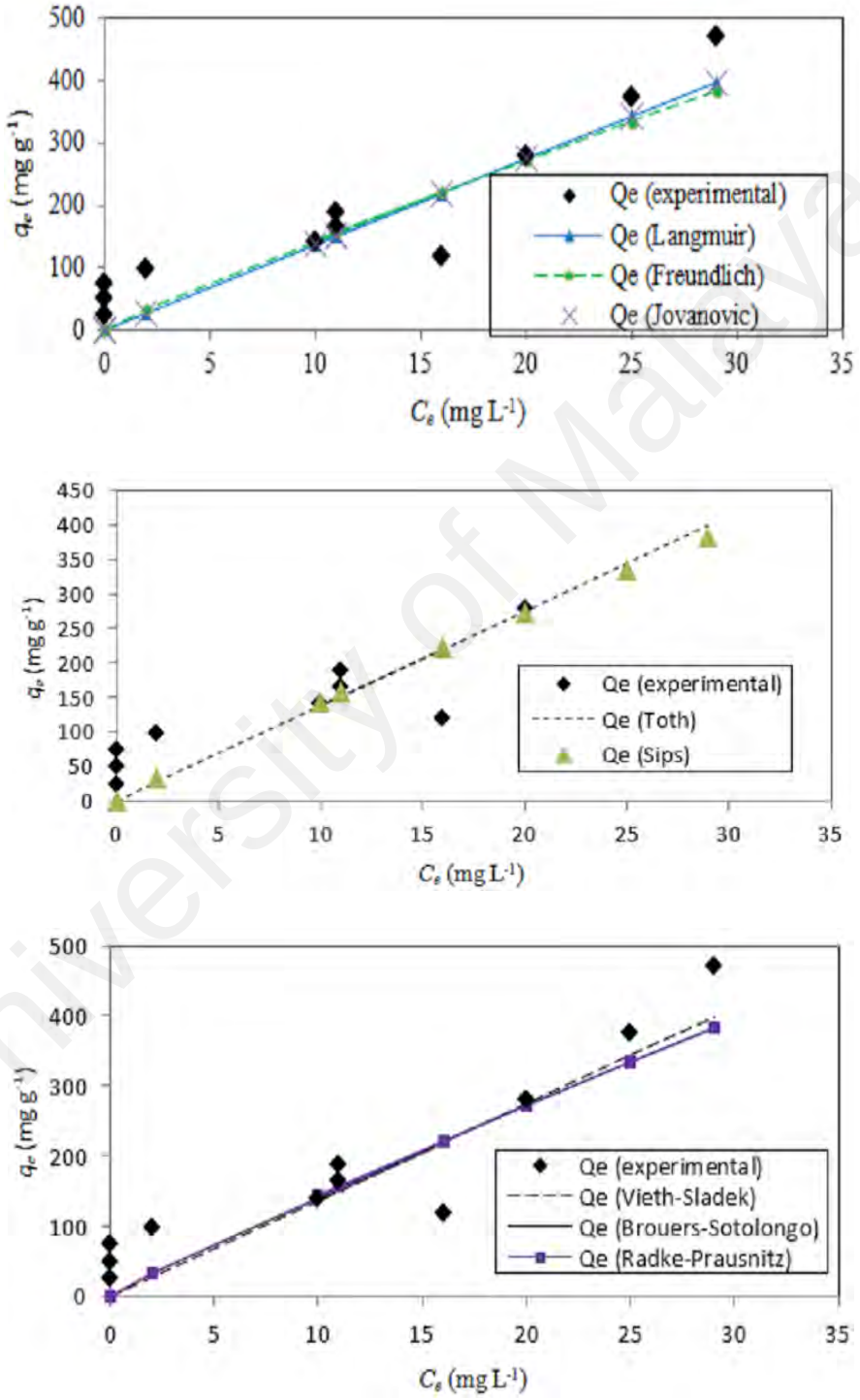

Figure 5.24: Fitting of adsorption data to Langmuir, Freundlich, Jovanovic, Toth, Sips, Vieth-Sladek, Brouers-Sotolongo and Radke-Prausnitz adsorption isotherm of AB52-NIFSS system

Table 5.11: Calculated and statistical parameters for adsorption isotherm models of AB52-NIFSS system

Error Functions	Two-parameter isotherms						Three-parameter isotherms									
	Langmuir		Freundlich		Jovanovic		Toth		Radke-Prausnitz		Sips		Vieth-Sladek		Brouers-Sotolongo	
	Q_m	2419975	K_F	110.32	Q_m	43966.20	Q_m	708884.1	Q_m	0.04	Q_m	530089.70	Q_m	1596817	Q_m	2720657
							n_{To}	0.971	K_{rp}	641.731	K_s	1.33E-05	K_{vs}	0.061	K_{Bs}	6.37E-06
	K_S	0	n_F	1.087	K_J	0.001	b_{To}	37735.180	m_{rp}	0.079	m_s	0.919	β_{vs}	11.72E-06	α	0.920
SSE	26516.9		26360.4		265210.8		265111.2		26360.6		26362.2		265110.2		26360.7	
χ^2	2910.604		292.978		2910.619		2910.606		292.993		292.939		2910.604		292.967	
R^2	0.84		0.83		0.84		0.84		0.83		0.83		0.84		0.83	

Table 5.12: Experimentally determined and theoretically predicted parameters for adsorption kinetics models of AB52-NIFSS system

Initial concentration	Temp		Pseudo-first order				Pseudo-second order			
[µg ml^{-1}]	[K]	$q_{e\ expt}$ [mg g^{-1}]	$Q_{m\ pred}$ [mg g^{-1}]	k_1	R^2	χ^2	$Q_{m\ pred}$ [mg g^{-1}]	k_2	R^2	χ^2
500	303	467	25.42	3.89E-02	0.83	1.57	30.24	1.58E-03	0.90	0.76
	313	458	26.21	4.16E-02	0.81	1.61	30.92	1.69E-03	0.90	0.76
	323	446	210.77	4.07E-02	0.79	1.98	32.82	1.55E-03	0.87	1.00

Based on coefficients of determination (R^2) and chi-square values (χ^2) the pseudo-second order model fitted better than pseudo-first order with the experimental data at initial AB52 dye concentrations of 500 µg ml^{-1} at different temperatures (Figure 5.25). The adsorption rate which was very high initially slowed down gradually to become stagnant when maximum adsorption was reached. The adsorption capacity (q_e) increased with increase in temperature. These results confirm that the adsorption processes are not rate-limiting. The data also indicate that adsorption process occurred in multiple steps where the solute molecules move from the bulk solution to solid surface followed by diffusion of the solute molecules to the pores of NIFSS.

The Dumwald-Wagner model (Figure 5.26a) calculates the true absorption rate constant (K) with corrections for observed diffusion effects (Table 5.13). According to Weber-Morris model (Figure 5.26b) the solute uptake varies with $t^{½}$ rather than time of contact (t). Therefore a plot of q_t versus $t^{½}$ should yield a straight line passing through the origin whose slope (k_{int}) is the diffusion rate constant. Adsorption kinetic is not always controlled by single mechanism. It is evident from our experimental data that at all solute concentrations there is multiple levels of linearity. At lower initial concentration (100 µg ml^{-1}) and at lower temperature, the adsorption rate is high and then there is a shift in the rate following a different linear trajectory and finally the rate stabilizes with respect to time. But at higher temperatures the rate gets more linear.

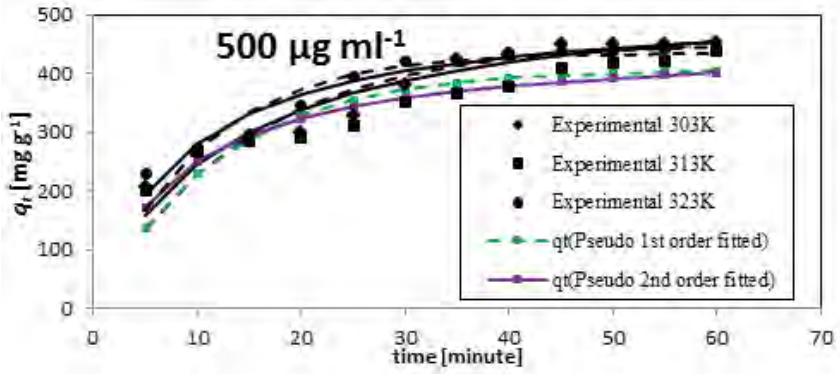

Figure 5.25: Kinetic model fits for 500 µg ml^{-1} initial concentration of AB52 dye onto NIFSS system at different temperatures

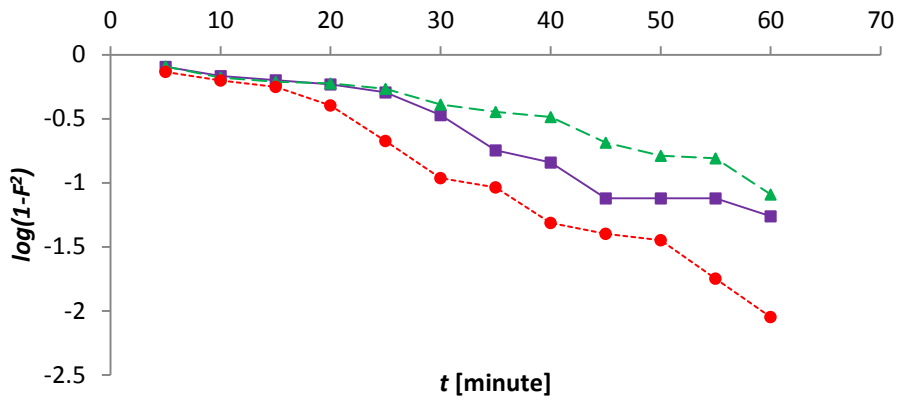

Figure 5.26a: Kinetics data fitted to the Dumwald-Wagner model with initial concentration of AB52 dye onto NIFSS system at 500 µg ml^{-1}

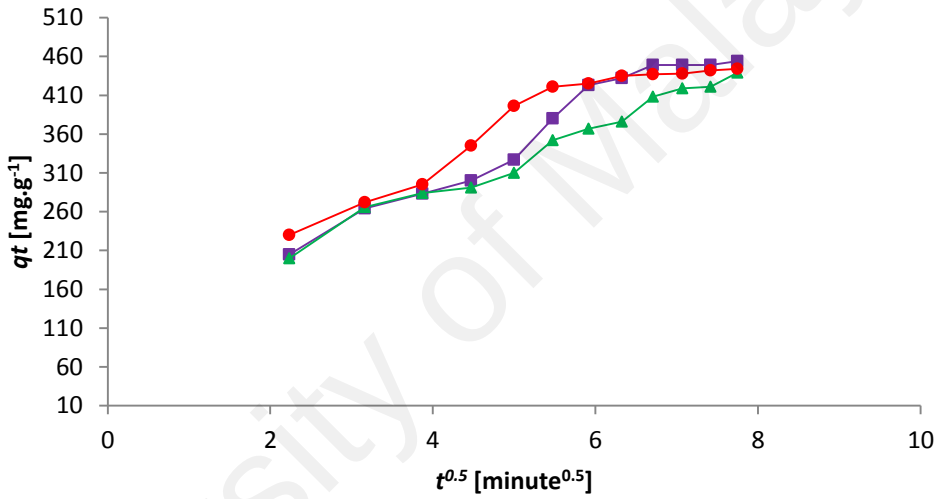

Figure 5.26b: Kinetics data fitted to the Weber- Morris model with initial concentration of AB52 dye onto NIFSS system at 500 µg ml^{-1}

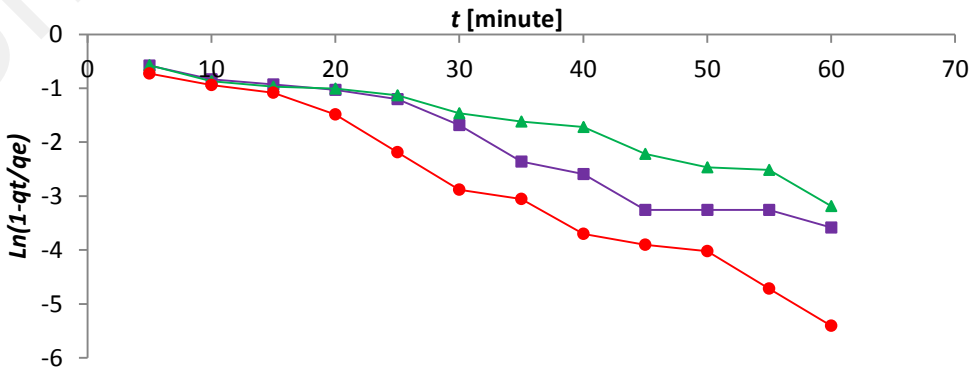

Figure 5.26c: Kinetics data fitted to the Film diffusion model with initial concentration of AB52 dye onto NIFSS system at 500 µg ml^{-1}

Higher concentration of solute (200 μg ml^{-1}) there are less apparent changes in the adsorption rate. This is more so when higher temperature data is fitted to the film diffusion model of Boyd et al., 1947. It is inferred from Figure 5.26c data that good adherence to the model with high R^2 and χ^2 values gives the liquid film diffusion constant R' (Table 5.13). This implies that at higher temperatures the hindrance to rate is adsorption negligible by diffusional limitations. It can be inferred that diffusion is a rate limiting process. Initially the solute gets absorbed quickly onto the surface of the particles forming a film which then retards further diffusion thereby effecting change in absorption rates.

ΔH°, ΔS° and E_a can be determined from the slope and the intercept of the Van't Hoff plots of ln (K_d) and ln (K_2) versus 1/T as shown in Figures 5.27a and 5.27b respectively.

The thermodynamic parameter estimates are provided in Table 5.14. The positive ΔH° value suggests the endothermic nature of adsorption and the negative ΔG° values indicate the feasibility and spontaneity of the adsorption process. The ΔG° is negative for all studied temperatures indicating that the adsorption of AB52 dye onto NIFSS follows spontaneous and favourable trend. The ΔG° value decreases with increase in temperature indicating an increase in adsorption at higher temperatures. The extremely low values of ΔH° suggests that the adsorption process is physical as the standard enthalpy change for chemical reaction is normally >200 KJ mol^{-1}. This has been further confirmed by activation energy values of the adsorption process at 500 μg ml^{-1} of initial concentration of ~-5.93 KJ mol^{-1} using the Arrhenius equation and the kinetic constant from the pseudo-second order model.

Table 5.13: Calculated parameters for diffusion models of AB52-NIFSS system

Initial concentration	Temp	Film diffusion model		Weber-Morris model		Dumwald-Wagner	
[µg ml^{-1}]	[K]	R^{l} [min^{-1}]	R^2	k_{ist} [mg g^{-1} s$^{-0.5}$]	R^2	K [min^{-1}]	R^2
500	303	0.0609	0.95	49.27	0.95	0.055	0.95
	313	0.0433	0.95	42.14	0.98	0.038	0.93
	323	0.0859	0.98	41.59	0.90	0.081	0.98

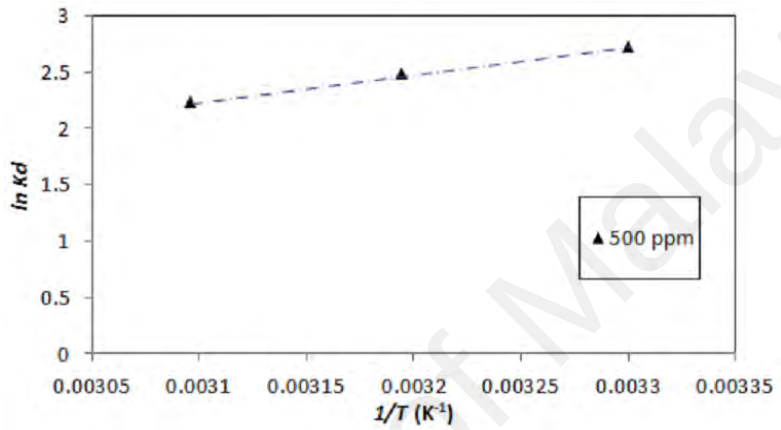

Figure 5.27a: Plot of thermodynamic equilibrium constant vs 1/T to determine the enthalpy and Gibbs free energy of the process of AB52-NIFSS onto NIFSS system and

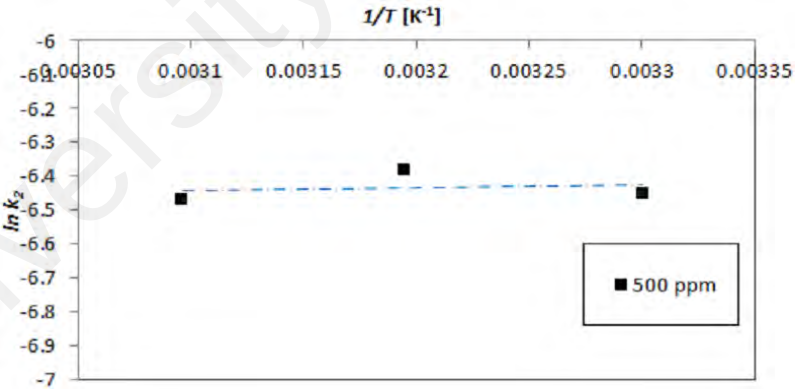

Figure 5.27b: Plot of pseudo – second order kinetic constant vs 1/T to determine the activation energy of the process of AB52-NIFSS onto NIFSS system

Table 5.14: Thermodynamic parameters of AB52-NIFSS system

Initial concentration	Temperature	ΔG°	ΔS°	ΔH°	ln A	E_a
[µg ml^{-1}]	[K]	[KJ mol^{-1}]	[J mol^{-1}K^{-1}]	[KJ mol^{-1}]		[KJ mol^{-1}]
500	303	-6.85	-43.46	20.03	-6.71	-5.93
	313	-6.44				
	323	-5.98				

5.3.4 Statistical optimization by fractional factorial experimental design

Experiments were carried out with different combinations of six independent variables to study the individual as well as combined effects. Analysis of variance (Table 5.15) obtained from the quadratic regression analysis clearly shows the significance of individual and combined effect of these factors. Significance of factors were considered at confidence interval of 95% with *p*-value < 0.05%. In this study A, C, D, E, F, A^2, B^2, C^2, E^2 and F^2 are significant model terms and rest of the variables is insignificant. Cross products AD, AE, BD, BE, BF, CD, CE, CF, DE, DF and EF are zero. The RSM model is highly significant with model *F-Value* of 172.9. The predicted R^2 value of 810.4% is in reasonable agreement with the adjusted R^2 value of 96.7%. High R^2 value of 910.2% and coefficient of variance of 11.1% assure that model can be used to navigate the design space. The comparison graph for actual versus predicted values (Figure 5.28) indicates a strong relationship between the experimental and predicted responses. The regression equation obtained from the study is shown below:

$$\text{Adsorption}=-160.9+1211.7*A+1.1*B+323.3*C-149.0*D-234.8*E-90.1*F+1.5*AB$$
$$-239.2*A^2+29.2*B^2-123.6*C^2+10.4*D^2+193.2*E^2+179.1*F^2 \quad \textbf{(5.3)}$$

The optimal values of the variables determined by maximization of the second-order polynomial equation with interaction terms obtained by multiple regression analysis based on FFED. Maximum adsorption obtained by the statistical optimization experiment was 958 mg g^{-1} with optimized conditions established as a pH of 1.4, adsorbent dosage of 0.5 g L^{-1}, and particle size of 101 μ and an initial dye concentration of 958 mg L^{-1} for an adsorption time of 112 min with orbital shaking of 165 rpm at temperature 32°C.

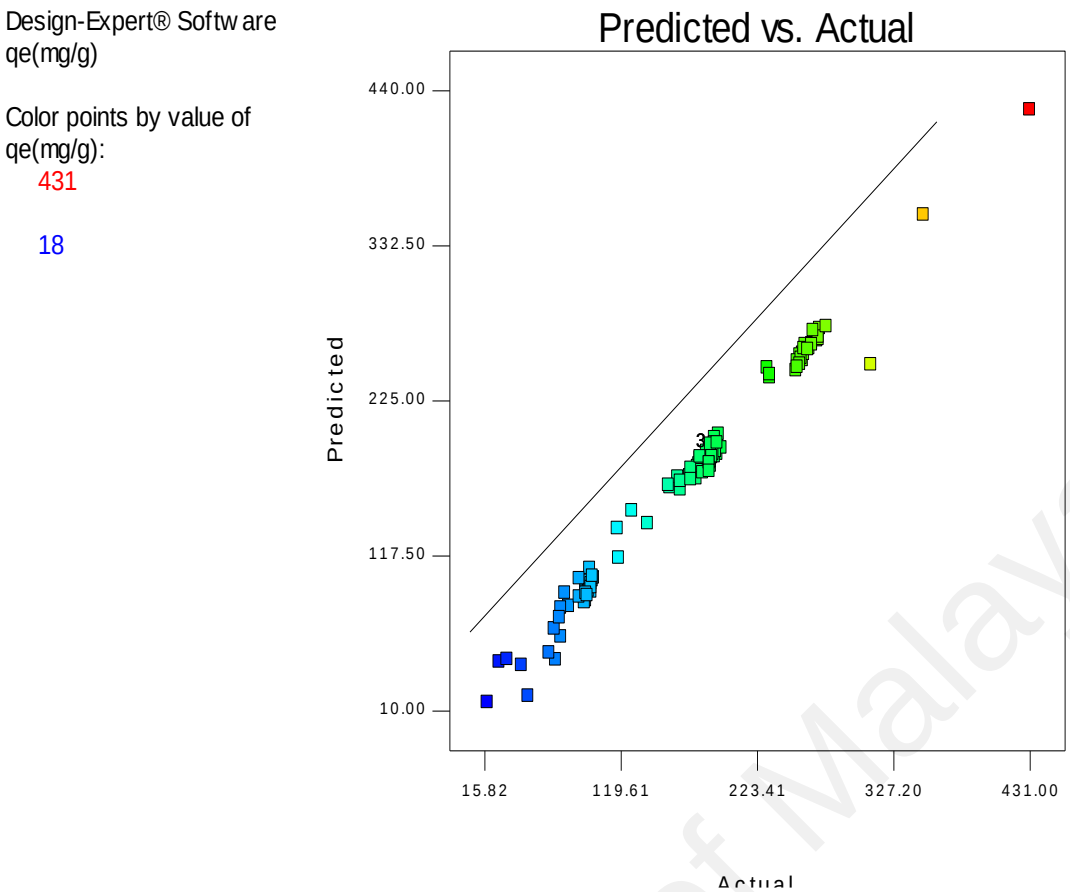

Figure 5.28: Comparison graph for actual versus predicted values of AB52-NIFSS onto NIFSS system

Statistical process optimization, in a given range of parameter values, allows not only for calculating the optimal condition, but also for determining the effect of the process conditions on the adsorption. 3D graphs plotted for time against temperature (AB), concentration (AC), adsorbent dosage (AE) and pH (AF) (Figure 5.29). By increasing time along with temperature, particle size and dye concentration, we can increase the process of adsorption. Maximum time of 113 min has shown maximum adsorption. Temperature does not make much difference on the process. Increase in pH beyond 2 decreases adsorption capacity even if time is increased. Absorbent dosage has negative effect on adsorption however increased time can improve the process of adsorption. Temperature plotted against other independent variables indicates that temperature has neutral effect with all other variable on the response. Initial dye concentration against other variables indicates that increase in the initial concentration

has positive effect for adsorption capacity. Increase in initial dye concentration increases the adsorption capacity. Increase in pH decreases the adsorption capacity of the adsorbent. Thus effect of two parameters together on the biosorption is graphically represented in the 3D-surface and 2D-contour plots (Figure 5.29).

Table 5.15: ANOVA for fractional factorial experimental design of AB52-NIFSS system

Source	Sum of Squares	Degree of freedom	Mean Square	F Value	P- Value
Model	16106410.8	13	123896.0	172.9	< 0.001**
A	2255810.8	1	2255810.8	314.8	< 0.001**
B	22.5	1	22.5	0.0	0.8600
C	657481.5	1	657481.5	9110.6	< 0.001**
D	87862.5	1	87862.5	122.6	< 0.001**
E	227023.5	1	227023.5	316.8	< 0.001**
F	379910.7	1	379910.7	53.0	< 0.001**
AB	23.4	1	23.4	0.0	0.8572
A^2	2264310.0	1	2264310.0	316.0	< 0.001**
B^2	4993.9	1	4993.9	10.0	0.0104**
C^2	43522.2	1	43522.2	60.7	< 0.001**
D^2	101.9	1	101.9	0.1	0.7073
E^2	42440.6	1	42440.6	59.2	< 0.001**
F^2	56703.4	1	56703.4	79.1	< 0.001**
Residual	458511.0	64	716.5		
Total	1656505.8	77			

Significant figures
Suggestive significance (p value: $0.05 < p < 0.10$)
Moderately significant (p value: $0.01 < p \leq 0.05$)
** Strongly significant (p value: $p \leq 0.01$)

a

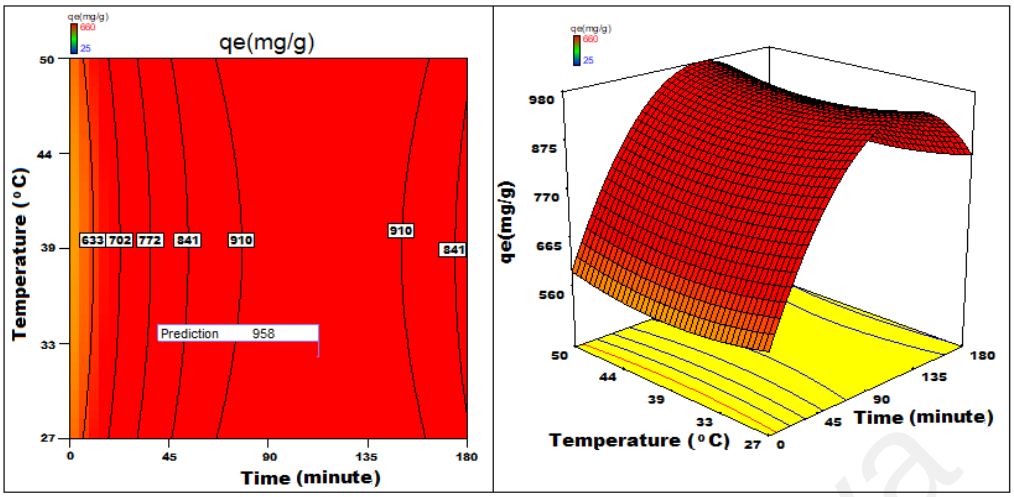

b

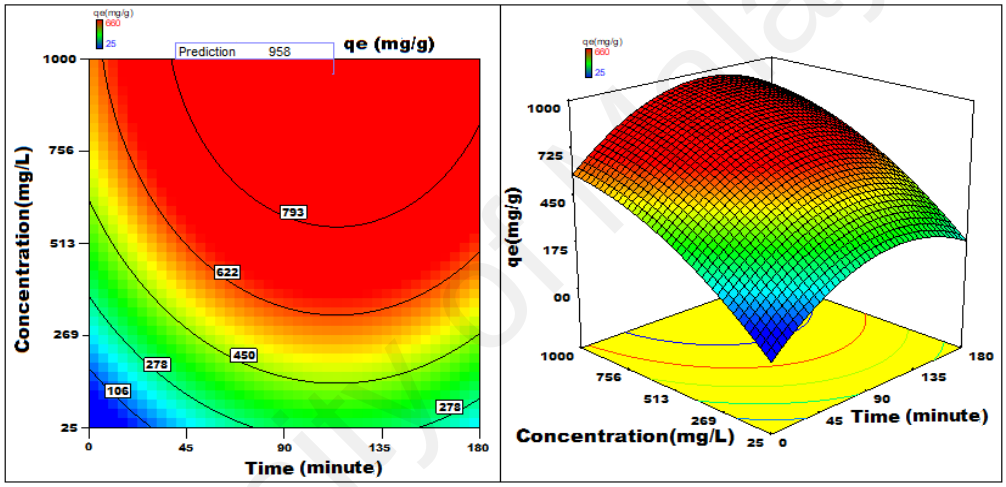

c

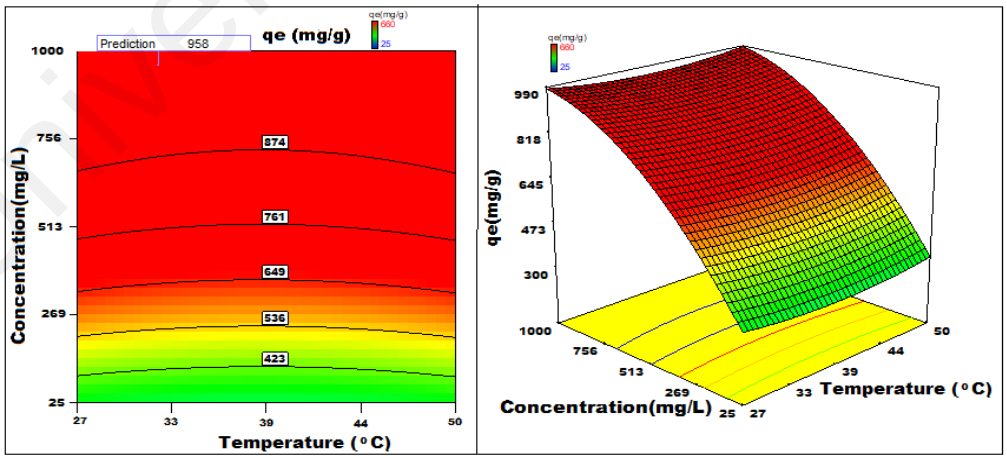

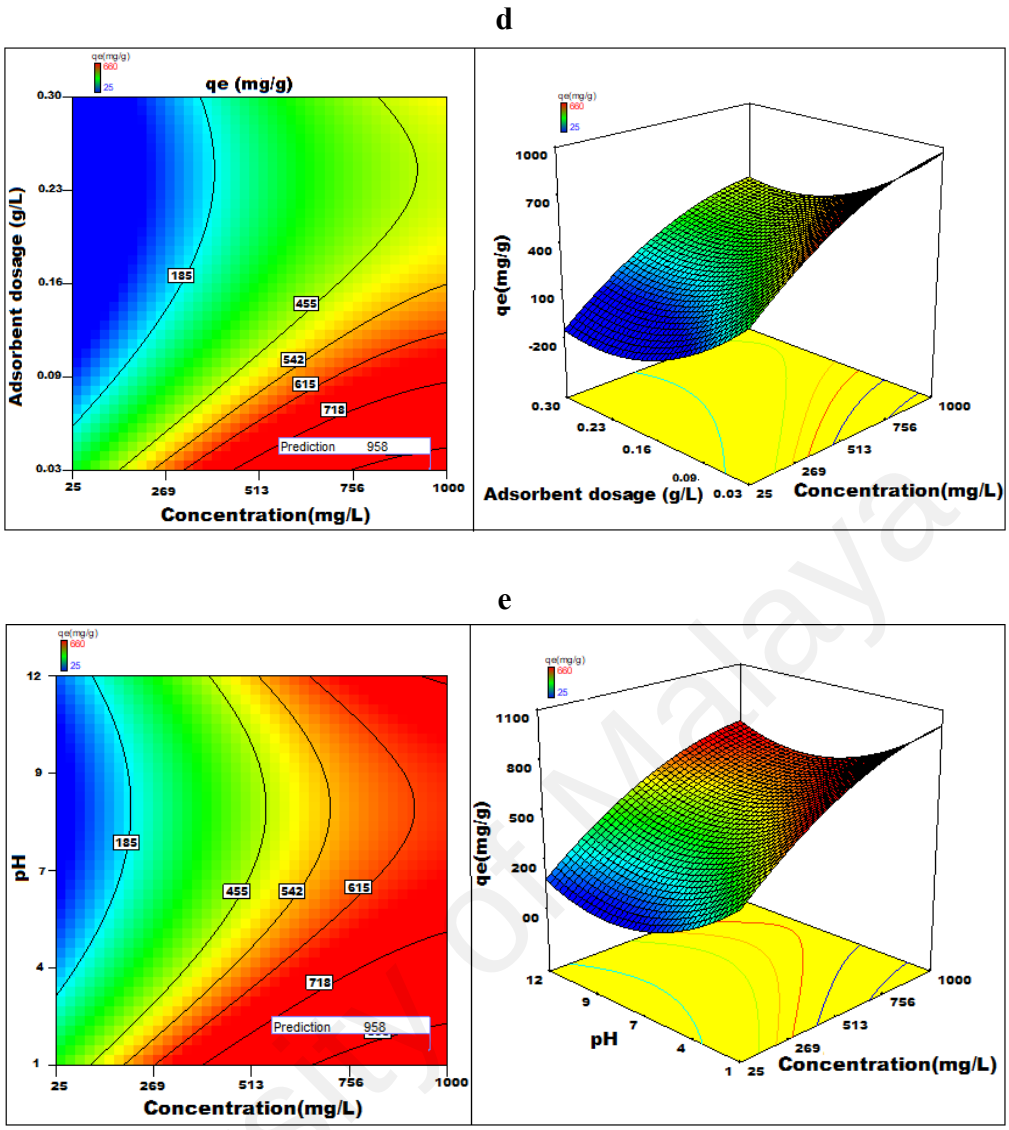

Figure 5.29: 2D-contour plot and 3D-surface plot of AB52-NIFSS system showing the variation of adsorption capacity with a) time versus temperature, b) time versus concentration, c) temperature versus concentration, d) adsorbent dosage versus concentration and e) pH versus concentration

5.3.5 Measurement of molar absorption coefficient (ε) of the dye

Six different concentrations (1.00 x 10^{-4}; 1.25 x 10^{-4}; 2.50 x 10^{-4}; 5.00 x 10^{-4}; 7.50 x 10^{-4} and 10.00 x 10^{-4}) of AB52 dye were prepared in distilled water and the absorbance was measured at 571 nm using distilled water as reference (Figure 5.30a).

5.3.6 Application of Proposed Method to Textile Industrial Effluent (TIE)

The powder and filtrate solutions after the adsorption of constituents of Solution 2 on NIFSS are shown in Figures 5.30b and 5.30c. Preliminary trial study revealed that better results could be obtained by scaling up to two-orders of the adsorbent and the adsorbate and to one order of the volume of the solution. In an interesting observation the Solution 2 showed about 20% decrease in absorbance compared to Solution 1.

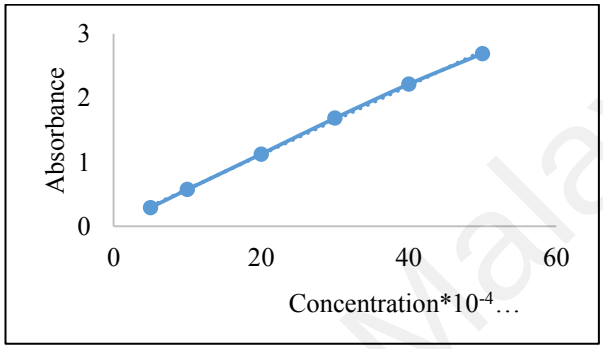

Figure 5.30a: Determination of molecular extinction coefficient of AB52 dye

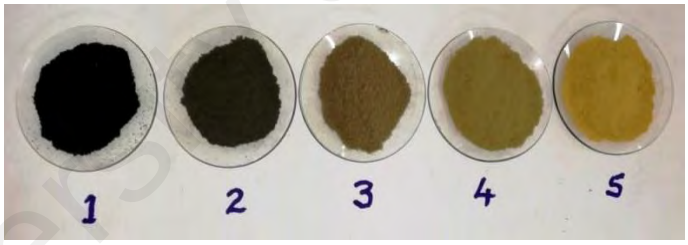

Figure 5.30b: Powders 1 to 4: Fresh samples of NIFSS added to AB52-TIE solution after every 15 min, filtered and the residue dried in oven. Sample 5: NIFSS

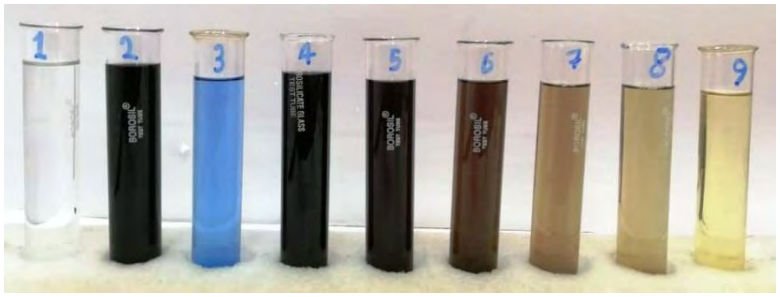

Figure 5.30c: Colour of the solutions before and after adsorption: 1. Distilled water; 2. AB52 dye in distilled water; 3. TIE; 4. AB52 dye in TIE; 5. Filtrate after adsorption of dye on NIFSS after 15 min; 6. 30 min; 10. 45 min; 11. 60 min; 9. Filtrate of NIFSS in distilled water

This may be due to the absorbance of the dye by varied undefined constituents present in TIE. Also, it was observed that additional fresh samples of the adsorbent after every 15 min enhanced the efficiency of removal of the dye from TIE. The recovery of the dye and allied substances from Solution 2 to an extent of 75%, 90%, 93% and 95% after 15, 30, 45 and 60 min respectively was observed. This observation is in accordance with the kinetic results according to which the solute adsorbs quickly onto the surface of the particles forming a film which then gets retarded further diffusion thereby bringing change in absorption rates.

The experiment was scaled up to 10 g, 20 g, and 50 g of NIFSS using 1, 2, and 5 L of Solution 2 taken in polyethylene beakers. The solutions were vigorously stirred using a magnetic stirrer and the procedure repeated as indicated earlier and the results obtained were almost uniform. All experiments were carried out in triplicate and the mean of three results are reported. The coefficients of variance of all results did not vary from ± 2% error.

In brief, an attempt to increase the scale of experiment by about three orders of its initial set up has given promising results. The industrial effluents may have many variables that may not be exactly interpreted from the initial data. This is always a serious limitation in such studies. The outcome could be pin pointedly focused by resorting to much larger pilot scale study. However, the fact that the limitations of scale have been recognized, and that the enhanced scale experimental data will definitely continue to show promise and reliability of the process, which fact may be sufficient to prove that the principles of the method when put into development on a larger scale in industries will show its usefulness.

Section 5.8 AB52-NICSS system and Section 5.9 AB52-NICUS behave almost similar to AB52-NIFSS. The figures and the tables are incorporated in Appendix A5 and Appendix A6 respectively.

CHAPTER 6: CONCLUSION

The major conclusions of the study are: first, Nutraceutical Industrial Spent (NIS) have been developed as efficient, environmental-friendly and cost-effective biosorbent for the remediation of toxic dyes; second, operational parameters influenced the adsorption efficiency of NIS; third, the adsorption isotherms and kinetic studies confirmed the complexity involved in the dye adsorption mechanism; fourth, thermodynamic study demonstrated the spontaneous and endothermic nature of biosorption process; fifth, NIS as alternate to activated carbon has better claim due to the least E-factor and low-cost; sixth, an alternate to burning/incineration/landfills of NIS to reduce carbon foot print has been explored; seventh, NIS is ready-to-use matrix in field of adsorption science; eighth, NIS-plastic composites proved to be viable propositions for sustainability; ninth, NIS and the dye adsorbed NIS have potential as filler materials in the fabrication of thermoplastics and thermosets composites by utilizing either virgin or waste synthetic polymer matrices; tenth, the products have high commercial viability and environmental sustainability and eleventh, the author envisages that the concept proposed and the template developed associated with dwindling resources will create an alternate paradigm to transform "waste-to-wealth".

In summary, the economic importance of the renewable resources has been neglected in most countries in the past. However, as their value becomes increasingly recognized for a multiplicity of uses, they represent a substantial potential source of renewable raw material for the future. It is univocally clear from the preceding chapters that Nutraceutical Industrial Spent may represent a more realistic approach to the design of adsorbent systems. Thus, it will not be surprising if the coming few

years will witness the growth – if not the dominance - of research on inorganic materials and Nutraceutical Industrial Spent as hybrid adsorbents.

REFERENCES

Acemioğlu, B. (2004). Adsorption of Congo red from aqueous solution onto calcium-rich fly ash. *Journal of Colloid and Interface Science*, *274*(2), 371-379.

Adams, C.D., & Gorg, S. (2002). Effect of pH and gas-phase ozone concentration on the decolorization of common textile dyes. *Journal of Environmental Engineering*, *128*(3), 293-298.

Afkhami, A., & Moosavi, R. (2010). Adsorptive removal of Congo red, a carcinogenic textile dye, from aqueous solutions by maghemite nanoparticles. *Journal of Hazardous Materials*, *174*(1-3), 398-403.

Ahmad, R., & Kumar, R. (2010). Adsorption studies of hazardous malachite green onto treated ginger waste. *Journal of Environmental Management*, *91*(4), 1032-1038.

Ahmad, A., Mohd-Setapar, S.H., Chuong, C.S., Khatoon, A., Wani, W.A., Kumar, R., & Rafatullah, M. (2015). Recent advances in new generation dye removal technologies: novel search for approaches to reprocess wastewater. *RSC Advances*, *5*(39), 30801-30818.

Ahmedna, M., Marshall, W.E., & Rao, R.M. (2000). Production of granular activated carbons from select agricultural by-products and evaluation of their physical, chemical and adsorption properties. *Bioresource Technology*, *71*(2), 113-123.

Aksu, Z., & Tezer, S. (2005). Biosorption of reactive dyes on the green alga Chlorella vulgaris. *Process Biochemistry*, *40*(3-4), 1347-1361.

Albano, C., Ichazo, M., González, J., Delgado, M., & Poleo, R. (2001). Effects of filler treatments on the mechanical and morphological behavior of PP+ wood flour and PP+ sisal fiber. *Materials Research Innovations*, *4*(5-6), 284-293.

Ali, H. (2010). Biodegradation of synthetic dyes—a review. *Water, Air, & Soil Pollution*, *213*(1-4), 251-273.

Alkan, M., Demirbaş, Ö., & Doğan, M. (2007). Adsorption kinetics and thermodynamics of an anionic dye onto sepiolite. *Microporous and Mesoporous Materials*, *101*(3), 388-396.

Allen, S.J., Mckay, G., & Porter, J. F. (2004). Adsorption isotherm models for basic dye adsorption by peat in single and binary component systems. *Journal of Colloid and Interface Science*, *280*(2), 322-333.

Altın, O., Özbelge, H. Ö., & Doğu, T. (1998). Use of general purpose adsorption isotherms for heavy metal–clay mineral interactions. *Journal of Colloid and Interface Science*, *198*(1), 130-140.

Anastopoulos, I., & Kyzas, G.Z. (2014). Agricultural peels for dye adsorption: a review of recent literature. *Journal of Molecular Liquids*, *200*, 381-389.

Anjaneyulu, Y., Chary, N.S., & Raj, D.S.S. (2005). Decolourization of industrial effluents–available methods and emerging technologies–a review. *Reviews in Environmental Science and Bio/Technology*, *4*(4), 245-273.

Anliker, R., Clarke, E.A., & Moser, P. (1981). Use of the partition coefficient as an indicator of bioaccumulation tendency of dyestuffs in fish. *Chemosphere*, *10*(3), 263-274.

Apak, R., & Hugül, M. (1996). Photooxidation of some mono-, di-, and trichlorophenols in aqueous solution by hydrogen peroxide/UV combinations. *Journal of Chemical Technology & Biotechnology: International Research in Process, Environmental and Clean Technology*, *67*(3), 221-226.

Apostol, L.C., Pereira, L., Pereira, R., Gavrilescu, M., & Alves, M.M. (2012). Biological decolorization of xanthene dyes by anaerobic granular biomass. *Biodegradation*, *23*(5), 725-737.

ASTM D 638-94b. (1995). *Standard Test Method for Tensile Properties of Plastics*. Annual Book of ASTM Standards. American Society for Testing and Materials Publishing, Philadelphia.

ASTM D 638-95. (1995). *Standard test method for tensile properties of plastics*.

ASTM D 790-92. (1995). *Standard Test Method for Flexural Properties of unreinforced and reinforced Plastics and Electrical Insulating Materials*. Annual Book of ASTM Standards, American Society for Testing and Materials Publishing, Philadelphia.

ASTM D 256-93a. (1998). *Standard Test Method for determining the Pendulum Impact Resistance of notched specimens of Plastics*. Annual Book of ASTM Standards, American Society for Testing and Materials Publishing, Philadelphia.

ASTM D 792-00. (2004). *Standard test methods for density and specific gravity (relative density) of plastics by displacement*. Annual Book of ASTM Standards, American Society for Testing and Materials Publishing, Philadelphia.

ASTM D 2240. (2005). *Standard test method for rubber property durometer hardness*. Annual Book of ASTM Standards, American Society for Testing and Materials Publishing, Philadelphia.

ASTM D 570-98. (2010). *Standard test method for water absorption of plastics*. Annual Book of ASTM Standards, American Society for Testing and Materials Publishing, Philadelphia

ASTM G65. (2000). *Standard Test Method for Measuring Abrasion Using the Dry Sand/Rubber Wheel Apparatus*. ASTM, USA.

Aurrekoetxea, J., Sarrionandia, M., & Gómez, X. (2008). Effects of microstructure on wear behaviour of wood reinforced polypropylene composite. *Wear*, *265* (56), 606-611.

Aygün, A., Yenisoy-Karakaş, S., & Duman, I. (2003). Production of granular activated carbon from fruit stones and nutshells and evaluation of their physical, chemical and adsorption properties. *Microporous and Mesoporous Materials*, *66*(2-3), 189-195.

Azarang, M., Shuhaimi, A., Yousefi, R., Golsheikh, A.M., & Sookhakian, M. (2014). Synthesis and characterization of ZnO NPs/reduced graphene oxide nanocomposite prepared in gelatin medium as highly efficient photo-degradation of MB. *Ceramics International, 40*(7*)*, 10217-10221.

Azarang, M., Shuhaimi, A., Yousefi, R., & Jahromi, S.P. (2015). One-pot sol–gel synthesis of reduced graphene oxide uniformly decorated zinc oxide nanoparticles in starch environment for highly efficient photodegradation of Methylene Blue. *RSC Advances*, *5*(28), 21888-21896.

Azarang, M., Shuhaimi, A., & Sookhakian, M. (2015a). Crystalline quality assessment, photocurrent response and optical properties of reduced graphene oxide uniformly decorated zinc oxide nanoparticles based on the graphene oxide concentration. *RSC Advances*, *5*(65), 53117-53128.

Babel, S., & Kurniawan, T.A. (2003). Low-cost adsorbents for heavy metals uptake from contaminated water: a review. *Journal of Hazardous Materials*, *97*(1-3), 219-243.

Bafana, A., Devi, S.S., Krishnamurthi, K., & Chakrabarti, T. (2007). Kinetics of decolourisation and biotransformation of direct black 38 by C. hominis and P. stutzeri. *Applied Microbiology and Biotechnology*, *74*(5), 1145-1152.

Bafana, A., & Chakrabarti, T. (2008). Lateral gene transfer in phylogeny of azoreductase enzyme. *Computational Biology and Chemistry*, *32*(3), 191-197.

Bafana, A., Devi, S.S., & Chakrabarti, T. (2011). Azo dyes: past, present and the future. *Environmental Reviews*, *19*(NA), 350-371.

Bahorsky, M. (1998, June). Emerging Technologies for Color Removal. In *No. Caroline. Div Pollu. Prevention Seminar, Sure* (Vol. 17).

Bailey, S.E., Olin, T.J., Bricka, R.M., & Adrian, D.D. (1999). A review of potentially low-cost sorbents for heavy metals. *Water Research*, *33*(11), 2469-2479.

Banat, I.M., Nigam, P., Singh, D., & Marchant, R. (1996). Microbial decolorization of textile-dyecontaining effluents: a review. *Bioresource Technology*, *58*(3), 217-227.

Baouab, M.H.V., Gauthier, R., Gauthier, H., & El Baker Rammah, M. (2001). Cationized sawdust as ion exchanger for anionic residual dyes. *Journal of Applied Polymer Science*, *82*(1), 31-37.

Bataille, P., Boisse, S., & Schreiber, H.P. (1984). Mica as filler for PVC compounds: effects of particle size and surface treatment. *Journal of Vinyl Technology*, *6*(4), 147-151.

Batzias, F.A., & Sidiras, D.K. (2004). Dye adsorption by calcium chloride treated beech sawdust in batch and fixed-bed systems. *Journal of Hazardous Materials*, *114*(1-3), 167-174.

Beerbaum, S., & Heidhues, F. (1996). Policy reform and natural resource management week 4: Day 4b impact of environmental regulations on trade relations for developing countries. A case study of indian-german textile trade.

Belem, M.A. (1999). Application of biotechnology in the product development of nutraceuticals in Canada. *Trends in Food Science & Technology*, *10*(3), 101-106.

Bello, O.S., Bello, I.A., & Adegoke, K.A. (2013). Adsorption of dyes using different types of sand: a review. *South African Journal of Chemistry*, *66*(1), 117-129.

Bigda, R.J. (1995). Consider Fentons chemistry for wastewater treatment. *Chemical Engineering Progress*, *91*(12).

Birch, R. R., Biver, C., Campagna, R., Gledhill, W. E., Pagga, U., Steber, J., & Bontinck, W. J. (1989). Screening of chemicals for anaerobic biodegradability. *Chemosphere*, *19*(10-11), 1527-1550.

Biron, M. (2012). *Thermoplastics and Thermoplastic Compo*sites. 2nd ed, William Andrew Publishing, New York.

Birt, D.F., Hendrich, S., & Wang, W. (2001). Dietary agents in cancer prevention: flavonoids and isoflavonoids. *Pharmacology & Therapeutics*, *90*(2-3), 157-177.

Bhattacharyya, K.G., & Sarma, A. (2003). Adsorption characteristics of the dye, Brilliant Green, on Neem leaf powder. *Dyes and pigments*, *57*(3), 211-222.

Bhattacharyya, K.G., & Sharma, A. (2004). Azadirachta indica leaf powder as an effective biosorbent for dyes: a case study with aqueous Congo Red solutions. *Journal of Environmental Management*, *71*(3), 217-229.

Bledzki, A.K., Letman, M., Viksne, A., & Rence, L. (2005). A comparison of compounding processes and wood type for wood fibre—PP composites. *Composites Part A: Applied Science and Manufacturing*, *36*(6), 789-797.

Borrely, S.I., Cruz, A.C., Del Mastro, N.L., Sampa, M.H.O., & Somessari, E.S. (1998). Radiation processing of sewage and sludge. A review. *Progress in Nuclear Energy*, *33*(1-2), 3-21.

Boyd, G.E., Adamson, A.W., & Myers Jr, L.S. (1947). The exchange adsorption of ions from aqueous solutions by organic zeolites. II. Kinetics1. *Journal of the American Chemical Society*, *69*(11), 2836-2848.

Brouers, F., Sotolongo, O., Marquez, F., & Pirard, J.P. (2005). Microporous and heterogeneous surface adsorption isotherms arising from Levy distributions. *Physica A: Statistical Mechanics and its Applications*, *349*(1-2), 271-282.

Brown, S.C., & Schoenberg, M. (2008). Cancer incidence and mortality among workers exposed to benzidine and 3, 3-dichlorobenzidine. *Epidemiology*, *19*(6), S112.

Calzaferri, G., Brühwiler, D., Megelski, S., Pfenniger, M., Pauchard, M., Hennessy, B., Devaux, A., & Graf, U. (2000). Playing with dye molecules at the inner and outer surface of zeolite L. *Solid State Sciences*, *2*(4), 421-447.

Carliell, C.M., Barclay, S.J., Shaw, C., Wheatley, A.D., & Buckley, C.A. (1998). The effect of salts used in textile dyeing on microbial decolourisation of a reactive azo dye. *Environmental Technology*, *19*(11), 1133-1137.

Carrasco-Marin, F., Alvarez-Merino, M.A., & Moreno-Castilla, C. (1996). Microporous activated carbons from a bituminous coal. *Fuel*, *75*(8), 966-970.

Carvalho, M.C., Pereira, C., Goncalves, I.C., Pinheiro, H.M., Santos, A.R., Lopes, A., & Ferra, M.I. (2008). Assessment of the biodegradability of a monosulfonated azo dye and aromatic amines. *International Biodeterioration & Biodegradation*, *62*(2), 96-103.

Cervantes, F.J., Garcia-Espinosa, A., Moreno-Reynosa, M.A., & Rangel-Mendez, J.R. (2010). Immobilized redox mediators on anion exchange resins and their role on the reductive decolorization of azo dyes. *Environmental Science & Technology*, *44*(5), 1747-1753.

Chakraborty, S., Purkait, M.K., DasGupta, S., De, S., & Basu, J.K. (2003). Nanofiltration of textile plant effluent for color removal and reduction in COD. *Separation and Purification Technology*, *31*(2), 141-151.

Chen, B., Hui, C.W., & McKay, G. (2001). Film-pore diffusion modeling and contact time optimization for the adsorption of dyestuffs on pith. *Chemical Engineering Journal*, *84*(2), 77-94.

Chequer, F.M.D., Dorta, D.J., & de Oliveira, D.P. (2011). Azo dyes and their metabolites: does the discharge of the azo dye into water bodies represent human and ecological risks? *In Advances in treating textile effluent*, InTech.

Chequer, F.M.D., de Oliveira, G.A.R., Ferraz, E.R.A., Cardoso, J.C., Zanoni, M.V.B., & de Oliveira, D.P. (2013). Textile dyes: Dyeing process and environmental impact. *In Eco-friendly textile dyeing and finishing*, InTech.

Chung, K.T. (1983). The significance of azo-reduction in the mutagenesis and carcinogenesis of azo dyes. *Mutation Research/Reviews in Genetic Toxicology*, *114*(3), 269-281.

Chung, K.T., & Cerniglia, C.E. (1992). Mutagenicity of azo dyes: structure-activity relationships. *Mutation Research/Reviews in Genetic Toxicology*, *277*(3), 201-220.

Clarke, E.A., & Anliker, R. (1980). Handbook of environmental chemistry. *Organic Dyes and Pigments, Springer-Verlag, Heidelberg*, 181-215.

Clift, R. (1997). Overview clean technology—The idea and the practice. *Journal of Chemical Technology and Biotechnology: International Research in Process, Environmental and Clean Technology*, *68*(4), 347-350.

Crini, G. (2006). Non-conventional low-cost adsorbents for dye removal: a review. *Bioresource Technology*, *97*(9), 1061-1085.

Dányádi, L., Janecska, T., Szabo, Z., Nagy, G., Moczo, J., & Pukánszky, B. (2007). Wood flour filled PP composites: compatibilization and adhesion. *Composites Science and Technology*, *67*(13), 2838-2846.

Davies, L.C., Cabrita, G.J.M., Ferreira, R.A., Carias, C.C., Novais, J.M., & Martins-Dias, S. (2009). Integrated study of the role of Phragmites australis in azo-dye treatment in a constructed wetland: From pilot to molecular scale. *Ecological Engineering*, *35*(6), 961-970.

Dawood, S., & Sen, T. (2014). Review on dye removal from its aqueous solution into alternative cost effective and non-conventional adsorbents. *Journal of Chemical and Process Engineering*, *1*(104), 1-11.

De, A.K., Chaudhuri, B., Bhattacharjee, S., & Dutta, B.K. (1999). A practical application of the advanced oxidation processes for wastewater treatment. *Indian Chemical Engineer*, *41*(2), 121-126.

DeFelice, S.L. (1995). The nutraceutical revolution: its impact on food industry R&D. *Trends in Food Science & Technology*, *6*(2), 59-61.

de Lima, R.O.A., Bazo, A.P., Salvadori, D.M.F., Rech, C.M., de Palma Oliveira, D., & de Aragão Umbuzeiro, G. (2007). Mutagenic and carcinogenic potential of a textile azo dye processing plant effluent that impacts a drinking water source. *Mutation Research/Genetic Toxicology and Environmental Mutagenesis*, *626*(1), 53-60.

Demirbas, A. (2009). Agricultural based activated carbons for the removal of dyes from aqueous solutions: a review. *Journal of Hazardous Materials*, *167*(1-3), 1-9.

Devi, L.G., Kumar, S.G., Reddy, K.M., & Munikrishnappa, C. (2009). Photo degradation of Methyl Orange an azo dye by Advanced Fenton Process using zero valent metallic iron: Influence of various reaction parameters and its degradation mechanism. *Journal of Hazardous Materials*, *164*(2-3), 459-467.

Dharajiya, D., Shah, M., & Bajpai, B. (2015). Biosorption of acid black 52, an azo dye from aqueous solution using pre-treated biomass of aspergillus fumigatus A23. *Pollution Research*, *34*(4), 667-676.

Domínguez, J.R., Beltrán, J., & Rodríguez, O. (2005). Vis and UV photocatalytic detoxification methods (using TiO_2, TiO_2/H_2O_2,TiO_2/O_3,$TiO_2/S_2O_8^{2-}$, O_3, H_2O_2, $S_2O_8^{2-}$, Fe^{3+}/H_2O_2 and $Fe^{3+}/H_2O_2/C_2O_4^{2-}$) for dyes treatment. *Catalysis today*, *101*(3-4), 389-395.

Dubinin, M.M. (1947). The equation of the characteristic curve of activated charcoal. In *Dokl. Akad. Nauk. SSSR.* 55, 327-329.

El-Gohary, F., El-Hawarry, S., Badr, S., & Rashed, Y. (1995). Wastewater treatment and reuse for aquaculture. *Water Science and Technology*, *32*(11), 127-136.

Entezari, M.H., & Kruus, P. (1996). Effect of frequency on sonochemical reactions II. Temperature and intensity effects. *Ultrasonics Sonochemistry*, *3*(1), 19-24.

EPRI (1996) The Efficacy of colour removal technique in textile wastewater treatment. *Hydroscience*, EPRI project, 3329–01.

Eskandarian, M., Mahdizadeh, F., Ghalamchi, L., & Naghavi, S. (2014). Bio-Fenton process for Acid Blue 113 textile azo dye decolorization: characteristics and neural network modeling. *Desalination and Water Treatment*, *52*(25-27), 4990-4998.

Espert, A., Vilaplana, F., & Karlsson, S. (2004). Comparison of water absorption in natural cellulosic fibres from wood and one-year crops polypropylene composites and its influence on their mechanical properties. *Composites Part A: Applied science and manufacturing*, *35*(11), 1267-1276.

Finkbeiner, M., Schau, E. M., Lehmann, A., & Traverso, M. (2010). Towards life cycle sustainability assessment. *Sustainability*, *2*(10), 3309-3322.

Forgacs, E., Cserhati, T., & Oros, G. (2004). Removal of synthetic dyes from wastewaters: a review. *Environment International*, *30*(7), 953-971.

Fowler, M.W. (2006). Plants, medicines and man. *Journal of the Science of Food and Agriculture*, *86*(12), 1797-1804.

Freundlich, H.M.F. (1906). Over the adsorption in solution. *Journal of Physical Chemistry, 57*(385), e470.

Garfield, S. (2002). *Mauve: how one man invented a color that changed the world*. WW Norton & Company.

Garg, V.K., Gupta, R., Yadav, A.B., & Kumar, R. (2003). Dye removal from aqueous solution by adsorption on treated sawdust. *Bioresource Technology*, *89*(2), 121-124.

Garg, V.K., Amita, M., Kumar, R., & Gupta, R. (2004). Basic dye (methylene blue) removal from simulated wastewater by adsorption using Indian Rosewood sawdust: a timber industry waste. *Dyes and Pigments*, *63*(3), 243-250.

Garg, V.K., Kumar, R., & Gupta, R. (2004a). Removal of malachite green dye from aqueous solution by adsorption using agro-industry waste: a case study of Prosopis cineraria. *Dyes and Pigments*, *62*(1), 1-10.

Glavič, P., & Lukman, R. (2007). Review of sustainability terms and their definitions. *Journal of Cleaner Production*, *15*(18), 1875-1885.

Glaze, W H., Kang, J.W., & Chapin, D.H. (1987). The chemistry of water treatment processes involving ozone, hydrogen peroxide and ultraviolet radiation. *Ozone Science and Engineering*, 9, 335-352.

Green, F.J. (1990). *The Sigma-Aldrich handbook of stains, dyes and indicators*. Milwaukee: Aldrich Chemical Company, 628-629.

Guibal, E. (2004). Interactions of metal ions with chitosan-based sorbents: a review. *Separation and Purification Technology*, *38*(1), 43-74.

Guo, Y., Yang, S., Fu, W., Qi, J., Li, R., Wang, Z., & Xu, H. (2003). Adsorption of malachite green on micro-and mesoporous rice husk-based active carbon. *Dyes and Pigments*, *56*(3), 219-229.

Gupta, G.S., Prasad, G., & Singh, V.N. (1990). Removal of chrome dye from aqueous solutions by mixed adsorbents: fly ash and coal. *Water Research*, *24*(1), 45-50.

Gupta, V.K., Mohan, D., Sharma, S., & Sharma, M. (2000). Removal of basic dyes (rhodamine B and methylene blue) from aqueous solutions using bagasse fly ash. *eparation Science and Technology*, *35*(13), 2097-2113.

Gupta, V.K., Ali, I., & Mohan, D. (2003). Equilibrium uptake and sorption dynamics for the removal of a basic dye (basic red) using low-cost adsorbents. *Journal of Colloid and Interface Science*, *265*(2), 257-264.

Gupta, V.K., & Sharma, S.K. (2006). Plants as natural antioxidants.

Gupta, V.K., & Suhas (2009). Application of low-cost adsorbents for dye removal–A review. *Journal of Environmental Management*, *90*(8), 2313-2342.

Hameed, B.H., & El-Khaiary, M.I. (2008). Malachite green adsorption by rattan sawdust: Isotherm, kinetic and mechanism modeling. *Journal of Hazardous Materials*, *159*(2-3), 574-579.

Hashmi, S.A.R., Dwivedi, U.K., Naik, A., & Chand, N. (2002). Effect of Chemical Treatments on High-Stress Abrasive Wear Behaviour of Polypropylene based Lining Materials. *Metals Materials and Processes*, *14*(3), 235-240.

Hatakeyama, T. & F.X. Quinn, (1999). *Thermal Analysis: Fundamentals and Applications to Polymer Science*. Wiley Publishing, New Jersey.

Ho, Y.S., & McKay, G. (1998). Kinetic models for the sorption of dye from aqueous solution by wood. *Process Safety and Environmental Protection*, *76*(2), 183-191.

Ho, Y.S., & McKay, G. (1998a). Sorption of dye from aqueous solution by peat. *Chemical Engineering Journal, 70*(2), 115-124.

Ho, Y.S., & McKay, G. (1999). A kinetic study of dye sorption by biosorbent waste product pith. *Resources, Conservation and Recycling*, *25*(3-4), 171-193.

Ho, Y.S., & McKay, G. (1999a). Comparative sorption kinetic studies of dye and aromatic compounds onto fly ash. *Journal of Environmental Science & Health Part A*, *34*(5), 1179-1204.

Ho, Y.S., & McKay, G. (2003). Sorption of dyes and copper ions onto biosorbents. *Process Biochemistry*, *38*(7), 1047-1061.

Ho, Y.S., Chiang, T.H., & Hsueh, Y.M. (2005). Removal of basic dye from aqueous solution using tree fern as a biosorbent. *Process Biochemistry*, *40*(1), 119-124.

Hoekstra, A.Y., & Wiedmann, T.O. (2014). Humanity's unsustainable environmental footprint. *Science*, *344*(6188), 1114-1117.

http://agriexchange.apeda.gov.in/MarketReport/Reports/Hides_Skins%20-(accessed 2018 May 9).

https://committee.iso.org/files/live/sites/tc61/files/The%20Plastic%20Industry%20Berlin%20Aug%202016%20-%20Copy.pdf (accessed 2018 March 5).

http://www.dnaindia.com/india/report-ranipet-among-world-s-top-ten-polluted-cities-1087070 (accessed 2018 April 15).

https://www.ibef.org/industry/textiles.aspx (accessed 2018 September 29).

https://www.ibef.org/archives/detail/b3ZlcnZpZXcmMzc3NDEmMTEy (accessed 2018 September 29).

http://www.indiaenvironmentportal.org.in/content/5589/polluting-industries/ (accessed 2018 April 15).

http://www.mrssindia.com/uploads/reports/pdf/assocham-knowledge-report-on nutracuticals released-at-3rd-national-symposium-6.pdf (accessed 2018 March 28).

https://www.prnewswire.com/news-releases/plastics-marketworth-65438-billion-by-2020 grand-view-research-inc-51172 0541.html (accessed 2018 March 5).

http://www.royalspices.com/products/cumin-seed/ (accessed 2018 April 22).

http://www.spices.res.in/ (accessed 2018 September 29).

http://www.worstpolluted.org/2016-report.html (accessed 2018 March 5).

Hua, I., & Hoffmann, M. R. (1997). Optimization of ultrasonic irradiation as an advanced oxidation technology. *Environmental Science & Technology*, *31*(8), 2237-2243.

Hunger, K., Mischke, P., Rieper, W., & Zhang, S. (2000). Azo Dyes, 1. General. *Ullmann's Encyclopedia of Industrial Chemistry*, 1-24.

Husain, Q., Karim, Z., & Banday, Z.Z. (2010). Decolorization of textile effluent by soluble fenugreek (Trigonella foenum-graecum L) seeds peroxidase, *Water Air Soil Pollution*, 212(1-4), 319-328.

Illán-Gómez, M.J., Garcia-Garcia, A., Salinas-Martinez de Lecea, C., & Linares-Solano, A. (1996). Activated carbons from Spanish coals. 2. Chemical activation. *Energy & Fuels*, *10*(5), 1108-1114.

Ince, N. H., & Gönenç, D. T. (1997). Treatability of a textile azo dye by UV/H_2O_2. *Environmental Technology*, *18*(2), 179-185.

Işik, M., & Sponza, D.T. (2007). Fate and toxicity of azo dye metabolites under batch long-term anaerobic incubations. *Enzyme and Microbial Technology*, *40*(4):934-939.

Jain, A.K., Gupta, V.K., & Bhatnagar, A. (2003). Utilization of industrial waste products as adsorbents for the removal of dyes. *Journal of Hazardous Materials*, *101*(1), 31-42.

Janos, P., Buchtová, H., & Rýznarová, M. (2003). Sorption of dyes from aqueous solutions onto fly ash. *Water Research*, *37*(20), 4938-4944.

Jovanović, D.S. (1969). Physical adsorption of gases. *Kolloid-Zeitschrift und Zeitschrift für Polymere, 235*(1), 1214-1225.

Juang, R.S., Tseng, R.L., & Wu, F.C. (2001). Role of microporosity of activated carbons on their adsorption abilities for phenols and dyes. *Adsorption*, *7*(1), 65-72.

Juang, R.S., Wu, F.C., & Tseng, R.L. (2002). Characterization and use of activated carbons prepared from bagasses for liquid-phase adsorption. *Colloid and Surfaces A: Physicochemical and Engineering Aspects*, *201*(1-3), 191-199.

Kadirvelu, K., Palanival, M., Kalpana, R., & Rajeswari, S. (2000). Activated carbon from an agricultural by-product, for the treatment of dyeing industry wastewater. *Bioresource Technology*, *74*(3), 263-265.

Kadirvelu, K., Kavipriya, M., Karthika, C., Radhika, M., Vennilamani, N., & Pattabhi, S. (2003). Utilization of various agricultural wastes for activated carbon preparation and application for the removal of dye and metal ions from aqueous solutions. *Bioresource technology*, *87*(1),129-132.

Kalra, E.K. (2003). Nutraceutical-definition and introduction. *Aaps Pharmsci*, *5*(3), 27-28.

Kannan, N., & Sundaram, M. M. (2001). Kinetics and mechanism of removal of methylene blue by adsorption on various carbons—a comparative study. *Dyes and Pigments*, *51*(1), 25-40.

Karaca, S., Gürses, A., & Bayrak, R. (2004). Effect of some pre-treatments on the adsorption of methylene blue by Balkaya lignite. *Energy Conversion and Management*, *45*(11-12), 1693-1704.

Kargi, F., & Ozmıhcı, S. (2004). Biosorption performance of powdered activated sludge for removal of different dyestuffs. *Enzyme and Microbial Technology*, *35*(2-3), 267-271.

Kellner, H.M., Christ, O.E., & Lötzsch, K. (1973). Animal studies on the kinetics of benzidine and 3, 3′-dichlorobenzidine. *Archiv für Toxikologie*, *31*(1), 61-79.

Khare, S.K., Panday, K.K., Srivastava, R.M., & Singh, V.N. (1987). Removal of victoria blue from aqueous solution by fly ash. *Journal of Chemical Technology & Biotechnology*, *38*(2), 99-104.

Khan, M.S., Knapp, J., Clemett, A., Chadwick, M., Mahmood, M., & Sharif, M.I. (2006). Managing and Monitoring Effluent treatment plants. *Managing Industrial Pollution from Small and Medium Scale Industries in Bangladesh Booklet Serie,* SEI, BCAS, University of Leeds, Dhaka, Bangladesh.

Khattri, S.D., & Singh, M.K. (2000). Colour removal from synthetic dye wastewater using a bioadsorbent. *Water, Air, and Soil Pollution*, *120*(3-4), 283-294.

Khehra, M.S., Saini, H.S., Sharma, D.K., Chadha, B.S., & Chimni, S.S. (2005). Comparative studies on potential of consortium and constituent pure bacterial isolates to decolorize azo dyes. *Water Research*, *39*(20), 5135-5141.

Kumar, M.N.R. (2000). A review of chitin and chitosan applications. *Reactive and Functional Polymers*, *46*(1), 1-27.

Kumar, P., Prasad, B., Mishra, I.M., & Chand, S. (2007). Catalytic thermal treatment of desizing wastewaters. *Journal of Hazardous Materials*, *149*(1), 26-34.

Langmuir, I. (1917). The constitution and fundamental properties of solids and liquids. *Journal of the Franklin Institute, 183*(1), 102-105.

Largegren, S. (1898). About the theory of so-called adsorption of soluble substances. *Kungliga Suensk Vetenskapsakademiens Handlinga, 241*(1).

Lee, L.Y., Chin, D.Z.B., Lee, X.J., Chemmangattuvalappil, N., & Gan, S. (2015). Evaluation of Abelmoschus esculentus (lady's finger) seed as a novel biosorbent for the removal of Acid Blue 113 dye from aqueous solutions. *Process Safety and Environmental Protection*, *94*, 329-338.

Li, L., Gao, H.W., Ren, J.R., Chen, L., Li, Y.C., Zhao, J.F., & Yuan, Y. (2007). Binding of Sudan II and IV to lecithin liposomes and E. coli membranes: insights into the toxicity of hydrophobic azo dyes. *BMC Structural Biology*, *7*(1), 16.

Li, W.Y., Chen, F.F., & Wang, S.L. (2010). Binding of reactive brilliant red to human serum albumin: insights into the molecular toxicity of sulfonic azo dyes. *Protein and Peptide Letters*, *17*(5), 621-629.

Lin, Q., Zhou, X., Dai, G., & Bi, Y. (2002). Some studies on mechanical properties of wood flour/continuous glass mat/polypropylene composite. *Journal of Applied Polymer Science*, *85*(3), 536-544.

Liu, G.F., Zhou, J.T., Qu, Y.Y., & Ma, X. (2007). Decolorization of sulfonated azo dyes with two photosynthetic bacterial strains and a genetically engineered Escherichia coli strain. *World Journal of Microbiology and Biotechnology*, *23*(7), 931-937.

Low, K.S., Lee, C.K., & Tan, B.F. (2000). Quaternized wood as sorbent for reactive dyes. *Applied Biochemistry and Biotechnology*, *87*(3), 233-245.

Maiti, S.N., & Lopez, B.H. (1992). Tensile properties of polypropylene/kaolin composites. *Journal of Applied Polymer Science*, *44*(2), 353-360.

Malik, P. K. (2003). Use of activated carbons prepared from sawdust and rice-husk for adsorption of acid dyes: a case study of Acid Yellow 36. *Dyes and Pigments*, *56*(3), 239-249.

Malkapuram, R., Kumar, V., & Negi, Y.S. (2009). Recent development in natural fibre reinforced polypropylene composites. *Journal of Reinforced Plastics and Composites*, *28*(10), 1169-1189.

McKay, G., Porter, J.F., & Prasad, G.R. (1999). The removal of dye colours from aqueous solutions by adsorption on low-cost materials. *Water, Air, & Soil Pollution*, *114*(3-4), 423-438.

Mohamed, M.M. (2004). Acid dye removal: comparison of surfactant-modified mesoporous FSM-16 with activated carbon derived from rice husk. *Journal of Colloid and Interface Science*, *272*(1), 28-34.

Mohammadi, A., Daemi, H., & Barikani, M. (2014). Fast removal of malachite green dye using novel superparamagnetic sodium alginate-coated Fe_3O_4 nanoparticles. *International Journal of Biological Macromolecules*, *69*, 447-455.

Mohan, S.V., Sailaja, P., Srimurali, M., & Karthikeyan, J. (1998). Color removal of monoazo acid dye from aqueous solution by adsorption and chemical coagulation. *Environmental Engineering and Policy*, *1*(3), 149-154.

Mohan, S.V., Rao, N.C., & Karthikeyan, J. (2002). Adsorptive removal of direct azo dye from aqueous phase onto coal based sorbents: a kinetic and mechanistic study. *Journal of Hazardous Materials*, *90*(2), 189-204.

Mondal, S. (2008). Methods of dye removal from dye house effluent—an overview. *Environmental Engineering Science*, *25*(3), 383-396.

Morais, L.C., Freitas, O.M., Goncalves, E.P., Vasconcelos, L. T., & Beca, C.G. (1999). Reactive dyes removal from wastewaters by adsorption on eucalyptus bark: variables that define the process. *Water Research*, *33*(4), 979-988.

Muthukumar, M., Sargunamani, D., & Selvakumar, N. (2005). Statistical analysis of the effect of aromatic, azo and sulphonic acid groups on decolouration of acid dye effluents using advanced oxidation processes. *Dyes and Pigments*, *65*(2), 151-158.

Mutje, P., Lopez, A., Vallejos, M.E., Lopez, J.P., & Vilaseca, F. (2007). Full exploitation of Cannabis sativa as reinforcement/filler of thermoplastic composite materials. *Composites Part A: Applied Science and Manufacturing*, *38*(2), 369-377.

Naidu, A.S. (2000). Indian leather industry in 21st century: challenges and opportunities. *Yojana-Delhi*, *44*(3), 13-17.

Nakagawa, K., Namba, A., Mukai, S.R., Tamon, H., Ariyadejwanich, P., & Tanthapanichakoon, W. (2004). Adsorption of phenol and reactive dye from aqueous solution on activated carbons derived from solid wastes. *Water Research*, *38*(7), 1791-1798.

Namasivayam, C., & Arasi, D.J.S.E. (1997). Removal of congo red from wastewater by adsorption onto waste red mud. *Chemosphere*, *34*(2), 401-417.

Namasiyam, C., & Chandrasekaran, B. (1991). Treatment of dying industry wastewaters using Fe (III)/Cr (III) Sludge and red Mud. *Journal of Indian Assoiation of Environmental Manage*ment *18*, 93-99.

Namasivayam, C., & Kadirvelu, K. (1994). Coirpith, an agricultural waste by-product, for the treatment of dyeing wastewater. *Bioresource Technology*, *48*(1), 79-81.

Namasivayam, C., & Kavitha, D. (2002). Removal of Congo Red from water by adsorption onto activated carbon prepared from coir pith, an Nagricultural solid waste. *Dyes and Pigments*, *54*(1), 47-58.

Namasivayam, C., & Sumithra, S. (2005). Removal of direct red 12B and methylene blue from water by adsorption onto Fe (III)/Cr (III) hydroxide, an industrial solid waste. *Journal of Environmental Management*, *74*(3), 207-215.

Namasivayam, C., Kanchana, N., & Yamuna, R.T. (1993). Waste banana pith as adsorbent for the removal of rhodamine-B from aqueous solutions. *Waste Management*, *13*(1), 89-95.

Namasivayam, C., Jeyakumar, R., & Yamuna, R. T. (1994). Dye removal from wastewater by adsorption on 'waste'Fe (III)/Cr (III) hydroxide. *Waste Management*, *14*(7), 643-648.

Namasivayam, C., Muniasamy, N., Gayatri, K., Rani, M., & Ranganathan, K. (1996). Removal of dyes from aqueous solutions by cellulosic waste orange peel. *Bioresource Technology*, *57*(1), 37-43.

Namasivayam, C., Prabha, D., & Kumutha, M. (1998). Removal of direct red and acid brilliant blue by adsorption on to banana pith. *Bioresource Technology*, *64*(1), 77-79.

Namasivayam, C., Kumar, M.D., Selvi, K., Begum, R.A., Vanathi, T., & Yamuna, R.T. (2001). 'Waste'coir pith—a potential biomass for the treatment of dyeing wastewaters. *Biomass and Bioenergy*, *21*(6), 477-483.

Namasivayam, C., Radhika, R., & Suba, S. (2001a). Uptake of dyes by a promising locally available agricultural solid waste: coir pith. *Waste Management*, *21*(4), 381-387.

Ness, B., Urbel-Piirsalu, E., Anderberg, S., & Olsson, L. (2007). Categorising tools or sustainability assessment. *Ecological Economics*, *60*(3):498-508.

Neagu, R.C., Gamstedt, E.K., & Berthold, F. (2006). Stiffness contribution of various wood fibers to composite materials. *Journal of Composite Materials*, *40*(8), 663-699.

Netpradit, S., Thiravetyan, P., & Towprayoon, S. (2003). Application of 'waste'metal hydroxide sludge for adsorption of azo reactive dyes. *Water Research*, *37*(4), 763-772.

Netpradit, S., Thiravetyan, P., & Towprayoon, S. (2004). Adsorption of three azo reactive dyes by metal hydroxide sludge: effect of temperature, pH, and electrolytes. *Journal of Colloid and Interface Science*, *270*(2), 255-261.

Netpradit, S., Thiravetyan, P., & Towprayoon, S. (2004). Evaluation of metal hydroxide sludge for reactive dye adsorption in a fixed-bed column system. *Water Research*, *38*(1), 71-78.

Ngah, W.W., Teong, L.C., & Hanafiah, M.A.K.M. (2011). Adsorption of dyes and heavy metal ions by chitosan composites: A review. *Carbohydrate Polymers*, *83*(4), 1446-1456.

Nicolais, L., & Narkis, M. (1971). Stress-strain behavior of styrene-acrylonitrile/glass bead composites in the glassy region. *Polymer Engineering & Science*, *11*(3), 194-199.

Nigam, P., Armour, G., Banat, I.M., Singh, D., & Marchant, R. (2000). Physical removal of textile dyes from effluents and solid-state fermentation of dye adsorbed agricultural residues. *Bioresource technology*, *72*(3), 219-226.

Ohr, L.M. (2005). Novelty of nutraceuticals. *Food Technology*.

Okada, K., Yamamoto, N., Kameshima, Y., & Yasumori, A. (2003). Adsorption properties of activated carbon from waste newspaper prepared by chemical and physical activation. *Journal of Colloid and Interface Science*, *262*(1), 194-199.

Ong, S.A., Toorisaka, E., Hirata, M., & Hano, T. (2005). Treatment of azo dye Orange II in aerobic and anaerobic-SBR systems. *Process Biochemistry*, *40*(8), 2907-2914.

Organisation for economic cooperation and development (2005). Environmental requirements and market access. Chapter 2: Limits on aromatic amines in textiles coloured with azo dyes.

Otero, M., Rozada, F., Calvo, L.F., Garcıa, A.I., & Moran, A. (2003). Kinetic and equilibrium modelling of the methylene blue removal from solution by adsorbent materials produced from sewage sludges. *Biochemical Engineering Journal*, *15*(1), 59-68.

Otero, M., Rozada, F., Calvo, L. F., Garcıa, A. I., & Moran, A. (2003). Elimination of organic water pollutants using adsorbents obtained from sewage sludge. *Dyes and Pigments*, *57*(1), 55-65.

Özacar, M., & Şengil, İ.A. (2005). Adsorption of metal complex dyes from aqueous solutions by pine sawdust. *Bioresource Technology*, *96*(7), 791-795.

Pagga, U., & Brown, D. (1986). The degradation of dyestuffs: Part II Behaviour of dyestuffs in aerobic biodegradation tests. *Chemosphere*, *15*(4), 479-491.

Park, B.D., & Balatinecz, J.J. (1997). Mechanical properties of wood-fiber/toughened isotactic polypropylene composites. *Polymer Composites*, *18*(1), 79-89.

Patwardhan, B., Warude, D., Pushpangadan, P., & Bhatt, N. (2005). Ayurveda and traditional Chinese medicine: a comparative overview. *Evidence-Based Complementary and Alternative Medicine*, *2*(4), 465-473.

Pearce, C.I., Lloyd, J.R., & Guthrie, J.T. (2003). The removal of colour from textile wastewater using whole bacterial cells: a review. *Dyes and Pigments*, *58*(3), 179-196.

Pelegrini, R., Peralta-Zamora, P., de Andrade, A.R., Reyes, J., & Duran, N. (1999). Electrochemically assisted photocatalytic degradation of reactive dyes. *Applied Catalysis B, Environmental*, *22*(2), 83-90.

Peralta-Zamora, P., Kunz, A., de Moraes, S. G., Pelegrini, R., de Campos Moleiro, P., Reyes, J., & Duran, N. (1999). Degradation of reactive dyes I. A comparative study of ozonation, enzymatic and photochemical processes. *Chemosphere*, *38*(4), 835-852.

Peter, K.V. (2006). *Handbook of herbs and spices*. 3: Woodhead publishing.

Petrier, C., Jeunet, A., Luche, J.L., & Reverdy, G. (1992). Unexpected frequency effects on the rate of oxidative processes induced by ultrasound. *Journal of the American Chemical Society*, *114*(8), 3148-3150.

Pinheiro, H.M., Touraud, E., & Thomas, O. (2004). Aromatic amines from azo dye eduction: status review with emphasis on direct UV spectrophotometric detection in textile industry wastewaters. *Dyes and pigments*, *61*(2), 121-139.

Pollard, S.J.T., Fowler, G.D., Sollars, C.J., & Perry, R. (1992). Low-cost adsorbents for waste and wastewater treatment: a review. *Science of the Total Environment*, *116*(1-2), 31-52.

Puntener, A., & Page, C. (2004). European Ban on certain azo dyes. *Quality and Environment*, 1-3.

Puvaneswari, N., Muthukrishnan, J., & Gunasekaran, P. (2006). Toxicity assessment and microbial degradation of azo dyes.

Raaman, N. (2006). Categories of phytochemicals. *Phytochemical Techniques*, 197-274.

Radke, C.J., & Prausnitz, J.M. (1972). Thermodynamics of multi-solute adsorption from dilute liquid solutions. *AIChE Journal*, *18*(4), 761-768.

Raghavachary, C. (1997). Colour removal form industrial effluents. A comparative review of available technologies. *Chemical engineering world*, *32*, 53-54.

Raj, R.G., Kokta, B.V., & Daneault, C. (1990). A comparative study on the effect of aging on mechanical properties of LLDPE–glass fiber, mica, and wood fiber composites. *Journal of Applied Polymer Science*, *40*(5-6), 645-655.

Ramakrishna, K.R., & Viraraghavan, T. (1997). Dye removal using low cost adsorbents. *Water Science and Technology*, *36*(2-3), 189-196.

Ramaraj, B. (2007). Crosslinked poly (vinyl alcohol) and starch composite films: tudy of their physicomechanical, thermal, and swelling properties. *Journal of Applied Polymer Science*, *103*(2), 1127-1132.

Ramasami, T., Rajamani, S., & Rao, J.R. (1994). Pollution control in leather industry: Emerging technological options. *International symposium on surface and colloid science and its relevance to soil pollution*.

Ramasami, T., Rajamani, S., & Rao, J.R. (1995). Pollution Control in Leather Industry: Emerging Technological Options. *CLRI, Adyar*, Madras, India.

Ramos, E.U., Vaal, M.A., & Hermens, J.L. (2002). Interspecies sensitivity in the aquatic toxicity of aromatic amines. *Environmental Toxicology and Pharmacology*, *11*(3-4), 149-158.

Redlich, O.J.D.L., & Peterson, D.L. (1959). A useful adsorption isotherm. *Journal of Physical Chemistry*, *63*(6), 1024-1024.

Report by LGC. (1999). The risk of cancer caused by textiles and leather goods coloured with azo dyes. Presented, CSTEE plenary meeting, Brussels.

Robin, J., & Breton, Y. (2001). Reinforcement of recycled polyethylene with wood fibers heat treated. *Journal of Reinforced Plastics and Composites*, *20*(14-15), 1253-1262.

Robinson, T., McMullan, G., Marchant, R., & Nigam, P. (2001). Remediation of dyes in textile effluent: a critical review on current treatment technologies with a proposed alternative. *Bioresource technology*, *77*(3), 247-255.

Robinson, T., Chandran, B., & Nigam, P. (2002). Removal of dyes from an artificial textile dye effluent by two agricultural waste residues, corncob and barley husk. *Environment International*, *28*(1-2), 29-33.

Robinson, T., Chandran, B., & Nigam, P. (2002a). Studies on desorption of individual textile dyes and a synthetic dye effluent from dye-adsorbed agricultural residues using solvents. *Bioresource Technology*, *84*(3), 299-301.

Robinson, T., Chandran, B., & Nigam, P. (2002b). Removal of dyes from a synthetic textile dye effluent by biosorption on apple pomace and wheat straw. *Water Research*, *36*(11), 2824-2830.

Robinson, T., & Nigam, P.S. (2008). Remediation of textile dye waste water using a white-rot fungus Bjerkandera adusta through solid-state fermentation (SSF). *Applied Biochemistry and Biotechnology*, *151*(2-3), 618.

Rodriguez-Reinoso, F. (1997). Activated Carbon In "Introduction to Carbon Technologies". *University Alicante*, 35-61.

Rozada, F., Calvo, L.F., Garcıa, A.I., Martın-Villacorta, J., & Otero, M. (2003). Dye adsorption by sewage sludge-based activated carbons in batch and fixed-bed systems. *Bioresource Technology*, *87*(3), 221-230.

Salleh, M.A.M., Mahmoud, D.K., Karim, W.A.W.A., & Idris, A. (2011). Cationic and anionic dye adsorption by agricultural solid wastes: A comprehensive review. *Desalination*, *280*(1-3), 1-13.

Sarkar, K.T. (1981). *Theory and practice of leather manufacture*. Ajoy Sorcar.

Sato, Y., & Furukawa, J. (1963). A molecular theory of filler reinforcement based upon the conception of internal deformation (a rough approximation of the internal deformation). *Rubber Chemistry and Technology*, *36*(4), 1081-1106.

Serpone, N., & Colarusso, P. (1994). Sonochemistry I. Effects of ultrasounds on heterogeneous chemical reactions–a useful tool to generate radicals and to examine reaction mechanisms. *Research on Chemical Intermediates*, *20*(6), 635-679.

Sips, R. (1948). Combined form of Langmuir and Freundlich equations. *Journal of Physical Chemistry, 16*(429), 490-495.

Sharma, P., Kaur, H., Sharma, M., & Sahore, V. (2011). A review on applicability of naturally available adsorbents for the removal of hazardous dyes from aqueous waste. *Environmental Monitoring and Assessment*, *183*(1-4), 151-195.

Sheldon, R.A. (1992). Organic synthesis-past, present and future. *Chemistry and Industry*, (23), 903-906.

Shu, H.Y., Chang, M.C., & Huang, S.W. (2015). UV irradiation catalyzed persulfate advanced oxidation process for decolorization of Acid Blue 113 wastewater. *Desalination and Water Treatment*, *54*(4-5), 1013-1021.

Shu, H.Y., Chang, M.C., & Huang, S.W. (2016). Decolorization and mineralization of azo dye Acid Blue 113 by the UV/Oxone process and optimization of operating parameters. *Desalination and Water Treatment*, *57*(17), 7951-7962.

Shu, H.Y., Huang, S.W., & Tsai, M.K. (2016a). Comparative study of acid blue 113wastewater degradation and mineralization by UV/persulfate and UV/Oxone processes. *Desalination and Water Treatment*, *57*(60), 29517-29530.

Shu, H.Y., Chang, M.C., & Liu, J.J. (2016b). Reductive decolorization of acid blue 113 azo dye by nanoscale zero-valent iron and iron-based bimetallic particles. *Desalination and Water Treatment*, *57*(17), 7963-7975.

Shukla, A., Zhang, Y. H., Dubey, P., Margrave, J. L., & Shukla, S. S. (2002). The role of sawdust in the removal of unwanted materials from water. *Journal of Hazardous Materials*, *95*(1-2), 137-152.

Sivakumar, S., Senthilkumar, P., & Subburam, V. (2001). Carbon from cassava peel, an agricultural waste, as an adsorbent in the removal of dyes and metal ions from aqueous solution. *Bioresource Technology*, *80*(3), 233-235.

Sivaraj, R., Namasivayam, C., & Kadirvelu, K. (2001). Orange peel as an adsorbent in the removal of acid violet 17 (acid dye) from aqueous solutions *Waste Management*, *21*(1), 105-110.

Sivashankar, R., Sathya, A. B., Vasantharaj, K., & Sivasubramanian, V. (2014). agnetic composite an environmental super adsorbent for dye sequestration–A review. *Environmental Nanotechnology, Monitoring & Management*, *1*, 36-49.

Slokar, Y.M., & Le Marechal, A.M. (1998). Methods of decoloration of textile wastewaters. *Dyes and pigments*, *37*(4), 335-356.

Solís, M., Solís, A., Pérez, H. I., Manjarrez, N., & Flores, M. (2012). Microbial decolouration of azo dyes: a review. *Process Biochemistry*, *47*(12), 1723-1748.

Srinivasan, R., & Mishra, A. (2008). Okra (Hibiscus esculentus) and fenugreek (Trigonella foenum graceum) mucilage: Characterization and application as flocculants for textile effluent treatments. *Chinese Journal of Polymer Science*, *26*(06), 679-687.

Srinivasan, A., & Viraraghavan, T. (2010). Decolorization of dye wastewaters by biosorbents: a review. *Journal of Environmental Management*, *91*(10), 1915-1929.

Standard methods for the examination of water and wastewater. (2002). 20th edn, American Public Health Association: Washington DC.

Suslick, K.S. (1990). Sonochemistry. *Science*, *247*(4949), 1439-1445.

Talarposhti, A.M., Donnelly, T., & Anderson, G.K. (2001). Colour removal from a simulated dye wastewater using a two-phase anaerobic packed bed reactor. *Water Research*, *35*(2), 425-432.

Tanthapanichakoon, W., Ariyadejwanich, P., Japthong, P., Nakagawa, K., Mukai, S. R., & Tamon, H. (2005). Adsorption–desorption characteristics of phenol and reactive dyes from aqueous solution on mesoporous activated carbon prepared from waste tires. *Water Research*, *39*(7), 1347-1353.

Taqui, S.N., Yahya, R., Hassan, A., Nayak, N., & Syed, A.A. (2017). Development of sustainable dye adsorption system using nutraceutical industrial fennel seed spent—studies using Congo red dye. *International Journal of Phytoremediation*, *19*(7), 686-694.

Taqui, S.N., Yahya, R., Hassan, A., Nayak, N., & Syed, A.A. (2018). A novel sustainable design to develop polypropylene and unsaturated polyester resin polymer composites from waste of major polluting industries and investigation on their physicomechanical and wear properties. *Polymer Composites, 40*(3), 1142-1157.

Temkin, M., & Pyzhev, V. (1940). Kinetics of the synthesis of ammonia on promoted iron catalysts. *Journal of Physical Chemistry (USSR)*, *13*, 851-867.

Toth, J. (1971). State equation of the solid-gas interface layers. *Acta Chimica Hungaricae*, *69*, 311-328.

Tsai, W.T., Chang, C.Y., Lin, M.C., Chien, S.F., Sun, H.F., & Hsieh, M.F. (2001). Adsorption of acid dye onto activated carbons prepared from agricultural waste bagasse by $ZnCl_2$ activation. *Chemosphere*, *45*(1), 51-58.

Tseng, R.L., Wu, F.C., & Juang, R.S. (2003). Liquid-phase adsorption of dyes and phenols using pinewood-based activated carbons. *Carbon*, *41*(3), 487-495.

United States Patent. (1996). 4, 792, 407 & 4,849.114 to *Ultrox International*, 1996.

Valix, M., Cheung, W.H., & McKay, G. (2004). Preparation of activated carbon using low temperature carbonisation and physical activation of high ash raw bagasse for acid dye adsorption. *Chemosphere*, *56*(5), 493-501.

Varma, A.J., Deshpande, S.V., & Kennedy, J.F. (2004). Metal complexation by chitosan and its derivatives: a review. *Carbohydrate Polymers*, *55*(1), 77-93.

Vieth, W.R., & Sladek, K.J. (1965). A model for diffusion in a glassy polymer. *Journal of Colloid Science*, *20*(9), 1014-1033.

Wang, H.L., Chen, J.L., & Zhai, Z.C. (2004). Study on thermodynamics and kinetics of adsorption of p-toluidine from aqueous solution by hypercrosslinked polymeric adsorbents. *Environmental Chemistry-Beijing, 23*(2), 192-196.

Wang, S., Boyjoo, Y., Choueib, A., & Zhu, Z.H. (2005). Removal of dyes from aqueous solution using fly ash and red mud. *Water Research*, *39*(1), 129-138.

Webber, T.W., & Chakravorti, R.K. (1974). Pore and solid diffusion models for fixed-bed adsorbers. *AIChE Journal, 20*(2), 228-238.

Weisburger, J. H. (2002). Comments on the history and importance of aromatic and heterocyclic amines in public health. *Mutation Research/ Fundamental and Molecular Mechanisms of Mutagenesis*, *506*, 9-20.

Wu, F.C., Tseng, R.L., & Juang, R.S. (1999). Preparation of activated carbons from bamboo and their adsorption abilities for dyes and phenol. *Journal of Environmental Science & Health Part A*, *34*(9), 1753-1775.

Wuhrmann, K., Mechsner, K.L., & Kappeler, T.H. (1980). Investigation on rate—Determining factors in the microbial reduction of azo dyes. *European Journal of Applied Microbiology and Biotechnology*, *9*(4), 325-338.

Xiaoyue, S. (1999). Impacts of Environmental Standards and Requirements in EU Countries on China's Textile Industry. *Policy Research Center for Environment and Economy, China*.

Xu, Y. (2001).Comparative studies of the $Fe^{3+/2+}$–UV, H_2O_2–UV, TiO_2–UV/vis systems for the decolorization of a textile dye X-3B in water. *Chemosphere*, *43*(8), 1103-1107.

Xu, Y., Lebrun, R.E., Gallo, P.J., & Blond, P. (1999). Treatment of textile dye plant effluent by nanofiltration membrane. *Separation Science and Technology*, *34*(13), 2501-2519.

Yagub, M.T., Sen, T.K., Afroze, S., & Ang, H.M. (2014). Dye and its removal from aqueous solution by adsorption: a review. *Advances in Colloid and Interface Science*, *209*, 172-184.

Yang, H.S., Kim, H.J., Son, J., Park, H.J., Lee, B.J., & Hwang, T.S. (2004). Rice-husk flour filled polypropylene composites; mechanical and morphological study. *Composite Structures*, *63*(3-4), 305-312.

Zaffalon, V. (2010). Climate change, carbon mitigation and textiles. *Textile World*, 160, 34-35.

LIST OF PUBLICATIONS AND PAPER PRESENTED

List of Publications

1. **Taqui, S.N**., Yahya, R., Hassan, A., Nayak, N., & Syed, A.A. (2019). Adsorption of Acid blue 113 from aqueous solution onto nutraceutical industrial coriander seed spent: Isotherm, kinetics, thermodynamics and modeling studies. *Desalination and Water Treatment*, *153,* 321-337.

2. Taqui, S.N., Yahya, R., Hassan, A., Khanum, F., & Syed, A.A. (2019). Valorization of nutraceutical industrial coriander seed spent by the process of sustainable adsorption system of Acid Black 52 from aqueous solution. *International Journal of Environmental Research*, 1-21.

3. Taqui, S.N., Yahya, R., Hassan, A., Nayak, N., & Syed, A.A. (2018). A novel sustainable design to develop polypropylene and unsaturated polyester resin polymer composites from waste of major polluting industries and investigation on their physicomechanical and wear properties. *Polymer Composites, 40*(3), 1142-1157.

4. Taqui, S.N., Yahya, R., Hassan, A., Nayak, N., & Syed, A.A. (2017). Development of sustainable dye adsorption system using nutraceutical industrial fennel seed spent—studies using Congo red dye. *International Journal of Phytoremediation, 19*(7), 686-694.

List of Paper Presented

1. **Taqui, S.N**., Yahya, R., Hassan, A., Nayak, N., & Syed, A.A. Nutraceutical Industrial Spent as Sustainable Materials for the Remediation of Toxic Dyes from Textile Industries. National Conference on Trends in Bioactive natural products and health care (BNPHC 2017), 05-06 October 2017, Mangalore University, Post Graduate Centre, Chikka Aluvara, Kodagu, Karnataka, India.

2. **Taqui, S.N**., Yahya, R., Hassan, A., & Syed, A.A. A novel sustainable approach to develop green thermoplastic and thermoset composites from waste generated from textile and nutraceutical industries: Evaluation of physico-mechanical properties. 7th National Conference on Novel Polymeric Materials (Synthesis, Processing & Characterization), 15-16 September 2017, SJCE, Mysuru, Karnataka, India.

3. **Taqui, S.N**., Yahya, R., Hassan, A., & Syed, A.A. Mechanistic and kinetic studies using novel adsorbent for the remediation of Acid Black 52 from tanneries effluent. National Conference on Advances in Materials Research (NCAMR-2017), 18-19 August 2017, Ramaiah University of Applied Sciences, Bengaluru, Karnataka, India.

4. **Taqui, S.N**., Yahya, R., Hassan, A., Nayak, N., & Syed, A.A. Feasibility studies of Acid Blue 113 dye adsorption on nutracetuical industrial spent and novel use of resulting sludge as filler material for the fabrication of "green" composites. National Seminar on Role of Chemistry in Human Health & Environmental Protection, 30-31 January 2017, Government Science College (Autonomous), Anantpur, Andhra Pradesh, India.

5. **Taqui, S.N**., Yahya, R., Hassan, A., Nayak, N., & Syed, A.A. "Innovative Method for the use of "sludge" obtained after Bioremediation of toxic dyes as Filler Material for the Fabrication of "Green" Composites". International Conference on

Science & Technology: Future Challenges & Solutions (STFCS-2016), 08-09 August 2016, University of Mysore, Mysuru, Karnataka, India.

6. **Taqui, S.N**., Yahya, R., Hassan, A., Nayak, N., & Syed, A.A. Studies on the mechanism and thermodynamic feasibility of fennel seed spent for the bioremediation of Congo red dye in water. 2nd International Conference on Emerging Trends in Multidisciplinary Research (ETMR 2016), 02-03 August 2016, Bangkok, Thailand.

7. **Taqui, S.N**., Yahya, R., Hassan, A., Nayak, N., & Syed, A.A. Novel Studies on the Bioremediation of Toxic Dye and Reuse of Resulting Sludge as Filler Material for the Fabrication of "Green" Composites. International Conference on Emerging Research in Sciences & Humanities (ERSH-2016), 16-17 May 2016, Kuala Lumpur, Malaysia.